Technische Universität München

Wissenschaftszentrum Weihenstephan für Ernährung, Landnutzung und Umwelt

Lehrstuhl für Phytopathologie

Molecular Characterization of Retroelement Encoded ROPIP1 as Virulence Effector of *Blumeria graminis* f.sp. *hordei*

Mathias Nottensteiner

Vollständiger Abdruck der von der Fakultät Wissenschaftszentrum Weihenstephan für Ernährung, Landnutzung und Umwelt der Technischen Universität München zur Erlangung des akademischen Grades eines

Doktors der Naturwissenschaften

genehmigten Dissertation.

Vorsitzender:	Univ.-Prof. Dr. A. Gierl
Prüfer der Dissertation:	1. Univ.-Prof. Dr. R. Hückelhoven
	2. Univ.-Prof. Dr. A. Tellier
	3. apl. Prof. Dr. E. Glawischnig

Die Dissertation wurde am 13. August 2015 bei der Technischen Universität München eingereicht und durch die Fakultät Wissenschaftszentrum Weihenstephan für Ernährung, Landnutzung und Umwelt am 09. November 2015 angenommen.

3-AT	3-Amino-1,2,4-triazole
AF	Actin filaments
At	*Arabidopsis thaliana*
AVR	Avirulence
BEC	*Bgh* effector candidate
Bgh	*Blumeria graminis* f.sp. *hordei*
Bgt	*Blumeria graminis* f.sp. *tritici*
BiFC	Bimolecular fluorescence complementation
CA	Constituitvely active
CC-NB-LRR	Coiled-coil nucleotide binding leucine rich repeat receptor
CLSM	Confocal laser scanning microscopy
CRIB	Cdc42/Rac interactive binding
CSC	Cellulose synthase complex
CSEP	Candidate secreted effector protein
CW	Cell wall
CWA	Cell wall apposition (papillae)
CWDEs	Cell wall degrading enzymes
d	day(s)
dai	Days after inoculation
DAMP	Damage-associated molecular pattern
DN	Dominant negative
dsRNA	double-stranded RNA
EKA	Effectors paralogous to Avr_{a10} and Avr_{k1}
ER	Endoplasmatic reticulum
ETI	Effector-triggered immunity
ETS	Effector-triggered susceptibility
F-actin	Filamentous actin
GAP	GTPase-activating protein
GDI	Guanine nucleotide dissociation inhibitor
GEF	Guanine nucleotide exchange factor
GNBP	Guanine-nucleotide binding proteins
hai	Hours after inoculation
hat	Hours after transformation
HIGS	Host-induced gene silencing
HR	Hypersensitive response
Hrp	Horseradish peroxidase
ORF	Open reading frame
p	p-value
PAMP	Pathogen-associated molecular pattern
PCD	Programmed cell death
PCR	Polymerase chain reaction
PM	Plasma membrane
PRR	Pattern recognition receptor
PS	Preimmune serum
PTI	PAMP-triggered immunity
PTI	Pattern triggered immunity
RACE-PCR	Rapid amplification of cDNA-ends-PCR
R-gene	Resistance gene
RLCK	Receptor-like cytoplasmic kinase
RLK	Receptor like kinase
RLP	Receptor like protein
RNAi	RNA interference
ROP	Rho of plants
ROS	Reactive oxygen species
R-protein	Resistance protein
S gene	Susceptibility gene
S.E.	Standard error
SA	Salicylic acid
SAR	Systemic acquired resistance
SDS-PAGE	Sodium dodecyl sulfate polyacrylamide gel electrophoresis
SEP	Short open reading frame encoded polypeptides
SINE	Short interspersed element
sRNA	small non-coding RNA
STD	Standard deviation
T3SS	Type three secretion system
TE	Transposable element
TEM	Transmission electron microscopy
TM	Transmembrane
TSD	Target site duplication
WB	Western blot
WT	Wild-type
Y2H	Yeast two-hybrid system

1 Introduction

1.1 Plant Immunity

1.1.1 Pattern-Triggered Immunity

Plant immunity is executed autonomously on the single cell level as plants lack a circulation system required for adaptive immunity [Spoel and Dong 2012]. Plant pathogens generally stay separated from the host cell interior by the host Plasma Membrane (PM) [Dodds and Rathjen 2010]. The host PM is wrapped with a rigid Cell Wall (CW) mainly consistent of cellulose, hemicelluloses and pectin. Epidermal cells of aerial parts of herbaceous plants are additionally overlapped with cuticular layers of cutin and wax. Some plant pathogens secrete lytic enzymes that degrade the CW and the cuticula (Cell Wall Degrading Enzymes, CWDEs) and some additionally exert mechanical force to push through their infection structure. Fragments of extracellular matrix components but also presence of intracellular molecules in the apoplast act as elicitors for defense signaling and for wound sealing. The perception of these Damage-Associated Molecular Patterns (DAMPs) by PM-spanning Pattern Recognition Receptors (PRRs) is conserved across all kingdoms [Heil and Land 2014]. Amongst others, pectin fragments and the release of intracellular ATP into the apoplast are described as DAMPs in plant cells. Oligogalacturonides (OGs) are fragments of the pectin polysaccharide homogalacturonan produced by lytic activity of CWDEs or mechanical force. OGs are perceived by the EGF-like domain containing receptor kinase Wall-Associated Kinase 1 (AtWAK1) in *Arabidopsis thaliana* (*At*) [Brutus et al. 2010]. Intracellular ATP gets released upon biotic (pathogen attack), abiotic stress and during plant cell growth. Extracelluar ATP is then recognized by the lectin receptor kinase DORN1 of Arabidopsis [Tanaka et al. 2014]. Plants not only recognize manipulation of themselves by pathogens but they also recognize potential intruders directly by Pathogen-Associated Molecular Patterns (PAMPs) which are alternatively called Microbe-Associated Molecular Patterns (MAMPs). PAMPs are conserved structural or other components that cannot be easily changed by the pathogen. The most prominent PAMPs are flagellin oligopeptides (flg22) of bacterial flagella and chitin fragments derived from fungal cell walls. Flg22 gets recognized by the Leucine-Rich

Repeat (LRR) ectodomain of the Receptor-Like Kinase (RLK) Flagellin Sensing 2 (AtFLS2) in Arabidopsis. Upon ligand binding AtFLS2 heterodimerizes with the co-receptor Brassinosteroid Insensitive 1-Associated Kinase 1 (AtBAK1) and further proteins to form a receptor complex. Fungal chitin oligomers are perceived by the LysM-ecotodomain of the Arabidopsis Chitin Elicitor Receptor Kinase 1 (AtCERK1) RLK. AtCERK1 homo-dimerizes upon ligand binding. Chitin fragments are likewise bound by Lys-M ectodomain-containing TM proteins in rice. In contrast to RLK, Receptor-Like Proteins (RLPs), like rice Chitin Elicitor Binding Protein (OsCEBiP) lack the intracellular kinase domain. Like AtCERK1, OsCeBIP1 homodimerizes upon ligand binding but additionally recruits the rice homologue of AtCERK1, OsCERK1 for signal transduction. Like the AtFLS2-AtBAK1 complex, the OsCERK1-OsCEBiP complex recruits further proteins to form a functional immune receptor complex. Both, the AtFLS2 and the OsCERK1 immune receptor complexes can promote the activation of Mitogen-Activated Protein Kinase (MAPK) cascades. MAPK cascades end up in the nucleus where they lead to differential regulation of transcription factors. As a result the transcription of defense-associated genes gets upregulated. Further, PRR signaling promotes the extracellular generation of Reactive Oxygen Species (ROS) generated from superoxide ($O_2^{\cdot -}$) produced by PM-spanning NADPH oxidases [Macho and Zipfel 2014; Zipfel 2014; Trdá et al. 2015]. Plant cells react to PAMP treatment with a strong accumulation of extracellular ROS (oxidative burst) that directly poison the pathogen but also act as second messenger in defense signaling. Further ROS contribute to enhancement of CW rigidity by cross-linking of phenolic CW components mediated by peroxidases [Lehmann et al. 2014]. All wannabe intruders have to overcome this so called Pattern-Triggered Immunity (PTI). Besides ROS generation and altered gene expression patterns the PTI defense responses includes further defense reactions. The cell-wall gets thickened by focused secretion of CW material beneath the site of attack to form a Cell Wall Apposition (CWA) which is also referred to as papillae. Antimicrobial compounds get secreted. These include low molecular weight toxins that are either constitutively present (phytoanticipines) or get induced upon pathogen perception (phytoalexins) and proteins with antimicrobial properties. Additionally Pathogenesis-Related proteins (PR-proteins) get secreted. PR-proteins, like chitinases or proteinases, have lytic activity but are also discussed to inhibit CWDEs of the pathogens [Hückelhoven 2007].

1.1.2 Effector-Triggered Susceptibility and Immunity

Plant pathogens deploy effectors to overcome PTI (see below) and to establish Effector-Triggered Susceptibility (ETS). The co-evolution of plant pathogens and host plants is driven by the ability of plants to detect manipulation through pathogen effectors via Resistance Proteins (R proteins). In most cases effector recognition is achieved by one particular class of R-proteins, the intracellular Nucleotide-Binding/Leucine Rich-Repeat (NLR) receptors. Detection of pathogen effectors triggers a boosted immune response that often cumulates in massive ROS generation going in hand with a localized Programmed Cell Death (PCD), referred to as the Hypersensitive Response (HR). The re-established immunity is then called Effector-Triggered Immunity (ETI). Recognized effectors are consequently called Avirulence Proteins (AVRs). ETI also primes the plant through systemic signaling for faster PTI execution. ETI is thought to be causative for rapidly diversifying effector repertoires of plant pathogens which ultimately re-establish ETS. The ‘arms race’ of pathogen effectors and plant R-proteins is thought to cause host adaption of the pathogen on the one hand and a race-specific resistance of the plant on the other [Jones and Dangl 2006].

This co-evolution of plants and pathogens is mirrored by NLRs being one of the most rapidly evolving plant genes [Jacob et al. 2013; Cui et al. 2014]. Plant genomes harbor several hundred variants of NLR genes. NLRs are generally composed of a Nucleotide-Binding Site (NBS) which is followed by Leucine-Rich-Repeat (LRR) domain. NLRs can get divided into two major subgroups depending on the presence of a Coiled-Coil (CC) or of an alternative Toll-Interleukin 1 (TIR) domain at their amino terminus. NLRs are kept inactive as long the NBS is ADP-bound. Activation of NLRs requires exchange of ADP for ATP. The precise mechanism regulating ADP/ATP exchange and hence receptor activation remain to be explored but likely includes NLR dimerization or oligomerization. Given the importance of NLR inactivity for cell survival, NLR activation is thought to be tightly regulated. There are two models in the field that aim to explain how the presence of pathogenic effectors inside plant host cells triggers NLR activation. The first model states direct protein-protein interaction of one pathogen effector and a corresponding NLR, which is based on Flor’s gene-for-gene hypothesis [Flor 1971]. The second model, another interpretation of Flor’s gene-gene hypothesis, states indirect

recognition of intracellular pathogen effectors by monitoring of host proteins targets by NLRs [Dangl and Jones 2001]. NLRs are thought to recognize modification of the effector target protein (guard hypothesis) in a kind of modified-self detection reaction. Additionally plants are thought to have evolved proteins that are without major function for the plant cells but act as NLR-guarded ‘decoys’ due to their structural resemblance to the real pathogen effector target protein. Direct and indirect effector perception by NLRs is not seen mutually exclusive but rather to be present simultaneously (see Cui et al. 2014 for recent review on ETI).

1.1.3 The Role of Phytohormones

Additional to protein-interaction relayed defense pathways, plant hormone signaling is involved in pathogen defense, too. Principally, one can distinguish Salicylic Acid (SA)-mediated resistance against biotrophic pathogens from Jasmonic Acid (JA)/ethylene-mediated resistance against necrotrophic pathogens [Glazebrook 2005].

SA signaling in pathogen defense is reviewed in Vlot et al. [2009]. Elevated SA levels contribute to enhanced resistance against viral, bacterial and fungal pathogens by triggering Pathogenesis-Related gene (PR gene) expression and amplifying ROS mediated HR in *At*. In pathogen challenged leaves, increasing SA concentrations temporally coincide with PR-gene expression and subsequent elevated SA concentrations in the phloem sap and in systemic tissue. Hence, SA is a component of Systemic Acquired Resistance (SAR) signaling although it is not the translocated signal. Most of the work in SA signaling is done in tobacco and Arabidopsis and it is less well understood in monocots.

Like typical for phytohormone signaling, SA pathways cross-react with other phytohormone pathways. SA signaling negatively interferes with JA and Abscisic Acid (ABA) defense signaling against necrotrophic pathogens and insects. JA and ABA signaling in return negatively interferes with SA signaling. High auxin concentrations do not only promote growth but also susceptibility towards pathogens. High SA concentrations inhibit auxin signaling and therewith susceptibility.

Major protein components upstream and downstream of SA were identified genetically. Enhanced Disease Susceptibility 1 (EDS1) and Phytoalexin Deficient 4 (PAD4) act

upstream of SA in PTI and ETI. Downstream signaling mainly depends on the SA signal transducer Non-Expressor of Pathogenesis-Related Genes 1 (NPR1) that via interaction with transcription factors of the TGA family induces PR-gene expression, e.g of *PR1*. However, there are also SA-dependent but NPR1-independent changes in gene expression. The SA response is potentiated by positive feedback regulation of SA levels by ROS and Nitric Oxide (NO) as well as by EDS1 and PAD4. High SA levels together with ROS and NO lead to cell death in the pathogen response [Vlot et al. 2009]. Arabidopsis SA signaling mutants (*pad4*, *eds5*, *npr1*) are more susceptible towards the powdery mildew fungus *Golovinomyces* (syn. *Erysiphe*) *orontii* (*G. orontii*). Exogenous JA treatment also impairs *G. orontii* growth on *At*. However, no induction of JA-mediated defense pathways is observed upon infection with *G. orontii* [Glazebrook 2005].

1.2 Plant Pathogen Effectors

Plant pathogens have evolved diverse effectors that act together in circumventing plant defense responses and to reprogram their hosts to the benefit of the pathogen.

1.2.1 Avoidance of Recognition

One strategy is to hide MAMPs and DAMPs. The fungal pathogen *Cladosporium fulvum* (*C. fulvum*) of tomato secretes Avr4 which binds to long-chained chitin oligomers of the fungal cell wall thereby shielding it from secreted host chitinase lytic degradation [van den Burg et al. 2006]. *C. fulvum* additionally secretes the apoplastic LysM domain-containing effector Ecp6 that binds to short-chained chitin oligomers with great affinity such that chitin recognizing PRRs are outcompeted [De Jonge et al. 2010]. *Pseudomonas syringae* (*P. syringae*) and other bacteria secrete the alkaline protease AprA which cleaves flg22 into smaller fragments that cannot be perceived by FLS2 anymore and that way supports virulence of *P. syringae* on tomato [Pel et al. 2014].

Another strategy is to directly interfere with the receptors that recognize them. *P. syringae* AvrPto and AvrPtoB have a kinase inhibitor domain and interact with the protein kinase Pto of tomato which is guarded by the R protein Prf. Binding of AvrPto or AvrPtoB to Pto likely changes the conformation of the Pto-Prf dimer, thereby activating the R-protein Prf. The plant PRRs AtFLS2 and AtEFR are further targets of AvrPto, while AvrPtoB additionally targets AtFLS2 and AtCERK1. Likely further PRRs are

targeted by both. Besides a kinase inhibitor domain at its N-terminal part, AvrPtoB carries an additional E3 ligase domain at its C-terminus [Xiang et al. 2011; Dou and Zhou 2012]. AvrPtoB was shown to promote ubiquitination of AtFLS2 [Göhre et al. 2008] and AtCERK1 [Gimenez-Ibanez et al. 2009] leading to their proteasomal degradation. The versatile *P.syringae* Type Three Secretion System (T3SS) effector HopZ1 acts as acetyltransferase on multiple host proteins. It *inter alia* acetylates the non-functional Receptor-Like Cytoplasmic Kinase (RLCK) AtZED1 of Arabidopsis which likely acts as decoy for HopZ1a recognition by the AtZAR1 R-protein in ETI. Deletion of AtZED1 abolished AtZAR1-triggered HR but did not affect the virulence function of HopZ1a [Lewis et al. 2013].

1.2.2 Mitigation of Defense Response

PRRs induce a MAPK cascade by phosphorylation which is targeted by plant pathogen effectors. HopA1 of *P. syringae* removes the phosphate from phosphorylated kinases by its phosphothreonine lyase activity thereby stopping the phosphorylation cascade of MAPK cascades [Zhang et al. 2007; Zhang et al. 2012b]. HopF2 of *P. syringae* localizes to the host PM where it exerts ADP ribosyltransferase activity on MAPKs, which blocks their kinase activity [Wang et al. 2010; Wu et al. 2011]. Further, HopF2 directly interacts with AtBAK1 which prevents phosphorylation of AtBIK1 which is required for initial MAPK cascade activation [Zhou et al. 2014].

The SA phytohormonal pathway is also targeted by plant pathogen effectors. *P. syringae* secretes the toxin coronatine which structurally mimics the SA antagonistic JA and forces stomatal opening for bacterial entry into tomato and Arabidopsis leaves [Melotto et al. 2006]. The *Ustilago maydis* (*U. maydis*) effector Cmu1 is a cytoplasmic effector with functional chorismate mutase activity. Interaction of Cmu1 with the cytoplasmic Chorimate Mutase 2 (Cm2) of mays is thought to promote chorismate efflux from chloroplasts to the cytoplasm which was supposed to reduce the amount of the available SA precursor chorismate inside chloroplasts [Djamei et al. 2011]. The necrotrophic ascomycete fungus *Cochliobolus victoriae* secretes the toxin Victorin that directly binds to the active site of the thioredoxin TRX-h5 resulting in a stabilized NPR1 oligomer. NPR1 is one key regulator of the SA-dependent response. The prevented interaction of NPR1 monomers with TGA transcription factors inhibits SA-responsive

defense genes (e.g. PR-genes) and SAR. TRX-h5 is in turn guarded by the R-protein LOV1 and cell-death triggered via LOV1 is then beneficial for the necrotropic pathogen [Kazan and Lyons 2014; Caarls et al. 2015].

PRR signaling and phytohormonal pathways both end up with differential transcription of defense-related genes. Their transcription and subsequent translation are targeted by plant pathogen effectors. The effector Pi03192 of *Phytophthora infestans* (*P. infestans*) directly interacts with the two NAC transcription factors StNTP1 and StNTP2 of potato. Heterologous expression in *Nicotiana benthamiana* (*N. benthamiana*) showed that Pi03192 prevents the relocation of StNTP1 and StNTP2 from their native localization at the ER into the nucleus after defense induction with culture filtrates of *P. infestans* [McLellan et al. 2013]. HopD1 of *P. syringae* is a further example. It physically interacts with the NAC transcription factor NTL9 at the ER. NTL9 is a positive regulator of ETI response gene expression. HopD1 suppresses ETI responsive genes but not PTI response genes [Block et al. 2014]. HopU1, a T3SS effector of *P. syringae* is a functional ADP ribosyltransferase. It was shown to ADP ribosylate the RNA recognition motif of the RNA binding protein GRP7 of Arabidopsis [Fu et al. 2007]. ADP-ribosylation of AtGRP7 hampers its RNA binding capabililty. AtGRP7 associates with the 43S pre-initiation protein translation complex that joins together mRNA and ribosomes. AtGRP7 was found to bind to the mRNA of the PRRs AtFLS2 and AtEFR. Addition of HopU1 disrupts the binding capacity of AtGRP7 for AtFLS2 and AtEFR mRNA. This resulted in reduced AtFLS2 and AtEFR protein abundancy upon *P. syringae* infection [Nicaise et al. 2013].

Transcribed and translated apoplastic acting defense proteins, like PR-proteins and other defense compounds need to be secreted and there are plant pathogen effectors that impair the secretion machinery of the host cells. HopM1 of *P. syringae* promotes ubiquitination of host proteins. It *inter alia* targets AtMIN7 for proteasomal degradation. AtMIN7 is an ADP-Ribosylation Factor-Guanine Nucleotide Exchange Factor (ARF-GEF) that activate ARF GTPases required for coated vesicle formation at the Golgi. Therefore, HopM1 is thought to inhibit the host vesicle trafficking pathway, which was substantiated by a reduced and non-polarized callose deposition in PTI [Nomura et al. 2006; Yorimitsu et al. 2014].

In case defense compounds of the host cell are secreted then there are plant pathogen effectors that inhibit these defense compounds or that mitigate the effect of these defense compounds. *Phytophthora* species secrete Glucanase Inhibitor Proteins (GIPs) that structurally resemble serine proteases but are non-functional. GIPs inhibit secreted endo-β-1,3-glucanases (EGase) of soybean and tomato by direct binding in the apoplast. Pathogenic GIPs and host EGases are both transcriptionally induced in the host pathogen interaction and show signs of co-evolution [Rose et al. 2002; Damasceno et al. 2008]. The fungus *C. fulvum* secretes the apoplastic effector Avr2 that inhibits secreted host cysteine proteases, like Rcr3 of tomato. The Avr2-Rcr3 complex is perceived by the RLP Cf2 [Rooney et al. 2005]. Further apoplastic tomato cysteine proteases are also inhibited by Avr2 which are not guarded by R-proteins. Avr2 is also functional in inhibiting Arabidopsis secreted cysteine proteases [van Esse et al. 2008]. Two independently evolved apoplastic effectors of *P. infestans*, EPIC1 and EPIC2b, also inhibit Rcr3 [Song et al. 2009]. However, EPICs selectively prefer binding to the apoplastic papain-like cysteine protease C14 of *solanaceae* under more stringent conditions. EPICs physically interact with C14 likely in the apoplast, likely blocking its protease activity [Kaschani et al. 2010]. Avrblb2 of *P. infestans* appears to be localized in the apoplastic extrahaustorial matrix surrounding haustoria. Avrblb2 associates with C14 and apparently prevents its secretion into the apoplast. The C14 protein amount was lowered in presence of Avrblb2 in protein extracts prepared from apoplastic fluids [Bozkurt et al. 2011]. Apoplastic ROS produced in the oxidative burst is another important PTI response. ROS are directly poisonous to pathogens as their oxidative capacity damages proteins, lipids and DNA but are also involved in plant CW reinforcement and act as second messenger in SA response [Apel and Hirt 2004; Doehlemann and Hemetsberger 2013].The *U. maydis* apoplastic effector Pep1 attenuates apoplastic H_2O_2 accumulation. Pep1 physically interacts with the maize apoplastic class III heme peroxidase POX12 in the apoplast and directly inhibits its peroxidase activity *in vitro* [Hemetsberger et al. 2012].

1.2.3 Reprogamming of the Host

A major aim of biotrophic plant pathogens is avoidance of host cell-death:

HopPtoN is a secreted cysteine protease of *P. syringae* that partially suppresses cell-death in incompatible and in compatible interactions. Mutational inactivation of its cysteine protease domain abolishes its effect in HR suppression [López-Solanilla et al. 2004].

Action of T3SS effector XopJ of *X. campestris* keeps SA levels in the host cell low which ultimately contributes to prevention of cell death. XopJ has protease activity and localizes to the host PM where interacts with the proteasomal subunit Regulatory Particle AAA-ATPase6 (RPT6). RPT6 is thought to contribute to correct 26S proteasome assembly. Proteolytic cleavage of RPT6 by XopJ degrades RPT6 resulting in malfunction of the host proteasome which was seen by an increase in ubiquitinated host proteins. XopJ activity leads to decreased SA levels and SA-dependent responses in host cells. This was reasoned to be due to disturbances in NPR1 steady state protein turnover resulting in an accumulation of ubiquitinated NPR1. An increase in NPR1 protein abundance was observed upon transient expression of XopJ or silencing of *RPT6* [Üstün et al. 2013; Üstün and Börnke 2015].

A summary of the effectors mentioned in the text is given in chronological order in Table1.

Table 1: Described effectors and their functions

Pathogen	Effector	Function	Reference
Avoidance of Recognition			
Cladiosporum fulvum	Avr4	Shields chitin from host chitinases	Van den Burg et al. (2006)
	Ecp6	Prevents PRR activation by interception of chitin fragments	De Jonge et al. (2010)
Pseudomonas syringae	Arp6	Prevents PRR activation by lytic degradation of flg22	Pel et al. (2014)
	AvrPto	PRR kinase inhibitor	Xiang et al. (2011); Dou and Zhou (2012)
	AvrPtoB	PRR kinase inhibitor; Ubiquitination of PRRs	Göhre et al. (2008); Gimenez-Ibanez et al. (2009)
	HopZ1a	Acetylation of RLCKs in ETI signalling	Lewis et al. (2013)
Mitigation of Defense Responses			
Pseudomonas syringae	HopAI1	Inhibition of MAPK cascades by dephosphorylation of MPKs	Zhang et al. (2007, 2012b)
	HopF2	Inhibition of MAPK cascades by inhibiting kinase activity	Wu et al (2010, 2011); Zhou et al. (2014)
	Coronatine	Structural mimicry of SA antagonist JA	Melotto et al. (2006)
Ustilago maydis	Cmu	Reduction of SA levels in plastids by likely promoting SA efflux into cytoplasm	Djamei et al. (2011)
Cochliobolus victoriae	Victorin	Inhibition of SA-induced signalling for defense gene expression	Kazan and Lyons (2014); Caarls et al. (2015)
Pseudomonas syringae	HopD1	Suppression of defense gene expression by binding to host transcription factor	Block et al. (2014)
Phytophthora infestans	Pi03192	Prevents migration of host transcription factors into nucleus	McLellan et al. (2013)
Pseudomonas syringae	HopU1	Reduction of AtFLS3 and AtEFR PRR translation by acetyltation of mRNA binding proteins	Nicaise et al. (2013)
Pseudomonas syringae	HopM1	Prevention of host secretion by induction of proteasomal degradation of an ARF-GEF.	Nomura et al. (2006)
Phytophthora sojae	GIPs	Inhibition of lytic PR-proteins in the apoplast	Rose et al. (2002); Damasceno et al. (2008)
Clasoporium fulvum	Avr2	Inhibition of apoplastic host proteases	Rooney et al. (2005); van Esse et al. (2008);
Phytophthora infestans	EPIC1; EPIC2b	Inhibition of apoplastic host proteases	Song et al. (2009); Kaschani et al. (2010)
	Avrblb2	Prevention of secretion of host proteases into apoplast	Bozkurt et al. (2011)
Ustilago maydis	Pep1	Inhibition of apoplastic ROS generation	Hemetsbeger et al. (2012)
Reprogamming of the Host			
Pseudomonas syringae	Hopavr2PtoN	Host cell death suppression	López-Solanilla et al. (2004)
Xanthomonas campestris	XopJ	Decreases host SA level by inhibiting host protein turn-over	Üstün et al. (2013); Üstün and Börnke (2015)

1.3 The Pathogen *Blumeria graminis*

Blumeria graminis DC. forma specialis (f.sp.) *hordei* (Marchal; *Bgh*), the causal agent of the powdery mildew disease on the crop barley (*Hordeum vulgare* L.), is a member of the kingdom fungi, phylum *Ascomycota*, order *Erysiphales* (powdery mildew fungi), genus *Blumeria* (powdery mildew of cereals and grasses). Powdery mildews are a widespread disease of aerial plant parts of angiosperms causing the name-giving symptom of whitish to grey powdery pustules that later can merge into a dusty appearing cover of wider plant parts. They are obligate biotrophic ecto-parasites and cannot grow or reproduce being absent from their host plant which also excludes their axenical cultivation in the laboratory. Powdery mildews of true grasses (*Poaceae*, syn. *Graminae*) have evolved a high degree of host specificity as e.g. *Bgh* hardly can infect other cereal crops than barley and barley is vice versa largely resistant to non-adapted *Blumeria* species, like *Blumeria gramins* f.sp. tritici (*Bgt*) of wheat [Agrios 2005; Inuma et al. 2007]. However, powdery mildews of cereals can infect several wild grasses [Troch et al. 2014] which might act as temporary hosts between seasons and common host for different formae specialis. It is further suggested, that the strict host specificity of powdery mildews observed with cereal crops is rather the result of host adaption than of host specialization. Suggestion on the divergence time of *Blumeria graminis* into the formae speciales *hordei* and *tritici* range from 14.000 to 10 million years ago and the topic is under current debate [Troch et al. 2014].

The life cycle of *Bgh* is well described in Bélanger [2002]. The asexual (anamorph) or imperfect stage is mainly relevant for the epidemiology of *Blumeria graminis*. Dormant mycelium overwinters at autumn-sawn grains, volunteer grain and wild grasses from where air current-spread asexual spores, called conidia, cause primary infection in the following vegetation period. The primary infection can also be a result of ascospore release from asci formed in sexual fruiting bodies called cleistothecia (syn. chasmothecia). Ascospores of *Bgh* germinate by producing a single germtube that directly penetrates host epidermal cells via appressoria formation. Water soaking of cleistothecia is a prerequisite for ascospore differentiation in asci within days that otherwise, under dry conditions, contain undefined protoplasm. Dry cleistothecia remain their ability to form ascospores over years when kept dry at cool temperatures.

However, upcoming data question the role of cleistothecia as source of primary infection in the following vegetation period and place them rather as a structure for survival of unfavorable conditions during summer [Jankovics et al. 2015].

Conidida germiniation of *Blumeria graminis* is inhibited by the presence of free water on the leaf surface, which can actually lead to bursting of conidia, but conidia germination is promoted by a high relative humidity above 90 percent at temperate temperatures in the range of 10-22 °C. In contrast to ascospores, conidia of *Blumeria* first develop a short Primary Germ Tube (PGT) within 2 hours after inoculation (hai). PGTs adhere conidia to the plant surface but do not form an appressorium. They pierce the plant cuticle for water and solute uptake from the host [Bélanger 2002]. PGTs actively sense the hydrophobic environment of the cuticle by secretion of lytic enzymes. Especially very long-chained aldehydes of plant cuticular waxes have been shown to act as developmental cues for conidia germination and differentiation [Hansjakob et al. 2012]. In angiosperms, the cuticle on the adaxial leaf surface is thicker than on the abaxial leaf surface which might explain why powdery mildew symptoms are preferably seen at the upper leaf side.

A longer secondary germ tube, which is also referred to as Appressorial Germ Tube (AGT) emerges, which forms a hook-shaped appressorium. From there a cone-shaped penetration peg is getting pushed through the cell wall, which is softened lytically by CWDEs, at 12-15 hai [Bélanger 2002]. In case of succesfull circumvention of non-specific basal defense fungal haustoria get established in host epidermal cells that stay separated from the host cytoplasm by a modified host membrane (the extrahaustorial membrane) which is separated from the fungal PM by the extrahaustorial matrix and the fungal cell wall. Haustoria of *Blumeria graminis* are of oval shape with characteristic finger-like protrusions at their distal ends and are fully expanded at 48 hai. Besides their importance for nutrient uptake, like sugars and amino acids [Voegele et al. 2001], haustoria also play a pivotal role in effector delivery [Petre et al. 2014]. Growth of Elongated Secondary Hyphae (ESH) initially branching off from the AGT on successfully invaded barley epidermal cells is observed at 24-36 hai. Further haustoria get established in epidermal cells passed by growing ESH eventually building up the epiphytic mycelium creating the symptomatic mildew pustules which can be seen by eye

around 5 days after infection (dai). At the same time multiple conidiophores erect from the mycelium, septate and differentiate into chains of oval-shaped single cell conidia emerging from a conidial mother cell. Conidiophores are fully developed 6 dai and start releasing the topmost conidium [Moriura et al. 2006] leading to the dispersal of conidia in large quantities over kilometers mainly by air current. Finally, brownish to black round cleistothecia form as sexual fruiting bodies in matured pustules.

First symptoms are observed at lower leaves in the field which is due to the favorable microclimate for conidiogenesis there. Later, powdery mildew pustules may spread to upper leaves, stems and ears, given appropriate weather conditions.

Heavy powdery mildew infection can cause economic important yield loss [Oerke 2006] due to redirection of metabolic flux to the infected area which is transformed into a sink tissue [Walter and McRoberts 2006].

1.4 Effectors of *Bgh*

Initially 248 Candidate Secreted Effector Proteins (CSEPs) were predicted from the *Bgh* genome of the isolate DH14. Criteria were a positive prediction for a signal peptide for secretion, a negative prediction for Trans-Membrane (TM) localization and being small proteins specific to *Bgh* [Spanu et al. 2010]. The number was later extended to 491 CSEPs which group into 72 families [Pedersen et al. 2012]. Many CSEPs cluster family-wise on genomic sequence scaffolds suggesting abundant sequence duplications. Remarkably, not all CSEPs being located closest to each other originated from the same CSEP family. The level of nucleotide sequence identity upstream and downstream of a pairwise-compared set of CSEP loci was found to be very high (in most cases 90-100%). This high sequence similarity is extended up to ~1kb in both directions until it noticeably drops in front of the *Bgh* Short Interspersed Element (SINE)-like retroelemtens Eg-R1, Egh24 or a repetitive DNA sequence (AJ002007.1). In a different set of CSEP loci comparisons SINEs and repetitive elements were also found to be included as the distal ends of the high sequence similarity regions [Pedersen et al. 2012]. Hence, the *Bgh* SINE-like retroelements Eg-R1 and Egh24 are found in the very proximity of CSEPs in genomic regions showing patterns of frequent sequence duplications. Repetitive elements were also made responsible for the inability to create a

complete genome assembly of the independently sequenced *Bgh* isolates A6 and K1. Roughly half of the genome sizes could get assembled. Apart from that, the mapped contigs of *Bgh* isolates A6, DH14 and K1 were found to be nearly identical. This also holds true for their sets of CSEP orthologues. The CSEP genes of the geographically separated isolates A6 and K1 showed above average nonsynonymous substitution (dN) rates suggesting a need for adaptation to hosts that likely differ in their defense repertoire [Hacquard et al. 2013].

Expression profiles of CSEPs were generated by RNA sequencing (RNAseq) of the *Bgh*-infected Arabidopsis *pen2 pad4 sag101* triple mutant [Lipka et al. 2005; Maekawa et al. 2012] that is susceptible to *Bgh*. The first induction of a group of CSEPs is at the stage of plant epidermal penetration (12 hai), a second induction of a distinct set of CSEPs follows at the stage of haustorial differentiation (18-24 hai). The CSEPs of the latter group showed higher dN rates than other CSEP families and are enlarged in *Bgh* in comparison to the wheat powdery mildew *Bgt*. [Hacquard et al. 2013].

The existence of in total 97 CSEPs at the protein level was shown by a proteogenomics approach. Thereof 62 CSEPs were unique to a protein preparation from haustoria-containing barley epidermal cells [Bindschedler et al. 2009; Bindschedler et al. 2011; Pedersen et al. 2012]. Tertiary structure predictions revealed a ribonuclease-like fold of some CSEPs [Pedersen et al. 2012] whereas to others no structural domains could get assigned, thus they might represent novel folds [Bindschedler et al. 2011]. Roughly two-thirds of all CSEPs carry a conserved YxC motif near their predicted signal peptide cleavage site [Godfrey et al. 2010; Pedersen et al. 2012], albeit no further characterization of the motif is available to date.

Some of the predicted CSEPs have been characterized further yet. The contribution of a set of 50 CSEPs, which are alternatively referred to as *Blumeria* Effector Candidates (BEC), to virulence of *Bgh* was investigated by Host-Induced Gene Silencing (HIGS) of single candidates [Pliego et al. 2013]. HIGS takes advantage of the phenomenon that expression of anti-sense or double-strand RNA in the host can silence pathogen transcripts by an yet unknown mechanism of RNA exchange [Nowara et al. 2010]. Eight of them significantly reduced the number of successfully established haustoria of *Bgh* in

barley. The strongest effect was shown for BEC1011 and the highly sequence-similar BEC1054. The effect could be complemented by the co-expression of an RNAi rescue construct. Tertiary structure modelling indicated a ribonuclease-like fold of BEC1054. Transient over-expression of BEC1011 led to more viable barley epidermal cells in a cell death assay suggesting BEC1011 to act as cell-death repressor albeit the underlying host process is unclear yet [Pliego et al. 2013]. BEC2 and BEC4 were identified from *Bgh* Expressed Sequence Tags (ESTs). Both show a predicted eight-cysteine-containing domain present in fungal extracellular membrane proteins (CFEM domain). They do not show signs of diversifying selection and are present as single copy in the genome of *Bgh*. BEC2 and BEC4 orthologous sequences were found in the genomes of *Bgt* and the more distal related powdery mildews *Erysiphe pisi* (*E. pisi*) of pea and *G. orontii* of Arabidopsis. Arabidopsis lines expressing the BEC2 orthologue GoEC2 of *G.orontii* were more susceptible to the non-adapted *E. pisi*. A Yeast Two-Hybrid Screen (Y2H) identified an ubiquitin-conjugating enzyme (E2 protein) and an ARF-GAP as putative host targets of BEC4. The *in planta* interaction with the ubiquitin-conjugating enzyme was shown by Bimolecular Fluorescence Complementation (BiFC) [Schmidt et al. 2014]. A more comprehensively studied single *Bgh* CSEP–host target interaction was reported on CSEP0055 and the barley PR-protein PR17c [Zhang et al. 2012a]. A contribution of CSEP0055 to *Bgh* virulence was suggested by HIGS in barley epidermal cells. The putative host target protein PR17c was identified in an Y2H screen. Transient over-expression of Pr17c increased resistance of barley against *Bgh* whereas RNA interference (RNAi)-mediated gene silencing of *PR17c* increased susceptibility. *In planta* interaction of CSEP0055 and PR17c was indicated to be principally possible by BiFC in tobacco cells. A PR17c-mCherry fusion protein located to the apoplast of barley epidermal cells where it accumulated beneath sites of attempted *Bgh* entry, likely representing papillae. The CSEP0055 transcript gets induced with the establishment of the first haustorium and continuously increases over at least 6 days. Expression profiles of CSEP0055 and PR17c indicate a role of CSEP0055 in secondary haustoria establishment [Godfrey et al. 2010; Zhang et al. 2012a].

Another class of *Bgh* effectors is referred to as EKAs (Effectors paralogous to *Bgh* AVR_{k1} and AVR_{a10}). The huge EKA gene family comprises at least 1350 paralogues in

the *Bgh* genome [Spanu et al. 2010] which might be due to a co-evolution with a TE1a retrotransposon (LINE-1 retrotransposon, Cgt-like) and subsequent gene duplications. The TE1a retrotransposon was found in close proximity to EKAs but commonly to be located within the same predicted Open Reading Frame (ORF) in genomic sequences. Moreover, EKAs and TE1a retrotransposons were also reported to be localized together on single cDNA transcripts [Ridout et al. 2006; Sacristán et al. 2009] and it was suggested that they might translocate together. The *Bgh* SINE-like retroelements Eg-R1 and Egh24, a repetitive DNA sequence (AJ002007.1) and further retrotransposable elements were found in proximity to EKAs but not to be associated with EKAs. [Skamnioti et al. 2008; Sacristán et al. 2009]. EKA loci have been identified genetically by their avirulence function in barley, but are also present in other powdery mildew fungi mainly of *Poaceae* [Sacristán et al. 2009]. In barley, more than 85 Resistance genes (R-genes) are described that confer resistance to *Bgh* isolates [Jørgensen and Wolfe 1994]. Among them are about 30 alleles of the Mildew resistance locus a (Mla) that mediate resistance to *Bgh* isolates with corresponding AVRs. Mla proteins belong to the class of intracellular CC-NB-LRR immune receptors [Seeholzer et al. 2010]. AVR_{k1} and AVR_{a10}, which are recognized by barley MLK1 and MLA10, respectively, have been isolated by a map based cloning approach. Both specifically induced cell death upon transient expression in barley cultivars carrying MLK1 or Mla10, respectively. AVR_{a10} was found to be required for the nuclear association of Mla10 with WRKY1 and WRKY2 transcription factors thereby de-repressing basal defense genes [Shen et al. 2007]. *Bgh* strains not carrying AVR_{k1} or AVR_{a10} were significantly impaired in their virulence on barley cultivars lacking MLK1 or MLA10, respectively. Whereas transient over-expression of AVR_{k1} or AVR_{a10} induced super-susceptibility [Ridout et al. 2006] and HIGS of AVR_{a10} reduced fungal virulence on susceptible barley [Nowara et al. 2010]. EKAs lack N-terminal signal peptides for secretion via the conventional secretory pathway but, given their intracellular functionality, are thought to be secreted into the host cell by an alternative route [Ridout et al. 2006].

1.5 Host Susceptibility Genes

Resistance breeding against fungal plant pathogens is mainly based on the introduction of dominantly inherited R-genes and on quantitative trait loci. However, an alternative

strategy is to make use of the loss of Susceptibility genes (S-genes). S-genes are all host genes that contribute to the accommodation and the maintenance of the pathogen in the host plant. Loss of susceptibility is mostly inherited recessively and has the potential for durable race nonspecific resistance as long as possible negative pleiotropic effects are tolerable for plant development [Pavan et al. 2010; van Schie and Takken 2014].

Besides barley MLO and RACB, which are described below, some further examples of barley susceptibility factors are: The cell death suppressor protein BAX-Inhibitor-1 (BI-1), which over-expression can break *mlo*-broadspectrum resistance [Hückelhoven et al. 2003; Eichmann et al. 2010] and the BI-1-like Lifeguard (LFG) proteins [Weis et al. 2013], the WRKY1/2 transcription factors that repress defense gene transcription [Shen et al. 2007] and Alcohol Dehydrogenase 1 (ADH1) which supports carbohydrate metabolism under stress conditions [Pathuri et al. 2011].

1.5.1 The *mlo*-Mediated Resistance – The Classic Loss of an S-gene

Mildew Locus O (MLO) proteins are plant specific and functionally conserved in many plant species [Acevedo-Garcia et al. 2014]. Structurally they are made up of seven transmembrane domains residing in the plasma membrane, resembling animal G-protein-coupled receptors [Devoto et al. 1999]. Genetic evidence suggests a role of the barley MLO protein as repressor of the syntaxin ROR2 [Freialdenhoven et al. 1996; Collins et al. 2003]. Both, barley MLO and ROR2, were found to accumulate beneath *Bgh* appressorial germ tubes in plasma membrane microdomains. Whereby the redistribution of MLO into the microdomain was pathogen-dependent leading to a hypothesized *Bgh* effector triggered cooption of MLO [Bhat et al. 2005]. The AtMLO2 orthologue was recently identified to be targeted by the *P. syringae* effector HopZ2 [Lewis et al. 2012]. The nature of MLO proteins remains somewhat elusive but mutant alleles can confer to long-lasting, broad-spectrum resistance against powdery mildews. In barley cultivation, it has been made use of recessively inherited *mlo* mutant alleles since the 1980s and the obtained non-race specific resistance in the field has not been broken by the fungus since [Jørgensen 1992; Reinstadler et al. 2010]. Mechanistically, barley *mlo* mutant genotypes are thought to be derepressed in the focal secretion pathway involved in cell wall apposition (CWA; also papillae) formation and/or delivery of

defense compounds at sites of attempted pathogen entry. Biochemical and cell biological evidence point to the formation of a ternary SNARE complex involving the barley syntaxin ROR2, the SNAP-25-like protein HvSNAP34 and the R-SNARE HvVAMP721 [Collins et al. 2003; Kwon et al. 2008; Meyer et al. 2009; Kwaaitaal et al. 2010]. The use of *mlo* mutants has to be regarded as a tradeoff between benefiting from reduced powdery mildew infection and some negative pleiotropic effects. Axenic grown barley plants carrying homozygous *mlo* alleles show spontaneous formation of CWAs. [Wolter et al. 1993]. Further, leaf mesophyll cells of these genotypes undergo spontaneous cell death due to accelerated leaf senescence [Piffanelli et al. 2002]. The hemi-biotrophic rice blast fungus *Magnaporthe oryzae* and the necrotrophic fungus *Bipolaris sorokiniana*, causal agent of leaf spot blotch disease, were shown to profit from non-functional *MLO* alleles at least under laboratory conditions [Jarosch et al. 1999; Kumar et al. 2001].

1.6 Plant ROP Small GTPases

1.6.1 The Rho of Plants (ROPs)

The mammalian Ras superfamily is subdivided into 5 subfamilies: Ras, Rho, Rab, Ran and Arf. The Rho subfamily is further subdivided into Rac, Cdc42, RhoA and other Rho-GTPases and includes in total 22 members. It is conserved in all eukaryotes. Small monomeric GTPases function as molecular switch in multiple signaling pathways. One activated Rho-GTPase has something around 20-30 downstream protein interaction partners [Hall 2012]. Therefore the activity of one particular Rho-GTPase is very likely not restricted to one signaling pathway. Eukaryotic Rho-GTPases have a prominent role in regulation of the actin cytoskeleton upon perception of extracellular stimuli by the cell. Their regulation through Rho-GEFs (see below) is thought to determine spatiotemporal Rho-GTPase activity. In cell biology Rho-GTPase signaling is involved in cell migration, endocytosis, phagocytosis, morphogenesis and cytokinesis. Point-mutated, constitutively activavted (CA) Ras subfamily GTPases are oncogenes. For Rho-GTPase subfamily members several Rho-GEFs and Rho-GAPs are studied as oncogenes and tumor suppressors, respectively [Hall 2012].

Rho-GTPases of plants are not further subdivided. ROPs (Rho-GTPases of plants) resemble most Rac-type Rho-GTPases and are alternatively referred to as RACs. Plant ROP signaling is involved in polarized cell growth (root hair growth, pollen tube growth), cell morphology establishment (pavement cells and xylem vessel formation), abiotic hypoxia response, pathogen response as well as in regulation of phytohormonal pathways (ABA and auxin). ROP signaling has been shown to influence the actin cytoskeleton organization, the microtubule cytoskeleton organization, polar exocytosis and polar endocytosis. In sum ROPs are key components of cell polarity establishment. The spatiotemporal regulation of ROP activity through GEFs, GAPs and GDIs (see below) is thought to be important as ROPs cannot be excluded to act redundantly [Berken 2006; Craddock et al. 2012].

Plant ROPs are conserved in the G-domain (G1-G5) but feature some aberrations in their protein domains that make them distinct from non-plant Rho GTPases. These are e.g. a putative serine/threonine kinase phosphorylation site downstream of switch II and a shortened Rho insert region that might be responsible for plant-specific ROP effector interaction. Plant ROPs group into two types which are distinguished by whether the hypervariable region at their C-terminus gets prenylated (type I) and/or they get palmitoylated. (type II) [Berken 2006]. Lipid modification is required for attachment to membranes, where ROPs reside in their active GTP-bound form. The G-domain of Guanine Nucleotide-Binding Proteins (GNBPs) is highly conserved. Switch I and switch II (G2 and G3 in ROPs) are clamped together by binding to the γ-phosphate of GTP leading to a conformational change that enables the binding of downstream effector proteins. Effector proteins possessing a CRIB (Cdc42/Rac interactive binding) domain directly bind to the switch region where they are in direct competition with the GNBP regulators GTPase Activating Proteins (GAPs), Guanine Nucleotide Exchange Factors (GEFs) and Guanine Nucleotide Dissociation Inhibitors (GDIs) [Vetter and Wittinghofer 2001]. GEFs activate GNBPs by catalyzing the exchange from GDP to GTP. ROP-GEFs contain a unique Plant-specific ROP Nucleotide Exchanger (PRONE) domain that specifically regulates ROPs but is unable to regulate animal Rho family members [Berken et al. 2005]. In plants, among others, members of the CrRLK family of membrane spanning RLKs have been identified to act upstream of some ROP-GEFs

involved in polar cell growth of pollen tubes and root hairs. One of them, FERONIA (FER) of Arabidopsis, is involved in tissue specific perception of diverse stimuli and was found to directly interact with AtROP-GEF1 in an AtROP2 and auxin dependent pathway regulating NADPH oxidase mediated ROS generation required in polar root hair growth [Duan et al. 2010]. Originally FER was described to induce the burst of incoming pollen tubes at female gametophytes [Escobar-Restrepo et al. 2007]. However, *Atfer* mutants were also found to have enhanced resistance towards powdery mildew in a manner phenotypically reminiscent of the *Atmlo2* mutant [Kessler et al. 2010].

GNBPs possess an intrinsic GTPase activity but its catalytic rates are slow. GAP proteins accelerate the hydrolysis of GTP to GDP. GAPs of the animal small G-proteins Ras, Rho and Rab families bind to the switch region of the G-domain and possess a conserved arginine-finger in their GAP domain which is essential for their catalytic activity [Scheffzek and Ahmadian 2005; Bos et al. 2007]. The largest and best studied group of ROP-GAPs, CRIB-type like ROP-GAPs, is most homologous to Rho-GAPs of the animal system. The architecture of their GAP-domains as well as their functionality is conserved as they were found to be able of regulating human RAC1 protein [Klahre and Kost 2006; Wu et al. 2000]. However, their CRIB domain in front of the GAP domain, which is absent in GAPs of all other kingdoms, makes them unique to plants [Schaefer et al. 2011a; Schaefer et al. 2011b].

The main purpose of GDIs is the extraction of GDP-bound Rho-GTPases from the PM. Therefore GDI bind to the switch region of the G-domain followed by an encasement of the lipid-modified C-terminus by their hydrophobic pocket. The heterodimer subsequently moves to the cytoplasm [Dovas and Couchman 2005]. Plant ROP-GDIs are structurally related to Rho-GDIs. They are thought to be involved in spatial distribution of ROP activity in growing root hairs and pollen tubes [Carol et al. 2005; Kost 2008].

1.6.2 ROP Signaling

ROP signaling plays a central role in cellular processes affecting many aspects of plant cell fate which can also be interconnected. This includes polarized cell growth, cell morphology, cell development, pathogen and abiotic stress response. ROP activity was

found to act on the cytoskeleton, vesicular trafficking, ROS production, local Ca^{2+} levels, gene expression and protein turnover [Berken 2006; Nibau et al. 2006]. ROP signaling has a somewhat non-linear character in the overall view. Some ROPs act in the same pathways and are therefore functional redundant, whereas one specific ROP can influence several pathways or just one. This is further complicated by tissue-dependent alterations of the pathway setup downstream of one and the same ROP. Antagonistically regulation of each other ROPs and antagonistic regulation of each other downstream effectors of a single ROP may be the underlying principle of a self-organized ROP signaling network [Craddock et al. 2012].

AtROP2 and AtROP4 act functionally redundant on the actin cytoskeleton in the development of jigsaw-shaped epidermal cells [Fu et al. 2005]. In their active form AtROP2/4 directly bind to Arabidopsis ROP Interactive CRIB motif protein (RIC) 4 (AtRIC4) which in turn mediates the formation of a fine filamentous (F)-actin mesh that is seen together with lobe outgrowth. AtROP2/4 activity also inhibits AtRIC1 mediated reorientation of cortical microtubules (MTs) by direct protein-protein interaction and detaching AtRIC1 from MT. AtRIC1 is in turn a downstream target of AtROP6 signaling which promotes AtRIC1-MT association. AtRIC1 unties MT at branch points which subsequently orient in a parallel and bundled manner at indentation of pavement cells. AtRIC1 or parallel oriented MT negatively interfere with the AtROP2/4-AtRIC4 pathway. AtROP2/4 and AtROP6 pathways are thought to influence each other antagonistically at the border of adjacent growing cells which subsequently forms the characteristic jigsaw shape of Arabidopsis epidermal cells (reviewed in Craddock et al. [2012]). AtROP2 is also involved in the generation of ROS at the tip of growing root hairs. The activity of AtRBOH C NADPH oxidase is regulated by AtROP2 [Jones et al. 2007]. Oscillatory root hair growth correlates with oscillatory ROS production at the root hair tip which is AtRBOH C-dependent [Foreman et al. 2003; Monshausen et al. 2007].

Auxin-induced changes in MT orientation within minutes has recently been shown to depend on AtROP6, AtRIC1 and the microtubule severing protein Katanin 1 (KTN1) that unties branched MTs. In the growing regions of primary roots, the transition zone, and of etiolated hypocotyls, the elongation zone, MT are predominantly arranged in transverse orientation. Transversely oriented MTs promote cell elongation whereas longitudinal

oriented MTs inhibit cell elongation. Within minutes after exogenous application of auxin MTs reoriented from transverse orientation to longitudinal orientation. Single mutants of the whole chain, *Atrop6*-1, *Atric1-1*, *Atktn1*, each was less auxin responsive seen as no significant MT reorientation after exogenous auxin application [Chen et al. 2014]. AtROP6 was reported to be Auxin-inducible and to influence SA-dependent defense as wells as SA-independent defense responses presumably by sensing of cytoskeleton rearrangements of the plant cell [Poraty-Gavra et al. 2013].

The transcription of SA-related defense genes was upregulated in Dominant Negative (DN) *AtROP6* lines which showed constitutively elevated levels SA. The SA levels of *DN AtROP6* plants doubled those of the controls after inoculation with the adapted powdery mildew fungus *G. orontii*. Further, *DN AtROP6* lines were more resistant towards *G. orontii* which was also impaired in its reproductive fitness seen as a reduction of conidiophores. SA defense-*DN AtROP6* double mutant lines did not rescue the low number of conidiophores indicating that it mainly dependent on the DN mutation of *AtROP6* and not on the increased SA level. Interestingly, *DN AtROP6* as well as Constitutively Activated (CA) *AtROP6* lines, both were more susceptible towards the non-adapted barley powdery mildew *Bgh* [Poraty-Gavra et al. 2013].

Auxin and SA signaling are not the only phytohormonal pathways influenced by ROP activity. Activated AtROP6 was found to negatively interfere with abscisic acid (ABA)-mediated breakdown of F-actin in guard cells required for stomatal closure [Lemichez et al. 2001]. Further, AtROP10 and AtROP11 were also described as negative regulators of ABA signaling [Miyawaki and Yang 2014].

A further ROP acting on MT organization is AtROP11. Its activity has in contrast to AtROP6 an destabilizing effect on cortical MTs. Activated AtROP11 resides in the future site of secondary cell wall pits in differentiating xylem vessel cells. There it interacts with Microtubule Depletion Domain 1 (AtMIDD1, alternatively called AtRIP3) an MT-associated ROP effector of the RIP/ICR (ROP Interactive Partner/Interactor of Constitutive Active ROPs) family. Out of four AtROPs expressed in metaxylem cells only AtROP11 co-localized with AtMIDD1. The N-terminal part of AtMIDD1 binds MT whereas the C-terminal part anchors the AtMIDD1-AtROP11 dimer to the PM. AtMIDD1

cannot deplete MTs on its own but recruits MT depolarizing AtKinesin-13A (AtKin13A) [Oda and Fukuda 2013a; Mucha et al. 2010]. Kinesin 13 proteins are a unique class of kinesin motor proteins that specifically recognize MT plus ends and use their motor domain for bending MT ends instead of walking along MT [Moores and Milligan 2006]. Tight spatial regulation of AtROP11 activity is crucial for focal formation of a MT-depleted zone of future cell wall pits. Over-expression of CA AtROP11 abolished pit formation but led to a uniformly distributed and flattened secondary cell wall. AtROP11 activity was found to be regulated by AtROP-GAP3 and AtROP-GEF4 [Oda and Fukuda 2012]. Cortical MTs accumulate at sites of secondary cell wall thickening. Vesicles emerging from the trans-Golgi network travel to sites of high MT density. Cellulose synthase complexes use cortical MTs as tracks. The target membrane component AtEXO70A1 of the exocyst complex was shown to be required for proper formation of secondary cell wall thickening [Oda and Fukuda 2014; Li et al. 2010; Li et al. 2013].

Arabidopsis Interactor of constitutive active ROPs 1 (AtICR1), another AtRIP/ICR activated ROP downstream effector interacts with the exocyst-vesicle tethering complex subunit AtSEC3 [Lavy et al. 2007]. AtICR1 was identified as downstream effector of a bunch of type I and type II AtROPs including AtROP3, AtROP6, AtROP7, AtROP8, AtROP9, AtROP10 and AtROP11. It does interact with WT AtROPs and CA AtROPs but not with DN AtROPs. In its protein structure it is made up of two coiled-coil (CC) domains but no further protein domains are identifiable yet. AtICR1 is involved in auxin transport and Aticr1 knock-out lines show developmental defects of leaves and roots [Hazak et al. 2010; Hazak et al. 2014].

AtROP1, which is closely related to AtROP3 and AtROP5, is the key regulator of oscillatory pollen tube growth. Oscillatory activated AtROP1 is localized at the very tip of the pollen tube where it subsequently activates AtRIC3 and simultaneously AtRIC4. The latter promotes the assembly of F-actin mesh where arriving exocytic vesicles accumulate. The former mediates a tip focused Ca^{2+} accumulation likely by regulating Ca^{2+} influx channels which in turn depletes the F-actin meshwork. The subsequent release of vesicles is thought to be necessary for their membrane fusion. AtRIC4-mediated F-actin accumulation inhibits exocytosis whereas AtRIC3-mediated F-actin disassembly inhibits vesicle accumulation. F-actin/vesicle accumulation was found to

temporally precede Ca^{2+} influx, F-actin depletion, exocytosis and finally growth [Gu et al. 2005; Lee et al. 2008; Yan et al. 2009].

A summary of the described Arabidpsis ROP signaling pathways is given in Table 2.

Table 2: Described AtROPs, their interactors and functions

ROP	Pathway components	Biological Process/Mechanism	Reference
AtROP1	AtRIC3; AtRIC4	Promotes Ca^{2+} accumulation at pollen tube tips; Formation of F-actin mesh at pollen tube tip	Gu et al. (2005), Lee et al. (2008), Yan et al. (2009)
AtROP2	AtRIC4; AtRIC1	Formation of F-actin mesh at lobes of pavement cells; Inhibition of MT bundling of pavement cells;	Reviewed in Craddock et al. (2012)
		ROS generation at tip of root hairs	Jones (2007)
AtROP3	AtICR1	Exocyst complex mediated secretion in leaf epidermis	Lavy et al. (2007)
		Auxin distribution in root	Hazak et al. (2010, 2014)
AtROP4	AtRIC4; AtRIC1	Formation of F-actin mesh at lobes of pavement cells; Inhibition of MT bundling of pavement cells;	Reviewed in Craddock et al. (2012)
AtROP6	AtRIC1; AtKTN1	MT bundling at indentations of pavement cells	Reviewed in Craddock et al. (2012)
		Auxin mediated reorientation of MTs in roots and leaf epidermis	Chen et al. (2014); Poraty-Gavra et al. (2013)
		Negative regulator of SA-dependent defence	Poraty-Gavra et al. (2013)
		Negative regulator of ABA signalling in stomata closure	Lemichez et al. (2001)
	AtICR1	Exocyst complex mediated secretion in leaf epidermis	Lavy et al. (2007)
		Auxin distribution in root	Hazak et al. (2010, 2014)
AtROP7	AtICR1	Exocyst complex mediated secretion in leaf epidermis	Lavy et al. (2007)
		Auxin distribution in root	Hazak et al. (2010, 2014)
AtROP8	AtICR1	Exocyst complex mediated secretion in leaf epidermis	Lavy et al. (2007)
AtROP9	AtICR1	Exocyst complex mediated secretion in leaf epidermis	Lavy et al. (2007)
		Auxin distribution in root	Hazak et al. (2010, 2014)
AtROP10		Negative regulator of ABA signalling	Reviewed in Miyawaki and Yang (2024)
		Auxin distribution in root	Hazak et al. (2010, 2014)
AtROP11	AtMIDD1; AtKin13a	Depletion of MTs in future xylem vessel pits	Reviewed in Oda and Fukuda (2014)
		Negative regulator of ABA signalling	Reviewed in Miyawaki and Yang (2024)
	AtICR1	Exocyst complex mediated secretion in leaf epidermis	Lavy et al. (2007)
		Auxin distribution in root	Hazak et al. (2010, 2014)

1.6.3 OsRAC1 – A Central Player in the Defense Response of Rice

The type II ROP of rice OsRAC1 is a positive regulator of defense against fungal and bacterial pathogens. Transgenic rice expressing *CA OsRAC1* is more resistant towards the hemibiotrophic fungus *Magnaporthe oryzae* (*M. oryzae*) [Kawano et al. 2014] that causes the devastating rice blast disease on foliar tissue [Kankanala et al. 2007]. OsRAC1 plays a central role in PTI. Chitin oligosaccharide fragments are recognized as PAMPs by the LysM domains of the RLP OsCEBIP1 which then forms a receptor complex with the RLK OsCERK1, that also transduces perception of the bacterium *Xanthomonas oryzae* pv. *oryzae*. OsCERK1 subsequently interacts with OsRAC-GEF1 that activates OsRAC1. OsRAC-GEF1 additionally interacts with the flagellin receptor OsFLS2 [Akamatsu et al. 2013]. Activated OsRAC1 is proposed to initiate a multisubunit protein complex, called ‘defensome’. The scaffolding protein OsRACK1 links OsRAC1 to co-chaperons for OsCERK1 receptor maturation but also links OsRAC1 to RBOHb NADPH oxidase for ROS generation. The activity of the NADPH oxidase likely co-depends on Ca^{2+} influx. Simultaneously, OsRAC1 activity transcriptionally represses the ROS scavenger protein Metallothionein2b (MT2b). Active OsRAC1 likely triggers a MAPK cascade that eventually phosphorylates the transcription factor Rac Immunity 1 (OsRAI1). OsRAI1 likely acts upstream of transcription factor OsWRKY19 and of Phenylalanine Ammonia Lyase 1 (OsPAL1), a key enzyme of the phenylpropanoid pathway [Kawano et al. 2014]. Defense-related outputs are phytoalexins (Flavanones, Isoflavones, Isoflavanones), monolignol precursors and the defense-related phytohormone SA. Active OsRAC1 further activates Cinnamoyl-CoA Reductase (CCR) that is involved in synthesis of monolignols which are then ROS-dependent cross-linked in the cell wall [Kawasaki et al. 2006]. Further, PR-proteins expression gets induced, *inter alia* of the RNAse OsPBZ1 (Probenazole-induced Protein 1) which is a cell death executor. Besides acting in in PTI, OsRAC1 was shown to be inducible by the ETI receptor couple RGA4 and RGA5 and by the R-protein OsPit that both induce HR as well as by a heterotrimeric G-protein Gα subunit after sphingolipid treatment [Kawano et al. 2014]. RGA5 interacts with the *M. oryzae* avr-effector AvrPia or alternatively with AvrCO39, which frees RGA4 from the heterodimer with RGA5. RGA4 then triggers HR [Cesari et al. 2013; Cesari et al. 2014].

1.6.4 RACB of Barley – A Susceptibility Factor

The barley type I ROP RACB is a susceptibility factor in the interaction with *Bgh*. Transient Induced Gene Silencing (TIGS) of *RACB* reduced the virulence of *Bgh* in a susceptible barley background. Conversely, transient over-expression of a CA RACB mutant protein induced super-susceptibility, whereas over-expression of the wild-type allele of RACB had no influence on susceptibility. Neither did over-expression of DN RACB. Hence, GTP-bound RACB is beneficial for *Bgh* [Schultheiss et al. 2002; Schultheiss et al. 2003]. The requirement of RACB for full susceptibility of barley epidermal cells towards *Bgh* was seen in barley transgenic knockdown lines expressing a RNAi construct directed against *RACB*. The density of fungal colonies was significantly reduced as was the number of successfully established haustoria. In addition, established haustoria were significantly smaller in size showing that RACB is not only beneficial for fungal penetration but also for haustorial expansion [Hoefle et al. 2011]. The susceptibility inducing effect of CA RACB was further confirmed in transgenic barley lines expressing CA RACB from the *Zea mays* ubiquitin promoter. Besides a higher susceptibility towards *Bgh*, infection of these lines with the hemibiotrophic fungi *Bipolaris sorokiniana* or *Fusarium graminearum*, that later switch to a necrotrophic lifestyle, had no effect on their virulence and *Bgh* challenged leaves showed no elevation in HR frequency. This underlines the difference of RACB mediating susceptibility to OsRAC1 (see above) acting in PTI and ETI [Schultheiss et al. 2005; Pathuri et al. 2008]. Heterologous CA RACB expression in transgenic tobacco induced super-susceptibility towards the tobacco powdery mildew fungus *Golovinomyces cichoracearum*, whereas growth of the bacterial pathogen *Pseudomonas syringae* pv. *tabacci* remained unaffected [Pathuri et al. 2009b]. Together, this suggests that RACB activity is especially required for susceptibility of barley towards powdery mildew.

Besides RACB, there are 5 additional ROPs in barley, 4 of them are expressed in the leaf epidermis. At least two of them, when activated, (CA RAC1, CA RAC3) also promote susceptibility of barley epidermal cells towards *Bgh* [Schultheiss et al. 2003; Pathuri et al. 2008].

Some proteins possibly acting downstream of activated RACB have been identified. RIC171 is a CRIB-domain protein sharing sequence similarities with other RICs.

Transient over-expression of RIC171 pheno-copied CA RACB in enhancing susceptibility towards *Bgh*. No additive effect was observed by transient co-expression together with CA RACB. RIC171 interacted with CA RACB, RACB WT and CA RAC3 but not with DN RACB, CA RACD and CA RAC1 in yeast. DsRED-tagged RIC171 was found to be preferentially PM-localized *in planta* where it also interacted with CA RACB and RACB WT in a BiFC assay. Upon inoculation with *Bgh* DsRED-RIC171 accumulates beneath the site of attack which can be weakened by co-expression of DN RACB which suggests a high ROP activity there [Schultheiss et al. 2008; Hückelhoven and Panstruga 2011].

ROP Binding Kinase 1 (RBK1) is a class VIA receptor like cytoplasmic kinase (RLCK)-like protein. It shares sequence similarities with the AtRLCK VIA family. RBK1 interacted with CA RACB as well as with CA RAC1 in yeast but not with their respective DN mutant proteins. The protein interaction with CA RACB was confirmed *in planta* by Fluorescence Resonance Energy Transfer (FRET) analysis. The kinase activity of RBK1 was stimulated by CA RACB or CA RAC1 in an *in vitro* kinase assay [Huesmann et al. 2012]. RBK1 was found to interact with a barley type II S-phase Kinase 1-associated (SKP1)-like subunit of the SKP1 cullin 1-F box (SCF)-E3 ubiquitin ligase complex. TIGS of *RBK1* or *SKP1-like* increased the protein abundancy of fluorophore-tagged RACB which suggested RBK1 to act via SKP1-like in proteasomal degradation of RACB. TIGS of *RBK1* or *SKP1-like* also increased susceptibility of barley epidermal cell towards *Bgh* [Huesmann et al. 2012; Reiner et al. 2015]. Together this places RBK1 as a negative regulator of RACB activity. Interestingly, TIGS of *RBK1* was found to destabilize the MT cytoskeleton [Huesmann et al. 2012] which may point to RACB acting as a negative regulator of MT network integrity.

A putative regulator of RACB that also acts on MTs and antagonizes RACB in susceptibility is barley Microtubule-Associated ROP-GTPase Activating Protein 1 (MAGAP1). It has a conserved CRIB domain for ROP binding followed by a GAP domain. MAGAP1 is a MT associated protein, which is a peculiarity in so far as ROP-GAPs usually appear to be located in the cytoplasm. Drug-induced depolymerization of MTs freed GFP-MAGAP1 from the cytoskeleton. However, no MT binding signature has been identified but a C-terminal fragment (MAGAP1-Cter) is sufficient for MT-binding. A

MAGAP1 mutant lacking its C-terminus, MAGAP1ΔCter, lost the MT association. MAGAP1 was found to interact with CA RACB or CA RAC1 but not DN RACB or DN RAC1 in yeast which was confirmed by FRET *in planta*. Co-expression of CA RACB, RFP-MAGAP1 as well as FRET showed recruitment of MAGAP1 from MTs to the cell periphery by activated RACB. The RFP-labelled C-terminus (MAGAP1-Cter), lacking all further protein domains, did label cortical MT but was not recruited by CA RACB. Together with showing no effect on susceptibility upon *Bgh* treatment, MAGAP1-Cter is predestined as MT marker protein. TIGS of *MAGAP1* revealed its CA RACB antagonizing character. It increased the relative susceptibility level of barley epidermal cells towards *Bgh* by 50 % whereas transient over-expression of MAGAP1 significantly decreased their susceptibility, which was independent of its localization on MTs. Transient over-expression of the catalytic inactive MAGAP1 R185G mutant, lacking the conserved arginine-finger of GAP domains, decreased susceptibility nearly identical to TIGS of *MAGAP1*. A strong focusing of cortical MTs to the site of attack was observed in resistant cells where *Bgh* was stopped at the prepenetration state. The MT network was not focused but appeared somewhat loosened in susceptible cells bearing an haustorium. Expression of RFP-MAGAP1 significantly increased resistance and focusing of cortical MTs to the site of attack in resistant cells. This effect was not observed by alternative expression of the catalytic inactive RFP-MAGAP1-R185G mutant. In susceptible cells bearing a haustorium, RFP-MAGAP1 fluorescence additionally appeared ring-shaped around the collar and the neck of haustoria, reminiscent of RIC171, which stresses the suggestion of high ROP activity at sites of ingrowing haustoria [Hoefle et al. 2011]. MAGAP1 might itself be negatively regulated by an Engulfment and Motility (ELMO) domain containing protein, ELMOD_C [Hoefle and Hückelhoven 2014].

Besides RACB activity influencing MTs, transient over-expression of CA RACB in barley epidermal cells also suggested RACB as negative regulator of actin filament polarity [Opalski et al. 2005]. *Bgh* resistant barley *mlo*-genotype epidermal cells showed strong and persistent polarization of Actin Filaments (AF) towards the site of attack upon challenge with *Bgh* whereas in non-penetrated cells of the susceptible *MLO*-genotype AF polarization was reduced. This suggests an inhibitory effect of functional MLO on AF

polarization ability. Over-expression of CA RACB negatively influenced AF in their ability to focus towards the site of attack in the susceptible *MLO* background as well as in the resistant *mlo* background. TIGS of *RACB* was seen to promote AF polarization in the *MLO* background. This suggests RACB to act upstream of AF regulatory elements [Opalski et al. 2005].

ROPs have a prominent role in cell polarity establishment, cell expansion and cell differentiation (see above). Transgenic CA RACB expressing seedlings grown on osmotic medium developed short, bulb-shaped roothairs suggesting an isotropic root hair growth resulting in a polar outgrowth deficit. Epidermal B-cells were significantly longer than in azygous control plants [Schultheiss et al. 2005; Pathuri et al. 2008; Pathuri et al. 2009b].

The RACB transcript was never found to be more reduced to than 50 % in leaves of transgenic *RACB* RNAi barley lines. This hinds to the requirement of an at least moderate amount of functional RACB protein for plant development. The introduced RACB RNAi cassette co-silenced the second barley type I ROP *RACD*, but none of the barley type II ROPs *RAC1*, *RAC3* or *ROP6*. Fully grown *RACB* RNAi plants did not reach the height of azygous control plants. Interestingly, *RACB* RNAi seedlings developed no or less root hairs depending on the level of *RACB* silencing. These two observations suggest RACB to be involved in cell expansion [Hoefle et al. 2011].

The observed phenotypes attribute a role to RACB in cell polarity establishment, cell expansion, cell differentiation and organ development. In combination with RACB having been identified as susceptibility gene, it is tempting to speculate that the biotrophic fungus *Bgh* might actively exploit a host cell developmental process in order to establish itself in the host cell. Haustorial ingrowth resembles root hair outgrowth as both processes depend on a polarized active growth process of the plant cell. These thoughts were formulated as the ‘inverted tip growth’ hypothesis [Schultheiss et al. 2003]

1.7 Objectives

Previous work has collected some preliminary hints that a small protein, likely derived from *Bgh*, may have the potential to interact with the barley susceptibility factor RACB in yeast and that it may have the potential to modulate the susceptibility level of barley epidermal cells towards *Bgh* (TUM, Chair of Phytopathology, unpublished). Interestingly, first database searches using the nucleotide sequence of candidate cDNA clone V42A, which was then named ROPIP1 in this study, located it on the retrotransposable element Eg-R1 of *Bgh*.

With this study, I wanted to follow the way of the *Bgh* effector candidate ROPIP1 starting from the genome of *Bgh* and ending with its putative mode of action inside the host cell to eventually answer the question: Is ROPIP1 an effector of *Bgh*?

An effector protein should be encoded in the DNA of the pathogen, therefore I wanted to learn about how ROPIP1, being at least partially encoded by the retroelement Eg-R1, is distributed in the genome of *Bgh*. ROPIP1 was discovered as clone V42A interacting with barley RACB protein in a Y2H-screen with barley RACB as bait against a cDNA library prepared from *Bgh*-infected barley leaves. Hence, I wanted to know whether *Bgh* native ROPIP1 gets translated into protein. For being an effector, a protein needs to get secreted by the pathogen. As RACB is localized in the barley leaf epidermis [Schultheiss et al. 2002], the question was, whether a putative ROPIP1 protein gets translocated into barley epidermal cells and whether a putative ROPIP1-RACB protein interaction might take place *in planta*. The mode of action of effector proteins without obvious enzymatic activity is difficult to determine. Therefore I underwent first steps to elucidate the mode of action of ROPIP1. Finally, the nature of effector proteins is to make their hosts susceptible to the pathogen and I wanted to find out whether ROPIP1 indeed triggers barley susceptibility to *Bgh*.

2 Results

2.1 Barley RACB Interacts with *Bgh* ROPIP1 in Yeast

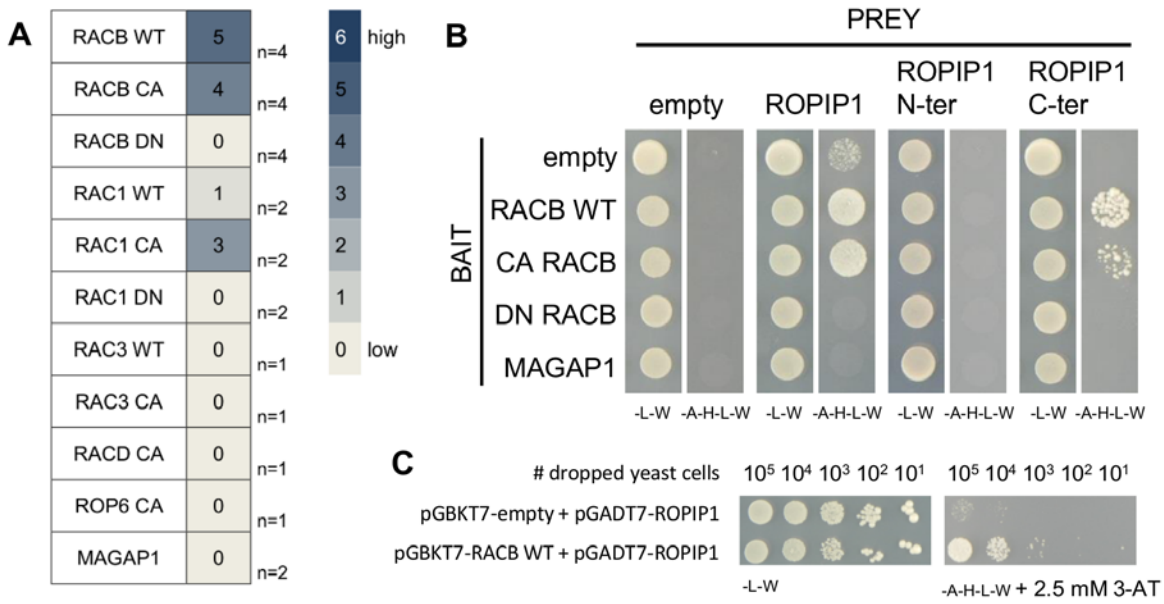

Figure 1: Targeted Y2Hs showing preferential and specific protein interaction of *Bgh* ROPIP1 with RACB WT and CA RACB. (A) A protein interaction strength evaluation score based on growth of transformed yeast cells, expressing ROPIP1 as prey and baits as indicated, on increasing *HIS3* gene inhibitor 3-AT concentrations in the selection medium was generated. A maximum score of 6 indicates strongest protein interaction, a minimum score of 0 no protein interaction in yeast. (B) Targeted Y2H with ROPIP1 and ROPIP1 N-terminal and C-terminal truncation mutants as preys and baits as indicated. The C-terminal ROPIP1 fragment (ROPIP1-Cter) comprises a small ORF. Left stripes: Transformation control medium (SD –L/-W); Right stripes: selection medium (SD –A/-H/-L/-W). Drops of 10^5 cells per combination are shown (C) Dilution series of dropped yeast cells in numbers and combinations as indicated on selection medium supplemented with 2.5 mM 3-AT (SD –A/-H/-L/-W) and transformation control medium (SD –L/-W) showing true positive interaction of ROPIP1 and RACB WT. pGBKT7: bait vector; pGADT7: prey vector.

Bgh ROPIP1 (ROP-Interacting Peptide 1), ROPIP1 paralogous sequences and partial and full Eg-R1 sequences were repeatedly retrieved as prey-cDNAs in a Y2H screen using cDNA libraries prepared form *Bgh*-infected barley leaves as prey and RACB WT, CA RACB and CA RAC1 as baits (Hoefle Caroline, Hückelhoven Ralph (TU München, Germany), Schultheiss Holger (University of Giessen, Germany), unpublished results personally communicated).

Bgh ROPIP1 was thus considered as a possible effector targeting the barley susceptibility factor RACB. An independent targeted Y2H with ROPIP1 cloned into the prey vector confirmed the protein interaction with RACB WT, CA RACB and CA RAC1.

Starting from these results further independent targeted Y2H assays had the following aims. In total, six ROPs were identified in barley, five of them to be expressed in the epidermis which is the relevant tissue for *Bgh* interaction [Schultheiss et al. 2003]. One aim was to check whether ROPIP1 preferentially interacts with a distinct subset of barley ROPs or whether it has the ability to interact redundantly with barley ROPs. Another aim was to verify the interaction of ROPIP1 with RACB WT and CA RACB by additional independent repetitions. The possibility of false-positive colony growth should also get addressed. ROPIP1 truncations should get tested in a structure function analysis to learn more about which sequence part of ROPIP1 mediates interaction with barley ROPs.

ROPIP1 in the prey vector was tested against barley ROPs and MAGAP1 as baits in a series of targeted Y2Hs. Colonies of co-transformed yeast AH109 cells were resuspended and plated in parallel on SD –L/-W medium for transformation control and on SD –A/-H–L/-W selection medium supplemented with 0, 0.5, 1.0, 1.5, 2.0, 2.5 mM 3-Amino-1,2,4-Triazole (3-AT). RACB WT, CA and DN were included in 3 independent experiments, RAC1 WT, CA and DN in one additional independent experiment. RAC3 WT, CA RAC3, CA RACD and CA ROP6 have not been tested for interaction with ROPIP1 in yeast before and the experiment was done once. MAGAP1 was included in one additional independent experiment as a potential key regulator of barley RAC/ROPs and because green fluorescing GFP-ROPIP1 co-localized with red fluorescing RFP-MAGAP1 on MTs of transiently transformed barley cells (see below). A dataset was created that included in total 4 independent repetitions with RACB (WT, CA; DN), 2 independent repetitions with RAC1 (WT, CA, DN) and one experiment with RAC3 (WT, CA), CA RACD, CA ROP6 as well as 2 independent repetitions with MAGAP1 as baits and ROPIP1 as prey. A protein interaction strength evaluation score was generated by applying the following rules: I) Each ROPIP1-bait combination dropped onto selection medium containing 0 to 2.5 mM 3-AT gets evaluated (6 data points for one ROPIP1-bait combination); II) Each data point gets the value 1 for yeast colony growth or 0 for no yeast growth; III) The value 1 is only true when yeast colony growth exceeds yeast background growth in the combination ROPIP1-empty bait vector, otherwise it is 0; IV) This is repeated for every available independent repetition of ROPIP1-bait combinations;

V)The values of each ROPIP1-bait combination are summed up and divided by the number of repetitions. The maximum score is 6, the minimum score is 0. 3-AT is a competitive inhibitor of the leaky nutritional selection marker Saccharomyces *HIS3* gene product. Additional to its application in reducing yeast background growth, increasing 3-AT concentrations give hints to the strength, or affinity of protein interactions. Usage of a 3-AT concentration series and the scoring-rules yielded the highest score for the combination ROPIP1-RACB WT (score = 5), followed by the combination ROPIP1-CA RACB (score = 4). The combination ROPIP1-CA RAC1 resulted in a score in the medium range (score = 3), whereas the combination ROPIP1-RAC1 WT resulted in a score in the low range (score = 1). All other combinations resulted in a score of 0 (Figure 1 A). These results suggested that ROPIP1 preferentially interacted with RACB WT and CA RACB in yeast. ROPIP1 was also indicated to interact with CA RAC1 in yeast albeit with a likely lower affinity.

Preferential and specific binding of ROPIP1 to RACB was further substantiated by usage of ROPIP1 truncations instead of ‘full-length’ ROPIP1. The ROPIP1 sequence was split into an N-terminal (ROPIP1-Nter) and a C-terminal (ROPIP1-Cter) part. ROPIP1-Nter comprises amino acid positions 1 to 31 and ROPIP1-Cter amino acid positions 32 to 75 as depicted in Table A 2 (Appendix). ROPIP1-Cter constitutes a small ORF of 44 amino acids. ROPIP1-Nter and C-term were PCR-amplified and cloned into the pGADT7 prey vector. Targeted Y2Hs with ROPIP1-Nter or ROPIP1-Cter as prey in combination with RACB (WT, CA, DN) and RAC1 (WT, CA, DN) as baits were performed. ROPIP1-Cter interacted with WT and CA RACB but not DN RACB (Figure 1 B) which indicated that the small ORF represented by ROPIP1-Cter is sufficient for ROPIP1-RACB (WT, CA) protein interaction in yeast. By contrast, the N-terminus of ROPIP1 alone was insufficient for interaction with RAC/ROPs, as indicated by the absence of colony growth upon alternative usage of ROPIP1-Nter as prey in the same experiment (Figure 1 B). Colonies of the combination ROPIP1-Cter – RACB WT grew denser than those of the combination ROPIP1-Cter – CA RACB, a pattern which was also observed in an independent repetition of the experiment and that is also reflected by the protein interaction strength evaluation score (Figure 1 A). However, colony growth with ROPIP1-Cter as prey was less dense when compared to ROPIP1 in the

same experiment (Figure 1 B) where 10^5 transformed yeast AH109 cells of each combination were dropped in parallel on transformation control medium and selection medium. Further, the interaction strength seemed to be weaker as colony growth was only observable until 1.0 mM 3-AT in the selection medium, whereas ROPIP1 positive interactions grew even at a concentration of 2.5 mM 3-AT in the selection medium. Interestingly, ROPIP1-Cter did not interact with RAC1 (WT, CA, DN, see Figure A 1, Appendix) which further stressed ROPIP1 preference of RACB over RAC1. Usage of test protein truncations and 3-AT supplement to the selection media are possibilities to counteract auto-activation of reporter genes in Y2H assays [Causier and Davies 2002]. The background growth observed with cells co-transformed with ROPIP1 in the prey vector and empty bait vector completely abolished upon substitution of ROPIP1 with ROPIP1-Cter or ROPIP1-Nter while the interaction pattern of ROPIP1-Cter with RACB WT and CA RACB remained as observed with ROPIP1. This strongly suggested that the observed protein interactions are true positive. This is further supported by an additional drop out of a dilution series of yeast AH109 cells having been co-transformed with pGADT7-ROPIP1 as prey vector and either pGBKT7-empty or pGBKT7-RACB WT as bait vectors. Yeast colonies of both combinations were resuspended in H_2O and adjusted to 10^5, 10^4, 10^3, 10^2, 10 cells per drop and dropped in parallel on transformation control medium and selection medium supplied with 2.5 mM 3-AT (Figure 1 C). Background colony growth on the selection medium in the combination ROPIP1-empty bait was low in comparison to the combination ROPIP1-RACB WT and almost vanished at 10^4 dropped cells. Whereas cell density in drops of the combination ROPIP1-RACB WT greatly exceeded that of the control combination with colony growth still observable at 10 dropped cells.

Together, the targeted Y2H studies indicated that ROPIP1 preferentially and specifically interacted with RACB WT and CA RACB in yeast and to a certain extent also with CA RAC1. Additionally, ROPIP1-Cter was shown to be sufficient for the protein interaction of ROPIP1 with RACB WT and CA RACB in yeast.

2.2 ROPIP1 Contributes to Virulence of *Bgh*

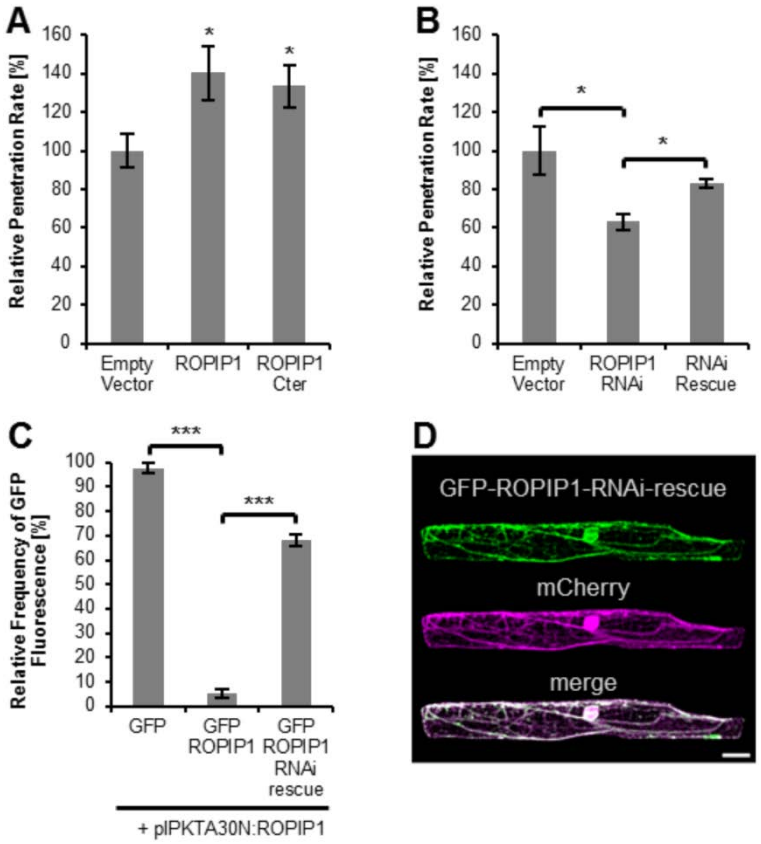

Figure 2: ROPIP1 modulates the susceptibility level of barley epidermal cells towards *Bgh*. (A) Transient over-expression of ROPIP1 and a ROPIP1 C-terminus truncation mutant (Cter) in barley epidermal cells driven from the 35S promoter. The penetration rates of *Bgh* in relation to the mean of the pGY1-empty vector control transformed cells which was set 100 % of 6 independent repetitions are shown. (B) The relative penetration rates of *Bgh* in a Host-Induced Gene Silencing (HIGS) experiment were calculated from 4 independent repetitions. Barley epidermal cells were transiently transformed with either an RNAi construct directed against *ROPIP1* (ROPIP1-RNAi), the ROPIP1-RNAi construct plus a synthetic ROPIP1-RNAi insensitive ROPIP1 mutant RNAi rescue construct (RNAi rescue) or empty pIPKTA30N vector control. (C) The pIPKTA30N-ROPIP1 RNAi vector was tested in its ability to silence GFP-ROPIP1, the GFP-ROPIP1 RNAi rescue construct, or GFP as control in 3 independent repetitions. Transiently transformed barley epidermal cells were identified by co-transformed red-fluorescing mCherry. Red-fluorescing transformed cells were judged whether GFP fluorescence was visible or not by fluorescence microscopy. (D) An exemplary barley epidermal cell showing translation of the GFP-ROPIP1-RNAi-rescue construct. The cell was taken from one repetition of C and imaged in parallel by confocal laser scanning microscopy. A maximum projection of a whole cell sequential scan in 2 µm increments is shown. The co-transformed mCherry labeled the cytoplasm and the nucleoplasm. Scale bar is 20 µm. * p ≤ 0.05, *** p ≤ 0.001, two-sided Student's t-test.

RACB, when over-expressed as its constitutively activated (CA) mutant induced super-susceptibility of barley epidermal cells against *Bgh* in transient assays [Schultheiss et al. 2002; Schultheiss et al. 2003] and in stable transgenic barley lines [Schultheiss et al. 2005; Pathuri et al. 2008]. As ROPIP1 interacted with CA and WT RACB in yeast, the next question was whether ROPIP1 would have the potential to influence the susceptibility level of barley epidermal cells towards establishment of haustoria by *Bgh*.

As a first approach, transient over-expression of ROPIP1 in barley epidermal cells and subsequent inoculation with *Bgh* was chosen as it is a routine method for the functional characterization of candidate proteins putatively modulating the susceptibility level of barley epidermal cells towards *Bgh*. The experiment was performed essentially as described in Schweizer et al. [1999] and Hückelhoven et al. [2003]. Detached barley primary leaves (7d old) were ballistically transformed with empty pGY1 plant expression vector [Schweizer et al. 1999] as control, pGY1-ROPIP1 with ROPIP1 equiped with an artificial ATG start codon or pGY1-ROPIP1-Cter. The pGY1-GFP plasmid was co-delivered as transformation marker. Transiently transformed barley leave segments were inoculated with *Bgh* conidiospores at 24 hat. Fungal development on transformed cells was evaluated at 48 hai by fluorescence microscopy. It was distinguished between susceptible transformed cells where *Bgh* established haustoria and exhibited secondary hyphae growth and resistant transformed cells where the infection process was stopped at the stage of appressorial germ tube formation by host CWAs (also papillae). The relative penetration rate (see Material and Methods for details) was calculated for each variant. In total the values of six independent experiments were combined for statistics.

Over-expression of ROPIP1 from the 35S promoter significantly increased the relative penetration rate by 40.25 % (Figure 2 A) compared to the control (two-sided Student's t-test; * $p \leq 0.05$). Hence, ROPIP1 induced super-susceptibility towards *Bgh* comparable to the effect of transient over-expression of CA RACB in barley [Schultheiss et al. 2003]. Additionally, over-expression of ROPIP1-Cter was sufficient (two-sided Student's t-test; * $p \leq 0.05$) for induction of super-susceptibility. The increase of the relative penetration rate was 33.40 % compared to the control (Figure 2 A). The susceptibility inducing effect of ROPIP1-Cter was not significantly different from that of ROPIP1 but tendentially weaker. This might reflect the less strong interaction of ROPIP1-Cter with RACB when

compared to that of ROPIP1 (Figure 1 B). Together with the results from the targeted Y2Hs this indicated the small ORF represented by ROPIP1-Cter to constitute the effector domain of ROPIP1.

Over-expressing a candidate protein gives a good indication for its functionality in the barley-*Bgh* interaction. However, due to the usage of strong promoters the protein amounts are very likely exaggerated, which does not represent the native situation. Now, having identified the potential of ROPIP1 in modulating the susceptibility level of barley epidermal cells towards *Bgh*, the next aim was to check whether this finding can get substantiated by posttranscriptional gene silencing.

Unfortunately, there is no applicable protocol for transformation of *Bgh* available which excluded direct genetic manipulation of *Bgh*. However, HIGS was shown to be functional in the barley-*Bgh* pathosystem [Nowara et al. 2010] and is well established in the community [Koch and Kogel 2014]. In brief, over-expression of double-stranded RNAi constructs in barley leads to silencing of *Bgh* transcripts which might involve an yet unknown RNA-translocation mechanism.

ROPIP1 was cloned into the RNAi Gateway destination vector pIPKTA30N and supplied to barley epidermal cells via microprojectile-mediated transient transformation [Douchkov et al. 2005]. Empty pIPKTA30N was delivered as negative control. In each variant pGY1-GFP vector was co-bombarded as transformation marker. Detached transformed barley leaves were inoculated with *Bgh* conidiospores at 24 hat. Evaluation of the susceptibility level of *Bgh* inoculated barley epidermal cells by fluorescence microscopy was done analogous to the ROPIP1 over-expression experiment (see above) at 48 hai. The experiment was repeated independently four times. Transient expression of pIPKTA30N-ROPIP1 (ROPIP1-RNAi) in barley epidermal cells significantly reduced the relative penetration rate of *Bgh* by 36.95 % (Figure 2 B) compared to the empty vector control (two-sided Student’s test, * $p \leq 0.05$). This supported the results of ROPIP1 over-expression and indicated a function of ROPIP1 in virulence of *Bgh*.

An RNAi rescue variant was included in the experiments to tackle the possibility of non-specific silencing of off-target transcripts [Nowara et al. 2010]. The ROPIP1-RNAi-

rescue construct was designed analogous to as described by Pliego et al. [2013]. The nucleotides in the wobble position of the ROPIP1 codons were exchanged for the codons being most different to *Bgh* but most commonly used by barley as retrieved from the Codon Usage Database (kazusa.or.jp/codon). The resulting ROPIP1-RNAi-rescue nucleotide sequence shared 64 % identity with the ROPIP1 nucleotide sequence (Table A 2, Appendix). The nucleotide exchange mutations were silent and putatively insensitive to RNAi-mediated gene silencing. The synthetic ROPIP1-RNAi-rescue construct was ordered at Eurofins Genomics GmbH (Ebersberg, Germany) and subcloned into the pGY1 plant expression vector [Schweizer et al. 1999].

The pGY1-ROPIP1-RNAi-rescue vector (RNAi rescue) was co-bombarded with pIPKTA30N-ROPIP1 and pGY1-GFP as additional variant to the ROPIP1-RNAi variant in the same experiments (Figure 2 B). Addition of pGY1-ROPIP1-RNAi-rescue elevated the relative penetration rate from 63.05 % to 82.86 %. The rescuing effect was significant at $p \leq 0.05$ when the mean relative penetrations rates of the ROPIP1-RNAi variant and the RNAi-rescue variant were compared in a two-sided Student's t-test. This indicated that ROPIP1-RNAi-rescue functionally complemented ROPIP1 and corroborated specific silencing of *ROPIP1* by pIPKTA30N-ROPIP1. However, there was also some indication that ROPIP1-RNAi-rescue was incomplete (Figure 2 C and see below). Therefore, the specificity of *ROPIP1* transcript silencing by pIPKTA30N-ROPIP1 was further assessed. Off-target predictions using the si-Fi (version 3.1.0-0001) software (labtools.ipk-gatersleben.de/index.html) with the ROPIP1 nucleotide sequence as query against the nucleotide databases barley_HighConf_genes_MIPS_23Mar12_CDSSeq and barley_LowConf_genes_MIPS_23Mar12_CDSSeq (pgsb.helmholtz-muenchen.de/plant/barley) for barley and bgh_dh14_v3.0.cds and mRNA_8_12_10 (blugen.org) for *Bgh* and using standard parameters produced no barley hits at all, nor *Bgh* off-target hits. The efficacy of pIPKTA30N-ROPIP1 in silencing *ROPIP1* was also quantitatively assessed. Therefore, pIPKTA30N-ROPIP1 was co-transformed with pGY1-GFP as control or pGY1-GFP-ROPIP1 or pGY1-GFP-ROPIP1-RNAi-rescue into barley epidermal cells by particle bombardment. To each combination pGY1-mCherry was added as an additional transformation marker. Analysis followed at 36 hat by fluorescence microscopy. Transformed cells were identified by red-fluorescing mCherry

and judged whether additional GFP-fluorescence was visible or not. The experiment was independently repeated 3 times. In each repetition at least 150 transformed cells of each combination were scored. The mean relative frequencies of GFP-fluorescing cells were compared. The mean relative frequencies of GFP-fluorescing cells were 97.60 % for the GFP control, 5.14 % for the GFP-ROPIP1 variant and 68.01 % for the GFP-ROPIP1-RNAi-rescue variant (Figure 2 C). GFP-ROPIP1 expressing cells were highly significant different from the GFP control (*** $p \leq 0.001$, two-sided Student's t-test). The relative frequency of GFP-expressing cells of the GFP-ROPIP1-RNAi-rescue variant was highly significant different from GFP-ROPIP1 expressing cells (*** $p \leq 0.001$, two-sided Student's t-test). Together, this showed a high potential of the pIPKTA30N-ROPIP1 HIGS construct for silencing *ROPIP1* and the potential of the GFP-ROPIP1-RNAi-rescue construct to mediate ROPIP1 expression despite presence of the pIPKTA30N-ROPIP1 HIGS construct.

A subset of transformed cells was imaged in parallel by confocal laser scanning microscopy in sequential scan mode showing that ROPIP1-RNAi-rescue as GFP-fusion was translated in barley epidermal cells. The observed GFP fluorescence pattern was identical to what was observed with GFP-ROPIP1 (Figure 2 D, compare to Figure 5 A).

2.3 Evidence of the Native ROPIP1 Peptide

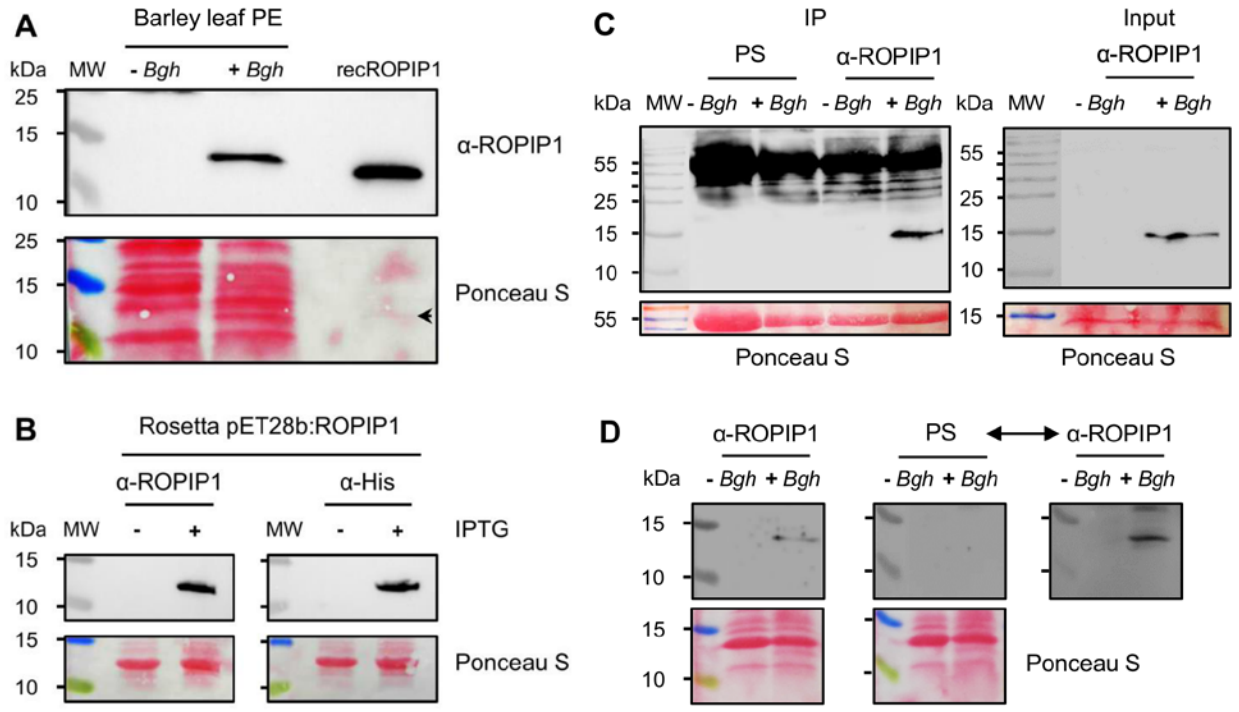

Figure 3: Western blot analyses using affinity purified polyclonal anti-peptide α-ROPIP1 as primary antibody. (A) Total protein extracts (PE) were prepared from barley primary leaves, mock treated (-*Bgh*) or *Bgh* infected (+ *Bgh*). A purified recombinant His-tagged ROPIP1 protein (recROPIP1) was run as positive control on the same gel. (B) Controls validating α-ROPIP1 specificity. Crude lysates were prepared from IPTG (+) –induced or non-induced (-) parallel small-scale *E. coli* Rosetta cell cultures expressing His-tagged recombinant ROPIP1 from an IPTG-inducible promoter (pET28b vector). Aliquots of the lysates were additionally probed with α-His antibody (right panel) as independent antibody control recognizing the same recombinant protein. (C) Immunoprecipitation (IP) using preimmune serum (PS) or α-ROPIP1 for immune complex formation in total protein extracts prepared from non-inoculated mock control (- *Bgh*) or *Bgh*-infected (+ *Bgh*) barley primary leaves. Immune complexes were captured, purified and probed with α-ROPIP1 as primary antibody in a western blot. Antibody heavy chains (~ 55 kDa) and light chain fragments (~ 25 kDa) were co-detected by α-rabbit-Hrp secondary antibodies. Aliquots of the input protein extracts (right panel) were probed with α-ROPIP1 as primary antibody in a parallel western blot to show the presence of the antigen. (D) Control validating specificity of α-ROPIP1 for the ~ 14.5 kDa signal seen in the *Bgh*-treated sample lane. Total protein extracts were prepared from non-inoculated (-*Bgh*) or *Bgh*-inoculated (+*Bgh*) barley primary leaves. Aliquots of the same extracts were run as duplicate on the same gel. Blotted membranes were cut into halves and incubated with either α-ROPIP1 (left panel) or PS (middle panel) as primary antibody. After chemiluminescence detection, antibodies were stripped from the PS blot followed by reprobing of the same blot with α-ROPIP1 as primary antibody instead (right panel). MW: Molecular weight marker. Ponceau S : loading and transfer control.

Ectopically expressed *Bgh* ROPIP1 showed potential to interact with the barley host susceptibility factor RACB and to manipulate the susceptibility level of barley epidermal cells against *Bgh*. Considering that ROPIPI1 might be a putative virulence effector of *Bgh* it should be present in proteinaceous form in the native situation. Western blot analysis using an antibody directed against ROPIP1 was chosen to answer the question whether ROPIP1 gets translated in the authentic interaction of barley and *Bgh*.

Therefore a polyclonal antipeptide antibody directed against the epitope NH_2-IPSRLRDLYRLHF-COOH in the C-terminal part of the ROPIP1 amino acid sequence was generated and provided by Pineda Antibody Service (Berlin, Germany). Off-target searches for the epitope yielded no significant hits. Two rabbits were immunized with the synthesized epitope peptide in a long immunization protocol (145 d). Periodically delivered antiserum samples were tested for their capability of recognizing recombinant ROPIP1 in crude cell lysates of *E. coli* small scale cultures and protein extracts prepared from non-inoculated and *Bgh* inoculated barley leaves in parallel by western blot. Once a slight signal unique to the *Bgh*-inoculated sample was observed, the immunization protocol was finalized. At the end, the monospecific IgG fraction was purified by affinity chromatography using the epitope peptide as antigen. This monospecific IgG fraction is referred to as α-ROPIP1 in this work.

Total protein extracts were prepared from *Bgh*-inoculated and non-inoculated control barley primary leaves. Notably, it turned out that methanol and acetone washing of liquid nitrogen ground leaf powder prior to protein extraction was greatly helpful for the success of the experiment (see Material and Methods for details). Besides, a high amount of fungal biomass (7-10 dai) and a high amount of total protein (100 µg) per sample loaded onto a SDS-PAGE gel was a prerequisite. This may point to low abundancy of the target protein, sensitivity to polyphenolic protein precipitation or low accessibility of the protein.

However, protein extracts prepared from non-inoculated and *Bgh*-inoculated barley primary leaves were separated by discontinuous tris-glycine SDS-PAGE [Laemmli 1970] and blotted onto nitrocellulose membrane. Blots were incubated with α-ROPIP1 or Preimmune Serum (PS) as primary antibody followed by horseradish peroxidase (hrp)-

conjugated anti-rabbit secondary antibody. Ponceau S staining of the blotted nitrocellulose membrane served as visualization of successful protein transfer and loading control.

A unique band labeled through α-ROPIP1 in the *Bgh*-inoculated sample lane as depicted in Figure 3 A was repeatedly (n > 10) observed in independent experiments. The mean molecular weight of the observed signal was estimated as 14.3±0.7 kDa (n = 27; mean ± STD). This signal was never seen in the non-inoculated sample lanes. Even not after prolonged exposition time in the chemiluminescence detector. Hence, α-ROPIP1 labeled a protein associated with *Bgh*-infection. The absence of the signal in the non-inoculated sample even at high protein amounts loaded (100 µg) onto the gel and after prolonged exposition time, as well as the absence of predictable significant off-targets in barley rather pointed to a fungal protein labeled by α-ROPIP1.

Besides protein extracts prepared from non-inoculated barley leaves as negative control, a recombinant in *E. coli* expressed and His-tag purified 6H-ROPIP1-6H (recROPIP1) was added as positive control (Figure 3 A). This experiment was repeated with nearly identical results.

Specificity of α-ROPIP1 was further tested with crude protein extracts from *E. coli* (Rosetta cells) small scale cell culture using an Isopropyl-β-D-thiogalactopyranosid (IPTG) inducible promoter for recROPIP1 expression (pET28b plasmid). The common starter culture was used to obtain parallel cultures with (+IPTG) and without (-IPTG) induction of the lac operon. Crude lysates of the cultures were prepared and submitted to western blot analysis using α-ROPIP1 as primary antibody. The blots were almost clean without major background signals. A unique signal fitting the size expectation of recROPIP1 (~12.5 kDa) was only seen in the IPTG-induced sample (Figure 3 B, left panel). The same crude lysates were used for probing with an independent antibody against recROPIP1 and run in parallel on the same gel. Usage of anti-His (α-His) antibody directed against the artificial His-tags of recombinant ROPIP1 resulted in the observation of an identical signal pattern (Figure 3 B, right panel), strongly suggesting specificity of α-ROPIP1 in detecting recROPIP1. This experiment was repeated with same results.

A slight signal at ~25 kDa was observed irrespective of whether α-ROPIP1 or α-His was used as primary antibody. This weak cross-labelling of a ~25 kDa band was also sometimes observable in non-inoculated and *Bgh*-inoculated samples prepared from barley leaves and therefore likely resulted from unspecific background staining. Sometimes weak signals >60 kDa were observable in all samples. They may also have arisen from the secondary antibody but incubation with anti-rabbit-hrp alone did not label the unique band delivered by α-ROPIP1.

However, most western blots using non-inoculated and *Bgh*-inoculated barley leaves protein extracts showed almost no background, there were also some without background at all as seen exemplary in Figure 3 C (Input).

Specificity of α-ROPIP1 for the ~14.3 kDa protein in the *Bgh*-inoculated sample was further demonstrated by two independent approaches. First, by usage of Immunoprecipitation (IP) as an independent method. Denaturing conditions had to be applied to the input protein extracts prior to addition of the antibodies. This is not astonishing, when considering that α-ROPIP1 was raised against a synthesized epitope peptide where the tertiary structure fold of the real protein is absent. Aliquots of the input samples were kept for western blot analysis to demonstrate the presence of the target protein (Figure 3 C, right panel). The input protein extracts derived from non-inoculated and *Bgh*-inoculated barley leaves were split and incubated in parallel with either α-ROPIP1 or preimmune serum. The formed antibody-antigen immune complexes were then captured by Protein A/G coupled agarose beads, purified and eluted by cooking in SDS sample buffer. The eluates consisting of antibodies and its precipitated proteins were separated by SDS-PAGE followed by transfer on nitrocellulose membranes. Blotted proteins were incubated with α-ROPIP1 as primary antibody followed by anti-rabbit hrp-conjugated secondary antibody for detection. This approach yielded exactly one band of 14.5$\pm$0.6 kDa (mean$\pm$STD, n = 5) in the *Bgh*-treated input when α-ROPIP1 was used to form the immune complex. No signal was obtained from the non-inoculated sample. Neither was a signal obtained in the non-inoculated nor *Bgh*-inoculated input upon usage of preimmune serum in the immunoprecipitation (Figure 3 C, left panel). Antibody heavy chains (~55 kDa) and light chain fragments (~25 kDa) were co-labelled by the anti-rabbit secondary antibody. This alternative method showed that the

preimmune serum did not precipitate proteins that are recognized by α-ROPIP1. It further strengthened the observation that the unique signal in *Bgh*-treated barley samples is depended on *Bgh*-inoculation of barley leaves and α-ROPIP1 as primary antibody. The IP with addition of α-ROPIP1 to the input samples was repeated in total 5-times with similar results, thereof 2-times with additional in parallel usage of preimmune serum.

Specificity of α-ROPIP1 was further substantiated by removal of antibodies and reprobing with different antibodies of the same nitrocellulose membrane. Protein extracts were prepared from barley leaves inoculated or non-inoculated with *Bgh* and subjected to western blot analysis. The extracts were split and aliquots run in parallel. One aliquot was incubated with α-ROPIP1, the other with preimmune serum as primary antibody. The protein labeled by α-ROPIP1 was present in the protein extract derived from the *Bgh*-treated sample (Figure 3 D, left panel) but not labeled by preimmune serum (Figure 3 D, middle panel). Antibodies were stripped under gentle conditions from the preimmune serum incubated nitrocellulose membrane and reprobed with α-ROPIP1 as primary antibody. A unique signal which was typically seen with α-ROPIP1 appeared in the *Bgh*-treated sample lane that was absent before (Figure 3 D, right panel). This further substantiated that the protein labeled by α-ROPIP1 was present in the samples first incubated with preimmune-serum but not recognized by preimmune serum. The experiment was repeated with similar results.

In sum, these experiments validated α-ROPIP1 to specifically recognize recROPIP1 as well as a unique protein in the *Bgh*-inoculated sample. However, the expected molecular weight of ROPIP1 as presented by Eg-R1, which was 8.3 kDa, differed from the observed molecular weight of the unique signal in *Bgh*-inoculated samples (~14.5 kDa). This may have several reasons. To name it first, Eg-R1 has multiply inserted itself into the genome of *Bgh*. Some insertion resulted in elongated ORFs (see Table A 3, Appendix). Further, many insertions may be unknown yet as high repeat areas are difficult to assemble and no physical maps of the *Bgh* genome have been generated. Hence, there is a high degree of uncertainty concerning the size of a putative native ROPIP1 protein as its localization of at least part of its sequence on the retroelement Eg-R1 and the multiple insertions of Eg-R1 which could give rise to paralog copy

variation of ROPIP1, clearly differing from classical gene encoded proteins. Other possible explanations may be competition between tertiary structure and SDS binding resulting in gel shifts as described for hydrophobic α-helices hairpins of transmembrane proteins [Rath et al. 2009], formation of SDS-resistant oligomers as described for amyloid-β peptide of Alzheimer's disease [Sandberg et al. 2010] or posttranscriptional modifications, like glycosylation, of the native ROPIP1 protein, formation of a stable oligomer of short ROPIP1 peptides and last, as with every antibody, it cannot be excluded that α-ROPIP1 cross-reacted with a completely unrelated protein, although this appears very unlikely. The long immunization protocol (145d) applied for production, the immunization with a synthesized epitope peptide and the affinity purification of the monospecific IgG fraction was intended to maturate and increase the affinity and specificity of the antigen binding site of α-ROPIP1 to the epitope peptide.

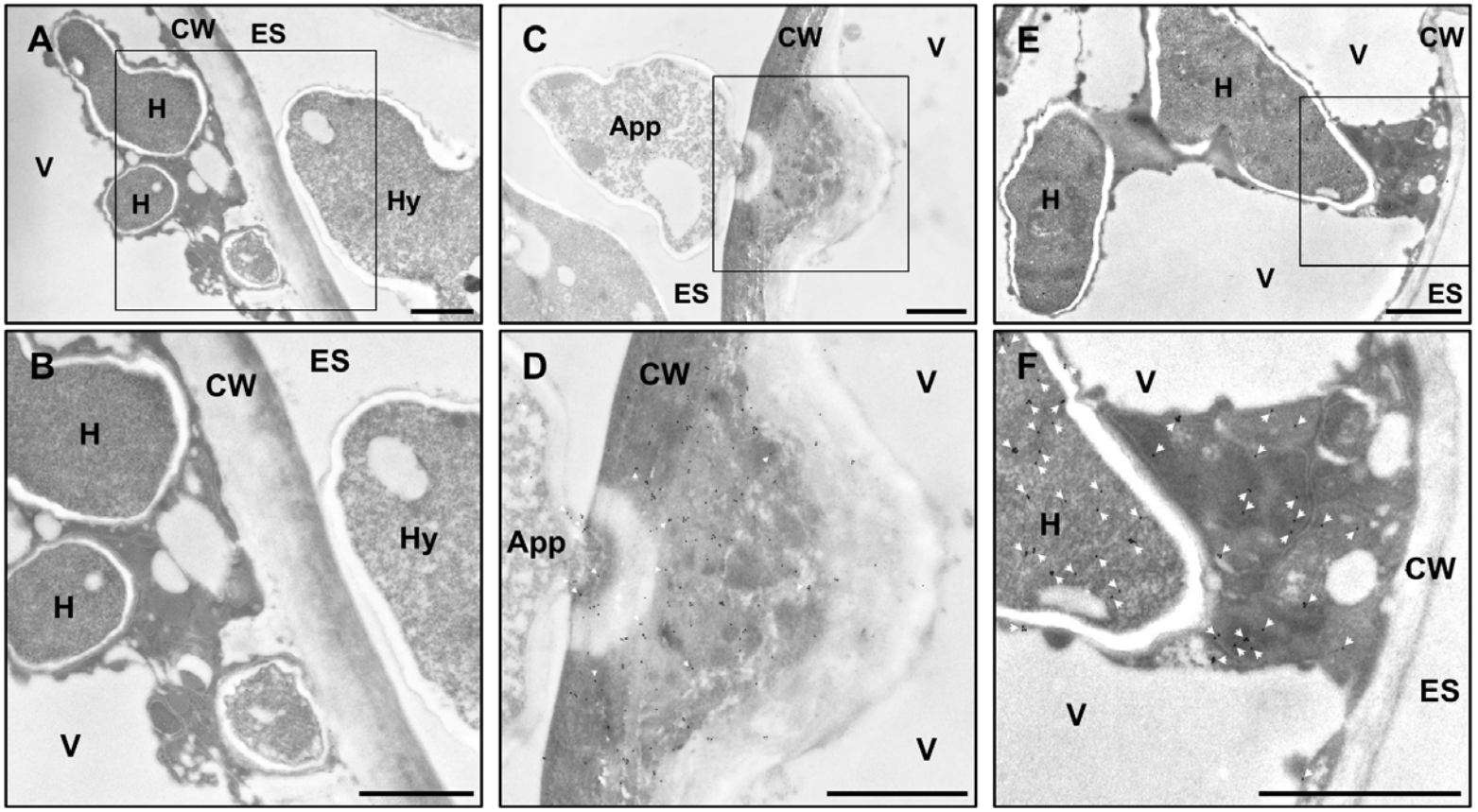

Figure 4: Transmission electron microscopy (TEM) micrographs of immunogold stained ultrathin cuts of epoxy resin embedded *Bgh*-infected barley primary leaves at 3 dai. (A and detail in B) Anti-rabbit secondary antibodies conjugated to 10 nm gold particels were hardly detecatble in the non-specific primary antibody control. (C and detail in D) A resistant barley epidermal cell where *Bgh* was stopped by a host papilla beneath its appressorium (App). Ultramicrotome prepared sections were incubated with α-ROPIP1 as primary antibody. Gold-particle conjugated secondary antibodies were detected in the *Bgh* App and in the barley CW and papilla. (E and detail in F) Ultrathin cut of a susceptible barley epidermal cell incubated with α-ROPIP1 as primary antibody. Gold-conjugated secondary antibodies decorated the lumen of a *Bgh* haustorium (H) and the cytoplasm of a barley epidermal cell. White arrowheads point to gold-particles. App: appressorium (*Bgh*). CW: cell wall (barley). ES: extracellular space. H: haustorium (*Bgh*). Hy: hyphae (*Bgh*). V: vacuole (barley). Scale bars are 1 µm.

2.4 TEM Localizes α-ROPIP1 in *Bgh* Structures and in the Host Cell Cytoplasm

The next aim was to detect the protein which is labeled by α-ROPIP1 *in situ*. Its localization *in situ* was of special interest as it would allow conclusions on whether it is *Bgh*-derived or *Bgh*-induced but possibly derived from barley, whether it gets secreted or not and whether it gets translocated into the host cytoplasm or remains in the apoplast. Immunogold-labeling and Transmission Electron Microscopy (TEM) was chosen to answer these questions.

The experiment was performed in cooperation with Dr. Bernd Zechmann at University of Graz (Austria). Barley primary leaves (7 d old) were densely inoculated with *Bgh* conidiospores. At 3 dai, ~ 1.5 mm^2 leaf discs were punched out and immediately chemically fixed with glutaraldhyde followed by dehydration in acetone and embedding in Epon™ epoxy resin. Ultrathin cuts were prepared with an Ultramicrotome and incubated with either α-ROPIP1 or an unspecific control antibody as primary antibodies. Primary antibodies were detected with 10 nm goldparticle coupled secondary antibodies by TEM.

In the unspecific antibody controls, almost no goldparticles were detectable in the extracellular space (ES), the cell wall (CW), the vacuole (V) and the cytoplasm of epidermal cells successfully invaded by *Bgh*. Also an extracellular hyphae of *Bgh* (Hy), likely representing an appressorium (App), as well as intracellular fungal haustorial structures (H) were almost free of goldparticles (Figure 4 A and detail in B).

By contrast, goldparticles were detected upon usage of α-ROPIP1 as primary antibody. In a resistant barley epidermal cell, where *Bgh* failed to invade the host cell but was stopped at the prepenetration stage in a host CWA (papilla), goldparticles decorated the extracellular fungal appressorium and appeared to spread from the tip of the appressorium into the apoplastic cell wall and CWA but were absent from the extracellular space and the vacuole (Figure 4 C and detail in D). This indicated α-ROPIP1 to bind to a secreted protein of *Bgh*. In a susceptible barley epidermal cell, where *Bgh* established a haustorium within the host cell, goldparticles were detected inside the haustorium and the host cytoplasm but only very rarely in the host vacuole

and cell wall and the extracellular space (Figure 4 E and detail in F). This patterning of gold particles suggested α-ROPIP1 to bind to a protein which gets translocated from the *Bgh* haustorium into the cytoplasm of barley epidermal cells. In ultrathin cuts of mesophyll cells from *Bgh*-inoculated barley leaves that were incubated with α-ROPIP1 as primary antibody the cytoplasm, the vacuole and the cell wall were almost free of goldparticles but showed sporadic localization of goldparticles in chloroplasts (see Figure A 2, Appendix). Together, immunogoldlabeling and TEM suggested α-ROPIP1 to bind to a *Bgh* cytoplasmatic protein acting in barley epidermal cells.

2.5 GFP-ROPIP1 is Recruited to Microtubules by RFP-MAGAP1

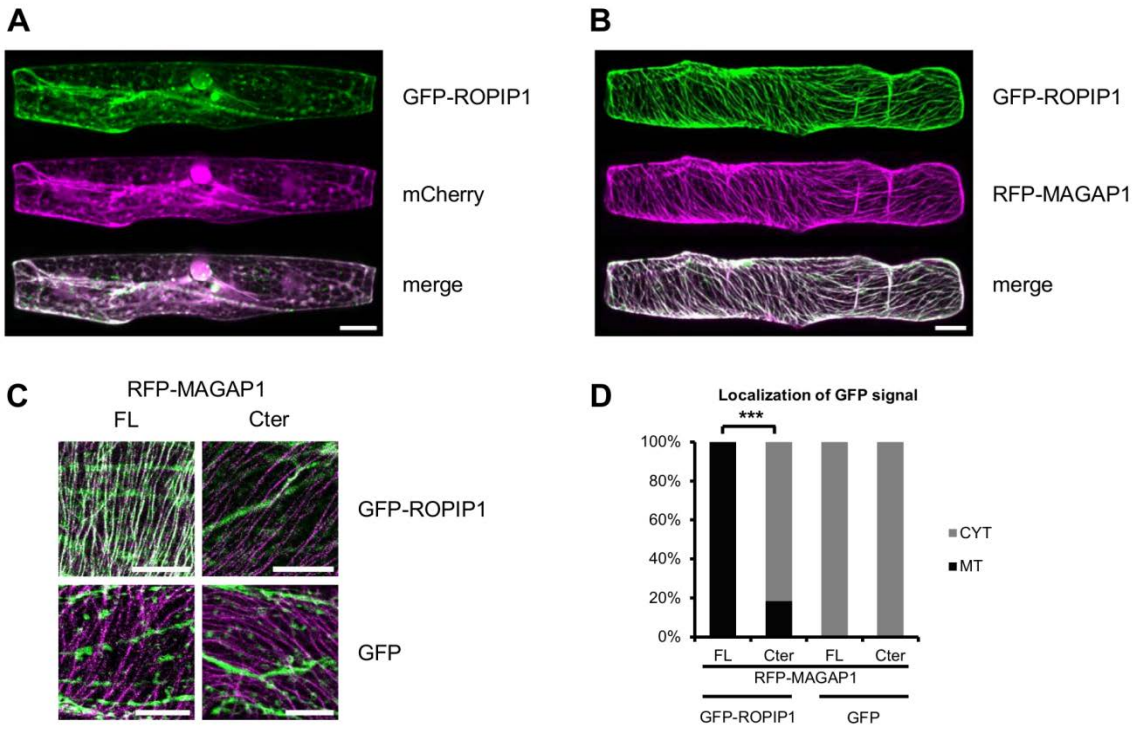

Figure 5: Co-expression of RFP-MAGAP1 recruited GFP-ROPIP1 to cortical microtubules (MTs). (A) GFP-ROPIP1 was localized in the cytoplasm and nucleoplasm as well as in moving dot-like structures. A maximum projection of a microprojectile transformed barley epidermal cell imaged with confocal laser scanning microscopy is shown. The cytoplasm and nucleoplasm was marked with co-bombarded mCherry fluorescence protein. (B) GFP-ROPIP1 got recruited to cortical MTs upon co-expression of MT-associated barley RFP-MAGAP1 fusion protein. Co-localization is indicated by white color in the merge picture. A maximum projection of a whole cell confocal laser microscope scan of a transiently transformed barley epidermal cell is shown. (C) Representative depiction of ectopically expressed fusion protein combinations used for quantitative analysis in D. FL: full-length, Cter: C-terminus. RFP-fluorescence is shown in mangenta, GFP fluorescence in green. Maximum projections of 10 optical sections à 2 µm of confocal laser microscopy imaged transiently transformed barley epidermal cells are shown. (D) Quantification of combinations as shown in C. Relative frequencies of GFP signals being located at MT or not are shown. CYT: cytoplasmatic localization of GFP signal. Cortical MT association of GFP-ROPIP1 depended on full-length (FL) MAGAP1 protein. The MT binding C-terminus of MAGAP1 (Cter) alone significantly abolished GFP-ROPIP1 MT association ($X^2 = 83.72$; $\alpha = 0.001$; df = 1; n = 61, 60, 53, 57 cells from left to right). *** $p \leq 0.001$ (X^2). Scale bars in A, B, C are 20 µm. All fusion proteins were expressed under control of 35S promoters.

Subcellular localization of transiently in barley epidermal cells expressed GFP-ROPIP1 fusion constructs showed GFP-ROPIP1 to be located in the cytoplasm and nucleoplasm when expressed together with cytoplasm and nucleoplasm marker proteins, like mCherry. In most cells GFP-ROPIP1 was also seen in freely floating dot-like structures of varying size, likely derived from aggregate formation of GFP-ROPIP1. The density of dot-like structures ranged from absent to dot-like structures only with most cells showing a few dot-like structures. Figure 5 A depicts an intermediate cell uniting cytoplasmic GFP-ROPIP1, dot-like structures in medium abundance, as well as smaller dot-like structures and one bigger aggregation of GFP-ROPIP1.

Upon transient co-expression of GFP-ROPIP1 together with the microtubule associated RACB antagonist RFP-MAGAP1 (see Introduction), GFP-ROPIP1 subcellular localization changed strikingly. GFP-ROPIP1 was recruited to cortical MT where it co-located with RFP-MAGAP1. Some cells as exemplary depicted in Figure 5 B showed almost complete recruitment of GFP-ROPIP1 to cortical MT, with GFP-ROPIP1 being absent from the nucleoplasm and the cytoplasm whereas in most cells a portion of GFP-ROPIP1 remained in the cytoplasm and nucleoplasm. An obvious next question was whether GFP-ROPIP1 recruitment to cortical MTs was MAGAP1-dependent.

Leaf segments of barley primary leaves were ballistically transformed with pGY1 [Schweizer et al. 1999] plant expression vectors containing 35S-driven fusion constructs coated to goldparticles. Imaging of transiently transformed barley epidermal cells was done with confocal laser scanning microscopy. Z-stacks of whole cells in 2 µm increments were generated and analyzed in maximum projection. All scans of this experiment were performed in sequential scan mode. GFP-ROPIP1 or GFP as control were co-bombarded with RFP-MAGAP1 or RFP-MAGAP1-Cter, respectively (Figure 5 C). RFP-MAGAP1-Cter is a truncation mutant consisting only of the MT-binding C-terminus of MAGAP1 fused to RFP. RFP-MAGAP1-Cter does not change susceptibility and does not interact with barley ROPs. Currently, it constitutes the best suitable MT-marker protein in barley [Hoefle et al. 2011]. Imaging was done at 12 – 24 hat.

Co-transformation of GFP-ROPIP1 and RFP-MAGAP1 confirmed recruitment of GFP-ROPIP1 to cortical MTs by RFP-MAGAP1. By contrast, GFP-ROPIP1 remained in its

cytoplasmic localization and was only rarely seen at cortical MTs labeled by RFP-MAGAP1-Cter. GFP, when co-expressed with RFP-MAGAP1 or RFP-MAGAP1-Cter was exclusively seen in the cytoplasm and nucleoplasm (Figure 5 C).

The subcellular localization of the GFP signal of all combinations was quantified. Maximum projections of the GFP-channel pictures were analyzed obtained from three independent experiments. At least 50 images of each combination were used for analysis. It was distinguished between the GFP signal being located at cortical MTs or being absent from cortical MTs but located in the cytoplasm. The relative frequency of the GFP signal being located at cortical MTs was calculated for each combination. It was 100 % for GFP-ROPIP1 plus RFP-MAGAP1, 18% for GFP-ROPIP1 plus RFP-MAGAP1-Cter and 0 % for GFP plus RFP-MAGAP1 or RFP-MAGAP1-Cter. The distribution of absolute values of the categories MT localization and no MT localization of the GFP signal of the combinations GFP-ROPIP1 plus RFP-MAGAP1 was compared to the combination GFP-ROPIP1 plus RFP-MAGAP1-Cter in a X^2 test ($X^2 = 83.72$; df = 1; $n_{RFP\text{-}MAGAP1} = 61$; $n_{RFP\text{-}MAGAP1\text{-}Cter} = 60$) and found to be significant at $\alpha = 0.001$ (***).

This indicated that recruitment of GFP-ROPIP1 to cortical MT depended on full-length MAGAP1 including its CRIB ROP binding domain and GAP ROP regulating catalytic domain and that GFP-ROPIP1 was not recruited to MT on its own.

2.6 ROPIP1-YFP^N and CA RACB-YFP^C Interact *in planta* Meeting at Microtubules

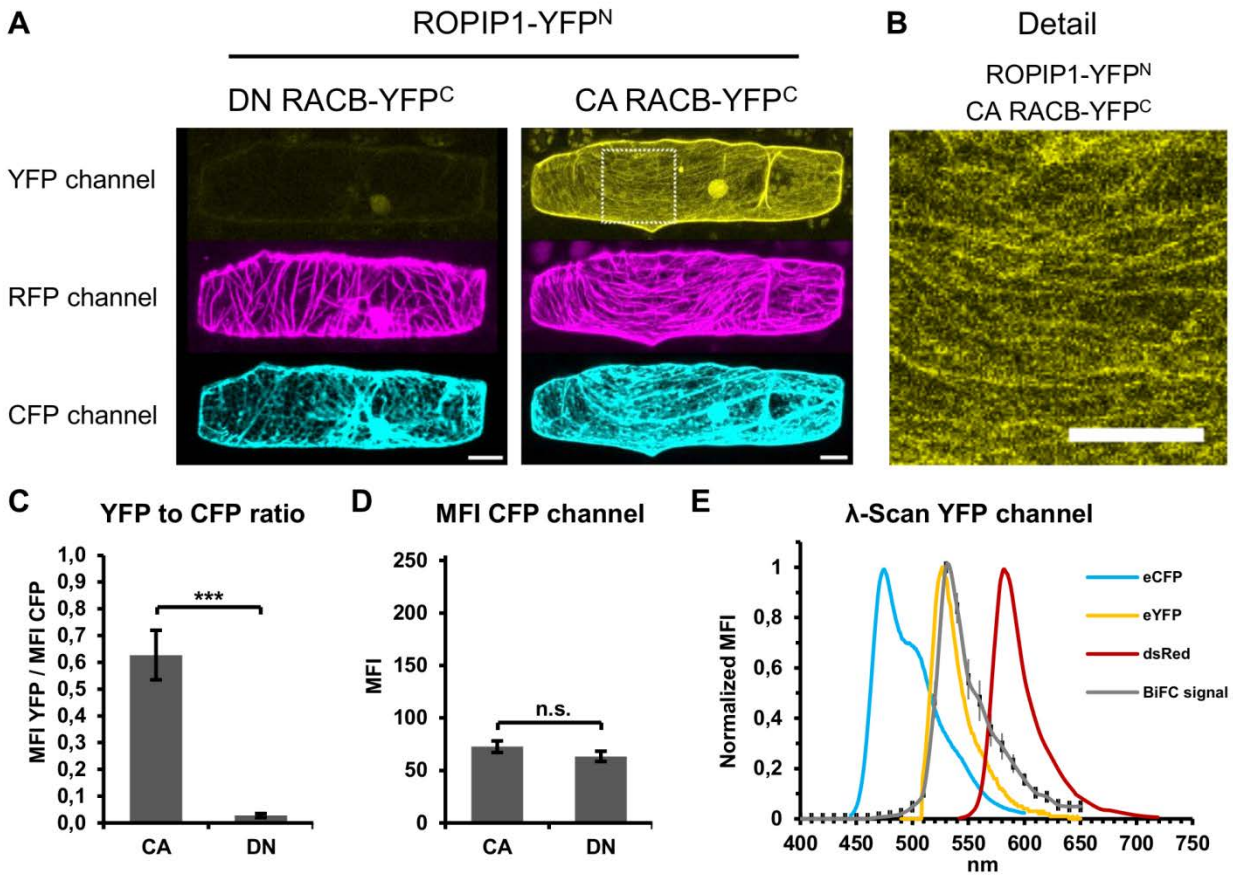

Figure 6: Split YFP Bimolecular Fluorescence Complementation (BiFC) assay. (A) ROPIP1-YFP^N was transiently co-expressed with DN (left) or CA (right) RACB-YFP^C, the catalytic inactive RFP-MAGAP1 R185G mutant and CFP as transformation marker in barley epidermal cells. Micrographs of confocal laser scanning microscopy whole cell maximum projections are shown. (B) Detail picture of the ROPIP1-YFP^N and CA RACB-YFP^C co-expressing cell from A. The depicted area is marked by dashed lines in A. A maximum projection of 10 optical sections à 2 µm from the adaxial cell border is shown. Scale bars in A and B are 20 µm. (C) A Mean Fluorescence Intensity (MFI) YFP to MFI CFP ratio was calculated for each cell after subtracting the background fluorescence in each channel. The depicted mean MFI YFP / MFI CFP ratios of each 45 CA RACB-YFP^C (CA) and DN RACB-YFP^C (DN) co-expressing cells of 2 independent repetitions were compared in a two-sided Student's t-test (p = 5.26E-09, *; p ≤ 0.001). Error bars are ± S.E.. (D) The MFIs of the CFP channel of CA RACB-YFP^C (CA) and DN RACB-YFP^C (DN) co-expressing cells were calculated from 45 cells of each combination obtained from 2 independent repetitions and compared in a two-sided Student's t-test (p = 0.20, n.s.: not significant at p ≤ 0.05). The CLSM picture would be fully saturated at a maximum MFI of 255. Error bars are ± S.E.. (E) The normalized mean MFI of three independent lambda scans in 10 nm increments of the YFP channel (BiFC signal) is shown together with the emission spectra of eCFP (blue), eYFP (yellow) and dsRED (red). The BiFC signal peaked at 530 nm. The emission maximum of eYFP is 527 nm. Error bars are ± S.E..**

ROPIP1 interacted with CA RACB but not MAGAP1 in targeted Y2Hs (see above). CA RACB interacted with MAGAP1 in yeast and *in planta* [Hoefle et al. 2011]. GFP-ROPIP1 was recruited to cortical MT upon co-expression of RFP-MAGAP1. This raised the question at what subcellular localization an interaction of ROPIP1 with CA RACB in combination with MAGAP1 might take place.

A split YFP Bimolecular Fluorescence Complementation (BiFC) assay with ROPIP1 fused to the N-terminal YFP part (YFP^N) and CA or DN RACB fused to the C-terminal part of YFP (YFP^C) combined with co-expression of RFP-MAGAP1 R185G was chosen to answer the question. The BiFC pair vectors pUC-SPYNE (YFP^N) and pUC-SPYCE (YFP^C) [Walter et al. 2004] with ROPIP1 fused to YFP^N and CA RACB, respectively DN RACB as negative control, fused to YFP^C were co-transformed with pGY1-RFP-MAGAP1-R185G and pGY1-CFP as transformation marker into barley epidermal cells (7 d old) via particle bombardment [Schweizer et al. 1999]. The catalytic inactive RFP-MAGAP R185G mutant [Hoefle et al. 2011] was chosen as co-expression together with GFP-ROPIP1 had a less severe effect on MT network organization (see below) while not influencing *in planta* interaction of CA RACB with MAGAP1 [Hoefle et al. 2011] or GFP-ROPIP1 recruitment to cortical MTs (see Figure A 3, Appendix). Transformed barley epidermal cells were imaged with confocal laser scanning microscopy at 48 hat. All cells were scanned with identical and fixed hardware and software settings. The laser scans were performed frame by frame, meaning each optical section was scanned independently with individual emission and detection settings for each fluorophore one after the other but combined in one file to counter possible cross-excitations of fluorophores. Whole cells were scanned as z-stacks in 2 µm increments and analyzed as maximum projection. A region of interest (ROI) was drawn as longitudinal line from cell to cell border. The nucleus was excluded. A second, copy-pasted, ROI was placed close to the cell in the surrounding background. The Mean Fluorescence Intensities (MFI) along the ROI lines of the YFP and CFP detector channel were determined by the Leica Application Suite Advanced Fluorescence (LAS AF version 2.5.1.6757) software quantification tool. The MFI of the background, which was mainly scattered mesophyll auto-fluorescence and other scattered light, was subtracted for each cell. The resulting cell-specific MFI of the YFP channel was divided by the cell-specific MFI of the CFP

channel for normalization, which resulted in an YFP to CFP MFI ratio for each cell. YFP/CFP ratios of n = 45 cells each in both combinations derived from two independent repetitions of CA RACB-YFP^{C} and DN RACB-YFP^{C} co-expressing cells were compared in a two-sided Student's t-test. The mean YFP/CFP ratio of 0.63 of CA-RACB-YFP^{C} co-expressing cells was highly significant (p = 5.26E-09, ***; p ≤ 0.001) different from the mean YFP/CFP ratio of 0.03 of DN-RACB-YFP^{C} co-expressing cells (Figure 6 C). Additionally, the means of CFP cell-specific MFIs of CA RACB-YFP^{C} and DN RACB-YFP^{C} co-expressing cells were statistically indistinguishable (two-sided Student's t-test; p = 0.20) showing that evenly bright fluorescing cells were used for analysis (Figure 6 D). Hence, a protein-protein interaction of CA RACB and ROPIP1 but not of DN RACB and ROPIP1 was observed *in planta*. This confirmed the results of the targeted Y2H *in planta*.

In each of the CFP, RFP and YFP detector channels, it was observed an individual fluorescence pattern. The co-expressed transformation marker CFP located to the cytoplasm and nucleoplasm. RFP-MAGAP1-R185G located predominantly to cortical MTs, weakly to the cytoplasm and occasionally to the nucleoplasm. Noticeably, RFP-MAGAP1-R185G was not obviously recruited to the PM upon co-expression of CA RACB-YFP^{C} as it was reported for CA RACB in combination with GFP or RFP-tagged MAGAP1 or RFP-MAGAP1-R185G which was also substantiated by a significant FRET efficiency of CFP-CA RACB and YFP-MAGAP1 [Hoefle et al. 2011]. This might indicate a sterical hindrance of an YFP^{C} fusion to CA RACB, alternatively an effect of ROPIP1 in fixing MAGAP1 to MTs, or something else. The BiFC signal in the YFP detector channel when ROPIP1-YFP^{N} was co-expressed with CA RACB-YFP^{C} was typically observed as being evenly distributed at the cell periphery, which indicated the PM, at cortical MTs marked by RFP-MAGAP1-R185G, in the nucleus and rather weakly in the cytoplasm (Figure 6 A and detail in B). The BiFC signal in DN RACB-YFPC co-expressing cells was over all very weak. In a few cells, where the BiFC signal was slightly brighter, it was exclusively seen in the cytoplasm and nucleoplasm. Hence, the specific subcellular site of *in planta* protein interaction of ROPIP1-YFP^{N} with CA RACB-YFP^{C} was observed to be a mixture of cortical MTs and likely PM localization.

The identity of the BiFC signal in the YFP detector channel was proven to be YFP by 3 in parallel performed lambda scans ranging from 400 nm to 650 nm in 10nm steps. The BiFC signals in the YFP channel peaked at 530 nm. The eYFP-emission maximum is 527 nm. No fluorescence of the BiFC signal was detected in the eCFP and dsRed emission spectra (Figure 6 E). This strongly indicated successful YFP complementation and further strengthened the BiFC signal to be true-positive.

Together, the BiFC experiment substantiated the protein-protein interaction of CA RACB with ROPIP1 *in planta*. Further, the alternative fusion of YFP^N instead of GFP to ROPIP1 confirmed the recruitment of ROPIP1 to cortical MTs by RFP-MAGAP1. It was also shown that ROPIP1, CA RACB and MAGAP1 meet at cortical MTs. ROPIP1 interacted with CA RACB at cortical MTs and likely the PM. The interaction of CA RACB and MAGAP1 at likely the PM and partially at cortical MTs was already reported by [Hoefle et al. 2011].

2.7 *Bgh* ROPIP1 has a MT Destabilizing Potential

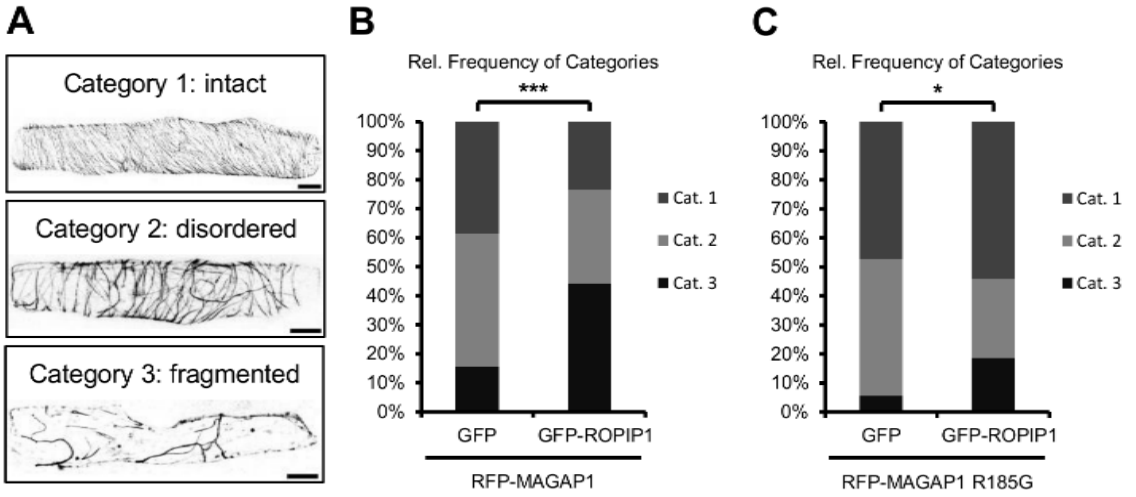

Figure 7: Co-expression of GFP-ROPIP1 and RFP-MAGAP1 promoted microtubule network destruction. (A) Example micrographs illustrating three distinguished categories of MT network organization in barley epidermal cells. Grey scale pictures were created from merged maximum projections of transiently transformed barley epidermal cells co-expressing GFP-ROPIP1 and RFP-MAGAP1 imaged with confocal laser scanning microscopy. Scale bars are 20 µm. (B) Distribution of the mean relative frequencies of the categories as depicted in A. The mean relative frequencies were obtained from n = 145 and n = 132 barley epidermal cells transiently co-expressing RFP-MAGAP1 with GFP or GFP-ROPIP1 in four independent repetitions. The distribution of the categories was highly significant different between the GFP control and GFP-ROPIP1 expressing cells (* $p \leq 0.001$; $\chi^2 = 27.92$; df = 2). (C) Microtubule-associated RFP-MAGAP1 was replaced by its catalytic inactive mutant RFP-MAGAP1-R185G in n = 59 GFP-ROPIP1 and n = 53 GFP co-expressing barley epidermal cells in 3 independent repetitions (* $p \leq 0.05$; $\chi^2 = 7.11$; df = 2).**

ROPIP1 interacted with WT and CA RACB in yeast. Two RACB interacting proteins affecting MT organization are published. MAGAP1 promoted focusing of cortical MTs towards the site of *Bgh* attack. Focused MTs were significantly less observed in susceptible cells where *Bgh* succeeded in establishing a haustorium. Further, MAGAP1 over-expression opposed RACB in susceptibility as it promoted resistance of barley epidermal cells towards *Bgh*. It was suggested that focusing of cortical MTs towards the interaction site might promote resistance of barley epidermal cells towards *Bgh* [Hoefle et al. 2011]. On the other hand, TIGS of another RACB interacting protein, RBK1, lead to increased fragmentation, or destruction, of cortical MTs that was seen together with enhanced susceptibility of barley epidermal cells towards *Bgh* [Huesmann et al. 2012]. With ROPIP1 over-expression enhancing susceptibility, the question arose whether RFP-MAGAP1-dependent recruitment of GFP-ROPIP1 influences cortical MT organization.

Leaf segments of 7d old barley epidermal cells were transiently transformed via particle bombardment. RFP-MAGAP1 was co-expressed with either GFP-ROPIP1 or GFP as control. Transformed cells were imaged with confocal laser scanning microscopy at 12 – 24 hat. Whole cells were scanned as z-stacks in 2 µm increments in sequential scan mode. Maximum projections were used for analysis. The pattern of RFP-MAGAP1 labeled cortical MT organization was distinguished by three categories in accordance to Huesmann et al. [2012] and Hoefle et al. [2011]. Cells were classified as category 1 when they showed intact and well-ordered MTs in parallel arrays, as category 2 when MTs were less well ordered, randomized, loosened but mainly intact and category 3 when the MT network was destroyed or fragmented (Figure 7 A). MTs of category 3 cells mostly appeared as few remaining thick and randomly bent bundles. Onset of MT network destruction was observed to emerge around the nucleus. Values of four independent experiments were combined for analysis. This resulted in total n = 145 cells for GFP and n = 132 cells for GFP-ROPIP1 plus RFP-MAGAP1 each. The relative frequencies of each category in both variants were determined and depicted in Figure 7 B. In the control, where GFP was combined with RFP-MAGAP1 38.6 % of cells exhibited an intact MT network (category 1), 45.9 % a disordered MT network (category 2) and 15.5 % a destroyed MT network (category 3). The percentage of category 3 cells

in the control was in the same range as reported by Huesmann et al. [2012]. Replacement of GFP by GFP-ROPIP1 changed the relative frequency of categories. The relative frequency of cells exhibiting a destroyed MT network almost tripled to 44.3%, whereas 32.2 % of cells were of category 2 and 23.5 % of category 1. The absolute frequencies of categories of both variants were compared in a X^2 test (X^2 = 27.92, df = 2; $n_{GFP+RFP\text{-}MAGAP1}$ = 145; $n_{GFP\text{-}ROPIP1+RFP\text{-}MAGAP1}$ = 132) and found to be highly significantly different at α = 0.001 (***).

This suggested that GFP-ROPIP1 in combination with RFP-MAGAP1 promoted MT network loosening eventually leading to MT network destruction.

Moreover, catalytic activity of MAGAP1 seemed therefore to be beneficial, as replacement of RFP-MAGAP1 by its catalytic inactive mutant RFP-MAGAP1 R185G [Hoefle et al. 2011] in combination with GFP-ROPIP1 had a less pronounced effect in MT network destruction albeit the GFP signal was seen co-located with the RFP signal (see Figure A 3, Appendix). The relative frequency of category 3 cells also tripled from 5.7 % in cells co-expressing GFP to 18.6 % in cells co-expressing GFP-ROPIP1 albeit at a low overall level of category 3 cells. More cells of both combinations were of category 1 (GFP: 47.3 %; GFP-ROPIP1: 54.2 %) showing an intact MT network compared to RFP-MAGAP1 co-expressing cells. Data of 3 independent experiments were combined for the analysis. Total number of cells were n= 59 for GFP-ROPIP1 and n = 53 for GFP each plus RFP-MAGAP1 R185G. The mitigating effect of RFP-MAGAP1 R185G on MT network destruction might also be reflected in a less significant difference in the distribution of categories compared between the two variants. The absolute frequencies of categories of GFP-ROPIP1 co-expressing cells was significantly different from GFP co-expressing cells at α = 0.05 (*) in a χ^2 test (χ^2 = 7.11; df = 2; $n_{GFP\text{-}ROPIP1+RFP\text{-}MAGAP1\ R185G}$ = 59; $n_{GFP+RFP\text{-}MAGAP1\ R185G}$ = 53).

Together, this on the one hand provided a clue on how ROPIP1 mechanistically might contribute to susceptibility and on the other strengthened the hypothesis that one branch of activated RACB downstream proteins can modulate cortical MT organization.

2.8 *In silico* Characterization of *Bgh* ROPIP1 and *Bgh* Eg-R1

2.8.1 BLAST Searches using ROPIP1 as Query

Initial BLAST searches of Y2H clone V42A (Hoefle Caroline, Hückelhoven Ralph (TU München, Germany), Schultheiss Holger (University of Giessen, Germany), personal communication), which was later named ROPIP1, located its nucleotide sequence to the 5'-region of the *Bgh* retroelement Eg-R1 [Wei et al. 1996]. The ROPIP1 nucleotide sequence showed a short C-terminal ORF with an endogenous ATG start codon. Because of a longer ORF in frame with the activation domain of the prey vector, which might suggest requirement of the longer ORF for RACB interaction, the ROPIP1 nucleotide sequence was equipped with an ATG start codon for *in planta* expression (Hoefle Caroline, Hückelhoven Ralph (TU München, Germany), Schultheiss Holger (University of Giessen, Germany), personal communication).

The ROPIP1 nucleotide sequence (see Table A 1, Appendix) without the artificial 5' ATG was used as query sequence in BLAST searches [Altschul et al. 1997] against several databases or datasets. BLASTn search against the NCBI nr database (nucleotide collection (nr/nt)) using NCBI standard settings (Megablast) yielded six hits exclusively to the organism *Blumeria graminis*. No hits to other organisms were retrieved. Alternative usage of the full repetitive element Eg-R1 nucleotide sequence (GenBank: X86077.1) as query yielded identical hits plus one *Bgt* microsatellite aligning to the 3'-end of Eg-R1. Besides the *Bgt* microsatellite, four hits were from *Bgh* and two from *Bgt*. This indicated that ROPIP1, respectively Eg-R1, of all deposited organisms, specifically matched to the organism *Blumeria graminis* and it further indicated the presence of homologous sequences in *Bgh* and *Bgt*. The *Bgt* sequence homologous to Eg-R1 is named *Bgt*_RSX_Lie [Parlange et al. 2011]. The 647 bp *Bgt*_RSX_Lie element shares 94 % sequence identity with the annotated 687 bp Eg-R1 sequence.

The ROPIP1 and Eg-R1 nucleotide sequences were additionally used as query sequences against genomic DNA sequence contigs of the three sequenced *Bgh* races DH14, A6 and K1. The online BLAST tool of the BluGen consortium (blugen.org) was set to BLASTn algorithm with a maximum e-value of 1 (Expect threshold). The ROPIP1 query yielded 2304 hits in the DH14 reference genome (BGH DH14 Genome v3b

(contigs)), whereas the Eg-R1 query yielded 2613 hits. The hit numbers in the *Bgh* races A6 (BGH A6 Genome contigs) and K1 (Bgh K1 Genome contigs) were higher but comparable to each other. The ROPIP1 query produced 2847 hits in race A6 and 2997 hits in race K1. The hit numbers for the Eg-R1 query were 3998 in race A6 and 4003 in race K1. The real numbers might even be higher due to the high repeat content which generally aggravates complete genome assembly and the lack of a physical map of the *Bgh* genome. The contig size of the *Bgh* genome was 87.9 Mbp whereas the scaffold size was 118.7 Mbp (blugen.org). Anyhow, ROPIP1, respectively Eg-R1 multiply inserted into the genome and is present in different *Bgh* races.

Transcripts of *ROPIP1* and *Eg-R1* were amplified from cDNA generated from total RNA or mRNA isolated from *Bgh* infected barley primary leaves and verified by sequencing (data not shown). The *ROPIP1* transcript was *Bgh*-specific (Figure A 4, Appendix). The ROPIP1 and Eg-R1 nucleotide sequences matched to expressed sequence tags (ESTs) provided by the BluGen consortium (blugen.org). The online BLAST tool was set to BLASTn algorithm with a maximum e-value set to 1. The ROPIP1 nucleotide query matched to 198 hits in the BGH DH14 All ESTs dataset. The number of hits matching to the nucleotide sequence of Eg-R1 was 373. A more general NCBI nucleotide BLAST (blast.ncbi.nlm.nih.gov/Blast.cgi) using BLASTn algorithm and with ROPIP1 or Eg-R1 nucleotide sequence as query against the expressed sequence tags (est) database retrieved 125 hits for the ROPIP1 query and 181 hits for the Eg-R1 query. The number of hits specific to the organism *Blumeria graminis* f.sp. *hordei* (taxid:62688) was 99 for ROPIP1 and 134 for Eg-R1 as query. The ROPIP1 query additionally matched to the organisms *Hordeum vulgare* (barley), *Triticum aestivum* (bread wheat) and *Lolium multiflorum* (Italian rye-grass). The Eg-R1 sequence matched to the same additional organisms plus to *Avena barbata* (slender wild oat). All hits in other organisms were monocots of the *Poaceae* family. This may point to that Eg-R1 homologous elements are generally active in powdery mildews of *Poaceae* grasses. The ROPIP1 query further retrieved at least 100 hits in RNAseq raw sequence data from *Bgh* race A6 grown on the susceptible *Arabidopsis thaliana* triple mutant Columbia-0 *pen2-1 pad4-1 sag101-2* [Hacquard et al. 2013] which is otherwise a non-host of *Bgh*. The sequence read archive (SRA) experiment set SRX160966 [Hacquard et al. 2013] deposited at the NCBI

Sequence Read Archive was searched against the ROPIP1 query using the Sequence Read Archive Nucleotide BLAST online tool with BLASTn algorithm and maximum e-value set to 1.

Together this substantiated that the ROPIP1, respectively Eg-R1 sequence gets transcribed and that it is specific for *Bgh* and not for barley. Further, an Eg-R1 homologous element, *Bgt*_RSX_Lie [Parlange et al. 2011] can be found in genomic sequences of the close *Bgh* relative wheat powdery mildew fungus *Bgt* and homologous elements might also be present in further powdery mildews of *Poaceae*.

2.8.2 *In silico* Characterization of the Eg-R1 Element

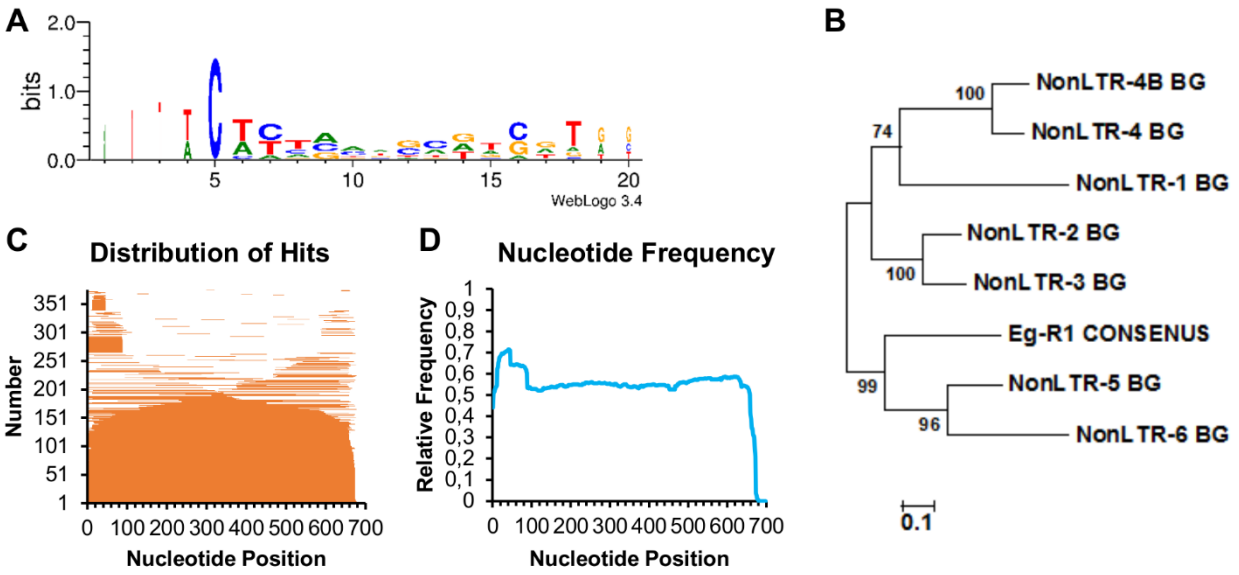

Figure 8: (A) Weblogo of Eg-R1 accompanied Target Side Duplications (TSDs) generated from a multiple alignment of 25 genomic insertions of Eg-R1. (B) Phylogenetic tree of 7 *Blumeria graminis* Non-LTR retrotransposons (NonLTR_BGs) plus Eg-R1 CONSENSUS which replaced EGRT1 Non-LTR Retrotransposon deposited in Repbase. EGRT1 Non-LTR Retrotransposon is identical in sequence to the Eg-R1 annotation (GenBank: X86077.1). NonLTR-4_BG and NonLTR-4B_BG are identical to previously reported Egh24I and Egh24II. The tree was calculated using the Maximum Likelihood method and 500 rounds of bootstrapping. Bootstrap support for each node is given at each node. The branch length mirrors substitutions per site as indicated by the scale. (C) Distribution of genomic insertions of Eg-R1 along the query Eg-R1 annotation (GenBank: X86077.1) which was extended with a newly identified 11 bp nucleotide stretch at the 5'-end. Hits were obtained from 376 BLASTn hits representing the topmost 100 *Bgh* genomic contigs from the output. The insertions were sorted by length. (D) Relative nucleotide frequency of the query sequence from C. The frequency of each nucleotide position was divided by the number of insertions which was 376.

Eg-R1 generally was referred to as SINE [Parlange et al. 2011; Pedersen et al. 2012] but it was also doubted whether it constitutes a classical SINE [Wei et al. 1996]. A small subset of genomic insertions of the Eg-R1 element was analyzed in order of getting an impression of the nature of the element as knowledge about Eg-R1 is very sparse.

The annotated Eg-R1 mRNA sequence (GenBank: X86077.1) of 687 bp was used as query sequence in a BLASTn search against the Bgh DH14 reference genome database BGH DH14 Genome v3b (contigs) using the BluGen online BLAST tool. The sequences of the topmost 25 hits were manually extracted from the respective 25 contigs. A first observation was that on almost every analyzed contig Eg-R1 was present as one full-length insertion plus a number of additional truncated insertions that varied in number and size (see below). Next, all Eg-R1 insertions were extracted with 100 bp upstream and downstream sequence extensions and manually searched for Target Site Duplications (TSDs). TSDs are short stretches of an identical nucleotide sequence that surround the insertion and that arose from the insertion mechanism of non-LTR retroelements that is referred to as target primed reverse transcription [Ostertag and Kazazian Jr 2001; Han 2010; Levin and Moran 2011]. In brief, the Long Interspersed Element (LINE) ORF2 protein has dual functionality as endonuclease and reverse transcriptase. A DNA single strand nick is generated by its endonuclease activity. The 3’-OH primes the reverse transcriptase activity of the ORF2 protein. Restriction enzyme-like sticky ends result in TSDs. Non-autonomous SINEs are thought to make use of the LINE retrotransposition machinery. Interestingly, TSDs were found nearly exclusively with the longest insertions of Eg-R1 whereas shorter insertions of Eg-R1 in almost all cases lacked TSDs. The 25 TSDs of Eg-R1 varied from 7 to 16 bp in length with a mean length of 12.44 ± 2.53 bp (Mean ± STD) and were of individual sequence composition. A multiple alignment file of the TSDs was created with ClustalW2 [Larkin et al. 2007; Goujon et al. 2010] which was used to create a weblogo [Crooks et al. 2004]. Only one cytosine nucleotide at position 5 of the multiple alignment was conserved (Figure 8 A). This may point to usage of an endonuclease with some target site specificity albeit not to a degree like human LINE L1 ORF2 protein which has a pronounced target site specificity for the sequence motif 5’-TTAAA-3’. Human L1 orthologues in zebrafish grouped into one clade exhibiting target site specificity like human L1, whereas one

other clade showed relaxed target site specificity likely due to evolution [Ichiyanagi et al. 2007]. Eg-R1 might rather make use of an endonuclease with relaxed target site specificity.

DNA sequences bordered by TSDs and being longer than 670 bp, which were in sum 23, were used to determine the full length of the Eg-R1 element. Their length was 678.26 ± 4.85 bp. They were aligned with ClustalW2 [Larkin et al. 2007; Goujon et al. 2010]. A consensus sequence was created from the multiple alignment file with GeneDoc [Nicholas et al. 1997]. The 670 bp Eg-R1 CONSENSUS sequence was 93 % identical to the annotated 687 bp Eg-R1 mRNA sequence (GenBank: X86077.1). Besides 6 SNPs after the 5´-ROPIP1 sequence part, the Eg-R1 CONSENSUS sequence differed from the annotated Eg-R1 mRNA sequence at both, the 5'-end and the 3'-end. Additional 11 nucleotides (5'-GGGGGACTATT-3') precede the Eg-R1 CONSENSUS 5'-end which are absent in the annotated Eg-R1 mRNA sequence. This 5'-extension of the Eg-R1 nucleotide sequence was also seen in the sequences of 5'-RACE PCR products with ROPIP1-specific primers (see exemplary sequence in Table A 1, Appendix) and in sequences of some prey clones of the initial Y2H screen with RACB (CA and WT) as bait (Hoefle Caroline, Hückelhoven Ralph (TU München), Schultheiss Holger (University of Giessen, Germany), unpublished data personally communicated). Hence, the 5'-GGGGGACTATT-3' 5'-end is an integral part of the Eg-R1 sequence which is missing in the Eg-R1 annotation (GenBank: X86077.1). The 3'-end of the genomic Eg-R1 CONSENSUS sequence is missing the poly(A) tail. Posttranscriptional polyadenylation of the Eg-R1 transcript was suggested by [Wei et al. 1996] and the presence of a polyadenylated Eg-R1 transcripts was confirmed by usage of Oligo(dT) 3'-primers in course of this study (data not shown). The Eg-R1 CONSENSUS sequence lacked 6 nucleotides directly upstream of the poly(A) tail of the Eg-R1 mRNA annotation. A little size variation at the very 3'-end of full-length Eg-R1 insertions was observed to be common.

A small family of 8 members of *Blumeria graminis* Non-LTR retrotransposons (BG_Non-LTRs) including Eg-R1 (EGRT1 Non-LTR Retrotransposon) as well as Egh24I and Egh24II (NonLTR-4_BG and NonLTR-4B_BG), another previously described SINE-like element of *Bgh* [Rasmussen et al. 1993], that share 35 % overall pairwise identity was

found in Repbase Reports (2011, Volume11, Issue 9, Jurka et al. [2005]). A phylogenetic tree was computed using the Maximum Likelihood method and 500 rounds of bootstrapping (Figure 8 B). Eg-R1 CONSENSUS and EGRT1 Non-LTR Retrotransposon (phylogenetic tree not shown) were closest related to NonLTR-5_BG and NonLTR-6_BG. EGRT1 Non-LTR Retrotransposon and BG_NonLTR-5 were similar at their 5'-ends. They shared 73 % pairwise identical residues in their first 100 bp. The percentage of pairwise identical residues within their 5' ends first 100 bp rose to 93 % when the Eg-R1 CONSENSUS sequence as deciphered in this work was used instead of the annotated Eg-R1 mRNA sequence. The first 88 bp of EGRT1 Non-LTR Retrotransposon and NonLTR-5_BG were, besides a single SNP, identical. NonLTR-5_BG is 914 bp in length and thus 244 bp longer than Eg-R1 CONSENSUS or 227 bp longer than the annotated Eg-R1 mRNA sequence. Following their nearly identical 5'-ends the sequences of both aligned scattered with insertions ranging from single nucleotides to stretches of more than 20 nucleotides provided by both elements. All BG_Non-LTR retroelements still shared ~56 % pairwise identity within the first 100 bp of their 5'ends (see Table A 2, Appendix). Wei et al. [1996] reported a stretch of nearly identical 31 nucleotides shared at the 5'-ends of Eg-R1, Egh24I and Egh24II. This 31 nucleotides are to 71 % pairwise identical in all 8 BG-Non-LTR family members. Together, this may point to evolutionary diversification of Eg-R1 related elements currently represented by the small BG_Non-LTR family.

A closer look was taken on the unequal insertion sizes of the Eg-R1 element. The annotated Eg-R1 mRNA sequence was equipped with the 5'-end as determined in this work. The resulting 698 bp query was used for a BLASTn search against the BGH DH14 Genome v3b (contigs) database of the *Bgh* reference genome (blugen.org). The hit ranges along the query sequence of the topmost 100 retrieved hits on individual contigs, which were 376 individual hits, were used for analysis. The individual hit lengths were sorted by size and depicted in relation to their position on the Eg-R1 query sequence (Figure 8 C). 75 of 376 hits (19.94 %) were greater or equal 670 bp. When taking the experience from the TSD search into account most of these insertions probably are surrounded by TSDs. The mean insertion size was 376.00 ± 270.56 (Mean ± STD) bp. The maximum insertion length was 679 bp, the shortest hit was 21 bp. The frequency of

individual nucleotides was calculated (Figure 8 D) by assigning ‘1’ for presence and ‘0’ for absence to every hit nucleotide compared to the query sequence. The sum for each nucleotide of the query was divided by the total number of insertions, which was 376. The increased nucleotide frequency within the first 5’ 88 nucleotides is likely due to the high sequence similarity of this sequence part with BG_NonLTR-5 (see above). The remaining nucleotides were rather evenly distributed. This pointed to that the incomplete Eg-R1 insertions unlikely resulted from an interrupted insertion process as known from 5’-truncated LINE element insertions [Pavlíček et al. 2002]. Further, seemingly no region of the Eg-R1 element was preferably inserted. It may be possible that individual full-length insertions of Eg-R1 were split by unequal crossing over. Pedersen et al. [2012] suggested Eg-R1 to provide hot spots for unequal crossing-over. Given the proportion of incomplete insertions that typically also lacked TSDs, the frequency of unequal crossing-over events in the *Bgh* genome would be quite high. Alternatively, the incomplete insertions may represent remainders of ancient insertions that have been silenced for the most part by accumulating point mutations over time.

Classical SINEs are of a tripartite structure. Their 5’-heads are derived from tRNA, 7SL RNA or 5S RNA which are followed by a body sequence of unknown origin. Many 3’-tail regions of SINEs share a common sequence with the 3’-end of LINEs from where it is supposed to be derived of. SINE/LINE pairs have been identified by their common 3’-end. The 3’-end of LINEs constitutes a 3’-UTR that is believed to be required for the initiation of first strand synthesis by the LINE ORF2 protein. It is further believed, that corresponding SINEs make use of their partner LINE ORF2 protein which is mediated through their common 3’-end [Ohshima and Okada 2005; Ohshima 2013].

Figure 9: Exemplary genomic sequence of the Eg-R1 retroelement. The insertion was extracted from contig CAUH010023330 at nucleotide position 34805-35675 from the *Bgh* genome (blugen.org). The surrounding genomic sequence is stroked-through. Likely retrotransposition-derived target site duplications (TSDs) are highlighted in orange. The newly identified 5'-end extension of 11 bp of Eg-R1 is highlighted in green. Nucleotides identical to Eg-R1 are underlined. Nucleotides identical to ROPIP1 are shaded in grey. A SINE-like region follows the ROPIP1 sequence part. Putative A- and B-Box-like sequences are shaded in yellow and turquoise. A-Box and B-Box pol III promoter consensus sequences [Marck et al. 2006] are given below the respective nucleotides. Matching nucleotides are in bold-type. Note that the putative A- and B-Box-like sequences are overlapping at one nucleotide highlighted in green. A putative tRNA-related sequence region is highlighted in violet. A region similar to a V-domain, which can be found in some SINEs, follows and is highlighted in blue. T-stretches (Oligo(T)) that terminate pol III transcription are in bold-type. A likely functional polyadenylation (Poly(A)) signal is indicated in bold-type near the 3'-end of Eg-R1.

The SINE2-1_BG /Tad1-24_BG LINE pair of *Bgh* was identified [Ohshima 2012] in the Repbase reference database of repetitive DNA elements [Jurka et al. 2005]. A local BLASTn search performed in analogy to Ohshima [2012] using the last 100 bp of the SINE2-1_BG element as query against the RepBase20.01 database yielded, besides SINE2-1_BG, Tad1-24_BG as topmost hit (e-value 2e-006) and 4 further Tad1 LINEs sharing a conserved stretch of 30 nucleotides with SINE2-1_BG at their 3' regions. No such a hit with a sufficient score or e-value was produced when the last 3'-end 100 bp of Eg-R1 were used as query instead. Although the 100 bp 3'-end of Tad1-24_BG aligned scattered to the 3'-region of Eg-R1 in a direct sequence comparison the alignment score was pretty poor. Repeat elements identified in the taxon *Blumeria graminis* were retrieved from Repbase Update [Jurka et al. 2005] and used as alternative database in a local BLASTn search. This delimited search also did not identify an autonomous retroelement sharing 3'-tail sequence similarity with the last 100 bp of the 3'-tail of Eg-R1. Therefore it was not possible to identify a corresponding to Eg-R1 autonomous retroelement which might assist non-autonomous Eg-R1 retrotransposition as it is known for a wide range of SINE/LINE pairs of different species [Ohshima 2013]. It does not exclude that Eg-R1 might engage a LINE ORF2 protein for retrotransposition. Human L1 LINEs share no sequence similarity with Alu SINE elements in their tail region but recognize Alu elements by their poly(A) tails which also leads to processed pseudogene formation by LINE ORF2 proteins [Ohshima 2013]. Alternative usage of full-length Eg-R1 as query against the set of all known *Blumeria graminis* repeats in a local BLASTn search neither identified a corresponding autonomous retroelement by sequence similarity.

Next, SINE2-1_BG and Eg-R1 were analyzed in regard to classical SINE characteristics using SINE Base [Vassetzky and Kramerov 2012] and its recommended protocol for SINE analysis. SINE2-1_BG was classifiable as classical SINE. Its 5'-head region matched to a tRNA-Val. Further, A-Box and B-Box pol III promoter consensus sequences, as determined for *Saccharomycetes* of the *Ascomycota* phylum [Marck et al. 2006] characteristically matched to the t-RNA related region of SINE2-1_BG. The body part of many SINEs is unique. None of four known and in SINE Base-deposited body-part domains (sines.eimb.ru) matched to SINE2-1_BG. The tRNA-related 5'-head region

together with the sequence similarity with Tad1-24_BG LINE at its 3'-tail region (see above) supported SINE2-1_BG being a classical SINE element. This suggestion was not possible for Eg-R1. A single tRNA-Gln (tdbD00008587|Homo_sapiens|9606|Gln|CTG) of the RNA Base database (sines.eimb.ru) matched to the Eg-R1 sequence with 63.9 % identity in a 61 nucleotide overlap, but beginning with nucleotide position 285. Further, A-Box and B-Box consensus sequences [Marck et al. 2006] aligned to that t-RNA region. The putative A-Box and B-Box motifs followed each other directly without interspacing nucleotides. This possibly t-RNA related region located amid the sequence of Eg-R1 interfered with Eg-R1 being a classical SINE as these are pol III transcribed which depends on the 5' tRNA related head sequence. Interestingly, a V-domain identified in body-parts of SINEs of fishes [Ogiwara et al. 2002], which constitutes one of four known conserved domains of the body sequence of classical SINEs, matched to the Eg-R1 sequence 3'-adjacent to the tRNA-Gln-related region of Eg-R1. This pattern may point to that the Eg-R1 sequence starting with nucleotide position 285 showed some relatedness to classical SINEs. However, Eg-R1 as concluded by Wei et al. [1996] is likely pol II transcribed, as internal T-stretches would stop pol III transcription prematurely. Pol III transcription likely would result in a short transcript of ~ 120 bp. It may be conceivable that an ancient read-through of a pol II transcript picked up an ancient SINE element such that the ROPIP1 sequence is followed by a SINE element on a single transcript. In this scenario the SINE properties of the newly formed element would have distributed that chimeric transcript.

SINE elements are further distinguished whether they carry an intrinsic terminator sequence for pol III transcription or not. T^- SINEs carry no intrinsic poly (T) terminator sequence and transcription is not stopped until pol III meets a T-stretch by chance in the downstream sequence. In contrast, T^+ SINEs carry pol III terminator signals at their 3'-end. Many T^+-SINEs get post-transcriptionally poly-adenylated. Their 5'-AAUAAA-3' poly-adenylation signal is placed closely upstream of their pol III terminator. Again Eg-R1 did not fit into that categories defined for classical SINEs. It does carry a 5'-AAUAAA-3' poly-adenylation signal [Wei et al. 1996] at nucleotide positions 641-646 close to its 3'-end. Further, the signal seemed to be functional. Wei et al. [1996] identified Eg-R1 from an mRNA preparation. Similarly, cDNA synthesis for construction

of the Y2H library started from poly(A)-RNA [Hoefle et al. 2011] and the original prey clones contained poly(A)-tails. In course of this work, Eg-R1 was PCR-amplified using a 5'-gene-specific primer and an 3'-anchored Oligo(dT) primer from total RNA preparation derived cDNA of *Bgh*-infected barley primary leaves. Further, Eg-R1 was identified in 5'-RACE PCRs using mRNA isolations prepared from *Bgh*-inoculated barley primary leaves for cDNA synthesis. The obtained Eg-R1 amplicons of both experiments were verified by sequencing. Functionality of the poly-adenylation signal was indicated by the absence of poly (A) stretches in genomic insertion of Eg-R1 as deciphered in this work (see Table A 1, Appendix, for consensus sequence of genomic Eg-R1 insertions). Whatever mechanism Eg-R1 may make use of for its insertion into new genomic regions, the mechanism might differ from processed pseudogene-formation by LINE ORF2-protein, as those have inserted with their poly (A) tails [Kazazian 2014]. However, the poly-adenylation signal of Eg-R1 is placed 240 bp downstream of the first of multiple poly (T) stretches in the Eg-R1 sequence. This further strengthened the assumption of pol II transcription of Eg-R1 and separated Eg-R1 further from classical SINEs.

Together, these findings state that Eg-R1 does not fit all criterions of classical SINEs. The nature of the Eg-R1 retroelement remained therefore obscure. Eg-R1 shared the characteristics short sequence length and absence of major ORFs with SINEs. From that one can conclude that it is very likely a non-autonomous element. But Eg-R1 is likely pol II transcribed and differs in architecture from classical SINEs. Wei et al. [1996] suggested ROPIP1 to be a novel class of retroposons. This view was supported by the findings in this work.

2.8.3 *In silico* Characterization of the ROPIP1 Nucleotide Sequence

Not only Eg-R1 differed from classical SINEs but also ROPIP1 from classical effectors or effector candidates. Effector candidates typically are identified through predicting signal peptides and the absence of transmembrane (TM) domains in their sequences of relatively short size by bioinformatics.

Absence of TM domains was indicated by HMMTOP [Tusnády and Simon 1998] and PHOBIUS [Käll et al. 2004] by submitting the ROPIP1 amino acid query to the Quick2D webserver of the MPI bioinformatics toolkit [Biegert et al. 2006]. PHOBIUS [Käll et al.

2004] is a combined tool that also includes a signal peptide prediction, which was negative for the ROPIP1 query. The ROPIP1 sequence also had a negative signal peptide prediction using the SignalP 4.1 server [Petersen et al. 2011]. Recently, Liu et al. [2014] reported on two effectors of *Phytophtora sojae* (*P*. *sojae*) and *Verticillium dahliae* (*V*. *dahliae*) that act as isochorismate synthase interfering with host SA-mediated defense. Interestingly, both were predicted to lack signal peptides but to be secreted by non-classical pathways. ROPIP1 and ROPIP1-Cter both had a good SecP score for non-classical secretion of 0.835 and 0.821 (threshold = 0.5) using the SecretomeP 2.0 server [Bendtsen et al. 2004a] analogous to Liu et al. [2014]. The SecP scores of ROPIP1 and ROPIP1-Cter were higher than that of the unconventionally secreted effector VdISC1 (SecP score = 0.66) of *V*. *dahliae* and equaled that of PsISC1 (SecP score = 0.81) of *P*. *sojae*.

However, the ROPIP1 sequence as inherited by Eg-R1 additionally lacked a classical ATG start codon at its 5'-end but one amid its sequence that would give rise to a ROPIP1-Cter peptide. The aim here was to inspect genomic insertion of Eg-R1 in terms of chimeric ORF formation that would equip ROPIP1 with a classical in frame ATG start codon and/or a signal peptide for classical secretion via the endomembrane system. The ROPIP1 nucleotide sequence was used as query sequence against the BGH DH14 Genome v3b database of *Bgh* genomic DNA contigs (blugen.org) in a BLASTn search. The topmost 45 hits were extracted as 1000 bp fragments and manually analyzed for 5'-elongated ORFs. This yielded in total 8 (18 % of analyzed ROPIP1 insertions) ATG start codons in front of and in frame with ROPIP1 that produced chimeric ORFs and that were in frame with ROPIP1 (see Table A 3, Appendix) 5 of the 8 ROPIP1 5'-extension additionally were predicted to be signal peptides using SignalP 3.0 [Bendtsen et al. 2004b]. Upstream promoter elements could get predicted to all of the 5 candidates with positive signal prediction using BDGP Neural Network Promoter Prediction (NNPP2.2; fruitfly.org; Reese 2001). Poly (A) signals were delivered by Eg-R1 and predicted to be Poly(A) signals by HCpolya (bioinfo4.itb.cnr.it/~webgene/wwwHC_polya.html; Milanesi et al. 1996) in 4 of 5 candidates. The one missing was likely due to its localization at the 3'-contig border which truncated the Eg-R1 sequence. Predicted promoter elements and poly adenylation signals may point to insertions of Eg-R1 into gene-like environments

that may trigger pol II transcription. Two of the 5 candidates were amplifiable from genomic DNA extracted from *Bgh*-infected barley leaves by usage of gene-specific primers and were sequence-verified. One was weakly seen once as a band in cDNA prepared from DNAseI digested total RNA preparations prepared from *Bgh*-infected barley leaves. Unfortunately, all 5 candidates lacked introns. Therefore it was not excludable that gene-specific bands derived from genomic DNA contaminations. Interestingly, short sequence duplication reminiscent of TSDs were discovered in two of these 5 insertions, by chance. In both cases the duplicated sequence was located 5' in front of the ATG start codon of the predicted signal peptides. Untypically, the sequence duplication at the 3'-end was not located closely to the 3'-end of the Eg-R1 element but 532 bp (BluGen contig: CAUH01010509), respectively 163 bp (BluGen contig: CAUH01002559) downstream of the Eg-R1 3'-end. One additional ROPIP1 candidate exhibiting a positive signal prediction and an intron-exon structure was kindly provided by Thomas Wicker (University of Zurich, Switzerland). It was PCR-amplifiable from genomic DNA but not upon usage of intron-exon boundary spanning primers and cDNA as template. One additional strategy for identifying 5'-extended ROPIP1 ORFs was a BLASTn search against the NCBI Trace archive database *Blumeria graminis* f sp *hordei* WGS which contains whole genome shotgun raw reads provided by the BluGen consortium. This yielded one additional hit for a 5'-elongated ROPIP1 ORF with positive signal peptide prediction (SignalP 3.0; Bendtsen et al. 2004b) in the first 10 hits. Another hit was retrieved from NCBI by using ROPIP1 nucleotide sequence in a BLASTn search against the non-redundant nucleotide collection database. ROPIP1 was as Eg-R1 located on the reverse strand in close distance (130bp) upstream of an AVRa10-like effector protein on the plus strand. The 5'-elongated ORF of this ROPIP1 insertion had a signal peptide prediction (SignalP 3.0; Bendtsen et al. 2004b) but the ROPIP1 ORF was 3'-truncated due to a premature stop codon. Noticeably, all 5'-ROPIP1 ORF extension were different to each other in size and amino acid composition. Their size ranged from 9 to 55 amino acids with a mean length of 28.00 ± 14.56 amino acids. This suggested that the 5'-ORF extensions were gained by chance. Additionally, cDNA synthesized from mRNA preparations from *Bgh*-infected barley primary leaves was used as template in 5'-RACE PCRs together with ROPIP1-specific primers. This approach only yielded Eg-R1 exhibiting a 5'-end like the Eg-R1 consensus sequence deciphered in this work (see

Table A 1, Appendix). It may be conceivable that highly abundant Eg-R1 transcripts outcompeted a putative 5'-elongated ROPIP1 transcript, which would be comparatively rare in the RACE-PCR. In sum 8 5'-elongated ROPIP1-ORFs from 53 checked ROPIP1 (2 kindly provided by Thomas Wicker, University of Zurich, Switzerland) insertions, which is 15 %, exhibited a positive signal peptide prediction. Roughly 3000 Eg-R1 insertions would extrapolate to 450 ROPIP1 candidates showing 5'-elongated ORFs with predicted signal peptide properties. The real number might even be higher as highly repetitive genomic regions could not get assembled in the *Bgh* genome and no physical map of the *Bgh* genome existed. Further, many more 5'-elongated ORFs, to which no signal peptide might be predictable, would provide a classical ATG start codon to ROPIP1. This may indicate the existence of 5'-extended ROPIP1 transcripts that gained classical ATG start codons and some even signal peptides.

2.8.4 *In silico* Characterization of the ROPIP1 Amino Acid Sequence

Subcellular protein localization prediction using the WoLF PSORT server [Horton et al. 2007] located the amino acid sequence of ROPIP1 in the cytoplasm albeit with a rather weak confidence. Alternative usage of the TargetP 1.1 server [Emanuelsson et al. 2000] predicted ROPIP1 a localization in chloroplasts with the second best of 5 reliability score classes. Plant epidermal cells lack chloroplasts but contain leukoplasts. No conclusive subcellular localization of ROPIP1 was predictable and the ROPIP1 amino acid sequence is free of known subcellular protein localization motifs.

No protein domains were detected in the ROPIP1 amino acid sequence using SMART (smart.embl-heidelberg.de), Pfam (pfam.xfam.org) and PROSITE (prosite.expasy.org).

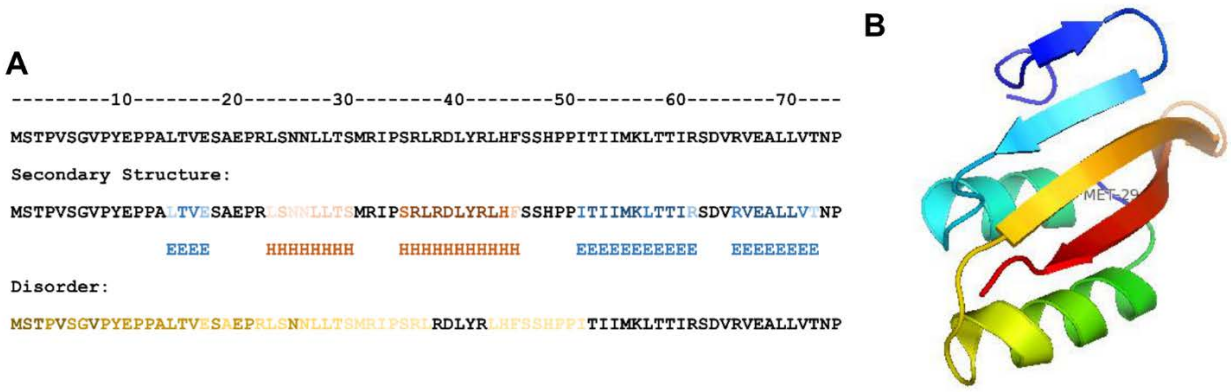

Figure 10: (A) Summary of ROPIP1 secondary structure and disorder predictions. The results of 5 algorithms for secondary structure prediction, respectively 4 algorithms for disorder prediction were combined. Identified amino acids were colored. The darker the color, the more algorithms predicted this residue. E: α-helices; B: β-sheets. Note that the first Met of the ROPIP1 sequence is artificial. (B) Tertiary structure prediction of ROPIP1 obtained from the QUARK ab initio tertiary structure prediction server. The image is given in rainbow color ranging from the N-terminus in blue to the C-terminus in red. Met29 of the submitted query which lacked the first 4 amino acids as depicted in A is marked in blue. Here, it represents the start of ROPIP1-Cter (amino acid position 32 in A).

Secondary structure predictions of the ROPIP1 amino acid were done with the Quick2D webserver of the MPI bioinformatics toolkit [Biegert et al. 2006] which delivered 4 independent secondary structure predictions. An additional 5th prediction was obtained from the results page of the QUARK server [Xu and Zhang 2012]. The outputs were combined (Figure 10 A). Each residue predicted to be part of α-helices was marked red (H), residues of β-sheets were marked blue (E). Residues having been predicted by more than one algorithm are depicted stepwise darkened. An α-helix followed by two β-sheets were predicted by all 5 engaged tools in the ROPIP1-Cter part of ROPIP1. A weak prediction for a short β-sheet and an α-helix was located to the N-terminal part of ROPIP1. Stretches of the N-terminal part of ROPIP1 were additionally predicted to be disordered in protein structure by Quick2D. Alternative usage of DisEMBL [Linding et al. 2003] confirmed the predicted region of intrinsically disorder by 3 applied algorithms. The predicted disordered residues were marked yellow and the outputs of 4 predictions combined analogous to the secondary structure prediction illustration and depicted in one sequence (Figure 10 A).

The ROPIP1 amino acid sequence was submitted to the QUARK server [Xu and Zhang 2012] for *ab initio* tertiary structure modelling. The first of ten predicted tertiary structure models of ROPIP1 is depicted in Figure 10 B. The estimated template modelling (TM-)

score of the model was 0.3561 ± 0.0833. The TM-score ranges from 0 to 1. A TM-score of 0.17 roughly equals a p-value of 1 and indicates a random model. At a TM-sore of 0.3, the model is significantly (p-value < 0.001) different from random structures. A TM-score > 0.5 indicates the existence of a protein with the same fold as the model [Xu and Zhang 2010]. This indicated that the ROPIP1 amino acid sequence has the potential to fold in a non-random manner, supporting evolution of the sequence at the protein level.

Next, the ROPIP1 amino acid sequence was submitted to the HHpred server [Söding et al. 2005] for protein homology detection. All databases were selected. Pre-selected default parameters were kept. Most hits were likely not true-positives, which might have been due to a lack of similar amino acid sequences. The HHpred algorithm is based on comparison of sequence alignments and secondary structure predictions. However, three indications were obtained from the 100 hits. First, 71 % of all hits matched to a stretch of 42 amino acids beginning 6 amino acids upstream of and largely spanning the ROPIP1-Cter part of the ROPIP1 query. This may substantiate the potential of ROPIP1 C-term to fold properly. Second, of all 42 hits with a probability score greater than 50 % and being bigger than 10 aligned amino acids, 80 % of hits contained a Structural Classification of Proteins (SCOP) domain of the YigF-like superfamily [55298] (see Table A 1, Appendix). This structural domain is found in proteins of all major kingdoms. The YigF-like domain promotes homo-trimerization but is of general unknown biochemical function. It is for instance found in protein translation inhibitors. This may indicate the possibility of homo-trimerization of a putative ROPIP1-Cter peptide. Third, the best match (probability score 79.19%) longer than 10 amino acids was Novel Protein Similar To Vertrebate MID1 Interacting Protein 1 of the Spot 14 family (IPR009786). Human Mid1-Interacting Protein 1 (MID-IP1, also Mig12) supposedly acts in stabilization and bundling of microtubules [Berti et al. 2004]. The hit spanned the first 10 amino acids of ROPIP1-Cter plus 6 upstream amino acid residues. However, there was a gap of 14 amino acids in the ROPIP1 sequence that was absent in the MID-IP1 similar novel protein match. Interestingly, HsMID-IP1 has a reportedly cytoplasmic localization and depends on microtubule-associated HsMID1 recruitment for microtubule localization [Berti et al. 2004]. This resembled ROPIP1 in so far, as GFP-ROPIP1 was located in the

cytoplasm but recruited to MTs by co-expression of MT-associated RFP-MAGAP1 recruitment for MT localization.

In sum, the secondary structure prediction, the tertiary structure modeling and the protein homology detection for ROPIP1 indicated that ROPIP1-Cter may fold in a proper way which supports the possibility that ROPIP1- Cter represents a peptide effector or a corresponding effector domain.

3 Discussion

This work places the retroelement-encoded ROPIP1 of *Bgh* as an secreted intracellular effector protein targeting the barley susceptibility factor RACB. ROPIP1 together with the microtubule-associated ROP regulator MAGAP1 promotes, microtubule networking loosening which was reported [Hoefle et al. 2011; Huesmann et al. 2012] to be associated with enhanced susceptibility of barley epidermal cells against *Bgh* attack.

3.1 ROPIP1 is an Effector Protein of *Bgh*

In this work, several indications were collected that show ROPIP1 to act as a secreted intracellular effector protein of *Bgh*. The affinity-purified custom α-ROPIP1 antibody specifically labelled a likely *Bgh*-derived protein in various immunoblots. It was exclusively observed in protein extracts prepared from *Bgh*-inoculated barley leaves. The signal was never seen in protein extracts prepared from mock-inoculated barley leaves. Antibody specificity of α-ROPIP1 was shown by using crude cell lysates of recombinant *E. coli* cultures expressing (IPTG induction of recombinant protein expression) or not expressing (no IPTG induction) a His-tagged recombinant ROPIP1 protein (recROPIP1). Further, the unique signal was not detectable by preimmune serum. Immunogoldlabeling confirmed that α-ROPIP1 labeled a *Bgh* protein. Gold-particles detected by TEM were observed in the fungal appressorium as well as inside haustorial protrusion of *Bgh*. The *Bgh* protein labeled by α-ROPIP1 seemed to be secreted as gold-particles were observed to spread from the tip of the appressorium to an apoplastic cell wall apposition of the attacked barley epidermal cell. Gold-particles were further seen in the host cytoplasm of a *Bgh*-invaded barley epidermal cell. This indicated a successful translocation of the α-ROPIP1 labeled protein from the *Bgh* haustorium into the barley host cell. The immunogoldlabeling seemed to be specific as almost no goldparticles were retrieved in the host vacuole, the fungus-unassociated host cell wall and the extracellular space. Transient ectopic over-expression of ROPIP1 in barley epidermal cells pointed to the capability of ROPIP1 in contributing to virulence of *Bgh*. This assumption was substantiated by transient double-stranded RNAi-mediated silencing of the native *ROPIP1* transcript. Transient HIGS [Nowara et al. 2010] of *ROPIP1* significantly diminished the number of established haustoria of *Bgh*. Co-expression of an RNAi insensitive ROPIP1 RNAi rescue construct significantly

complemented the relative penetration rate of *Bgh*. In addition, ROPIP1 was shown to physically interact with the barley susceptibility factor RACB and some first insights into the mechanistic contribution of ROPIP1 to barley susceptibility could get generated (discussed below).

3.1.1 Effector Proteins of *Bgh*

In general, effectors of plant pathogens are secreted molecules that manipulate their plant hosts to the benefit of the pathogen. One can distinguish between apoplastic and intracellular effectors depending on the localization of their host targets. Apoplastic pathogen effectors are currently known to act in avoidance of recognition by PRRs, in inhibition of host secreted lytic enzymes and in detoxification of host-generated defense molecules like ROS (see Introduction or Ökmen and Doehlemann 2014 for review). It is possible to show that there is at least one pathogen intracellular effector for each key component of the host cell defense network to suppress plant defense responses. Intracellular effectors are also reasoned to contribute to metabolic reprogramming of the host cell, e.g. by sink tissue induction and redirecting metabolite flow to the pathogen (see Introduction or Giraldo and Valent 2013 for review). Many effectors have been discovered by their avirulence function and the best studied effectors are AVR-effectors. Effectors of plant pathogenic bacteria are studied most intense. Less is known about effectors of filamentous plant pathogens but they are under current study and knowledge on them is emerging. Here most work was done with RXLR-family and CRN-family effectors of *P. infestans* [Schornack et al. 2009; Bozkurt et al. 2012; Anderson et al. 2015] while knowledge on fungal effectors is in comparison to their plurality sparse [Rafiqi et al. 2012]. In *Bgh* there are around 500 CSEP effector candidates as well as estimated 1350 EKA-type effector paralogues [Spanu et al. 2010; Pedersen et al. 2012; Sacristán et al. 2009]. The expression of a distinct subset of CSEPs peaks early in the infection process at appressorium formation of *Bgh*. The expression of another distinct subset of CSEPs peaks later when haustoria are nearly fully established in host barley epidermal cells [Hacquard et al. 2013]. Translation of around 100 CSEPs was confirmed by LC/MS/MS [Bindschedler et al. 2009; Bindschedler et al. 2011; Pedersen et al. 2012]. The host targets of CSEPs and EKAs, their mechanics of virulence and biochemistry are, except for a handful of CSEPs, unknown. Only CSEPs (also termed BECs) that

encode a predicted signal peptide for secretion have been investigated yet. For none of them host translocation has been shown. All were expressed in the plant for functional analysis except one, BEC1019, which was recently delivered using the T3SS of *Xanthomonas*, a novelty in the barley-*Bgh* system [Whigham et al. 2015]. BEC1011 has a predicted ribonuclease-like fold and might act as cell death suppressor [Pliego et al. 2013]. Nothing is known about its subcellular localization, its host targets and its mode of action or its biochemistry. BEC1019, likely a metalloprotease, likewise acts in suppression of cell-death. Again nothing is known about its subcellular localization, its host targets and its mode of action. Interestingly it is broadly conserved in the fungal kingdom [Whigham et al. 2015]. CSEP055 localizes to the apoplast. It interacts with the secreted PR17c protein in yeast and in tobacco. It is suggested to aid in secondary haustoria establishment [Zhang et al. 2012a]. CSEP1015 is the only *Bgh* effector with some insights in biochemistry and its mode of action. It physically interacts with barley small cytosolic heat shock proteins in yeast and in barley. Further it was shown to compromise their chaperone activity *in vitro*. Chaperones are important for host protein integrity in stress situations [Ahmed et al. 2015]. No pathway or functionality for Hsp16.9 and Hsp17.5 of barley are known yet. BEC3 was shown to interact with a barley thiopurine metalloprotease in yeast and *in planta*. No further information is available yet. BEC4 interacted with a barley ubiquitin-conjugating enzyme (E2 protein) in yeast and in barley. BEC4 additionally interacted with a barley ARF-GAP in yeast [Schmidt et al. 2014]. *In planta* interaction of BEC4 and the respective barley ARF-GAP has not been shown yet.

3.1.2 The *Bgh* Effector ROPIP1

Bgh ROPIP1 has to be placed as a completely new type of effector. It resembles EKA-type effectors in so far as both types do not encode signal peptides. But they are otherwise not related to each other. EKA-type effectors were found to co-evolve with a LINE retrotransposon and were also found joined together on single cDNAs [Ridout et al. 2006; Sacristán et al. 2009]. In general, transposable elements are discussed to aid effector evolution (see below). However, ROPIP1 is located as an integral part at the 5'-end of the Eg-R1 nucleotide sequence, which has not been reported before. Here, part of a retroelement serves as a virulence factor. This raises the question of what evolved

first, the retroelement or the effector? Has the retroelement itself adapted to virulence function or is a virulence domain dispersed in the genome by a retroelement to create variation that ends up with a functional new effector as output? The answering of this open question is further hampered by the sparse and imprecise knowledge on the nature of the Eg-R1 retroelement. It is sometimes classified as SINE, but this can also be doubted (discussed below). However, it is likely restricted to powdery mildew fungi of *Poaceae*. Additionally, it cannot be answered yet, whether ROPIP1 directly translates from Eg-R1. It might also be conceivable that at least one of the minimum 3000 genomic insertions of Eg-R1 gave rise to a chimeric transcript. A few hints were generated in this study that the ROPIP1 nucleotide sequence gained additional 5'-ATG start codons, with some of the extended ORFs bearing a positive prediction for a secretory signal peptide. Extrapolated, this adds roughly 500 ROPIP1 ORF candidates. Further possible options of ROPIP1 translation are discussed below. Hence, from the current knowledge it is impossible to conclude how the 'real' ROPIP1 effector or effector family looks like.

However, it is possible to state that ROPIP1-Cter is very likely the effector or virulence domain of ROPIP1. ROPIP1-Cter mediated the physical interaction of ROPIP1 and barley RACB (WT and CA) in yeast. It was further sufficient to induce super-susceptibility towards *Bgh* when ectopically over-expressed in barley epidermal cells. This was further supported by the higher likelihood of the ROPIP1-Cter part to be similar to database-deposited proteins. The secondary structure prediction output of 5 independent algorithms was consistent for the ROPIP-Cter part of the ROPIP1 nucleotide sequence, whereas it was not for the N-terminal sequence part. A SCOP protein domain matched to the ROPIP1-Cter part in the protein homology search. This and the tertiary structure prediction indicated that ROPIP1-Cter has the potential to fold properly. The SCOP domain YigF [55298] is a eukaryotic homo-trimerization domain. This raises the possibility that ROPIP1-Cter, directly translated from Eg-R1 may fold similarly and may form stable oligomers. In fact, a ROPIP1-Cter trimer would fit to the observed molecular weight of the protein which was labeled by α-ROPIP1 in western blots. However, the typical band-laddering of oligomers in SDS-PAGE was never observed. Moreover, the ROPIP1 protein showed a stronger protein interaction with RACB (WT and CA) than ROPIP1-Cter in yeast. It also interacted with RAC1 (WT and

CA) which ROPIP1-Cter did not. Additionally, transient over-expression of ROPIP1 rendered barley epidermal cells by trend more susceptible towards *Bgh* than ROPIP1-Cter. A potential virulence-supporting role of the N-terminal ROPIP1 part of ROPIP1 can therefore not be excluded.

The classical secretory pathway route mediated by a gained signal peptide is one possibility for ROPIP1 secretion. Lack of a signal peptide would not exclude ROPIP1 secretion as ROPIP1 and ROPIP1-Cter yielded good scores for non-classical secretion (SecretomeP 2.0 server). Secretion and host translocation of effectors from plant pathogenic fungi is only marginally understood. Plant pathogenic fungi might use different strategies for effector translocation into host cells [Lo Presti et al. 2015]. It is generally assumed that host cell uptake of RXLR translocation motif bearing oomycete effectors involves host cell plasma membrane lipid-raft formation and subsequent endocytosis [Rafiqi et al. 2012]. Interestingly, ROPIP1 harbors an arginine-rich RLRDLYR amino acid stretch at position 37-43 close to the N-terminus of ROPIP1-Cter (see Table A 1, Appendix). Powdery mildews might secret proteins and RNA into the host cell via fungal Multivesicular Bodies (MVBs) that release fungal intraluminal vesicles as exosomes into the extrahaustorial matrix [An et al. 2006a; An et al. 2006b]. The assumed following translocation process is unknown [Micali et al. 2011].

No protein domains were predictable for the ROPIP1 protein. Secreted proteins without functional protein annotation are typically found in fungal plant pathogens that have an obligate biotrophic lifestyle [Lo Presti et al. 2015], like *Bgh* is one. Combining several definitions of plant pathogen effectors, a model effector should be structured as follows. It is a small, secreted protein with some cysteines in its sequence. The signal peptide at its N-terminus is followed by a translocation motif or domain. Transmembrane domains are absent. Ideally it has enzymatic activity on top. Such a definition is undoubtedly useful to delimit the search for effector candidates but it does not cogently represent the full secretome of a pathogen. Sperschneider et al. [2013] used an different approach for identifying fungal pathogenicity effectors. They compared the genomes of pathogenic fungi to their respective apathogenic relatives and searched for protein-coding sequences that are only found in the pathogenic family members. The idea was that these proteins are present in pathogenic strains due to their role in pathogenicity. Sets

of effector candidates were generated including candidates that do not meet characteristic traits of definition of effectors used for prediction. Liu et al. [2014] showed secretion of effectors with isochorismate mutase activity of *P*. *sojae* and *V*. *dahliae* that do not encode signal peptides. Further examples are the EKA-type effectors Avr_{a10} and Avr_{k1} of *Bgh*. Avr_{a10} is perceived by the barley CC-NB-LRR resistance protein MLA10. Translocation of MLA10 from the cytoplasm to the nucleus is dependent on Avr_{a10}. In the nucleus, MLA10 interacts with the transcription factors WRKY1 and WRKY2 in an Avr_{a10}-supported manner to derepress PTI responses [Shen et al. 2007]. A signal peptide-independent effector delivery route is likely in *Bgh*, given that EKAs do not encode signal peptides [Ridout et al. 2006]. Cysteine-richness was thought to be required for travelling of effector proteins through the apoplast. Small cysteine-rich proteins form a distinct class of apoplastic effectors in *P. infestans* where di-sulfide bridges are thought to impede proteolytic degradation [Kamoun 2006]. But cysteine-richness is not a general criterion that can be applied to all effectors [Sperschneider et al. 2013]. There are described effectors without any cysteine in their sequences [Stergiopoulos and Wit 2009]. There are also several cysteine-free proteins in the putative secretome of *Bgh* (see supplementary file S6 of Sperschneider et al. 2013). The contribution of the oomycete RXLR effector translocation motif to pathogen-independent RXLR-effector uptake is under debate. Binding to Phosphatidylinositol 3-phosphate (PI3P) at the plant plasma membrane might be independent of the RXLR translocation motif [Rafiqi et al. 2012]. Whatever the precise host uptake mechanism might be like, the RXLR translocation motif undoubtedly led to the discovery of huge RXLR-effector families in *Phytophtora* species and downey mildews. For instance, *P. infestans* encodes at least 500 RXLR-effectors. The RXLR translocation domain is typically followed by diverse C-terminal effector domains that are of widely unknown biochemical functionality, due to their unrelatedness to characterized proteins. Functional characterization of some cloned RXLR-effectors showed their ability to suppress plant immunity which might be exerted in a collaborative manner of different RXLR effectors. Interestingly, RXLR effectors are located in gene-sparse genomic regions with high Transposable Element (TE) activity and high repetitive DNA content. It is assumed that this contributes to a fast evolution of RXLR effectors to escape recognition by R-proteins (see Anderson et al. 2015 for latest review on RXLR effectors). An effector molecule

must not be a protein, as *Botrytis cinerea* (*B*. *cinerea*) was found to secrete small non-coding RNAs (sRNAs) as effectors into the host cells of Arabidopsis and tomato where they manipulate plant defense by exploiting the host RNAi machinery. Inside the host cell, *B. cinerea* sRNAs load themselves into argonaute (AGO) proteins. AGO proteins mediate sRNA guided silencing of corresponding genes by mRNA cleavage, mRNA degradation, translational inhibition, DNA methylation and histone modification. Secreted *B. cinerea* sRNAs target host plant MAPKs, cell wall associated kinases and other defense components for posttranscriptional gene silencing. Interestingly, the *B. cinerea* sRNAs that lead to the discovery of cross-kingdom RNAi are derived from a LTR-type retrotransposon. TEs and effectors are often located in close vicinity and their transcription is often co-induced. There are also effector-gene derived sRNAs that function as effector sRNAs [Weiberg et al. 2013; Weiberg et al. 2014]. The direct physical interaction of ROPIP1 and RACB (WT and CA) in yeast and *in planta*, the results from the western blots using α-ROPIP1, the results from the immunogoldlabeling and the complementation of the virulence phenotype in the HIGS assay by ectopic expression of an RNAi rescue protein speak against a virulence function of ROPIP1-RNA or Eg-R1-RNA but favor a ROPIP1 peptide as the causal agent of biological function. In the latest review on fungal effectors they are defined as ‘any secreted molecule that modulates the interaction between the fungus and its host’ [Lo Presti et al. 2015].

3.2 ROP Small GTPases

In this work, the barley ROP protein RACB was found to physically interact with the *Bgh* effector protein ROPIP1. ROPIP1 interacted with RACB WT and CA RACB but not DN RACB in targeted Y2Hs. The direct protein-protein interaction of CA RACB and ROPIP1 but not DN RACB was confirmed *in planta* by BiFC. This suggested that GTP-bound, activated, RACB is the host target of ROPIP1. Barley RACB is a susceptibility factor of barley in the barley-*Bgh* interaction (see Introduction). Activated RACB was found to be beneficial for *Bgh* establishment into barley epidermal cells. Transient over-expression of CA RACB, but not WT RACB or DN RACB induces super-susceptibility of barley towards *Bgh*. The relative penetration rate was increased by 45 % [Schultheiss et al. 2003]. Transient knock-down of RACB significantly reduced the relative penetration rate

of *Bgh* showing that RACB is required for full virulence of *Bgh* on barley. The results from the transient experiments were confirmed by usage of stable transgenic barley lines [Schultheiss et al. 2005; Pathuri et al. 2008; Hoefle et al. 2011]. Transient over-expression of ROPIP1 increased the relative penetration rate of *Bgh* on barley epidermal cells by 40.25 % which is in the same dimension as transient over-expression of CA RACB. Transient HIGS-mediated silencing of *ROPIP1* reduced the relative fungal penetration rate by 36.95 %. This suggested that ROPIP1 is required for full virulence of *Bgh* on barley. This adds to RACB being the host target of ROPIP1. It further suggests that the mode of action of ROPIP1 is interfering with the regulation of RACB activity.

3.2.1 Effector Proteins Manipulating Host Small GTPases

Diverse bacterial pathogens of mammals manipulate host GTPase signaling to suppress immune responses. A major target of bacterial effectors are small monomeric GTPases that regulate the host cell cytoskeleton [Aktories 2011]. *Salmonella typhimurium* (*S. thyphimurium*) secrete effectors that sequentially trigger Rho GTPases first ‘on’ to induce their uptake into host cells and then ‘off’ to finish internalization. It is a gram-negative enterobacterium causing gastroenteritis. After attachment to intestinal epithelial cells, *S. thyphimurium* injects the T3SS effector SopE into the host cell. SopE is a molecular mimicry of GEFs that activates the Rho-GTPases Rac1 and Cdc42. Activated Rac1 and Cdc42 are key regulators of lamellipodia and filopodia formation. Lamellipodia and Filopodia are F-actin rich polar growing protrusions that mediate cell motility. Activation of Rac1 and Cdc42 by SopE leads to polymerization of an F-actin mesh beneath the bacterium. Subsequent membrane ruffling, a process similar to lamellipodium formation, encloses the bacterial invader. Inside the host cell, *S. thyphimurum* secretes a second Rho-GTPase manipulating effector, SptP, which is a molecular mimicry of GAPs. SopE is outcompeted by SptP resulting in the deactivation of Rac1 and Cdc42 signalling. The actin filaments depolymerize and *S. thyphimurium* establishes itself in an endosomal-like compartment, the Salmonella Containing Vacuole (SCV), where it proliferates before continuing with the infection process [Ham et al. 2011; Fàbrega and Vila 2013]. *Yersinia* species employ a contrasting strategy. They have evolved a whole repertoire of T3SS effectors to deactivate Rho GTPase signaling to prevent their internalization into macrophages (phagocytosis) in the early innate

immune response. This contributes to avoidance of recognition by the adaptive immune system which enables their extracellular proliferation in microcolonies [Cornelis 2002; Viboud and Bliska 2005]. *Yersinia pseudotuberculosis* virulence highly depends on the T3SS secreted effectors of the *Yersinia* outer protein family (Yop) which is conserved in further pathogenic *Yersinia* species, including the plague bacillus *Yersinia pestis* [Viboud and Bliska 2005]. *Yersinia* are gram-negative enterobacteria. The C-terminus of the multi-domain effector YpkA structurally mimics Rho-GDIs and inhibits GDP to GTP nucleotide exchange of the mammalian small GTPases RhoA and Rac1 [Prehna et al. 2006]. Activated RhoA and Rac1 positively regulate actin stress fiber formation and contractibility in non-muscle cells [Vallenius 2013]. YpkA action disrupts actin stress fibers leading to a deformed, rounded-up, cell shape of cultured human intestinal epithelial cells. Besides sequestration of RhoA and Rac1, YpkA (also termed YopO) was recently shown to physically bind to actin monomers which sterically hinders actin polymerization. Further, actin monomer binding activates the kinase domain of YpkA which subsequently phosphorylates actin polymerization regulators leading to misregulation of actin polymerization [Lee et al. 2015]. Unlike host GDIs YpkA likely cannot extract activated prenylated small GTPases from the plasma membrane [Prehna et al. 2006]. This part is executed by another member of the Yop effector family. YopT is a cysteine protease that cleaves the small GTPases RhoA, and Rac1 upstream of their prenylated cysteine at their C-terminus of their lipid anchor, thereby releasing them from the PM. This cleavage occurs irrespective of the activity status of the small GTPases [Shao et al. 2002; Shao et al. 2003]. A third T3SS effector of *Yersinia* species, YopE, directly de-activates Rho and Rac1 by exerting GAP activity on them. This depends on the arginine of its Arg-finger motif of Rho-GAPs as a mutation to alanine abolished GAP activity of YopE [Black and Bliska 2000]. The Arg-finger directly sticks into the GTP binding pocket of small GTPases thereby stimulating GTP hydrolysis. The versatile protein tyrosine phosphatase YopH completes the set of small GTPase negative regulating Yop effectors by interfering with the signaling network that ends up in RhoA and Rac1 activation through GEFs [Viboud and Bliska 2005]. Summed up, *Yersinia* YpkA, YopT, YopE and YopH act in concert in keeping the signaling proteins RhoA and Rac1 switched ‘off’ thereby provoking a breakdown of the host cell actin cytoskeleton which the pathogen profits from. In return, macrophages sense the manipulation of Rac1

by YopE which restricts the intracellular proliferation of *Yersinia pseudotuberculosis* in macrophages [Wang et al. 2014], which is likely an ETI reaction.

3.2.2 *Bgh* ROPIP1 and Barley RACB

ROPIP1 is the first example of a plant pathogen effector targeting a plant ROP small GTPase. Like Rho-GTPases in the mammalian system, RACB is a susceptibility factor in the barley-*Bgh* interaction and shares 65 % amino acid identity with human HsRAC1. Mammalian Rac1, Cdc42 and RhoA are key regulators of cell polarity establishment in lammelipodia and filopodia polar outgrowth. Likewise plant ROPs are well-established as regulators of cell polarity in polar growing root hairs and pollen tubes. Spatial regulation of ROP activity is pivotal for determining and maintaining the tip growth direction. This can exemplary be seen with tip growing tobacco pollen tubes. Active NtRAC5 localizes to the apex of elongating pollen tubes where it is thought to be involved in actin-based secretory vesicle delivery of new membrane material. Rho-GAPs at the borders of the pollen tube tip are thought to inactivate NtRAC5 to spatially restrict NtRAC5 activity to the apex. Rho-GDI then likely extract inactivated NtRAC5 from the plasma membrane. Inactive NtRAC5 eventually cycles back to the tip where it is thought to get activated by Rho-GEFs. Disturbing NtRAC5 activity regulation results in abnormalities in pollen tube tip growth. Expression of CA NtRAC5 causes an isotropic growth which results in a ballooning phenotype of the pollen tube tip that eventually bursts. By contrast expression of DN NtRAC5 arrests the tip growth process resulting in a stop of pollen tube elongation [Kost 2008]. Similar phenotypes were observed with root hairs of stable transgenic barley and tobacco lines expressing CA RACB. Root hairs of *CA RACB* mutant lines were bulb-shaped due to isotropic tip growth when cultivated on osmotic medium [Pathuri et al. 2008; Pathuri et al. 2009b]. By contrast, *RACB*-silenced barley plants were heavily impaired in root hair growth, with root hairs being almost absent [Hoefle et al. 2011]. Like effectors of enterobacteriaceae ROPIP1 likely manipulates the regulation of RACB activity. Activated RACB was specifically targeted by ROPIP1 in yeast and *in planta*. Further, GFP-ROPIP1 and the BiFC complex of ROPIP1- YFP^N and CA RACB- YFP^C were recruited by MAGAP1 to cortical MT (discussed below). ROPIP1 may enforce a local polar domain at the site of *Bgh* ingrowth. Barley RACB is a type I ROP like AtROP2/4 which play a prominent role in

lobe outgrowth in Arabidopsis pavement cell development (see Introduction). Lobe outgrowth is seen together with actin polymerization and branching which involves the Arp2/3 complex. Type I ROPs likely activate the WAVE complex at the Endoplasmic Reticulum (ER) which subsequent interaction with the Arp2/3 complex at the PM is required for actin polymerization. Activation of ROPs at the PM by ROP-GEFs is thought to result in a positive feedback loop that recruits further ROP-GEFs to the site of ROP activity which then enhances actin filament accumulation and polarized exocytosis. In this model, the site of ROP activity is restricted to an active polar domain with lipid raft properties by containment through surrounding ROP-GAPs and the mutually inhibitory effect of AFs and MTs [Bloch and Yalovsky 2013]. Besides lobe outgrowth, AtROP2 plays a prominent role as regulator of the actin cytoskeleton in the tip growth process of root hairs in Arabidopsis. Over-expression of AtROP2 resulted in the formation of elongated root hairs with branched, multiple tips. Transgenic Arabidopsis *CA AtROP2* mutants also exhibited increased root hair length. Further, multiple root hairs emerged from single cells such that roots had in total more root hairs compared to the wildtype. By contrast, *DN AtROP2* mutant lines had less and shorter root hairs than the wildtype plants. This impact of the activity status of AtROP2 on the tip growth process of root hairs could be further linked to the actin cytoskeleton. An excessive F-actin accumulation was observed in root hairs of *CA AtROP2* lines. Root hair tips showed depolarized, isotropic growth resulting in a bulb-shaped root hair tip when not grown inside the medium but in contact with the air [Jones et al. 2002]. This is reminiscent of the ballooning phenotype of CA NtRAC5 expressing tobacco pollen tubes (see above). This was in contrast to WT plants, where F-actin was restricted to the very tip of growing root hairs. The F-actin zone was located at the distal end of actin cables that traversed the subapical zone. The actin cables proceeded to the very tip of roothairs in *DN AtROP2* mutant lines where F-actin was absent. Thus, activated AtROP2 promotes F-actin assembly at the tip of growing root hairs which is linked to root hair growth [Jones et al. 2002]. Because of that, AtROP2 is discussed as key regulator of actin organization in polar root hair growth, albeit the mechanistic understanding is poor yet [Ketelaar 2013].

A bipartite role of the actin cytoskeleton in resistance as well as in susceptibility is likely in the interaction of barley epidermal cells with *Bgh*. Actin filaments strongly focus to the site of attempted entry in cells where *Bgh* was stopped at the pre-penetration stage. Here, the actin cytoskeleton is likely required for the polar secretion of defense compounds to the site of attempted entry. Over-expression of CA RACB partially reduced the focusing of actin filaments. However, this effect was neutral for the interaction outcome as *mlo*-mediated resistance was unaffected [Opalski et al. 2005], which might be due to the strong *mlo* effect. Besides the importance of the actin cytoskeleton for cell wall based defense reactions [Miklis et al. 2007], it might also be required for susceptibility. AFs followed and surrounded ingrowing *Bgh* haustoria as ring-shaped structures [Opalski et al. 2005]. Similarly, AFs accumulate at the apex of tip-growing pollen tubes and root hairs. The formed mesh of AF is thought to collect arriving secretory vesicles prior to their fusion with the PM for cell elongation [Mucha et al. 2011; Rounds and Bezanilla 2013]. Here AF might act in the delivery of new membrane material for ingrowing haustoria, which was discussed as an ‘inverted tip growth’ process [Schultheiss et al. 2003; Opalski et al. 2005]. It is conceivable that the susceptibility-enhancing effect of CA RACB in regard to the actin cytoskeleton is less due to the prevention of polar secretion of defense compounds but more due to a role in establishing a local polar domain for a host-aided active ingrowth of haustoria. A putative supportive role of the actin cytoskeleton for haustorial establishment would be worth further investigations. ROP signaling dependent rearrangement of the cytoskeleton is not restricted to the actin cytoskeleton. The organization of the cortical MT network is as well affected. Active AtROP2/4 on the one hand promotes F-actin assembly required for lobe outgrowth in Arabidopsis pavement cell development via its downstream effector AtRIC4. On the other hand, active AtROP2/4 also depletes AtRIC1 from cortical MTs by physical interaction which destabilizes cortical MTs at the site of lobe emergence. AtRIC1 is the actual target of AtROP6 signaling which has a MT stabilizing effect at sites of indentation formation. AtROP6 via AtRIC1 targets the MT unbranching protein AtKTN1. MTs get untied an orient in parallel arrays (see Introduction or Oda 2015 for review). The destabilizing effect of AtROP2 signaling on cortical MTs can also be seen at the tip of root hairs of transgenic Arabidosis lines expressing *CA AtROP2*. Stunted root hairs with depolarized, bulb-shaped root hair tips

show less well ordered MTs in random orientation [Yang et al. 2007]. To sum up, the site of activity of mammalian Rhos and plant ROPs determines the site of polar cell growth. Rho and ROP signaling influences the organization of the actin cytoskeleton, especially filamentous actin polymerization. In plants, ROP activity additionally includes regulation of the MT cytoskeleton for cell polarity establishment. The physical interaction of ROPIP1 with active RACB might promote and/or maintain a local domain for polar cell growth. In contrast to polar outgrowth of root hairs, pollen tubes or lobes of pavement cells, this polar domain in barley epidermal cells might be required for the ingrowth of a *Bgh* haustorium. Haustoria are enveloped by a host-derived lipid bilayer, the Extrahaustorial Membrane (EHM), which is separated from the host PM by the haustorial neckband. There is still a controversy on the origin of the EHM. Its composition differs from the host PM, e.g. TM proteins likely are absent in the EHM of G. orontii [Micali et al. 2011] as well as other typical PM proteins. One hypothesis is that the whole PM of the host cells enlarges upon fungal penetration. A high density of secretory vesicles containing new PM material would fuse to the PM near the site of fungal penetration. The host PM would invaginate as a lobe due to exerted pressure of the fungal appressorium. The composition of the host PM would be altered by being pushed through the haustorial neckband that would act as a molecular sieve. The alternative hypothesis is that host vesicles, derived from the nearby plant endomembrane system, deliver new membrane material of altered composition beneath the haustorial neckband from where it forms the haustorium surrounding EHM [Koh et al. 2005; Micali et al. 2011]. Anyhow, in both cases the establishment of a fungal haustorium in host cells depends on the active supply of new plasma membrane material by plant cells to the site of the enlarging haustorium which can be seen as a polar growth process.

3.3 Cortical Microtubules

MTs are predominantly known for their role in mitosis prior to cytokinesis. Plant cells show some MT-related peculiarities e.g. they lack centrosomes as Microtubule-Organizing Centers (MTOCs) from which the spindle apparatus emerges. Further plant MTs are essential for the plant-specific formation of a cell plate during cytokinesis. MTs define the zone of phragmoplast establishment in the center of the cell equator. MTs direct vesicles containing PM and cell wall material to the phragmoplast that expands

radially to the cell cortex. These peculiarities are exemplary for the two main characteristics of plant cell MTs. They form a self-organized network and function in anisotropic plant cell growth by being involved in cell wall formation [Wasteneys 2002; Rasmussen et al. 2013; Keijzer et al. 2014].

MTs are proteinaceous polymers of α-tubulin and β-tubulin heterodimers. The α-tubulin part of one dimer binds to the β-tubulin part of another dimer. Polymerized dimers align in a left-handed helix to form a tube of about 25 nm in diameter. MTs elongate in a directed and autonomous manner from their minus-end to their plus-end. They appear very dynamic due to their permanent elongation and shrinking, which is termed dynamic instability or treadmilling. MTs grow and shrink predominantly from their plus-ends. Both, α-tubulin and β-tubulin are GTP bound, while only β-tubulin can hydrolyse GTP to GDP. Only dimers with α- and β-tubulin being GTP loaded get integrated in an elongating MT at its plus-end. Subsequent GTPase activity of β-tubulin changes the conformation of the dimer that slightly turns thereby destabilizing the polymer. Permanent addition of GTP-bound tubulin dimers prevents the decay of the plus-end which is further stabilized by plus-end binding proteins (+TIPs). However, when the MT plus-end runs short of fresh GTP-bound dimers, the MT polymer starts a rapid dissociation directed from the plus-end to the minus-end, which is called ‘catastrophe’. This process is reversible with access to GTP-bound dimers that restart MT elongation, which is called ‘rescue’ [Horio and Murata 2014].

The nucleus acts as MTOC in plant cells. Some MT spread radially from the nucleus through the cytoplasm in postcytokinetic cells until they enter the cell cortex. The cortical MT array is the most prominent MT localization in interphase plant cells. At the cell cortex MTs are organized as a complex, self-organizing network without major MTOC [Ambrose and Wasteneys 2014]. Ring-formed γ-tubulin complexes get attached laterally to pre-existing MTs where they serve as nucleation sites. New MTs emerge at an angle of 40°. The consequence for a growing MT of collision with a pre-existing MT is also angle-dependent. A collision at a steep angle greater than 40° on the one hand can lead to crossing of the arriving MT over the pre-existing MT. On the other hand, it can also lead to catastrophe for the arriving MT. Junction of a growing MT with a pre-existing MT at a shallow angle less than 40° aligns the two MTs to a bundle which is referred to as

‘zippering’ [Horio and Murata 2014]. The MT Associated Protein 65 (MAP65) of Arabidopsis is localized laterally at MTs. It mediates alignment of two MTs in an antiparallel manner, such that the plus-ends and the minus-ends of two MTs oppose each other [Tulin et al. 2012]. However, there must be further factors or Microtubule-Associated Proteins (MAPs) that connect MTs to bundles as there are also bundles in parallel orientation and *map65* knock-out plants still show bundled MTs. Gamma-tubulin nucleated MTs get cut-off from the pre-existing MT by the MT severing protein AtKTN1 at their minus end at the branch point. AtKTN1 further cuts newly traversing MTs at the point of crossing but not the pre-existing MT. The growing plus-end part of the cut MT can grow further while the cut off rear part undergoes catastrophe from the newly generated plus-end unless it gets rescued. Action of AtKTN1 on MTs generates an atypical depolymerization of the minus-end, which is best explained to be exerted by yet unknown proteins. In the overall view, AtKTN1 serves in removing aparallel MTs to create the cortical array of parallel MT bundles [Horio and Murata 2014].

The Cellulose Synthase Complex (CSC) is a proposed hexamer complex of Cellulose Synthases (CESA) that forms a rosette at the PM. Cellulose fibrils emerge from its lumen into the apoplast where they get integrated into the plant cell wall. Visualization of fluorescence-tagged Arabidopsis Cellulose Synthase 6 (AtCESA6) together with a fluorescence-tagged α-tubulin MT-marker protein showed movement of AtCESA6 along tracks that co-incidence with the MT-marker. Further, the association of AtCESA6 with MTs persists upon reorganization of the MT cytoskeleton [Paredez et al. 2006]. MTs were additionally shown to be required for the delivery to and the correct positioning of CSCs at the PM [Gutierrez et al. 2009]. It has now become evident that CSCs and MTs are physically connected to each other via the linker protein Cellulose Synthase Interactive protein 1 (AtCSI1) in Arabidopsis. AtCS1 interacts with AtCESAs in yeast and with tubulin *in vitro*. The co-localization of fluorescence-tagged AtCESAs and MT-marker proteins depends on the presence of AtCSI1. Drug-induced depolymerization of MTs by oryzalin or usage of *csi1* knock-out mutants, both lead to an atypical positioning of CSCs as well as a slowed down CSC movement. In sum, correct positioning and motility of CSCs depends on an intact cortical MT array. Subsequent cellulose deposition and the accompanied enforcement of the cell wall, restricts cell expansion to anisotropic cell

growth in the longitudinal direction [Li et al. 2012]. Mechanical force transmitted on the cortical MT array biases their self-organization capability. Compressive force promotes shrinkage of an individual MT while tensile force promotes MT growth. Starting from a mesh-like architecture of the cortical MT array, MTs oriented in direction of maximum tension are favored in growth whereas MTs oriented perpendicular to the axis of force get compressed and shrink leading to their extinction. As an observed result, cortical MT bundles appear oriented in parallel to the axis of maximum tension. The underlying mechanistic factors for that model have not been identified yet. Another observation made was, that the stiffness of the cell wall has an impact on MT network dynamic. Lytic degradation of the cell wall induces the reorientation of cortical MTs [Landrein and Hamant 2013].

ROPs have been identified as plant factors influencing MT organization. AtROP6 via its downstream effector AtRIC1 induces AtKTN1 activity leading to parallel MT bundles in indentation formation of Arabidopsis epidermal pavement cells. By contrast, activity of AtROP11 via the scaffolding protein AtMIDD1 promotes AtKin13A-mediated decomposition of MTs leading to MT-depleted zones in differentiating protoxylem cells to form cell wall pits. AtROP11 activity is spatially restricted to cell wall pits by AtROP-GAP3 and AtROP-GEF4 as well as by surrounding MTs. The intact MT network outside of cell wall pits is seen to be required for the massive deposition of secondary cell wall material that contributes to the stability of xylem vessels (see Introduction or Oda and Fukuda 2013b). Besides, MT reorientation can be triggered by light signals and phytohormone treatment. Blue light, absicic acid and ethylene reorient the cortical MT array from transverse to longitudinal direction. Dark conditions, gibberellic acid and auxin treatment orient the MT array back from longitudinal to transverse direction [Oda and Fukuda 2013b].

3.3.1 MTs in Pathogen Attack

Touching of the plant cell surface with a fine glass or tungsten needle causes a rapid reorganization of the cytoskeleton, peroxisomes and the ER. This is a very similar pattern to the plant response in penetration resistance irrespective of whether the plant is susceptible or resistant to the wannabe intruder [Hardham et al. 2008]. Cytoplasmic aggregation beneath the site of attack, rearrangement of the endomembrane system

and focusing of the cytoskeleton are microscopically observable during basal resistance in the early defense reaction against fungal pathogens [Hückelhoven 2007]. This suggests an at least partially common mechanism which is triggered by physical force. Melanized fungal appressoria build up compressive pressure to push the penetration peg through the host cell wall. Anyhow, compressive force alone, as exerted by touching the cell surface with a needle rather promotes a response of the actin cytoskeleton than of the MT cytoskeleton. Upon contact of the needle tip, the actin cytoskeleton first accumulates as a diffuse patch beneath the contact point before actin cables focus towards the site of contact. This is seen together with an agglomeration of the ER and peroxisomes. The MT cytoskeleton, however, appears to be depleted beneath the needle tip but forms a diffuse tubulin ring around the site [Hardham et al. 2008]. An observed GFP-α-tubulin ring (Figure 4 in Hardham et al. 2008) is strikingly similar to the ring of RFP-MAGAP1 fluorescence that surrounds ingrowing *Bgh* hyphae in susceptible barley epidermal cells (Figure 6 in Hoefle et al. 2011). Another similarity between a penetrating *Bgh* hyphae and touching with a needle is focusing of the actin cytoskeleton towards the site of contact. However, MTs were similarly found to focus towards the site of attack in barley epidermal cells in a similar pattern to focused actin cables (Compare Figure 1B in Hückelhoven 2007 and Figure 6B in Hoefle et al. 2011; Opalski et al. 2005; Kobayashi et al. 1997). Further, both, the actin as well as the MT cytoskeleton are required for full non-host penetration resistance of barley epidermal cells against the non-adapted pathogen *E*. *pisi*. Pharmaceutical inhibition of the actin or the MT cytoskeleton allowed entry of *E. pisi* into the non-host barley with inhibition of the actin cytoskeleton having a more pronounced effect. Simultaneous chemical inhibition of both cytoskeletal components abolished cytoplasmic aggregations beneath the site of attack and prevented papillae formation [Kobayashi et al. 1997]. Likewise depolymerization of the actin cytoskeleton by transient expression of Actin-Depolymerizing Factor 3 (ADF3) in barley epidermal cells partially breaks *mlo*-mediated broad-spectrum resistance. The non-adapted *Bgt* and *E. pisi* mildew fungi were able to penetrate barley epidermal cells when a depolymerized actin cytoskeleton was combined with *MLO* [Miklis et al. 2007].

This raises two questions. First, what might be the difference between touching with a needle and a pathogen attack that causes additional focusing of MTs in the pathogen

attack? The answer must lie in a signal that is absent when using a needle. The difference is likely lytic cell-wall degradation by the fungus. Phytopathogenic fungi and oomycetes secrete CWDEs into the apoplast that digest the plant cuticle and the plant cell wall. CWDEs comprise cutinases (cutin), cellulases (cellulose), polygalacturonases (pectin), xylanases (hemicellulose) and proteinases [Hückelhoven 2007]. Together they act in cell-wall softening under release of fragments of their substrates that are perceivable by the plant. Membrane spanning extracellular receptor proteins, like Wall Associated Kinases (WAKs), monitor the integrity of the cell wall and transduce extracellular alterations into intracellular signaling upon ligand perception [Anderson et al. 2001; Seifert and Blaukopf 2010]. Further, they are discussed to initiate signaling pathways that function in MT cytoskeleton reorganization [Landrein and Hamant 2013]. That would make sense in so far as perception of cell-wall weakening would activate a positive feedback loop that attracts MTs to the site of potential cell wall breaching for cell-wall reinforcement via CSCs and likely secretion of further cell-wall components.
The second question is why arrange actin cables and MTs in such a strikingly similar pattern in the early basal defense reaction? Part of the answer might be that the actin cytoskeleton and the MT cytoskeleton cannot be considered separately but have to be viewed collectively. A collaborative role for AFs and MTs is known for the movement of organelles and vesicles where AFs are required for general motility and MTs for positioning. AFs further actively assist MT reorganization that requires detachment of cortical MTs from the PM. There are several eukaryotic proteins conserved in plants that likely physically connect AFs and MTs in a direct manner. These *inter alia* include the motor proteins Kinesins, Myosins and the potential cross-linker protein Formin (Petrásek and Schwarzerová 2009 and see below). As simultaneous focusing of AFs and MTs to site of *Bgh*-attack is required for papillae formation in barley epidermal cells, the next interesting question is what has to happen to overcome papillae formation. To date knowledge on the mechanistic contribution of the cytoskeleton in haustorium establishment is comparatively sparse. However, contributions of the plant MT cytoskeleton to the uptake of invaders, pathogenic or not, across all kingdoms have been reported. Symbiotic rhizobia are bacterial invaders of roots of mainly *Fabaceae* that establish themselves in characteristic root nodules where they fix atmospheric N_2. Their infection process starts at the tip of root hairs where they initiate root hair tip

curling by so called Nodulation (Nod) factors. The cortical MT network of host root hairs depolarizes then reassembles as an array connecting the nucleus and the root hair tip. The nucleus moves to the tip of the root hair. Whether or not the complete MT depolymerization at the onset of bacterial ingrowth may also happen in the native situation, or whether it was due to the application of Nod factors in an artificial high concentration is a matter of debate [Sieberer et al. 2005; Timmers 2008; Hardham 2013]. Undoubtedly, rhizobia grow through the root hair in a newly formed apoplastic tunnel, the so called infection-thread into the root cortex. The growth direction is headed by the nucleus in front of the infection thread to which MTs align in parallel to the growth direction. The tunnel inner side is lined with cell-wall components, like cellulose, pectin and hemi-cellulose [Rae et al. 1992; Hardham 2013]. Here, one role of MTs aligning with the growing infection thread might be in setting up the newly formed cell-wall in the inner of the apoplastic tunnel through the root hair. Attachment of hyphopodia of symbiontic Arbuscular Mycorrhizal Fungi (AMF) and appressoria of pathogenic *Bgh* resemble each other in so far as both cause an cytoplasmic aggregation beneath the contact point and movement of the nucleus into vicinity of the interaction site ([Kunoh et al. 1985; Genre et al. 2005; Hückelhoven 2007]. However, in case of AMF the plant cell initiates a ‘cytoplasmic bridge’ spanning root epidermal cells that is absent in the pathogenic interaction with *Bgh*. The so called Pre-Penetration Apparatus (PPA) forms inside the cytoplasmic aggregation and consists of AFs, MTs and ER. The nucleus subsequently heads the migration of the PPA through the cell interior in direction from the outer side to the inner side of epidermal root cells. AMF hyphae do not penetrate the root epidermal cell until this pre-defined route has been fully established. The ingrowing AMF PM is separated from the host plant cell by a perifungal matrix [Genre et al. 2005; Hardham 2013]. This is another resemblance to pathogenic fungal haustoria which are separated by the EHM. Anyhow, AFM must have means to circumvent host cell defense and to trigger an active uptake by the host cells that are obviously absent in pathogenic biotrophic fungi like *Bgh*.

3.3.2 Bacterial Pathogens Manipulate Host MTs to Gain Access

Bacterial pathogens of mammals secrete effector proteins into their host cells that either stabilize or destabilize the host MT network and that are required for their infection

process [Radhakrishnan and Splitter 2012]. After having been internalized, gastrointestinal *Salmonella* species localize in the endosomal-like SCV where they proliferate (see above or Fàbrega and Vila 2013). The maturated SCV migrates to MTOCs at the nucleus. From there the SCV produces filamentous protrusions that grow radially from the SCV to cell periphery. The best studied of those tubular networks are *Salmonella*-Induced Filaments (SIFs). SIFs are membranous extensions of the SCV that form on a MT backbone. In total five effectors of *Salmonella* are currently known to be involved in SIF formation. One thereof, SIFA, is essential for SIF formation, as *sifa*-mutant strains cannot form SIFs. This also holds true for its protein interaction partner SifA and Kinesin-Interacting Protein (SKIP). The SIFA-SKIP protein complex likely triggers membrane extension from the SCV towards the cell periphery along MTs. SIFA is localized outside at the SCV membrane where it likely exerts GEF activity on RhoA. Activated RhoA, likely recruits further proteins to form an active SIFA-SKIP complex that eventually recruits Kinesin-1. The motor protein Kinesin-1 then acts in concert with other proteins in pulling the SCV membrane in direction of the plus-end of MTs. Two other effectors of Salmonella, SSEF and SSEG promote MT bundling which stabilizes the MT network. SSEF and SSEG are further thought to redirect post-Golgi vesicles to the elongating SIF [Brumell et al. 2002; Kuhle et al. 2004; Schroeder et al. 2011]. Why SIF formation is beneficial for *Salmonella* has not been fully understood yet. There are additional examples of bacterial effectors inducing MT bundling which might possibly interfere with vesicle trafficking coming from *Streptococcus pneumonia* and *Brucella* spp. [Radhakrishnan and Splitter 2012]. Free tubulin dimer sequestration is a common mechanism for MT destabilization employed by intracellular pathogenic bacteria of mammals. The *Listeria monocytogenes* effector ACTA localizes to the tail pole of the bacterium where it recruits an Arp2/3 actin nucleation complex. Actin polymerization propels the bacterium through the host cytoplasm by forming impressive actin-composed ‘comet tails’. However, ACTA via another protein also recruits the MT destabilizing protein Stathmin. Stathmin hinders MT polymerization by sequestration of free tubulin dimers and additionally induces catastrophe of existing MTs. It is thought that MT depletion at the bacterial tail is a prerequisite for the massive actin nucleation activity in comet tail formation [Radhakrishnan and Splitter 2012]. *Chlamydia* species evolved independently a T3SS effector that shows Stathmin-like activity but does not

share sequence similarities with Stathmin. Like Stathmin, the effector COPN hinders MT assembly by physical binding to free tubulin dimers that by binding of COPN are altered in a way that prevents their integration into polymerizing MT plus-ends. Another resemblance of COPN and Stathmin is given by their functionality as inhibitors of cell division which is achieved by loss of metaphase mitotic spindles [Archuleta et al. 2011]. Enteropathogenic *E. coli* (EPEC) are gastrointestinal pathogens adhering to epithelial cells. EPEC secrete *inter alia* two redundantly acting effectors into their host cells. ESPG and ESPG2 destabilize MTs leading to a MT depleted zone beneath the adhering bacterium. ESPG and ESPG2 action involves direct tubulin binding but the exact mechanism for MT destruction remains unknown yet. MT fragmentation releases the MT-associated RhoA-GEF GEF-H1 from MTs which subsequently activates RhoA. RhoA signaling via the ROCK signaling pathway contributes to actin cytoskeleton rearrangement and might be responsible for actin stress fiber formation. Stress fibers likely exert actin-myosin-mediated contractile force on cell-cell-junctions. Cell-cell-junctions are protein complexes that link adjacent cells to each other and additionally form a physical barrier for paracellualar transport in endothelial cells. It is thought that stress fibers via their physical connection to cell-cell-junctions cause hyperpermeability of the paracellular transport route which is symptomatic for EPEC infections [Matsuzawa et al. 2004; Shaw et al. 2005; Caron et al. 2006]. ESPG and ESPG2 are homologous to VirA of *Shigella flexneri* that can replace each other in functionality. *Shigella flexneri* is a further gastrointestinal bacterial pathogen causing severe gastroenteritis. Besides activating RhoA signaling by VirA *Shigella* infection additionally activates RAC1 which was also attributed to MT depolymerization by VirA. Rac1 activity and RhoA activity are antagonistic to each other and it was unclear how *Shigella* might interfere with that antagonism. In contrast to EPEC, *Shigella* get internalized into endothelial cells at the basolateral site. This involves actin-driven lamellopodia-like membrane ruffles formation that depends on RAC1 and Cdc42 activity. Inside endothelial cells *Shigella* are transiently localized in a vacuole-like compartment that rapidly disintegrates thereby releasing *Shigella* into the cell cytoplasm. *Shigella* move like *Legionella* (see above) driven by an actin-tail through the host cytoplasm. Interestingly, intracellular *Shigella* movement causes a MT-depleted path. Immunostaining showed VirA to surround moving *Shigella*. *Shigella* motility depends on VirA as *VirA*-depleted mutant strains are

impaired in intracellular movement which can get complemented by VirA [Yoshida et al. 2002; Yoshida and Sasakawa 2003; Yoshida et al. 2006]. VirA was originally reported to act as a cysteine protease on α-tubulin, which was later heavily doubted based on the structure of the VirA protein and lack of protease activity on tubulin. It was then discussed to act as a scaffolding protein for other proteases [Davis et al. 2008; Germane et al. 2008]. However, VirA binding to tubulin was not questioned. Later it turned out that two other T3SS effector proteins activate Rac1, Cdc42 and RhoA instead of VirA. IgpB1 and IgpB2 both act as GEF mimicry like SopE of *Salmonella* (see above). IpgB1 activates Rac1 and Cdc42 for lamellopodia-like membrane protrusion formation via Arp2/3 complex induced actin filament polymerization. IpgB2 acts as GEF on RhoA which additionally requires the host GEF-H1 for RhoA activation. RhoA signaling acts in actomyosin contractility and cell adhesion. The RAC1-RhoA antagonism is likely subverted by the presence of either IpgB1 or IpgB2, where the presence of the one excludes the presence of the other. It has been shown that the functionality of IpgB2 depends on the absence of IpgB1 [Carayol and Tran Van Nhieu 2013]. However, VirA might still play a more indirect role activation than previously assumed. VirA promotes the degradation of calpstatin which is the negative regulator of calpain proteases thereby promoting calpain protease activity. Calpain travels to the PM where it is assumed to support F-actin assembly required for lamellipodia-like membrane protrusion uptake of *Shigella* [Bergounioux et al. 2012]. Calpaine proteases have versatile cellular targets including the cytoskeleton, PM proteins, signaling proteins and transcription factors [Bergounioux et al. 2012]. The 45kDa protein VirA has a GAP domain in its sequence that was shown to exert GAP activity on Rab-GTPases that regulate ER to Golgi vesicle trafficking. By de-activating Rab-GTPases, VirA inhibits secretion of proinflammatory cytokine IL-8 that stops the inflammatory response and prevents autophagy which enables *Shigella* residence in host cells [Dong et al. 2012].

To sum up, it seems to be a general virulence mechanism of bacterial invaders of eukaryotic cells to remove MTs to makes room for pronounced actin nucleation. The VirA function additionally tells that effector-triggered susceptibility is easily complicated with the observed host cell responses being less linear connected to the effector than first anticipated.

3.3.3 MT-Manipulating Effectors of Plant Pathogens

The knowledge on MT-manipulating effectors of plant pathogens is sparse and only vaguely understood. Harpin and Harpin-like proteins are associated with pilus formation and functionality of the T3SS of pathogenic bacteria. One thereof, HrpZ, integrates into artificial lipid bilayers *in vitro* and is thought to form an ion-conductive pore in vivo, also its real functionality is unknown yet. However, HrpZ can be used as a trigger of PCD in plant cells. Upon HrpZ elicitation, a rapid bundling of AFs is observed that then depolymerize and aggregate as punctuate structures. This is accompanied by loss of radially oriented cytoplasmic MTs with cortical MTs being unaffected [Guan et al. 2013]. So, HrpZ as cell-death elicitor has at best an indirect effect on MT organization, as the observed cytoskeletal reorientation are typically seen to precede plant PCD [Smertenko and Franklin-Tong 2011]. The YopJ-like effector AvrBsT of *Xanthomonas euvesicatoria* physically interacts with the putative MAP AtACIP1. Arabidopsis is a non-host for *X. euvesicatoria* but AvrBsT can get delivered into Arabidopsis using *Pst* DC3000. AvrBsT has acetyltransferase activity. AtACIP interacts with tubulin *in vitro* but is of general unknown function. It is localized as punctuate aggregates at the cell cortex and at cortical MTs. AvrBsT-dependent acetylation of AtACIP promotes its relocalization from the cell cortex and MTs to the cell lumen where it forms larger aggregates. AvrBsT triggers HR in a resistant Arabidopsis cultivar in an AtACIP-dependent manner. Further, acetylation of ACIP1 by AvrBsT is required for HR induction by AvrBst as a catalytic inactive AvrBsT mutation is unable to trigger HR in the resistant host background. However, the MT cytoskeleton organization is likely not affected by AvrBsT action [Cheong et al. 2014]. There is no functional connection between AtACIP MT localization and AtACIP functionality as cell-death trigger known yet. Further it is unclear whether AtACIP constitutes the real host target of AvrBsT or whether heterologous translocation of AvrBsT into the non-host Arabidopsis might have an effect. Especially when concerning that bacterial acetyltransferase effectors can have multiple targets. The YopJ/HopZ T3SS superfamily of acetyltransferase effectors is conserved in animal and plant pathogenic bacteria. HopZ1A of the bacterial plant pathogen *P. syringae* has at least two host targets in *At*. The first target is the pseudokinase AtZED1. AtZED1 directly interacts with HopZ1A and the NB-LRR R-protein AtZAR1 *in vitro* and *in planta*. Further, acetylation of AtZED1 by HopZ1A triggers AtZAR1 ETI-defense signaling. It is thought

that AtZED1 is a decoy that acts as a ‘kinase trap’ for kinase-acetylation by effectors which is then recognized by AtZAR1 [Lee et al. 2012]. The second host target of HopZ1A are cortical MTs. HopZ1A of *P. syringae* is therewith the first described plant pathogen effector directly targeting host cell MTs. HopZ1A was found to cause cell rounding and loss of cellular protrusions (lamellopodia) in human embryonic kidney cells in a heterologous screen for conserved eukaryotic host targets of bacterial T3SS effectors. Human tubulin was identified as interaction partner of HopZ1A by LC/MS/MS in a pull-down assay. In further attempts, HopZ1A was also found to physically interact with bovine and plant hetero-tubulins and taxol-stabilized MTs *in vitro*. *In vitro* acetylation assays showed strong auto-acetylation activity of HopZ1A and direct tubulin heterodimer acetylation by HopZ1A. HopZ1A gets myristoylated inside the host cell and associated with the inner face of the host PM where it meets the cortical MT network. HopZ1A activity was found to decrease the density of cortical MTs by 50 % whereas HopZ1A has no effect on the actin cytoskeleton. Acetylation of heterotubulins may interfere with MT polymerization. Drug-induced disruption of host MTs significantly enhances the proliferation of *P. syringae* in Arabidopsis. Heterologous expression of HopZ1A in Arabidopsis inhibited the classical secretory pathway and blocked callose deposition into papillae which is likely due to its effect on MT destabilization [Lee et al. 2012].

3.3.4 *Bgh* ROPIP1 and the Barley MT network

Live cell imaging of ectopically expressed GFP-ROPIP1 in barley epidermal cells showed recruitment of ROPIP1 to cortical MTs by the RFP-tagged MT-associated ROP-GAP MAGAP1. The MT association of GFP-ROPIP1 depended on co-expression of RFP-tagged full-length MAGAP1. Alternative co-expression of the truncation mutant RFP-MAGAP1-Cter, which is still MT-associated but lacks the CRIB domain for activated ROP interaction and the ROP regulatory GAP domain, highly significantly abolished recruitment of GFP-ROPIP1 to MTs. Further, transient expression of GFP-ROPIP1 alone localized GFP-ROPIP1 unspecifically to the cytoplasm and nucleoplasm of barley epidermal cells. Therefore, ROPIP1 likely does not have MT binding properties by itself but relies on MAGAP1 for MT association. However, ROPIP1 and MAGAP1 were not found to physically interact in targeted Y2Hs which suggests an indirect protein

interaction of ROPIP1 and MAGAP1. MAGAP1 is a putative ROP-GAP that interacts with the activated barley ROPs RACB and RAC1 [Hoefle et al. 2011 and Hoefle Caroline, Hückelhoven Ralph (TU München, Germany) unpublished results, personally communicated) in yeast and *in planta*. Physically interacting ROPIP1 and CA RACB were observed at RFP-MAGAP1 R185G decorated MTs by YFP-complementation of the BiFC pair ROPIP1-YFP^N and CA RACB-YFP^C. This suggests that the ROPIP1-MAGAP1 association is mediated by RACB. GFP-ROPIP1 recruitment to RFP-MAGAP1 decorated MTs in absence of co-expressed ROPs may be explained by the formation of a GFP-ROPIP1-native ROP-RFP-MAGAP1 complex. Activation of native RACB and likely RAC1 would first recruit ROPIP1 to form a dimeric protein complex which is then sequestered at MTs by direct ROP^{GTP}-MAGAP1 interaction upon formation of a heterotrimeric protein complex with ROPIP1. However, it cannot be ruled out that ROPIP1 binds to MAGAP1 *in planta* but that ROPIP1-MAGAP1 complex formation is hindered in yeast nuclei by unknown reasons. By associating with RFP-MAGAP1 at MTs, GFP-ROPIP1 promoted the collapse of the cortical MT network. The percentage of barley epidermal cells showing complete loss of MT organization tripled in comparison to control cells co-expressing GFP instead of GFP-ROPIP1. Contributing to cortical MT array breakdown provides a probable mechanistic link to the virulence inducing effect of ROPIP1. MTs contribute to penetration resistance in barley cells as oryzalin-induced disintegration of the MT cytoskeleton allowed entry of the non-adapted *E. pisi* which otherwise fails at the pre-penetration stage [Kobayashi et al. 1997]. As GFP-ROPIP1 and RFP-MAGAP1 expression was driven by the 35S promoter, it is likely that not the entire cortical MT array undergoes such dramatic change in the native situation. Especially as the complete loss of the host cell cytoskeleton is linked to PCD induction [Smertenko and Franklin-Tong 2011] which would be detrimental for *Bgh* as an biotrophic pathogen. It is conceivable that ROPIP1 contributes to local cortical MT disorganization beneath the fungal appressorium. This is likely the spot of highest ROPIP1 concentration as goldparticles were observed apparently spreading from the tip of the appressorium in immunogoldlabeling (Figure 4D). The results of this work clearly indicate ROPIP1 to constitute the first plant pathogen effector whose virulence function links ROP signaling to MT reorganization of the host cell. It further constitutes the first fungal plant pathogen effector manipulating the host MT network. This work further

substantiates that fail-regulation of the host MT cytoskeleton contributes to susceptibility of barley epidermal cell towards powdery mildew fungi which has already been suggested before [Kobayashi et al. 1997; Hoefle et al. 2011; Huesmann et al. 2012]. Additionally ROPIP1 is one of comparatively few plant pathogen effectors which have not been identified by their avirulence function but by their virulence function. ROPIP1 is the first plant fungal pathogen whose target is a host susceptibility factor. The results of this work together with the reported physical interaction of HopZ2 of *P. syringae* and the negative regulator of prepenetration defense AtMLO2 in yeast and *in planta* [Lee et al. 2012] add to the assumption that host susceptibility factors are *bona fide* pathogen effector targets [Hückelhoven et al. 2013; van Schie and Takken 2014].

The question why the MT destabilizing effect of ROPIP1 seems to be supported by catalytic activity of MAGAP1 remains unsolved. Under the assumption that ROPIP1 hinders deactivation of RACB signaling by probably sterical hindrance of MAGAP1, the catalytic inactive MAGAP1-R185G mutant should have the same effect. It binds to RACB and gets recruited to the PM by active RACB [Hoefle et al. 2011] but due to its lacking Arg-finger cannot shut RACB ‘off’. It probably could also form a stable complex with active RACB as GTP-bound RACB likely attracts MAGAP1-R185G by its CRIB-domain and/or by its GAP domain. Activated RACB recruits RFP-MAGAP1 and RFP-MAGAP1-R185G predominantly to the PM [Hoefle et al. 2011].The BiFC experiment showed that RFP-MAGAP1-R185G principally can interact with the ROPIP1-CA RACB complex at cortical MTs. This excludes the possibility that MT-association of the ROPIP1-RACB-MAGAP1 complex is hindered by the R185G mutation of MAGAP1. Hoefle et al. [2011] reported that over-expression of catalytic active MAGAP1 promotes focusing of cortical MTs to the site of *Bgh* attack, which was not seen when MAGAP1 was replaced by the catalytic inactive MAGAP1-R185G mutant. Hence, it is possible that catalytic activity of MAGAP1 has a positive effect on MT dynamics and that this is co-opted by ROPIP1. Anyhow, the possibility that MAGAP1 exerts GAP activity on RACB which then stays sequestered at cortical MT by ROPIP1 is unlikely. Only GTP-bound CA RACB induces super-susceptibility, whereas WT RACB and DN RACB are neutral in the defense reaction of barley against *Bgh* [Schultheiss et al. 2003]. ROPIP1 interacted with CA RACB in yeast and *in planta* but not with DN RACB. Over-expression of ROPIP1

induced super-susceptibility. As only active RACB is beneficial for *Bgh* it is likely that RACB cannot get regulated by MAGAP1 upon formation of an active RACB-ROPIP1 complex. The hindrance might be sterically like protecting the GTP binding pocket of RACB from the MAGAP1 GAP domain. This imperfect contact might be stabilized by the CRIB domain of MAGAP1 binding to active RACB. The BiFC experiment located the CA RACB-ROPIP1 complex likely to the PM and to cortical MTs, but was also seen to be located in the cytoplasm. A portion of fluorescence protein-tagged CA RACB with cytoplasmic localization is often seen in transient over-expression experiments and might be partly due to high protein abundancy. However, CA RACB can locate to the PM dependent on its C-terminal CAAX motif for prenylation [Schultheiss et al. 2003]. Localization of the CA RACB-ROPIP1 complex at likely the PM is a specific localization. GFP-ROPIP1 exclusively labeled the cytoplasm and was never seen at the cell periphery. As the PM is the predominant localization of CA RACB [Schultheiss et al. 2003], it is very likely that ROPIP1-YFP^{N} was recruited to the PM by CA RACB-YFP^{C}. Interestingly, RFP-MAGAP1-R185G was not recruited to the PM by the CA RACB-ROPIP1 BiFC complex. Co-localization and FRET-studies showed a near complete recruitment of RFP-MAGAP1 to the PM by CA RACB [Hoefle et al. 2011]. RFP-MAGAP1 R185G is not impaired in getting recruited to the PM by CA RACB [Hoefle et al. 2011]. Hence, the cortical MT localization of the CA RACB-ROPIP1 BiFC complex suggests cortical MTs to be the place of interaction of ROPIP1, activated RACB and MAGAP1. Together with the observed MT-destabilizing effect of GFP-ROPIP1 upon RFP-MAGAP1 co-expression, this indicates that local RACB activity negatively interferes with MT stability. The underlying mechanism of a possible RACB-mediated MT destabilization pathway is largely unknown. Besides RBK1 that might act as MT stabilizer possibly by restriction of RACB protein abundance (see Figure 11) [Huesmann et al. 2012; Reiner et al. 2015] further direct protein interaction partners acting on MT organization await their identification. Good candidates for a MT destabilizing pathway are proteins homologous to AtMIDD1 and AtKin13A [Mucha et al. 2010; Oda and Fukuda 2012]. Homologues to AtMIDD1 and AtKin13A have been identified in barley and are under current investigation. A combination of AtMIDD1 and AtKin13A is functional in MT destabilization in barley (Caroline Hoefle, Hückelhoven Ralph, TU München (Germany) unpublished results, personally communicated). This raises the

possibility of a conserved MT-destabilization pathway present in monocots and dicots (see also Figure 11).

3.3.5 MT Network Breakdown Might Restrict Papillae Formation

Papillae or CWAs are rapidly formed host cell wall enforcements that act as physical barriers against pathogens trying to penetrate the host cell. They are also sites of antimicrobial compound accumulation that act in poisoning the invader, like ROS [Hückelhoven 2014]. Papillae are structurally mainly composed of callose (β-1,3-glucan), cell wall polysaccharides (cellulose, hemicellulose, pectin) and cell wall proteoglycans (arabinogalactan proteins, hydroxyproline-rich glycoproteins). Lignification of phenolic monolignols and cross-linking of cell wall polysaccharides with further phenolic compounds mainly derived from the phenylpropanoid pathway further strengthen the secondary cell-wall like papillae [Underwood 2012; Bellincampi et al. 2014]. Tightening of cellulose fibrils by lignificiation further protects the plant cell wall from lytic digestion due to its water-rejecting nature. Lignification also contributes to penetration resistance of diploid wheat against the wheat powdery fungus *Bgt*, a close relative of *Bgh*. RNAi-mediated silencing of key regulators of the monolignol biosynthesis pathway decreased pre-penetration resistance. Co-silencing of *PAL* and *Cinnamyl Alcohol Dehydrogenase* (*CAD*) nearly doubled the penetration efficiency of *Bgt* on diploid wheat [Bhuiyan et al. 2009].

Callose deposition is discussed to be regulated by the cortical MT network in tobacco pollen tubes. Callose Synthase and tubulin can form protein complexes and Callose Synthase delivery to the PM might be independent of exocytotic vesicles. Further, oryzalin treatment inhibited Callose Synthase activity [Cai et al. 2011]. When assuming the existence of a similar mechanism in barley epidermal cells, ROPIP1-mediated MT fail-orientation would impair correct callose deposition at developing papillae. Papillae with reduced callose amount likely would not be sufficient to explain the virulence effect of ROPIP1. Over-expression of the Callose Synthase AtRPM4 led to complete penetration resistance of Arabidopsis against adapted and non-adapted powdery mildew fungi, likely by enhancing the resistance of plant cell walls against lytic enzymes. However, an *rpm4* knock-out mutation could only weakly break the non-host resistance of Arabidopsis against *Bgh* [Faulkner 2015]. The contribution of callose to penetration

resistance has not fully been served yet [Voigt 2014]. However, callose, the hemicellulose arabinoxylan and cellulose were found to be enriched in papillae that *Bgh* failed to overcome (effective papillae) in comparison to papillae that were penetrated in susceptible barley epidermal cells in an immunohistochemical study. Following initial deposition of phenolic compounds beneath the fungal appressorium, the amount of callose and arabinoxylan deposition in resistant cells exceeds the level seen in ineffective papillae. Arabinoxylan molecules are likely cross-linked to each other and are likely further cross-linked with phenolic acids. A large amount of callose and cross-linked arabinoxylan might be sufficient for entrapping the penetration peg eventually stopping the penetration process. Effective papillae are further encased by cellulose fibrils which are also likely cross-linked with arabinoxylan [Chowdhury et al. 2014].

Hence, the deposition of at least two components of an effective papillae, callose and cellulose, can get linked to the MT cytoskeleton. CSC are physically linked to cortical MTs by CSI1 (see above). Any negative effect on the MT-CSI1-CSC conjunction may promote atypical positioning of CSC and aberrations in CSC motility. Removal of the CSI1 component in a *csi1* null-mutant Arabidosis line reduced the cellulose content of hypocotyl and root cell walls with cells developing more isotropically in shape [Lei et al. 2014]. Knock-out mutants of *CESA6* or the cellulose biosynthesis-associated protein Korrigan (KOR1) were hypersensitive for oryzalin treatment and showed reduced CSC motility. It was concluded that CESA6 and KOR1 have a stabilizing effect on the cortical MT array and that CSC activity stabilizes the cortical MT array in a positive feedback loop via CESA6 and KOR1 [Paredez et al. 2008]. Likewise drug-induced destabilization of MTs disrupts directed positioning of CSCs leading to their atypical uniform localization throughout the cell cortex [Lei et al. 2014]. It is therefore conceivable that ROPIP1 induced destabilization of the cortical MT network negatively affects the association of CSCs and likely Callose Synthases with a developing papillae. This probably counteracts papillary rigidity rendering papillae less effective.

A recent study additionally linked the Golgi-based secretion of cell wall matrix polysaccharides to the cortical MT network. AtFRA1 is a kinesin4-family motor protein, which when silenced causes a reduction of cell wall thickness by 50%. GFP-AtFRA1 moves along cortical MTs and accumulates in rapidly growing cell regions. AtFRA1 likely

functions in transporting Golgi-derived secretory vesicles to sites of cell wall thickening. Pectin components were identified as cargo, but likely further Golgi exocytotic vesicles containing cell wall matrix polysaccharides like hemicelluloses (arabinoxylan, xyloglucan) are motor-driven transported to the cell cortex along cortical MTs via AtFRA1. The authors reasoned that MT-based transport of Golgi secretory vesicles provides an additional track to the actinomyosin system in the formation of cell walls [Zhu et al. 2015]. This adds hemicelluloses and pectins to the cell wall components whose directed secretion might at least be reduced by ROPIP1-triggered disorganization of the MT cytoskeleton. Especially a reduced amount of arabinoxylan, that likely glues together many polysaccharide and phenolic components of effective papillae, would likely contribute to accessibility of fungal hyphae into host plant cells.

Together, these recent findings make it conceivable that cortical MT array disintegration by ROPIP1 interference with RACB-MAGAP1 regulation may reduce the integration of key components into developing papillae rendering them less resistant to fungal penetration.

3.3.6 MT Network Breakdown Might Affect Secretion of Defense Compounds

In non-plant eukaryotic cells MTs participate in the motility and positioning of intracellular organelles. The actin and the MT cytoskeleton cooperate in movement of the nucleus. MTs are especially required for positioning of the nucleus. Unlike in plant and yeast cells ER movement and positioning predominantly depends on the MT network in mammalian cells. The ER moves kinesin-motor driven along preexisting MTs to the plus-end. The ER also extends with polymerizing MTs by formation of a Tip Attachment Complex (TAC) with the growing MT plus-end. MTs are additionally required for maintenance of the ER shape. MT depolymerization loosens the ER shape. The Golgi apparatus acts as MT nucleation center. MTs at the cis-Golgi site connect to the ER. COPII-coated vesicles travel Dynein-1 driven from the ER along MTs to their minus-end nucleated at the Golgi cis-site. COPI-coated vesicles in the retrograde route from the cis-Golgi back to the ER can move along MTs by Kinesin-2. Interestingly, barley COPIγ is required for penetration resistance to *Bgh* [Ostertag et al. 2013]. Clathrin-coated secretory vesicles emerging from the trans-Golgi network (TGN) under the help of the actin-myosin system subsequently travel to the cell periphery using MTs as tracks and kinesin1-3 as motors.

Like the ER, the Golgi apparatus relies on the cytoskeleton to maintain its shape. [Brownhill et al. 2009; Forges et al. 2012; Gurel et al. 2014].

For plant cells, the contribution of the MT cytoskeleton to secretion is far less understood. It has been agreed, that the MT cytoskeleton is pretty negligible for organelle movement and positioning. A view that is beginning to being challenged at least in part. Myosin motors move faster than kinesins and dyneins. Dyneins are absent in most plant species whereas kinesins have diversified into comparatively large protein families. The intracellular motility of organelles is actin-myosin driven in plant cells. This is attributed to the comparatively large size of plant cells where the velocity of myosin motors might be of advantage. The velocity of the actin-myosin system causes cytoplasmic streaming that can be watched using live cell imaging techniques. The Golgi apparatus moves fast along actin bundles that traverse the cytoplasm, its velocity gets reduced upon reaching F-actin where its movement gets less linear. Class-XI myosins associate with secretory vesicles and are likely involved in moving the ER and the Golgi apparatus. Unlike in animal cells, the MT cytoskeleton seems to be unimportant for ER and Golgi shape maintenance and motility. Further, vesicle exchange between the ER and the Golgi apparatus seems to be independent of the MT cytoskeleton as well as of the actin cytoskeleton. However there might be a connection of the Golgi apparatus, the actin cytoskeleton and the MT cytoskeleton at the cell cortex. The Golgi outer surface is wrapped with the kinesin AtKin13A which is thought to cause pausing of Golgi stacks at cortical MTs. Golgi pausing can be observed at sites of papillae formation in barley under attack from *Bgh* (Hückelhoven Ralph (TU München, Germany), personal communication). Further, cortical MTs are involved in local concentration of AtPIN2 Auxin efflux carrier endosomes. AtPIN2 endosomes travel to the TGN where they interact with Sorting Nexin 1 (SNX1). SNX1 is part of the retromer sorting complex that mediates recycling of AtPIN2 back to the PM. The MT-binding protein CLASP interacts with SNX1 tethering the PIN2-endosome to cortical MTs. SNX1-regulating proteins then promote the release of AtPIN2 back to the PM. A greater portion of AtPIN2 endosomes enter the degradation pathway when CLASP is missing [BOUTTE et al. 2007; Brandizzi and Wasteneys 2013]. The actin and the MT cytoskeleton act collaboratively in the transport of secretory vesicles in eukaryotic non-plant cells. The long-range transport to

the cell periphery is driven by Dynein and Kinesin motors. At the cell-periphery secretory vesicles enter the cortical F-actin network and move via myosin-motors. Secretory vesicles can cross from the MT network to the actin network and vice versa. This cross-reactivity is further required for movement and positioning of organelles [Ross et al. 2008; Barlan et al. 2013].

There is an obvious upside-down situation in plant cells, where the long-range transport of secretory vesicles through the cytoplasm to the cell cortex is driven by myosin motors along actin bundles. At the cell cortex actin bundles, F-actin and cortical MTs meet and the situation is getting more complex. Mitochondria that move along the actin cytoskeleton as well as along MTs and proteins that can bind to AF as well as to MTs give hints for an AF-MT connection in plant cells. Kinesins that contain a Calponin Homology Domain actin binding domain (KCHs) of rice and cotton can bind both AFs and MTs *in vitro* [Petrásek and Schwarzerová 2009]. Moreover, the cell cortex of plant cells seems to be highly interconnected by diverse Formin proteins. Formins are typically membrane-associated proteins. Class I Formins are TM proteins whose extracellular domain anchors the cell wall to the plasma membrane. Their intracellular part contains a Formin Homology 2 (FH2) domain that nucleates AFs. The intracellular part can further bind to MTs. Class II Formins lack the extracellular and the transmembrane domain but are membrane associated as well which includes endomembranes, the ER is known to be involved yet, localize at MT and contain the FH2 domain that inter alia acts as actin nucleation center. In sum, all major components of the cell cortex, the cell wall, PM, cortical MTs and AFs, have at least the ability to connect to each other via Formins. Further Formins might provide a link between the cytoskeleton and endomembranes in general, but might also provide a link between the endomembrane system and the plant cell cortex [Cvrčková et al. 2015]. The PM-based exocyst components AtExo70A and AtSEC3 were visualized as non-motile punctuate structures [Zárský et al. 2013]. Formins are discussed to fix the position of the exocyst complex at the PM through their anchorage of their extracellular domain in the cell wall. Lateral stabilization of the secretory machinery is a prerequisite for pointed secretion like in the process of exocyst-dependent pectin volcano cell wall formation at seed coats as lateral movement of the exocyst would lead to a more uniform pectin deposition [Synek

et al. 2014]. Activation of ROPs, likely by PRONE-GEFs, which in turn promotes the activity of PI4P 5-kinases creates lipid-raft-like Activated Microdomains (AMD) that are enriched in Phosphatidylinositol-4,5-bisphosphate (PtdIns(4,5)P2). These AMDs likely recruit AtExo70A. Further AtROP2 via its effector AtICR1 interacts with AtSEC3 at the PM. But AtSEC3 reportedly can also interact directly with membrane phospholipids. Hence, by ROP activity both PM-based exocyst subunits can get recruited to the PM. The other subunits of the octameric exocyst complex are provided by secretory vesicles. AMDs are seen together with dense underlying cortical MT arrays in plant cells. Dense cortical MT arrays are thought to promote secretion whereas cortical AF mesh inhibits secretion in plant cells. Therefore, the formation of dense cortical MT arrays in conjunction with ROP activity and the formation of AMDs might determine the site of regulated exocytosis [Zárský et al. 2009; Zárský et al. 2013; Synek et al. 2014].

Interestingly, a lipid-raft-like domain forms at the site of *Bgh* attack where the barley susceptibility factor *MLO* and the barley syntaxin ROR2 localize [Bhat et al. 2005]. A DsRed fusion of the activated RACB downstream effector RIC171 accumulated at papillae and penetration sites in *Bgh*-attacked barley epidermal cells which is likely indicative for local RACB activity beneath the invading hyphae [Schultheiss et al. 2008; Hückelhoven and Panstruga 2011]. Barley MAGAP1 promotes focusing of cortical MTs to the site of *Bgh* attack where they form a dense nest-like array surrounding the invading hyphae [Hoefle et al. 2011]. AtExo70 parlalogues are pathogen-responsive. A GFP-fusion of AtExo70A1 accumulated at papillae beneath *Bgh* appressoria in the non-host defense reaction of Arabidopsis. Knock-down of AtExo70B2 potentially inhibited vesicle fusion to the PM seen as vesicle accumulation beneath the contact site with *Bgh* appressoria. However, that was neutral in the non-host defense of Arabidopsis against *Bgh* [Zárský et al. 2013]. By contrast, a putative Exo70F protein is required for successful plant defense in the barley-*Bgh* interaction. TIGS of the *Exo70F* candidate rendered barley epidermal cells more susceptible towards *Bgh* [Ostertag et al. 2013]. There are 23 Exo70 paralog copies in Arabidopsis. This likely implies a functional diversification and a degree of pathway specificity of individual Exo70 paralogs. The exocyst complex is very likely required for papillae formation and may also be functional in endosomal and MVB recycling. A dependency on the PM-based exocyst components

for secondary cell wall formation was shown by *AtExo70A1* and *AtSEC3* knock-out mutants. At least pectin and hemicellulose (arabinoxylan and xyloglucan) deposition is dependent on AtExo70s and AtSec3 [Zárský et al. 2013; Krishnamoorthy et al. 2014]. This is very likely underestimated as vesicle tethering to the PM is to the current knowledge generally dependent on the exocyst complex. Further, exocytosis is not thought to be constitutive but to be regulated via regulation of the exocyst complex. Therefore, the exocyst complex is assumed to be required for secretion-based plant cell defense against pathogens [Zárský et al. 2009; Zárský et al. 2013].

While the focal delivery and concentration of secretory vesicle was largely attributed to the actin cytoskeleton [Day et al. 2011], recent work also adds the requirement of the MT cytoskeleton for targeted secretion in the development of the secondary cell wall of xylem vessels and opens a putative connection of Golgi-derived secretory vesicles and the cortical MT network. Two paralogous and likely redundant proteins of unknown function and a predicted coiled-coil structure scored highest in a screen for AtMIDD1 co-expressed proteins in developing Arabidopsis root xylem cells. GFP fusions of Vesicle Tethering 1 and 2 (AtVETH) localize to vesicle-like compartments that preferentially accumulate at growing plus-ends of MTs. AtVETH-decorated vesicle-like compartments (AtVETH-vesicles) were also observed at the side of MTs from where they moved to the MT plus-end and to cross from one MT to another, which suggests a kinesin-driven movement of AtVETH-vesicles. AtVETH proteins interact with an AtCOG2-like vesicle tethering Conserved Oligomeric Golgi Complex (COG) protein in yeast and interact physically with AtCOG2 *in planta*. Co-expression of AtVETH together with AtCOG2 recruited the exocyst subunit AtExo70A1 to cortical MTs which is likely mediated by AtCOG2. AtCOG2 is a putative COPI protein, that assist in the retrograde vesicle pathway from the Golgi back to the ER in metazoan cells. However, the functionality of COPI is not well understood in plant cells. The authors speculated that an AtVETH-AtCOG2 complex may connect the Golgi to cortical MTs for exocytosis of Golgi-derived vesicles along cortical MTs. In their model, AtVETH-vesicles containing secondary cell wall material are distributed to MT-dense areas where they get tethered to the PM by recruitment of the exocyst complex via an AtVETH-AtCOG2 protein complex [Oda et al. 2015]. Interestingly, Ostertag et al. [2013] identified, besides the putative Exo70F

exocyst subunit, additionally a putative COG3 protein to be required for full penetration resistance of barley epidermal cells towards *Bgh*. This raises the hypothetical possibility that not only targeted secretion of secondary cell wall material in xylem cells but also targeted secretion of antimicrobial compounds might involve a similar route.

Therefore destabilization of cortical MTs by ROPIP1 might also lead to a fail-positioned exocyst complex. A decrease in exocyst complex density at papillae might not only impair papillae structurally but might also lead to a decrease in secreted antimicrobial compounds.

The actin and the MT cytoskeleton focus towards the site of attack in the basal resistance reaction of barley epidermal cells against. Ectopic expression of GFP-ROPIP1 promoted MT loosening by co-expression of RFP-MAGAP1 possibly inducing ‘over-activation’ of RACB. This might I) enable the establishment of a local polar domain II) interfere with targeted secretion of defense compounds by disruption of MT order which also might affect a possible actin-MT connection III) may impair papillae formation.

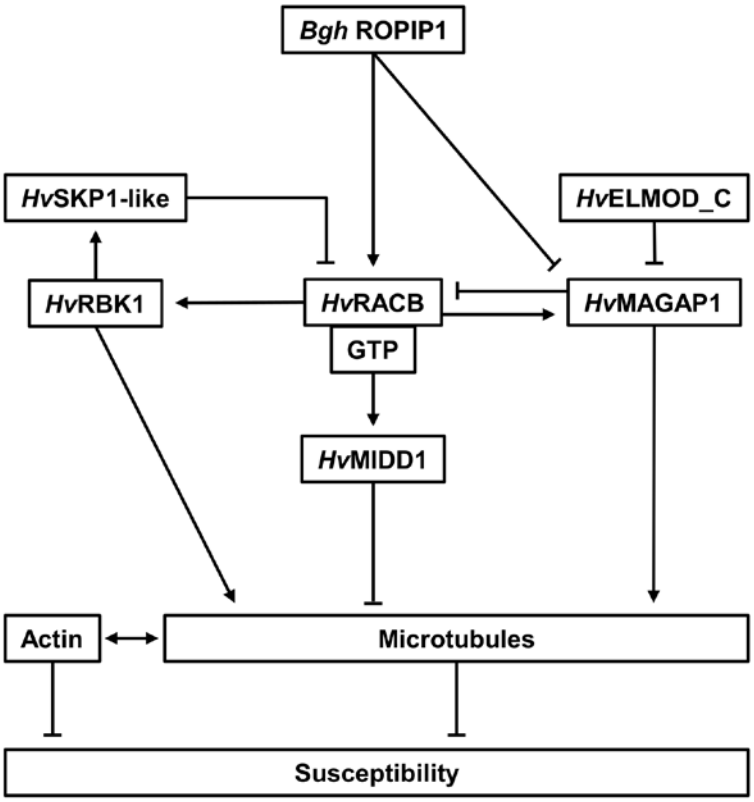

Figure 11: Current working model of the RACB effect on Microtubules in Susceptibility towards *Bgh*. Active, GTP-loaded RACB physically interacts with at least three downstream proteins that influence, or might influence, microtubule organization. RBK1 and MAGAP1 are supposed to stabilize MTs. A currently investigated MIDD1-like protein might, in analogy to AtMIDD1, have a destabilizing effect on MTs. The actin and the microtubule cytoskeleton might be interconnected. Both are required for resistance towards *Bgh*. MAGAP1 is supposed to negatively regulate RACB activity and might itself be negatively regulated by ELMOD_C. RBK1 physically interacts with SKP1-like that might lead to proteasomal degradation of RACB. MT breakdown is thought to correlate with the amount of GTP-bound RACB. *Bgh* ROPIP1 physically binds to GTP-bound RACB and might interfere with MAGAP1-mediated downreguation of RACB activity.

3.4 The Eg-R1 Retroelement

Until know, knowledge about the repetitive element Eg-R1 is sparse. A short nucleotide stretch located at the very 5'-end of Eg-R1 is highly identical to internal sequences of the *Bgh* SINEs EGH24-I and –II [Wei et al. 1996; Rasmussen et al. 1993]. Eg-R1 and EGH24 are located near CSEP families and might serve as spots for unequal crossing over [Pedersen et al. 2012]. They are also located close to EKAs [Skamnioti et al. 2008; Parlange et al. 2011].

Short interspersed nuclear elements (SINEs) are non-autonomous class I retrotransposons [Wicker et al. 2007]. SINEs are < 1 kb in length and lack major ORFs.

In this work, the Eg-R1 nucleotide sequence was found to harbor 11 additional nucleotides preceding the annotated 5'-end such that the Eg-R1 mRNA is of 698bp in length instead of 687bp. This is in line with classifying Eg-R1 as SINE. However, most SINEs are of a tripartite structure. Their 5' ends or 'heads' are derived from polymerase III (pol III) transcribed small RNAs, like tRNAs, 7SL RNA or 5SRNA which also serve as transcription initiation sites for pol III transcription of SINEs. The following 'body' sequence part is mostly of unknown origin and unique to individual SINEs. The 3'-ends of some SINEs 'body' show sequence similarities to autonomous LINEs which reverse transcriptase they depend on for inserting in new genomic locations. Their tail region can be A-rich, T-rich or be composed of short repeat sequences. Some SINEs carry intrinsic pol III terminator signals at their 3'-end (T^+ SINEs) whereas others are transcribed until stopped by a random stretch of T's in the genomic sequence (T^- SINEs). T^+ SINEs have been found to get post-transcriptionally poly-adenylated by functional AAUAAA poly-adenylation signals lying in front of their intrinsic pol III terminator sequence. In addition to the tripartite structure, SINEs can also be of simple structrure, missing the body, or of composite structures, where several short RNA-derived 'heads' and/or 'bodies' have combined [Kramerov and Vassetzky 2011].

However, Eg-R1 does not fit well into that definition of SINEs. Upon its discovery it has been described as novel class of retrotransposable element as it seems to be RNA polymerase II described (pol II; Wei et al. 1996). Eg-R1 includes a 5'- AAUAAA-3' polyadenylation signal at its 3' end and can get isolated as polyadenylated RNA [Wei et al. 1996] and my own data, not shown). The genomic insertions lack A-tails, which also points to posttranscriptional polyadenylation. Further, poly (T)-stretches which act as pol III termination signals are found amid its sequence and not at its distal end behind the polyadenylation signal. This is inconsistent with pol III transcription as it would result in a truncated element [Wei et al. 1996]. My own analysis of the Eg-R1 consensus sequence extracted from *Bgh* genomic contigs (BGH DH14 Genome v3b, www.blugen.org) using SINEBase tools for SINE analysis [Vassetzky and Kramerov 2012] would add to the hypothesis of Eg-R1 being a novel, or at least atypical SINE, retroelement. The Eg-R1 5'-'head'-region was hardly similar to small RNAs commonly found in SINEs. Instead Eg-R1 harbors a tRNA-related sequence part starting at nucleotide position 285 closely

following the ROPIP1 sequence part. Further, the t-RNA-related part lies in front of a region similar to the SINE ‘body’-part V-domain known from fish. This on the one hand adds to the assumption that Eg-R1 is pol II described and on the other may indicate that a putative ancient SINE element picked up the ROPIP1-sequence, possibly by an pol II read-through. Of course that does not exclude Eg-R1 from being possibly a SINE but it suggests that Eg-R1 clearly differs from currently known and characterized SINEs. Adding to that and even weighing more, a BLAST search against the Repbase Update (RepBase 20.01) reference collection of repetitive DNA in eukaryotic genomes using the Eg-R1 consensus sequence (as determined in this work) lead to not one single hit to a named autonomous repetitive DNA element, even not at very low significance levels. The non-specific TSDs identified in this work which are almost exclusively seen with ‘full-length’ Eg-R1 insertions rather points to a non-specific insertion mechanism by an autonomous retro-element with relaxed target site specificity. The unequal insertion size distribution of the Eg-R1 element has to my knowledge not been reported before. The sense of that is totally unclear in case it turns out not to be an assembly bias, or the result of *Eg-R1* transcript silencing by accumulation of point mutations. However, the finding of Eg-R1 belonging to a small family of 8 Non-LTR retrotransposons may point to diversification of a common ancestor element.

Together, this doubts whether Eg-R1 can get classified as true SINE and rather classifies it as novel SINE-like but pol II transcribed non-autonomous retroelement. Therefore, the Eg-R1 element does need a deeper characterization. This should include, to name a few, its structure, evolutionary origin, retrotransposition mode, copy number, physical distribution over the genome and its effect on genome remodeling.

3.5 Possibilities for ROPIP1 Translation

Whatever Eg-R1 being classified as SINE or not, the major question is how ROPIP1 would translate from Eg-R1. To make it short, this question can hardly be answered from the current knowledge. My results show ectopic translatability of the Eg-R1 derived ROPIP1 sequence in bacteria, yeast and *in planta*. Further, a possible similarity to the YigF-like superfamily (SCOP) homo-trimerization domain aligning to ROPIP1-Cter may hint to trimerization of a putatively translated ROPIP1-Cter which would fit to the size of the observed protein band in the western blot experiments. However, ROPIP1 by trend

performed better in the targeted Y2Hs and was slightly more efficient in inducing super-susceptibility. Hence, it cannot be excluded that the N-terminus of ROPIP1 constitutes a part of the native effector. So, what would be necessary to happen such that ROPIP1 gets translated directly from Eg-R1 and also gets secreted by the classical endomembrane route?

Long non-coding RNAs (lncRNAs) are more than >200 nucleotides in length. Most are pol II transcribed, while some are pol III transcribed, and are in general processed similar to mRNA including splicing, 5'-capping and polyadenylation [Nie et al. 2012]. Among them Alu and B2 SINE sequence containing transcripts can also be found [Geisler and Coller 2013]. Long intergenic non-coding RNAs (lincRNAs) are a subgroup that are not located in introns of classical genes, exert no antisense function, are of general unknown function and are not related to small non-coding RNAs (sncRNA) [Wright and Bruford 2011]. There were minor hints on the translation of lincRNAs in cancer cell lines [Banfai et al. 2012] but ncRNAs being translated also led to controversy [Guttman et al. 2013]. However, among 90 Short ORF Encoded Polypeptides (SEPs) identified under high stringency criteria in human cell lines, there were 8 which are derived from lincRNAs. SEPs are defined to be translated at ribosomes and to be shorter than 150 amino acids. The other classes of translated small ORFs were located in 5' and 3' UTRs, in the coding sequence of protein coding genes and as antisense transcripts. Due to the high stringency of the applied criteria the real number of SEPs in the human proteome might even be higher. The identified SEPs were 18 – 149 amino acids in length with most being smaller than 100 amino acids and the highest number was found in the category of 51 - 75 amino acids. The cellular concentration of SEPs was in the range from 10–1000 molecules per cell which resembled the physiological abundance of classical proteins. Interestingly, roughly 60 % of the SEPs showed non-ATG start codon initiation and some even bicistronic mRNA transcripts. Heterologous expression of SEPs substantiated their translatability, stability inside cells and their capability of translation from non-canonical start codons [Slavoff et al. 2012]. Recently the number of translated lincRNAs in the human proteome was risen 50 fold to 404 which were identified by high quality peptides in the human proteome [Wilhelm et al. 2014]. Small peptides encoded by ncRNAs have also been reported from Drosophila

[Galindo et al. 2007] where very short SEPs of 11 amino acids derived from an array of 33 nucleotide ncRNAs located on a polycystronic transcript showed bio-functionality in the morphogenesis of fly legs. Two further SEPs were identified in Drosophila that are conserved in many species including humans. In fact, these SEPs have been conserved for 550 million years. They were shown to exert functionality in regulation of Ca^{2+} transport in muscles. Disturbances in the protein level of the human homologue can cause pathological heart arrhythmias [Magny et al. 2013]. Another example comes from zebrafish. A Toddler named SEP is encoded by ncRNA. It gives rise to a 58 amino acid SEP containing a functional signal peptide for secretion. Homologous sequences are conserved within vertebrates. Additional to Toddler, 28 candidate secretory proteins representing 40 transcript isoforms ranging from 32 to 556 amino acids in length have been identified from ncRNA. Toddler was shown to promote movement of mesendodermal cells in the embryogenesis of the gastrula and constitutes a long-sought developmental signal in that process. Secreted Toddler is a ligand for a G-protein coupled receptor and was shown to activate its signaling [Pauli et al. 2014]. SEPs from ncRNAs have also been reported from yeast which is an ascomycete like *Bgh*. Unique RNA transcripts of previously unannotated non-coding RNAs have been identified by RNAseq. Their transcript amount was seen at physiological levels equivalent to mRNAs. A total of 39 peptides predicted from unannotated RNAs (uRNAs) show conservation within yeast strains. Ribosome profiling [Ingolia 2014], which is a combination of polysome preparation, nuclease treatment and RNAseq, revealed a subset of these uRNAs to be protected by the ribosome and hence indicated their translation. Five intergenic uRNAs (= lincRNAs)-derived transcripts were epitope-tagged at their 3’ end and introduced into yeast. Two of them were detectable on a western blot proofing their translation *in vivo*. Further, by ribosome profiling, it was shown that putative translated regions are of 10 – 100 codons in size that mapped to the 5’-region of uRNAs whereas the remaining 3’ region of in average ~900 nucleotide length was not associated with ribosomes. These transcripts were more abundant in a yeast strain deficient in translation-dependent Nonsense-Mediated RNA Decay (NMD). This indicated that the 3’-region of likely translated uRNAs is sensitive to NMD, which also functions in hindering 3’-UTR of mRNAs to be translated. NMD-insensitive uRNAs

had a reduced likelihood for translation and their 3'-tails were significantly shorter. This substantiated uRNAs to be actively translated. [Smith et al. 2014].

Together, these upcoming data stress that there is a yet over-seen 'shade' in the proteomes of eukaryotes which expands current models but also demands for methodologies to be adapted e.g. as they are easily missed by LC/MS/MS. Based on that reports, additional possible explanations on how ROPIP1 may be translated can get created. It may get directly translated from Eg-R1 by usage of a non-classical start codon as reported from the translation of human lincRNAs [Slavoff et al. 2012]. SINEs can form RNA-protein complexes with poly (A) binding protein (PBP) [West et al. 2002]. Further, the transcript of murine B2 SINEs shows similarities to mRNAs. In addition to posttranscriptional poly-adenylation depending on its 5'-AAUAAA-3' signal and binding to PBP, it also forms a 5'-cap-like methylation of its γ-phosphate [Kramerov and Vassetzky 2011]. Given that Eg-R1 is likely pol II transcribed, an mRNA-like transcript of Eg-R1 is even more likely. Eg-R1 gets posttranscriptionally poly-adenylated and pol II transcription would also enable 5'-capping. ROPIP1 location at the 5'-end of a non-coding predicted longer RNA transcript of Eg-R1 resembles what has been found for the translation of SEPs from uRNAs in yeast [Smith et al. 2014]. Eg-R1 could also translate into a SEP, namely ROPIP1-Cter, from the internal ATG start codon of ROPIP1. There is increasing evidence for the translation of SEPs and their biological relevance [Galindo et al. 2007; Magny et al. 2013; Pauli et al. 2014]. Alternatively, ROPIP1 could also translate in a cap-independent manner by formation of RNA secondary structure with internal ribosomal entry sites (IRES) functionality. IRES sequences directly bind to the P-position of 80S ribosomes and initiate translation which does not necessarily depend on classical ATG start codons [Cevallos and Sarnow 2004]. Lack of a signal peptide not necessarily inhibits secretion as there are alternative secretion pathways [Nickel 2003; Liu et al. 2014] and effectors of the EKA family of *Bgh* don't encode a signal peptide but have a well-documented host intracellular functionality as avirulence protein [Ridout et al. 2006; Sacristán et al. 2009; Shen et al. 2007]. ROPIP1 or Eg-R1 may be part of a polycystronic transcript downstream of a secreted protein, e.g. a virulence effector, which would enable classical secretion via the ER pathway. EKA sequences, even though missing a secretion leader, have been found to be co-transcribed with

retrotransposons on single transcripts [Ridout et al. 2006; Skamnioti et al. 2008; Sacristán et al. 2009]. Recently, two non-classical secreted effectors of the economically relevant plant pathogens *V*. *dahliae* which is an ascomycete and the oomycete *P*. *sojae* were reported that show isochorismate synthtase fold and functionality leading to disruption of the plant SA synthesis pathway and suppression of SA-mediated defense responses. Both effectors, VdISC1 and PsISC1, showed negative prediction for secretory signal peptide leaders but positive prediction for non-classical secretion using the Secretome P 2.0 server [Bendtsen et al. 2004a]. Both proteins were specifically detectable in western blots performed from culture supernatants of *V*. *dahliae* and *P*. *sojae* strains expressing protein-tagged VdISC1 and PsISC1, respectively. Alternative transformation of *V*. *dahliae* and *P*. *sojae* strains with VdISC1 and PsISC1 mRFP fusion protein constructs lead to the specific observation of mRFP fluorescence in culture supernatants. Further, mRFP fluorescence was observed inside haustoria of VdISC1-mRFP and PsISC1-mRFP expressing *V*. *dahliae* and *P*. *sojae* strains upon host plant interaction, which suggested their secretion from haustoria. Host translocation of PsISC1 was shown by exploiting the *P*. *sojae*-soybean (*Glycine max*) AVR-effector-R-gene pair Avr1b-Rps1b. The N-terminal translocation domain of Avr1b consisting of a signal-peptide and the RxLR-dEER translocation domain were replaced by PsISC1 in a chimeric construct. A pathogenic *P*. *sojae* strain expressing the chimer of PsISC1 and the C-terminal effector domain of Avr1b was avirulent on soybean cultivars carrying the cognate R-gene to Avr1b, Rps1b, but virulent on soybean cultivars in which Rps1b was absent [Liu et al. 2014]. Together, this clearly demonstrated that non-classical secretion is present as an additional pathway of intracellular effector delivery into host plant cells. Usage of the ROPIP1 amino acid sequence as query for the Secretome P 2.0 server [Bendtsen et al. 2004a] resulted in a well above threshold positive prediction for non-classical secretion of ROPIP1. Usage of ROPIP1-Cter as query resulted in a similarly high score. ROPIP1 and ROPIP1-Cter scores were higher than those reported from VdISC1 and comparable to those from PsISC1.

Alternative to direct translation, Eg-R1 might get `exonized` to form a chimeric ROPIP1 gene. Two possibilities of transposable element insertion into protein-coding region have been suggested: direct insertion into a protein-coding exon and intronic insertion and

subsequent exonization. The former seemingly is a rather rare event and might contribute ~ 10 % to protein-coding genomic regions containing transposable elements in humans. Direct insertion into exons is seen as being rather deleterious for protein functionality due the introduction of premature stop codons by the TEs [Nekrutenko and Li 2001]. However, such an insertion in 5'-located exons of transcribed genes could provide all necessary regulatory elements for ROPIP1 transcription and subsequent translation especially if it should happen into an exon of a secreted protein. Indeed, genomic insertions of Eg-R1 that expand the ROPIP1 sequence in 5'-direction resulting in an ORF starting with ATG and the extended part of the ROPIP1 sequence showing a positive prediction for a signal peptide have been identified in this work. Here the premature stop codon introduced through the ROPIP1 sequence of Eg-R1 may lead to the formation of a novel, chimeric and shortened transcript including the polyadenylation signal provided by Eg-R1 that may get secreted via the ER as a virulence effector protein. The transcript might not be prone to nonsense-meditated decay as there are no further downstream exons on Eg-R1. More common and accounting for ~ 90 % of human protein coding regions showing transposable element signatures are intronic integrations. In total an estimate of 4 % of human genes [Nekrutenko and Li 2001], which is depending on the precise number of protein-coding genes, something around 1000 genes, contain transposable element sequences in their transcripts. Human intronic Alu SINE elements can become an integral part of mature mRNA in a process called exonization. Antisense localization in introns provides alternative 3' and 5' splice sites leading to the incorporation of Alu sequences into mature mRNAs which accounts for 5 % of all alternatively spliced transcripts in humans [Lev-Maor et al. 2003; Sorek et al. 2004]. TE derived exons are most often located near the 5' region of the coding sequence [Sela et al. 2010]. Alu SINE exonization into coding transcripts can affect the transcriptome in different ways. It may form a non-functional transcript that gets degraded by nonsense-mediated decay in case of introducing a premature stop codon. Some Alu exonization events may result in non-functional proteins [Zarnack et al. 2013], or can even cause human genetic diseases [Vorechovsky 2010]. Antisense insertion of Alu elements provides polypyrimidine tracts regulating its capability to be spliced. The heterologous nuclear ribonucleoproteins C1/C2 (hnRNP C) preferentially binds to continuous U-tracts and blocks them from binding by the core splicing factor U2AF65

leading to a repression of the weak Alu-SINE inserted alternative splice sites. Accumulated base pair exchanges impair hhRNP C binding and allow access of U2AF65 and subsequent Alu exonization [Zarnack et al. 2013]. Alternative splicing using transposable elements provides differential transcripts in addition to the actual transcript which can serve as playground for protein evolution. Alterations in proteins can be tested while keeping the original protein [Makalowski 2003]. Some exons derived from ancient Alu elements acquired constitutive splice sites and show tissue specificity indicating positive selection of beneficial Alu exonization events [Lin et al. 2008]. Besides Alu elements, Mammalian-wide Interspersed Repeats (MIR) elements show even stronger signs of expatation e.g. MIR exonization into a zinc finger protein (ZNF635) took place before specification of humans, so that all humans carry this exonized retroelement [Krull et al. 2007; Schmitz and Brosius 2011]. Exonized TEs can get translated and are found in the human proteome. The estimated occurrence ranges from 0.1 % [Gotea and Makalowski 2006] to 0.5 % [Wu et al. 2007] of human proteins. The required evolutionary period of time until exaptation is reached is a matter of debate [Schmitz and Brosius 2011; Wu et al. 2007; Gotea and Makalowski 2006]. Alternative and constitutive splice sites are also predictable in the Eg-R1 sequence using Alternative Splice Site Predictor [Wang and Marín 2006]. It contains e.g. a prediction for an alternative 3’ acceptor site at nucleotide position 59 of the annotated Eg-R1 sequence (gagtctgcagAGCCAAGATT) which would be in frame with ROPIP1 when exonized and translated. Providing a 3’ splicing acceptor site would be sufficient as the polyadenylation signal of Eg-R1 could give rise to a transcript free of further downstream exons. An intronic insertion of Eg-R1 in the 5’ region of a secreted protein is another possibility for ROPIP1 translation and secretion.

3.6 Transposable Elements in the Genomes of Filamentous Plant Pathogens

With every genome of fungal and oomycete plant pathogens published it becomes more and more apparent that many of them are inflated by transposable elements [Raffaele and Kamoun 2012]. For instance, this is the case with biotrophic fungi, like *Bgh* [Spanu et al. 2010] and its close wheat relative *Bgt* [Parlange et al. 2011], but also with the necrotrophic wheat fungal pathogen *Pyrenophora tritici-repentis* [Manning et al. 2013],

as well as oomycete pathogens like *Phytophthora infestans* [Haas et al. 2009]. In general filamentous plant pathogens tend to harbor bigger genomes than their apathogenic relatives. A biotrophic phase during host infection and host speciation seem to be associated with genome expansion and the highest TE and repetitive DNA contents can be found in the genomes of the hemibiotrophic oomycete *P. infestans* (~75%) and the biotrophic ascomycete *Bgh* (~65 %). However, an obligate biotrophic lifestyle must not result in a massive accumulation of TEs and repetitive DNA, as seen e.g. with the genome of *U*. *maydis* [Kämper et al. 2006] that ranges in the size of apathogenic fungi [Raffaele and Kamoun 2012].

Repeat-Induced Point mutation (R.I.P.) is a process that inhibits spread of mobile genetic elements in fungi by introducing point mutations eventually stopping their activity. The R.I.P. process is of seemingly unusual high activity in the ascomycete *Neurospora crassa* as it not only inactivated all mobile elements but also likely prevented gene duplications thereby stalling their further diversification [Galagan and Selker 2004]. The loss of the R.I.P. mechanism in the powdery mildews *Bgh*, *E*. *pisi* and *G*. *orontii* might have attributed to the vast expansion of their genomes [Spanu et al. 2010]. However, TEs contributed to the expansion of the genome and the speciation of the pathogenic ascomycete *Leptosphaeria maculans 'brassicae'* (*Lmb*) in which the R.I.P. mechanism is functional. Albeit the extent of TE proliferation is low (~35 %) compared to powdery mildews it is significantly higher than in genomes of apathogenic *Leptosphaeria maculans-Leptosphaeria biglobosa* species complex members (~5 %). One possible explanation provided is that R.I.P. is only active during sexual recombination and *Lmb* speciation might have been preceded by a prolonged phase of asexual proliferation that did not happen to the other members of the species complex [Grandaubert et al. 2014]. The TE influx, likely supported by horizontal gene transfer, resulted in an isochore genetic architecture of the *Lmb* genome. Large GC-isochores alternate with large AT-isochores which account for roughly one third of the genome size. The GC-rich regions harbor ~95 % of all predicted genes but hardly TEs while the GC-poor regions show low gene but high TE content and R.I.P. activity. Interestingly, AT-isochores are enriched in genes encoding small secreted proteins which are putative effectors. These 'effector'-isochores are unique as they are not reported form other

fungal or oomycete plant pathogens [Rouxel et al. 2011] and enable an exceptional insight into the mechanism of effector diversification. In *Lmb*, the active R.I.P. mechanism is supposed to influence host adaption via effectors in a double-sided manner. On the one hand, AVR-effectors, which are no longer beneficial due to their perception by a host R-gene, can get immobilized and undergo subsequent negative selection. DNA transposons are thought to act as shuttles that translocate effectors from other genomic locations into AT-isochores where they meet the R.I.P. machinery that mutates them. TE class II mediated relocation could be shown for five of seven characterized AVR-effectors of *Lmb*. A side effect of high R.I.P. activity may be the prevention of gene duplications and no duplicates of effector genes can be found in the *Lmb* genome which excludes a major source of genetic variation. The R.I.P. mechanism normally depends on duplicated DNA but is somewhat leaky such that it occasionally extends its action on adjacent to repeat DNA located single-copy genes. So, on the other hand, the leaky R.I.P. machinery is supposed to act as a source of variation in the sequences of effector genes that when beneficial undergo positive selection in the population. In fact, one third of the top 100 up-regulated genes in *Lmb*- rapeseed (*Brassica napus*) interaction are descended from AT-isochores, many of which were species-specific effector candidates [Van de Wouw et al. 2010; Rouxel et al. 2011; Grandaubert et al. 2014].

The genomic architecture and the process of effector diversification differ in *Bgh*. There are no TE-rich clusters. Instead TEs are evenly spread over the genome interspersed by small clusters of 2-10 protein coding genes. This might be due to the absence of the R.I.P. mechanism that is thought to promote TE spread. The high TE content not only led to an increase in size but was also made responsible for gene losses of the primary and secondary metabolism and the translocation of gene loci [Spanu et al. 2010]. Gene duplications and transduplications seem to be the driving force of effector diversification in the *Bgh* genome. Effectors of the EKA family are present in more than 1350 paralog copies. The tight association of EKAs with LINE retrotransposons, which were even found as a single ORF on transcripts, is thought to enable their massive proliferation [Ridout et al. 2006]. The diversification process of EKAs and *Lmb* effector candidates resemble each other in their genetic mobility mediated by adjacent TEs. The second

class of *Bgh* effectors, CSEPs, unlike atypical EKA effectors, encode N-terminal signal peptides and fit defined characteristics of secreted effectors. At least 491 CSEPs were identified in the *Bgh* genome. They are organized in 72 families with each family containing at least four paralogs and some additional families having less paralogs. The biggest family includes 59 paralog copies and belongs to the largest gene families in *Bgh*. All predicted CSEPs together account for 7 % of all predicted protein-coding ORFs of *Bgh*. Roughly 10 % of CSEPs have a predicted ribonuclease-like tertiary protein structure and likely evolved from secreted endoribonucleases. Two-thirds of all CSEPs are clustered family-wise with 2-18 adjacent members but there are also some peculiarities. First, CSEPs not being part of a cluster are spread throughout the genome. Second, the CSEPs adjacent to each other in one particular cluster are not necessarily closely related. Third, the upstream and downstream DNA sequence shows high sequence similarity that extends for a maximum of ~1kb in both directions until it sharply drops at insertion sites of the non-autonomous retroelements Eg-R1, the SINE Egh24 or the AJ002007.1 high copy repeat element. This indicated that CSEPs have diversified by multiple rounds of gene duplication including unequal crossing-over with repeat elements providing highly similar sequence sections facilitating misalignment [Pedersen et al. 2012]. However, loss of R.I.P. contributes to TE-based genome size expansion but does not fully explain the genome architecture of *Bgh*. The genome of the oomycete *P. infestans* is also devoid of the R.I.P. mechanism but structured in gene-rich region but TE poor regions and gene-poor but TE rich regions. Unlike in the *Lmb* genome, the GC content does not drop in genomic regions with high repetitive DNA concentration. Therefore they are not referred to as isochore-like but as gene-sparse regions or transposon islands. Similar to the *Lmb* genome, the transposon islands harbor a significant subset of secreted proteins and effectors [Raffaele et al. 2010; Raffaele and Kamoun 2012]. Interestingly, nearly 90 % of all effectors of *P. infestans* are excluded from genomic regions being orthologous with its relatives *P. sojae* and *P. ramorum*. In contrast roughly two-thirds of all effectors are located in transposon islands. Previously unknown effectors were identified by screening TE-rich genomic regions for secreted proteins. Roughly a quarter of transposon island residing effector candidates were up-regulated in the *P. infestans*-host plant (*Solanaceae*) interaction. The process of effector diversification by TEs was referred to as plasticity in reminiscence of bacterial

pathogenicity islands [Raffaele et al. 2010]. In general, the underlying mechanism of TE mediated plasticity of genomes of filamentous plant pathogens includes all major mechanisms of genetic variations. Single nucleotide polymorphisms (SNPs), epigenetic imprinting, small insertions and deletions, gene translocation, gene copy number variation, domain shuffling by segmental duplication or translocation, gene or chromosome loss and horizontal gene or chromosome transfer [Raffaele and Kamoun 2012].

Of special interest in regard to ROPIP1 is chimeric gene formation due to TE activity. Crinkler (CRN) effectors of *Phytophthora* species show modular protein architecture with a conserved N-terminus followed by diversified C-termini [Haas et al. 2009; Stam et al. 2013]. Their nearly identical N-termini are composed of a signal peptide followed by the LFLAK domain containing the highly conserved putative translocation motif LxLFLAK and a DWL domain containing the highly conserved motif HVLVVVP at its C-terminal end. The N-terminal module is thought to mediate effector uptake into host cells of varying C-terminal attached effector modules. The LxLFLAK and the HVLVVVP motif were identified as ‘hot spots’ for recombination between CRN clades. New chimeric CRN effector genes are likely created by non-allelic homologous recombination and tandem gene duplication mediated by helitron DNA transposons [Haas et al. 2009]. Among DNA transposons, the Helitron transposon shows a unique preferential accumulation in gene-sparse genomic regions. However, Helitron elements are largely outnumbered by Gypsy_Ty3 LTR retrotransposons which are also preferentially found in transposon islands. Gypsy retroelements contributed around 30 % to the increase in genome size and are therefore the most proliferated type of TEs in the *P. infestans* genome. Interestingly, a Novel_Gypsy_LTR_8 has inserted into the effector domain of the CRN gene PITG_23144. This also bears a possibility for ROPIP1 translation and secretion: An Eg-R1 insertion giving rise to chimeric ORF could result in a secreted chimeric protein using the regulatory elements and the signal peptide of the gene at the insertion site for transcription and secretion. The effector domain provided by ROPIP1-Cter might in this case, by chance, have acquired a host translocation domain. An exiting example of chimeric protein formation and copy number variation due to TE action was reported from the necrotropic ascomycete wheat pathogen *Pyrenophora*

tritici-repentis (*Ptr*). A Histone 3-like (H3-like) protein was found to be multiple transduplicated by its association with a hAT DNA transposon in the genome. Two variants of hAT transposon associated H3-like insertions that differed in the compositions of ORFs between the terminal inverted repeats (TIRs), which define the borders of the insertions, were deciphered. The longer 5.6 kb variant was composed of the hAT transpsosase ORF at its 5'-end, a central ORF of unknown function and the H3-like ORF at its 3'-end. This longer element is believed to be autonomous due to the hAT transposon ORF and is also present in apathogenic ancestors of *Ptr*. The second variant of the element is shorter (2.3 kb) and is only found in pathogenic relatives of *Ptr*. Therein, the hAT transposase ORF has formed a chimeric in frame ORF with the central ORF at a 5'-GACTAT-3' sequence present in both which truncated the hAT transposase ORFs at its 3'-end and the central ORF amid its sequence. The chimeric ORF is followed by the H3-like ORF in this element. Interestingly, the Eg-R1 consensus sequence in the *Bgh* genome starts with 5'-ggggGACTAT-3'. The hAT recombination site is located proximal to the 3'-end of the hAT dimerization domain of the hAT transposase ORF. Therefore the shorter element is very likely non-autonomous but has retained the hAT dimerization domain and likely still could proliferate as it was found in multiple copies in the genome. Interestingly, the chimeric ORF as well as the H3-like ORF can get aligned to ESTs which suggests their transcription. Besides the novel gene that might have been formed by recombination of the hAT transposase ORF and the ORF of unknown function, H3-like ORFs of both elements showed signs of amino acid sequence diversification due to the accumulation of SNPs. This novel, likely non-autonomous element having formed a chimeric protein raises the interesting question whether the Eg-R1 element might behave in a similar way. Of special interest would be if the 5'-terminal part of Eg-R1 and hence ROPIP1 shares sequence similarities with secreted proteins of *Bgh*.

Another aspect of close association of TEs and effector genes in the *P. infestans* genome was suggested to be transcriptional regulation of effector genes. Small non-coding RNAs (sRNAs) homologous to various RxLR and CRN effector and TEs were observed in the transcriptome of *P. infestans*. It was shown that an artificial fusion of the transcripts of a SINE element (InfSINE) and an AVR-effector of *P. infestans* (Avr3a) lead

to a temporarily transcriptional silencing of both, the endogenous *Avr3a* RxLR-type effector and the endogenous *InfSINE* transcript amount very likely due to an RNAi mechanism of *P. infestans*. It was suggested that sRNAs directed against effectors or AVR-effectors are a mean to control the set of transcriptional and translational present effectors. The further spread of retrotransposons is likely controlled by sRNAs directed against their transcripts. It was further speculated that, the sRNA mediated silencing of genes or retrotransposable elements, in general, might promote heterochromatin formation as an additional mean of controlling 'undesired' transcript amounts. It was further assumed that chimeric transcripts of effectors and retrotransposons might naturally occur in the transcriptome of *P. infestans*. This might happen in a way that sRNA generation directed against retrotransposons might spread from its target repetitive DNA to adjacent (effector) genes [Vetukuri et al. 2011; Vetukuri et al. 2012; Whisson et al. 2014]. Given the versatile functionalities of SINE elements in general [Kramerov and Vassetzky 2011] it is very likely that one particular SINE element in a single genome is in involved in multiple processes. Whatever the assumed sense behind, interestingly, it was hinted to chimeric transcripts possibly having formed by physically close located (effector) genes and retrotransposable elements in the genome of *P. infestans*.

To sum all this up, even if not all details of the mechanics behind are understood, one can clearly conclude that I) some non-coding termed RNAs can get translated II) TEs are linked with effector evolution and generation of new genes or gene functionalites III) ROPIP1 translation appears well possible.

3.7 Remark on the 'Stressed' Genome of *Bgh*

Stress may be defined as the status when an 'environmental demand exceeds the natural regulatory capacity of an organism, in particular situations that include unpredictability and uncontrollability' [Koolhaas et al. 2011]. Biotrophic plant pathogens meet that definition of stress as they totally rely on their hosts to survive and changes in their host physiology, e.g. the introduction of novel R-genes or changes within their host genotypes within their reachable population of hosts, pose a life-threatening danger to them. *Bgh,* for instance, has lost core genes of the primary and secondary metabolism which strengthens its host dependency and conclusively the danger of extinction when it

cannot exploit the host metabolism anymore. TE activity is induced upon stress and the genomes of some plant filamentous pathogens are highly enriched in TEs indicating they are meeting or having met high or recurring stress conditions. TE activity adds an asexual source of genetic variation that speeds up host evolution. This is of particular importance to biotrophic pathogens. Biotrophic plant pathogen are in a need to evolve faster than their hosts as a plant genome can tolerate a pathogen, especially when it is a biotroph, whereas a changed host genome can mean extinction for the pathogen. It may not be sufficient to vary existing proteins when the pathogen encounters major changes within its host or within their ecosystems. The pathogen might be in need of proteins with novel functionalities to tackle the challenge especially when the host population structure changes rapidly or when they might need to jump to new hosts in order to increase their host range. TEs contribute to the diversification of existing genes, the creation of novel genes and the acquisition of new genetic resources by horizontal gene transfer. Low abundance translation of experimental transcripts or some non-coding RNA, like lincRNAs, might be the test lab for novel protein functionalities without major disturbance of the current physiology. Under non-stressful conditions, individuals having gained beneficial low abundance novel translations might undergo mild positive selection in the population while others might be neutral or might lead to mild negative selection. Under stress conditions, the impact of novel low abundance translations on selection might be boosted. Numerous of asexually generated spores and the high flexibility of repeat-rich genomes give myriads of options for combination of new genetic variety. The loss of some individuals of the numerous asexual generated conidia might not be harmful for the pathogen population. Stable genomes that have enough options to stand their environment might not be in such a drastic need for genetic variation, such that they can reduce TE activity as additional source of genetic variation. For those it may be worse to lose some individuals of their population as they would have survived anyway. To my knowledge, independent thoughts along the same lines have been formulated by Chadha et al. [2014] and Kemen et al. [2015].

ROPIP1 might be an example of a novel translation that has been created by activity of the Eg-R1 element in the gene-interspersed repetitive DNA genome of *Bgh*. How ROPIP1 might translate from Eg-R1 or whether an Eg-R1 insertion gave rise to a

chimeric and translated transcript cannot be answered yet. However, the fact that α-ROPIP1 repeatedly labelled a unique band in the protein extract prepared from *Bgh* inoculated barley leaves in western blots suggested ROPIP1 to be translated. The specific patterning of gold-particles in the immunogold-labeling assay upon usage of α-ROPIP1 as primary antibody, which located to *Bgh* intra- and extracellular structures as well as to the cytoplasm and the apoplast of barley epidermal cells, further suggested ROPIP1 to be secreted and to be translocated into the host cytoplasm. Together with the functionality of ROPIP1 in virulence, the identification of host targets and hints on the mechanism behind its effect on susceptibility of barley epidermal cells against *Bgh*, one can conclude that ROPIP1 could constitute a bona fide virulence effector of *Bgh*. A virulence effector at least partially encoded by a retrotransposable element constitutes a novelty. Further it would add a never sought source of virulence effectors. Even in case such a creation of a novel virulence effector might be extremely rare and could have only happened in a genome of extreme plasticity it could add to the understanding of how completely new genes evolve. As there is upcoming evidence for the low abundance translation of non-coding termed RNAs with methods getting more sensitive, deeper insights into a exiting ‘primordial soup’ of novel proteins hidden in the shade of genomes are getting possible.

3.8 Outlook

This work is a first report on *Bgh* ROPIP1. It suggests that ROPIP1 exists as native peptide effector. More direct evidence is desirable to further support the conclusion that ROPIP1 is translated. This could be done by protein sequencing of immuno-precipitated ROPIP1 or by protein mass spectrometry approaches. Another method, albeit indirect, is given by ribosome profiling. As a result, this combination of polysome preparation, endonuclease digestion and RNAseq techniques, is able to decipher parts of RNA that are protected from endonucleases by a surrounding ribosome that strongly suggests their translation. In addition the translated part of a given RNA is determined through alignment of the protected RNA fragments. Alternatively, albeit less direct, *in vitro* translation and subsequent protein identification techniques may be used. Eg-R1 could get isolated from an mRNA preparation by usage of immobilized antisense probes against ROPIP1 followed by *in vitro* translation of the purified Eg-R1 RNA, e.g. through wheat germ extracts. Future questions might also be, where is ROPIP1 translated, in the cytosol or at the rough ER? Another important future issue concerning ROPIP1 is the mode of ROPIP1 transcription. Is it transcribed like a classical gene? What triggers ROPIP1 transcription? What are and where are possible regulatory elements? What machinery does Eg-R1 use for retrotransposition? Is it LINE-dependent? If yes, which LINE supports transposition? How specific are Eg-R1 insertions, is there a common sequence feature that attracts Eg-R1 integration? What is the evolution of Eg-R1, where is it derived from, how old is it and is it conserved in ancestors of *Bgh*? Does it show signs of diversification or does ROPIP1 show signs of purifying selection? How many copies of Eg-R1 are present in the genome of *Bgh*, how many of them are transcribed? Differ the transcribed insertions form those that are inactive and if yes in what? And finally are there more chimeric ORF insertions than those identified in this work? To what genes relates the non-ROPIP1 part of chimeric ORFs? Are they transcribed and translated or do they get non-sense degraded? Most of these questions are hard to answer using classical wet lab techniques but could get answered using transcriptomic approaches and/or sophisticated data analysis using bioinformatics.

4 Summary

Plants have a multilayered immune system that effectively prevents infection by non-adapted pathogens. Successful pathogens secrete effector proteins that interfere with plant immunity and promote the colonization of their host. However, the knowledge about host target proteins of fungal virulence effectors is sparse and mechanistic understanding of effector triggered susceptibility in crop plants is generally weak. *Blumeria graminis* f.sp*. hordei* (*Bgh*) causes the powdery mildew disease on barley (*Hordeum vulgare* L.). This work characterizes Rho of Plants (ROP)-Interacting Peptide 1 (*Bgh* ROPIP1) as a novel type effector of *Bgh*. The virulence of *Bgh* on barley epidermal cells was significantly reduced upon transient Host-Induced Gene Silencing (HIGS) of *ROPIP1*, which could get significantly restored upon co-expression of an RNA interference insensitive ROPIP1 rescue construct. Transient over-expression of ROPIP1 or a C-terminal fragment of ROPIP1 (ROPIP1-Cter) induced super-susceptibility of barley epidermal cells towards *Bgh*. The small signaling ROP GTPase RACB of barley, which is required for full susceptibility of barley towards *Bgh*, was identified as host target of ROPIP1. The protein-protein interaction of ROPIP1 and Constitutively Active (CA), but not inactive Dominant Negative (DN), RACB was shown in targeted yeast two-hybrid assays and *in planta* by Bimolecular Fluorescence Complementation (BiFC). An α-ROPIP1 antibody labeled a unique band on western blots of protein extracts prepared from *Bgh*-infected barley leaves. The same antibody was used for immunogoldlabeling of *Bgh*-infected barley leaf cuts. Transmission electron microscopy located ROPIP1 to intra- and extracellular structures of *Bgh* and suggested its secretion and translocation into barley epidermal cells. Live cell imaging using confocal laser scanning microscopy showed recruitment of fluorophore-tagged ROPIP1 to cortical microtubules. This depended on the co-expression of the microtubule-associated RACB-interacting protein MAGAP1. BiFC visualized the ROPIP1-CA RACB protein complex at microtubules and the cell periphery. Co-expression of GFP-ROPIP1 and RFP-MAGAP1 significantly promoted microtubule network breakdown, which gave a hint on the mechanistic virulence effect of ROPIP1. ROPIP1 is at least partially encoded by the active retroelement Eg-R1 of *Bgh*, which is numerously dispersed in the *Bgh* genome. This places ROPIP1 as the first member of a novel class of pathogen effectors.

5 Zusammenfassung

Pflanzen verfügen über eine natürliche Immunität, die deren Infektion mit nicht angepassten Pathogenen verhindert. Erfolgreiche Pathogene sekretieren Effektorproteine, die die pflanzliche Immunantwort manipulieren und zur Besiedelung des Wirts beitragen. Das Wissen über Wirkmechanismen pilzlicher Effektoren, sowie das Verständnis der Anfälligkeit von Kulturpflanzen ist momentan noch gering. *Blumeria graminis* f.sp. *hordei* (*Bgh*) verusacht den Echten Mehltau an Gerste (*Hordeum vulgare* L.). In dieser Arbeit wurde Rho of Plants (ROP)-Interacting Peptide 1 (ROPIP1) als ein neuartiger *Bgh* Effektor charakterisiert. Die Virulenz von *Bgh* auf Gerstenepidermiszellen war durch Host-Induced Gene Silencing (HIGS) des *ROPIP1* Transkripts signifikant reduziert, was durch Koexpression eines RNA Interferenz insensitiven ROPIP1 Konstrukts signifikant komplementiert wurde. Die transiente Überexpression von ROPIP1, oder eines C-terminalen ROPIP1 Fragments (ROPIP1-Cter) induzierte Super-Anfälligkeit. Das Signalprotein RACB der Gerste, eine kleine ROP GTPase die zur vollen Anfälligkeit der Gerste gegenüber *Bgh* nötig ist, wurde als Wirtsziel von ROPIP1 identifiziert. Die Protein-Protein Interaktion von ROPIP1 mit konstitutiv aktiviertem (CA) RACB, aber nicht mit dominant negativem (DN) RACB, konnte im Hefe-Zwei-Hybrid System und durch bimolekulare Fluoreszenzkomplementation (BiFC) *in planta* gezeigt werden. Ein in Western Blots eingesetzter α-ROPIP1 Antikörper lieferte ein spezifisches Signal in Proteinextrakten aus *Bgh*-infizierten Gerstenblättern. Der gleiche Antikörper wurde für transmissionselektronenmikroskopische Aufnahmen von Immunogold-gefärbten Gerstenblattschnitten eingesetzt. Das ROPIP1 Protein lokalisierte spezifisch in intra- und extrazellulären *Bgh* Strukturen was dessen Sekretion und Translokation in die Wirtszelle unterstützt. Lebendzell-konfokale Lasermikroskopie zeigte eine Rekrutierung von Fluorophor-markiertem ROPIP1 an kortikale Mikrotubuli durch das Mikrotubuli-assoziierte, RACB-interagierende Protein MAGAP1. BiFC lokalisierte den ROPIP1-CA RACB Proteinkomplex an Mikrotubuli und in der Zellperipherie. Die Koexpression von GFP-ROPIP1 und RFP-MAGAP1 verursachte einen signifikanten Zusammenbruch des Mikrotubuli Netzwerkes und gab einen Hinweis auf den Wirkmechanismus von ROPIP1. ROPIP1 ist auf dem aktiven Retroelement Eg-R1 kodiert, das in großer Anzahl im *Bgh* Genom verteilt ist. Das platziert ROPIP1 als den ersten Vertreter einer neuen Klasse von Pathogeneffektoren.

6 Material and Methods

6.1 Plant and Pathogen

Barley (*Hordeum vulgare* L.) cultivar ‘Golden Promise’ was grown in environmental test chambers (Conviron, Winnipeg, Canada) at 18 °C, 60 % relative humidity in a day period of 16 h with a photon flux of 150 µmol $s^{-1}m^{-2}$. Seeds were directly potted into standard potting soil (Typ ED 73, Einheitserde und Humuswerke, Gebr. Patzer GmbH & Co. KG, Sinntal-Jossa, Germany).

Blumeria graminis (DC) Speer f.sp. *hordei* Em. Marchal, race A6 [Wiberg 1974] was kept on barley cultivar ‘Golden Promise’ at 18 °C, 65 % relative humidity and a photon flux of 150 µmol $s^{-1}m^{-2}$ in a day period of 16 h in a separate environmental test chamber (Sanyo, Moriguchi, Japan). Inoculation of barley leaves was done in an infection hood by blowing conidia from infected plants.

6.2 Standard Molecular Biology Methods

Standard molecular biology methods were used to generate recombinant plasmids and inserts [GREEN , 2012]. Recombinant plasmids were sequence-verified. Buffers, media, etc., unless indicated other, were prepared using recipes provided by Cold Spring Harbor Protocols (http://cshprotocols.cshlp.org/) or by Green and Sambrook. [2012]. Main suppliers for enzymes were Thermo Scientific (Waltham, USA, formerly Fermentas), Promega (Fitchburg, USA), New England Biolabs (Ipswich, USA) and others. Main suppliers of kits were Macherey Nagel (Düren, Germany), Qiagen (Hilden, Germany) and others. Main suppliers of chemicals were Carl Roth (Karlsruhe, Germany), Sigma-Aldrich (St. Louis, USA), Applichem (Darmstadt, Germany) and others.

6.2.1 Polymerase Chain Reaction

Standard PCR was done in TPersonal, TProfessional, TProfessional TRIO (Analytik Jena, Jena, Germany), or in Primus 25 (Peqlab, Erlangen, Germany) thermocyclers. Usually SupraTherm Taq DNA polymerase (Genecraft, Köln, Germany) was used. It has an an error rate in the range of $1*10^{-4}$ to $1*10^{-5}$. PCR reaction using SupraTherm Taq were setup in Genecrafts 10x reaction buffer (160 mM $(NH_4)_2SO_4$, 670 mM Tris-HCl pH

8.8, 15 mM $MgCl_2$, 0.1% Tween 20). Alternatively, for the accurate amplification of templates, Phusion High-Fidelity DNA polymerase (Thermo Scientific, Waltham, USA) was used. Its error rate is in the dimension of $1*10^{-7}$. Phusion® High-Fidelity DNA polymerase PCR reactions were usually set up in the supplied 5x Phusion GC buffer. dNTP mixes (2 mM or 10 mM each) were ordered from Thermo Scientific (Waltham, USA). Primer were synthesized by Eurofins MWG Operon (Ebersberg, Germany). Primers were designed using PerlPrimer v1.1.21.

6.2.2 Restriction Enzyme Digestion

Restriction enzymes and their corresponding reaction buffers were ordered at Thermo Scientific (Waltham, USA). Restriction digestion reactions were incubated at the recommended temperature for at least 3 hours or overnight, followed by heat-inactivation of the enzyme or gel purification. If necessary, sticky ends were blunted with 0.1 mM dNTPs and 2.5 u T4 DNA Polymerase (Thermo Scientific, Waltham, USA) for 5-15 min at RT, before heat inactivation of the enzyme at 75 °C for 10 min. If necessary, the ends of cut plasmids were dephosphorylated with FastAP Thermosensitive Alkaline Phosphatase (Thermo Scientific, USA) following the instruction of the manufacturer.

6.2.3 Gel Extraction of DNA fragments

DNA fragments were cut out from usually 1.0-1.5 % agarose gels and purified with the QIAquick Gel Extraction Kit (Qiagen, Hilden, Germany) or the Macherey Nagel (Düren, Germany) NucleoSpin Gel and PCR Clean-up kit according to the manufacturer's instructions. The principle lies in silica membrane-containing spin columns that bind DNA under high salt concentrations and release it under low salt conditions.

6.2.4 Determination of Nucleic Acid Concentrations

Purity and concentrations of nucleic acids were determined with a NanoDrop® ND-1000 spectrophotometer (Wilmington, USA). A 260/280 ratio above 1.8 was accepted as pure DNA.

6.2.5 Transformation of Chemically Competent *E.coli*

The Gram-negative enterobacteria *Escherichia coli* (*E. coli*) strain K-12 Dh5α (*fhuA2 Δ(argF-lacZ)U169 phoA glnV44 Φ80 Δ(lacZ)M15 gyrA96 recA1 relA1 endA1 thi-1 hsdR17*) (Clontech, Mountain View, USA) was mainly used for the amplification of

plasmid vectors. *E. coli* strain K-12 Dh5α was made chemically competent using the RbCl method as described in Green and Sambrook [2012]. Chemically competent cells were thawn on ice before 10-20 µl of cool ligation reaction mixture was mixed with 90-180 µl of them by gentle stirring with a pipette. The mixture was then kept on ice for half an hour. Afterwards, a heat shock at 42°C in a heating block for one minute was given followed by incubation on ice for another 2 minutes. 500 µl of LB medium were added to the transformation mixture, which then got incubated at 37°C for one hour with shaking at 250 rpm. Cells got spun down at 5000 rpm for 2 minutes, the supernatant removed and the pellet resuspended in 250 µl LB medium containing appropriate antibiotics. The resuspension was plated on LB agar containing appropriate antibiotics with a glass spatula. Plates were incubated at 37°C over night. A number of putative recombinant *E. coli* colonies were transferred with a sterile micropipette tip to a routine PCR mix, and routine PCR was performed with 5 min initial denaturation.

6.2.6 Plasmid Preparation

Plasmid preparation from recombinant *E. coli*, was done in small and medium-size scale (mini- and midi-preparation). The Nucleospin Plasmid and the Nucleobond Xtra Midi kit (Macherey-Nagel, Düren, Germany), respectively, were used according to the manufacturer's instructions. For mini-preparation, an over-night culture of recombinant *E. coli* was set up by transferring a small amount of a colony into 5 ml of LB medium containing the appropriate antibiotic followed by incubation at 37°C at 250 rpm. For midi-preparation, an over-night culture of 100 ml was prepared. Both kits follow the principle of cell lysis after the SDS/alkaline lysis method and the purification of the lysate via a silica anion-exchange matrix. Tables containing plasmids and primers used in this study can be found in the Appendix.

Table 3: Overview on Cloning Procedures of Plasmids.

Plasmid	Cloning Procedure
pGEM-T putX80677 K15	Eg-R1 was PCR amplified from cDNA prepared from pooling total RNA of *Bgh*-infected (0, 4, 8, 12, 24, 48 hai) barley primary leaves using primer V42fwd and X80677_anchored_dT. A nested PCR with V42A,V20B-BamH1kurz and X80677_anchored_dT followed. The fragment was gel-purified and cloned into pGEM-T vector.
pGEM-T sp42-2 K1	Sp42-2 was PCR amplified from genomic DNA prepared from *Bgh*-infected (9dai) primary leaves using primer S42A_EcoRI-fwd-2 and V42rev. The fragment was gel-purified and cloned into pGEM-T vector.
pGEM-T sp42-3 K2	Sp42-3 was PCR amplified from genomic DNA prepared from *Bgh*-infected (9dai) primary leaves using primer S42A_EcoRI-fwd-3 and V42rev. The fragment was gel-purified and cloned into pGEM-T vector.
pGEM-T sp42-5 K4	Sp42-3 was PCR amplified from genomic DNA prepared from *Bgh*-infected (9dai) primary leaves using primer S42A_EcoRI-fwd-5 and 42A,42k-NotI-rev. The fragment was gel-purified and cloned into pGEM-T vector
pGY1-ROPIP1-RNAi-rescue	ROPIP1-RNAi-rescue was subcloned from pEX-A2-ROPIP1-RNAi-rescue into pGY1 plant expression via BamHI/SalI.
pGY1-GFP-ROPIP1-RNAi-rescue	BamHI-GFP+2-BamHI was cut from pGY1-GFP+2 by BamHI and ligated into BamHI-digested pGY1-GFP-ROPIP-RNAi-rescue.
pGY1-mCherry-RACB WT	BamHI-mCherry-BamHI was PCR-amplified from pGY1-mCherry using primer GFP5'BamHI and GFP3'BamHI and cloned into pGEM-T. BamHI-mCherry-BamHI was cut from pGEM-T BamHI-mCherry-BamHI with BamHI, gel purified and cloned into BamHI-digested pGY1-RACB WT.
pGY1-mCherry- CA RACB	BamHI-mCherry-BamHI was PCR-amplified from pGY1-mCherry using primer GFP5'BamHI and GFP3'BamHI and cloned into pGEM-T. BamHI-mCherry-BamHI was cut from pGEM-T BamHI-mCherry-BamHI with BamHI, gel purified and cloned into BamHI-digested pGY1-CA RACB.
pGY1-mCherry-DN RACB	BamHI-mCherry-BamHI was PCR-amplified from pGY1-mCherry using primer GFP5'BamHI and GFP3'BamHI and cloned into pGEM-T. BamHI-mCherry-BamHI was cut from pGEM-T BamHI-mCherry-BamHI with BamHI, gel purified and cloned into BamHI-digested pGY1-DN RACB
pIPKTA30N-ROPIP1	ROPIP1 was recombined from the pIPKTA38N-ROPIP1 entry vector into pIPKTA30N destination vector using LR clonase
pGADT7-ROPIP1-Nter	ROPIP1-Nter was PCR-amplified from pGADT7-ROPIP1 using primer V42A_SmaI_F and R_V42A_Nter_BamHI and cloned into pGEM-T. SmaI-ROPIP1-Nter-BamHI was SmaI/BamHI cloned into pGADT7-empty.
pGADT7-ROPIP1-Cter	ROPIP1-Cter was PCR-amplified from pGADT7-ROPIP1 using primer V42A_SmaI_F and R_V42ACter_Bam and cloned into pGEM-T. SmaI-ROPIP1-Cter-BamHI was SmaI/BamHI cloned into pGADT7-empty
pET28b 6H-V42A-6H	BamHI-ROPIP1-SalI was PCR amplified from pGEM-T sp42-2 using primer B8B,V21B_BamH1fwd and V42A,V20Bsalrev and cloned into pGEM-T. pGEM-T- BamHI-ROPIP1-SalI was sequentially digested with first SpeI then BamHI/SalI to get rid of an pGEM-T derived second SalI site. BamHI-ROPIP1-SalI was then subcloned via BamHI/SalI into pET28b. The resulting pET28b-ROPIP1-6H was digested with NdeI/BamHI to get rid of additional ATG start codons in the MCS. Sticky ends were blunted with dNTPs and T4 DNA polymerase and the plasmid got finally religated.

6.3 Targeted Yeast Two-Hybrid Assays

Saccharomyces cerevisiae (baker's or brewer's yeast) strain AH109 (MATa, trp1-901, leu2-3, 112, ura3-52, his3-200, gal4Δ, gal80Δ, LYS2::$GAL1_{UAS}$-$GAL1_{TATA}$-HIS3, MEL1, $GAL2_{UAS}$-$GAL2_{TATA}$-ADE2, URA3::$MEL1_{UAS}$-$MEL1_{TATA}$-lacZ) was purchased from Clontech (Mountain View, USA). Yeast strain AH109 was transformed with pGADT7 (Protocol Number PT3530-5, Clontech, Mountain View, USA) as bait vector and pGBKT7 (Protocol Number PT3248-5, Clontech, Mountain View, USA) as prey vector following the Small-scale LiAc Yeast Transformation Procedure (Yeast Protocols Handbook, protocol V(E), Product Number PT3024-1, Clontech, Mountain View, USA). For transformation control, 150 µl of resuspended cells got plated with as few strokes as possible on synthetic, defined minimal medium lacking L-Leucine and L-Tryptophane (SD/-Leu/-Trp)(Yeast Protocols Handbook, Appendix C.(A), Product Number PT3024-1, Clontech, Mountain View, USA) and were kept in a 30°C incubator until yeast colonies appeared after usually 2-3 days. Two mid-sized colonies per transformation were picked with a sterile micropipette tip, got resupendend in H_2O_{bidest} and were adjusted to a concentration of 10^5 cells/µl using a counting chamber (Fuchs-Rosenthal). 10 µl thereof, which corresponds to 10^6 transformed cells, were dropped in parallel onto SD/-Leu/-Trp plates and SD medium lacking L-Adenine, L-Histidine, L-Leucine, L-Tryptophane (Quadruple Dropout, QDO) plates and kept at 30°C for ~7 d. Optional, 3-amino-1,2,4-triazole (3-AT) was added from a 1 M stock solution (Yeast Protocols Handbook, Appendix C.(A), Product Number PT3024-1, Clontech, Mountain View, USA) to the ~50°C medium prior to pouring plates to create QDO plates containing 3-AT in the range from 0.5 mM to 2.5mM in order to mitigate HIS3 reporter gene leakiness. Plates were photographed with a Nikon Coolpix P500 (Nikon, Chiyoda, Japan) camera.

6.4 Transient Transformation of Barley Leaf Epidermal Cells

Barley leaf epidermal cells got transiently transfected using the PDS-1000/He Particle Delivery System (Bio-Rad, Hercules, USA). Unless otherwise indicated, test constructs were cloned into the pGY1 plant expression vector [Schweizer et al. 1999]. The pGY1 vector is based on a pUC18 backbone with a Multiple Cloning Site (MCS) being surrounded by the strong constitutive Cauliflower Mosaic Virus 35S (CaMV35S) promoter and terminator. 1.0 µm Gold Microcarriers (Catalog # 165-2263, Bio-Rad,

Hercules, USA) were prepared according to the PDS-1000/He instruction manual and set to a final concentration of 60 mg/ml in 50 % glycerol and kept at -20 °C. Plasmids were coated to sonicated gold particles by mixing 11 µl of prepared gold-particles with test plasmids (usual range 0.5 – 1.0 µg/shot and plasmid, in sum max. 3.0 µg/shot) in a 1.5 ml test tube. An equal volume of 1 M $CaNO_3$ (pH 10) was added drop by drop while vortexing. The mixture was incubated at room temperature (RT) for ~20 minutes. In the meantime, 5 to 7 first leaves of seven day old barley seedlings were cut and placed side by side with the adaxial side facing up on 0.5% (w/v) water agar in 90 mm Petri dishes. After removal of the supernatant the gold particle pellet was washed with first 1 ml 70 % EtOH, second with 100 % EtOH. Droplets of remaining supernatant were collected by a short pulse of the centrifuge and discarded .The pellet got resuspended in 6 µl/shot 100% EtOH by shortly dipping the test tube in an ultrasonic bath. 6 µl/shot of plasmid coated goldparticles were pipetted on a Biolistic Macrocarrier (Catalog # 1652335, Bio-Rad, Hercules, USA) and the ethanol was let evaporate. A 900 psi Rupture Disc (Catalog # 1652328, Bio-Rad, Hercules, USA) was installed into the PDS-1000/He system. Petri dishes were placed in the second lowest slot of the particle delivery system. The chamber was evacuated to 26.5” Hg and the shot released. Petri dishes were then kept in the lab close to a window facing to the north

6.5 Over-Expression of ROPIP1 and ROPIP1-Cter

Barley detached leaf segments cut from 7 d old primary leaves were transiently transformed by particle bombardment. Gold particles were coated with 1.0 µg of either pGY1-empty (no insert), pGY1-ROPIP1 or pGY1-ROPIP1-Cter plus 0.5 µg pGY1-GFP each. Transfected leaf segments were inoculated with ~150 conidia/mm² of *Bgh* at 24 hours after transformation (hat). Samples were encrypted and screened manually for green fluorescing cells by fluorescence microscopy (Axio Imager Z1m, Zeiss, Jena, Germany) at 48 hours after inoculation (hai). The development of *Bgh* on transformed epidermal B-cells was judged according to the three categories: (I) Cell w/o fungal contact, respectively conidia not germinated, (II) penetration attempt of the secondary germ tube stopped by a visible papillae and (III) successful establishment of an visible haustorium and development of elongating secondary hyphae. At least 50 cells having been judged category (II) or (III) were counted per plasmid combination and repetition.

The relative penetration efficiency was calculated for each combination in each repetition by dividing the sum of category (III) cells by the sum of category (II) plus category (III) cells and multiplying the quotient by 100 to show it as percentage. In each repetition, the relative penetration rate was then calculated by forming the quotient of the penetration efficiency of each sample divided by the penetration efficiency of the control and multiplying with 100 to show it as percentage. The variation of the control samples was kept by dividing the penetration efficiency from one repetition by the arithmetic mean of all penetration efficiencies of the control samples and multiplying with 100 to show it as percentage. The arithmetic means calculated from the relative penetration efficiencies of the test samples were first tested by Grubb's test for outliers and then pairwise compared to the arithmetic means of the relative penetrations efficiencies of the control in a two-sided Student's t-test

6.6 HIGS of *ROPIP1* and RNAi rescue

The ROPIP1-RNAi-rescue construct was designed based on the principle described in Pliego et al. [2013]. The codon usage frequency of barley was obtained from the Codon Usage Database by searching for the organism *Hordeum vulgare* subsp. *vulgare* (http://www.kazusa.or.jp/codon/cgi-bin/showcodon.cgi?species=112509). The codon usage frequency of *Bgh* and the codon usage frequency in the ROPIP1 nucleotide sequence were obtained by submitting the ROPIP1 nucleotide sequence to the Graphical Codon Usage Analyzer (http://gcua.schoedl.de/) and choosing 'each codon vs. usage table' and the codon usage table of the organism *Blumeria graminis* f.sp. *hordei* (http://www.kazusa.or.jp/codon/cgi-bin/showcodon.cgi?species=62688 &aa=1&style=N). The codon usage frequency of each triplet of the ROPIP1 nucleotide sequence, respectively *Bgh* was then divided from the codon usage frequency of the respective triplet of barley. The codon yielding the maximum difference was chosen to replace the original codon in the ROPIP1 nucleotide sequence provided it is not a rare codon in barley. The resulting artificial ROPIP1-RNAi-rescue nucleotide sequence was ordered as synthetic gene at Eurofins MWG Operon (Ebersberg, Germany). ROPIP1-RNAi-rescue was subcloned from the MCS of the delivered pEX-A2 plasmid into the pGY1 plant expression vector [Schweizer et al. 1999] via BamHI/SalI restriction enzyme digestion resulting in pGY1-ROPIP1-RNAi-rescue. GFP from pGY1-GFP+2 was cloned

in frame with ROPIP1-RNAi-rescue using the 5'-end located BamHI restriction enzyme cleavage site resulting in pGY1-GFP-ROPIP1-RNAi-rescue. The resulting plasmids were sequence verified.

The sensitivity of ROPIP1, respectively the insensitivity of ROPIP1-RNAi-rescue towards RNAi directed against ROPIP1 was tested in advance. A double-stranded RNA of ROPIP1 was generated by Gateway (Gateway LR Clonase Enzyme mix, Catalogue Number 11791-019, Thermo Scientific, Waltham, USA) cloning of the ROPIP1 nucleotide sequence into the pIPKTA30N destination vector [Douchkov et al. 2005]. 1.0 µg pGY1-GFP, respectively pGY1-GFP-ROPIP1, respectively pGY1-GFP-ROPIP1-RNAi-rescue were co-bombarded with 1.0 µg pIPKTA30N-ROPIP1 and 0.5 µg pGY1-mCherry per shot into barley epidermal cells of detached leaves cut from 7 d old seedlings. Transformed cells were identified by mCherry-mediated red fluorescence by fluorescence microscopy (Axio Imager Z1m, Zeiss, Jena, Germany) at 36 hat. Red-fluorescing cells were categorized in (I) GFP-fluorescence visible and (II) GFP-fluorescence not visible. At least 150 transformed cells were analyzed per combination and repetition. The relative frequency of GFP-fluorescing cells per combination was calculated by dividing the number of GFP-fluorescing cells by the total number of mCherry-fluorescing cells and multiplied by 100 to show the value as percentage. The arithmetic means of the relative frequencies of GFP-fluorescing cells were pairwise compared with a two-sided Student's t-test. The green signal emerging in pGY1-GFP-ROPIP1-RNAi-rescue cells was additionally visualized by confocal laser scanning microscopy in a sequential scan with settings fitting GFP fluorescence and mCherry fluorescence (see below).For the evaluation of the effect of RNAi-mediated silencing of the native *ROPIP1* transcript as well as the effect of the ROPIP1-RNAi-rescue construct on the relative penetration efficiency of *Bgh* on barley, epidermal cells of detached leaf segments cut from 7 d old primary leaves got transiently transformed by particle bombardment using plasmid combinations (com) and plasmid amounts per shot (AMT) as depicted:

com	Plasmid	AMT	Plasmid	AMT	Plasmid	AMT
1	pIPKTA30N-empty	1.0 µg	pGY1-empty	1.0 µg	pGY1-GFP	0.5 µg
2	pIPKTA30N-ROPIP1	1.0 µg	pGY1-empty	1.0 µg	pGY1-GFP	0.5 µg
3	pIPKTA30N-ROPIP1	1.0 µg	pGY1-ROPIP1-RNAi-rescue	1.0 µg	pGY1-GFP	0.5 µg

Transformed barley leaf segments were inoculated with ~150 *Bgh* conidia/mm² at 24 hat. The relative penetration efficiencies were determined as described for the over-expression experiment (see above). Fluorescence microscopy took place at 48 hai. The arithmetic means of the relative penetration efficiencies of the combinations were pairwise compared by two-sided Student's t-tests.

6.7 Confocal Laser Scanning Microscopy

Live cell imaging of barley epidermal cells expressing fluorescing proteins was done with a Leica TCS SP5 system (Leica Microsystems, Wetzlar, Germany). Unless otherwise indicated, whole barley epidermal cells were scanned in xyz acquisition modes as z-stacks in 2 µm increments in sequential scan mode, between lines, with a line average of 2. As standard hardware setting the argon laser was set to 20% power, a DPSS 561 nm laser was additionally turned on for excitation of red-fluorescing proteins, the pinhole was set to 60.00 µm, the scan speed was 400 Hz and the HCX PL APO lambda blue 20.0x0.70 IMM UV objective was used. Standard settings for the excitation wavelengths (Ex λ) and the corresponding emission detector settings (Em. Range) of frequently used fluorophores are depicted:

Fluorophore	Ex λ	Em Range
GFP	488 nm	495-535 nm
mCherry/RFP/dsRed	561 nm	570-610 nm
YFP	514 nm	525-550 nm
CFP	458 nm	465-495 nm

The Leica TCS SP5 hardware was operated with Leica LAS AF software (version 2.5.1, Leica, Wetzlar, Germany) which was also used for analysis, to merge z-stacks into one picture and to export pictures in tif or jpeg format.

6.8 Standard Western Blot Workflow

Protein concentrations in prepared protein extracts were determined by a Bradford assay using the Bio-Rad Protein Assay Dye Reagent Concentrate (Catalogue Number 5000006) in the microtiter plate scale and a Tecan infinite 200 (Männedorf, Switzerland) microplate reader. BSA dilution rows (from 1 to 10 mg/ml) and protein extracts were diluted 1:10 in ultrapure H_20. The OD was measured as duplicate with 5 measuring points per well at 595 nm and RT. Alternatively, especially in case of buffers containing higher amounts of detergents, the Pierce BCA Protein Assay Kit (Catalogue Number

23225) was used following the manufacturer's instructions for the microplate procedure. The OD was measured at 562 nm at RT.

Handcast SDS-PAGE minigels were run in the Laemmli buffer system [Laemmli 1970] using the Bio-Rad Mini-Protean Tetra Cell system (Catalogue Number 165-8000). Stacking gels were prepared as 4% gel, resolving gels were prepared as 15% gel using the following recipes:

For 2 gels	**15% Resolving Gel**	**4% Stacking Gel**
Ultrapure H_20	2.4 ml	3.0 ml
Rotiphorese Gel 30[1]	5.0 ml	650 µl
1.5 M Tris-HCl, pH 8.8	2.5 ml	-
0.5 M Tris-HCl, pH 6.8	-	1.25 ml
10% (w/v) SDS	100 µl	50 µl
10% (w/v) APS	50 µl	25 µl
TEMED[2]	5 µl	5 µl
	∑ 10 ml	∑ 5 ml

[1]: Rotiphorese Gel: 30% Acrylamide with 0.8% Bisacrylamide 30 (37.5:1), degassed (Catalogue Number 3029, Carl Roth, Karlsruhe, Germany); [2]:TEMED (Catalogue Number 2367.1, Carl Roth, Karlsruhe, Germany)

Protein samples were mixed with 1x SDS loading buffer (5x stock: 250 mM Tris-HCl (pH 6.8), 10 % (w/v) SDS, 50 % (v/v) glycerol, 0.25 % (w/v) Bromophenol Blue, 5 % (v/v) β-mercaptoethanol) and denatured at 95 °C for 5 min. Usually 100 µg (minimum 50 µg) of total protein were loaded per lane. 5 µl of PageRuler Plus Prestained Protein Ladder (Catalogue Number 26620, Thermo Scientific, Waltham, USA) was loaded as molecular weight marker in a separate well. Gels were run in 1x SDS Running Buffer (25 mM Tris base, 192 mM glycine, 0.1 % (w/v) SDS, pH 8.3) at 200 V for up to 45 min.

After the SDS-PAGE run, proteins of the resolving gel part were transferred onto 0.2 µm nitrocellulose membranes (Protran BA83 Nitrocellulose Blotting Membrane) in a semi-dry blot using the continuous buffer system. 1.2 mm thick blotting paper (Whatman GB005) was soaked in transfer buffer (25 mM Tris base, 192 mM glycine, 10 % (v/v) methanol, pH 8.3). The sandwich was built up by each 2 two layers of soaked filter paper placed at the anode-side and the cathode-side with the gel placed on top of the nitrocellulose membrane in-between. A current of 5 mA/cm^2 of gel was applied for 25 min in a Fastblot B43 system (Biometra, Göttingen, Germany) with a cooling water flow of 0.5 l/min. Transferred proteins were visualized by Ponceau S (0.5 % (w/v) Ponceau S in 1.0 % acetic acid) staining and photographed with a Nikon Coolpix P500 (Nikon, Chiyoda, Japan) camera. Nitrocellulose membranes were then destained by 2 rounds of

incubation in 1x PBS for 10 min under agitation (3D shaker). Blocking was done with 5.0% non-fat dry milk in PBS-T (‘BLOTTO’) for 1 h at RT under agitation. Primary antibodies were also diluted in BLOTTO (1:100 for α-ROPIP1 and Preimmune Serum). The nitrocellulose membrane was placed together with diluted antibodies in a piece of a fresh autoclave bag and the edges were sealed with a laminator. Incubation with primary antibodies was done over-night at 4 °C. Afterwards, the nitrocellulose membrane was washed 3-times with PBS-T for 15 min at RT under agitation.The nitrocellulose membrane was again placed in a piece of an autoclaving bag and incubated with anti-rabbit-Hrp (Catalogue Number A0545-1ML, Sigma-Aldrich, St. Louis, USA, 1:80 aliquots in PBS were stored at -20°C) as secondary antibody in a 1:80.000 dilution in BLOTTO for 2 h at RT under gentle agitation. Afterwards, the nitrocellulose membrane was washed 3-times with PBS-T for 15 min at RT under agitation and was kept in PBS-T until subsequent chemiluminescene detection. The nitrocellulose membrane was covered with equal parts of SuperSignal West Femto Luminol/Enhancer Solution and SuperSignal West Femto Stable Peroxide Solution (SuperSignal West Femto Maximum Sensitivity Substrate, Catalogue Number 34096, Thermo Scientific, Waltham, USA) and a piece of an autoclave bag. Chemiluminescence was detected with a Vilber-Lourmat Fusion-SL4 (Marne la Valée, France) system run with FusionCapt Advance Solo 4 (version 16.06) software. Chemiluminescence pictures were taken using the default chemiluminescence mode with supersensitivity resolution and a pixel depth of 16 bits per pixel. The first picture was taken in autoexposure mode, when necessary the exposition time was stepwise increased until image saturation in manual mode. Brightfield images and chemiluminescence images were merged using the FusionCapt Advance Solo 4 (version 16.06) software tools Merge Marker or Paste Marker and exported in TIFF or JPEG format. The FusionCapt Advance Solo 4 (version 16.06) software was also used for molecular weight estimation.

6.9 ROPIP1 Western Blot

6.9.1 Protein Extraction Method

Various protein extraction protocols and protein extraction buffers failed, the following protocol worked. It is based on the Technical Bulletin of the Plant Total Protein Extraction Kit (Catalog Number PE0230, Sigma-Aldrich, St. Louis, USA). Seeds were

laid as rows of 5 seeds per pot. Primary leaves of potted barley plants were heavily inoculated at growth day 7 on their adaxial side. Control plants were mock treated. Inoculated plants were grown until the epiphytical mycelium has formed as big as possible colonies but the leaves still not becoming chlorotic (around 10 dai). Inoculated and mock treated pots were grown in separate environmental test chambers of the same type (Conviron, Winnipeg, Canada). Each 10 leaves were cut, placed in a 50 ml falcon tube and immediately placed in liquid N_2 and then stored at -70°C. For total protein extraction, leaves were ground in liquid N_2 and the powder was kept in liquid N_2 until the next step. A precooled spatula was used to transfer the powder into precooled 2.0 ml cryotubes (kept in liquid N_2) to a level of 0.5 ml which roughly corresponds to 200 mg of ground leaf material and placed back into liquid N_2 before proceeding with the next step. Test tubes were placed in a precooled (-20°C) massive test tube rack and 1.5 ml of precooled (-20 °C) methanol (optional including 1:100 diluted Protease Inhibitor Cocktail, Sigma-Aldrich, Catalog Number M3641) was added, followed by vortexing. Test tubes were then placed in -20 °C for 5 min before centrifugation at 16.000xg in a precooled centrifuge (4 °C) and discarding of the supernatant. The methanol wash step was repeated 2-times, or until the supernatant became more or less colorless. Inverted test tubes got shortly tapped onto a paper towel to remove droplets of remaining methanol. Precooled (-20 °C) acetone was added and the pellet got resuspended by brief, sharp vortexing. Test tubes were placed in -20 °C for up to 2 h before centrifugation at 16.000xg at 4 °C for 5 min. The supernatant was discarded; remaining acetone droplets were collected by a short pulse of the centrifuge and got discarded. The pellet was air dried for a couple of minutes before getting resuspended in 250 µl of Protein Extraction Reagent Type 4 (Sigma-Aldrich, Catalog Number C0356) by vortexing. The Protein Extraction Reagent Type 4 contains 7.0 M urea, 2.0 M thiourea, 4 mM Trizma base, 1.0% C7BzO at pH 10.4. The test tubes were then rotated overhead for 30 minutes in a lab rotator at room temperature (RT) before centrifugation at 16.000xg for 30 min at RT. The clean supernatant was transferred into a fresh 1.5 ml test tube. The protein concentration was determined by a Bradford Assay (see above). Samples were stored at -20°C.

6.9.2 Generation of Anti-ROPIP1 Antibody

The custom α-ROPIP1 anti-peptide antibody was ordered at Pineda Antibody-Service (Berlin, Germany). Epitope analysis based on Parker et al. [1986] of the ROPIP1 amino acid sequence suggested amino-acids 31 to 43 as antigenic with good avidity properties. Off-target searches yielded no significant hits. It was synthesized as CIPSRLRDLYRLHFSSH (ROPIP1-sequence underlined) and purified to ≥ 85 %. The epitope peptide was coupled to protein carriers (*inter alia* KLH). 2 rabbits were immunized in a 2 month lasting basal immunization protocol including 4 boosts. Preimmunesera and monthly delivered antisera were used for testing by western blots (see above) of recombinant ROPIP1 (see below) and protein extracts of barley leaves inoculated and non-inoculated with *Bgh*. The immunization protocol was extended with monthly boosts until, additional to the signal originating from recROPIP1, a slight specific signal appeared in the *Bgh*-treated barley leaf protein extract on a western blot, which was obtained with antisera of immunization day 120. Bleeding of the rabbits was at immunization day 145. The mono-specific IgG fraction was affinity-purified to ≥ 95% by affinity chromatography. The epitope peptide was coupled to Sepharose 6B via its thiol group. The monospecific IgG fraction was eluted in Tris-glycine buffer pH 7.5-8.0, 0.5 M NaCl, 1 mg/ml BSA, 0.02 % NaN_3 from the column and eventually delivered. Further testing showed the monospecific IgG fraction of both rabbits to deliver specific signals, with the monospecific IgG fraction of rabbit 1 delivering brighter signals, which was then named α-ROPIP1. Delivered monospecific IgG fractions were aliquoted and stored at -20°C.

6.10 Immunoprecipitation Experiment

In my hands, immunoprecipitation of the protein labeled by α-ROPIP1 only worked under denaturing conditions as described in the following final protocol which was repeatedly used successfully. Total protein extracts of *Bgh*-inoculated and non-inoculated barley leaves were prepared as described above. As the Protein Extraction Reagent Type 4 is not suitable for usage in immunoprecipitations and to meet the requirement of 500-1000 µg of total protein in a small volume, proteins got first precipitated by the TCA (trichloroacetic acid)/acetone method. 500 µl of ice-cold 20 % TCA was added to 500 µl of total protein extract ([c] ≥ 2.0 µg protein/µl), vortexed,

followed by incubation at -20 °C for 1 h and centrifugation at 21.000xg at 4 °C for 30 min. The supernatant was discarded. The pellet got washed 3-times with 500 µl of ice-cold acetone and the pellet resolved completely by vortexing or by dipping the test tube shortly into an ultrasonic bath, when necessary, followed by centrifugation at 21.000xg at 4 °C for 5 min, then the acetone was removed and discarded. After the last wash step, remaining acetone was let evaporate from the open test tube until the pellet just started to appear slightly cracked (~5-10 min).

50 µl of Denaturing Lysis Buffer based on Bonifacino et al. [2001] were added, which was composed of 1 % (w/v) SDS, 50 mM Tris-HCl (pH 7.4), 5 mM EDTA, and freshly added 10 mM DTT, 1:100 Protease Inhibitor Cocktail (Sigma-Aldrich, Catalog Number M3641) and optional 62.5 u/ml Benzonase (Catalogue Number 70746, Merck Millipore, Darmstadt, Germany). The pellet was then resuspended completely by vortexing and dipping the test tube shortly into an ultrasonic bath, if necessary. Proteins were then denatured by incubation at 95 °C for 5 minutes in a heating block. The SDS was diluted to 0.1 % by addition of 450 µl IP Lysis/Wash Buffer (25 mM Tris, 150 mM NaCl, 1 mM EDTA, 1% NP40, 5% glycerol at pH7) of the Pierce Classic IP Kit (Catalogue Number 26146, Thermo Scientific, Waltham, USA) and kept on ice for 15 min with occasional vortexing. A centrifugation stepped at 21.000xg for 5 min at 4 °C followed. The supernatant was transferred to a fresh test tube and kept on ice. 50 µl thereof were transferred to a separate test tube, denatured at 95°C for 5 min in 1x SDS sample buffer and kept as input sample for the western blot. The following steps were performed using the Pierce Classic IP kit (Catalogue Number 26146, Thermo Scientific, Waltham, USA) based on instruction manual (version 2137.6) starting from point C. (Preparation of Immune Complex). 25 µl of antibody (α-ROPIP1 or Preimmune Serum) which corresponds to ca. 12.5 µg and 5 µl of Protease Inhibitor Cocktail (Sigma-Aldrich, Catalog Number M3641) were added to 450 µl of the kept supernatants of the last step. The immune complex was let formed for 1.5 h at 4 °C under gentle rotation of the test tube. In the next step, the formed immune complex was captured (step D.) by Protein A/G coupled to 6 % beaded agarose (CL-6B). 20 µl of Pierce Protein A/G Plus Agarose (Catalogue Number 20423) slurry were placed into Pierce Spin Columns–Screw Cap (Catalogue Number 69705) and washed as recommended before adding the immune

complex sample of step C. The mixture was incubated at 4 °C for 1.5 h under gentle rotation and subsequently washed as recommended by the manufacturer's protocol. The immune complex was eluted from the column by sample-buffer elution (step E.) following the protocol: 50 µl 2x Non-reducing Lane Marker Sample Buffer (5x: 0.3 M Tris-HCl, 5 % SDS, 50 % glycerol, lane marker tracking dye; pH 6.8, Catalogue Number 39001) including 20 mM DTT and cooking at 95°C for 5 min. The flow-through was collected in a fresh test tube by centrifugation at 5.000xg for 1 min. The standard western blot workflow (see above) followed. Equal amounts were loaded on the SDS-PAGE gels. For the input protein extracts, usually 50 µg per lane as determined by BCA protein assay (Pierce BCA Protein Assay Kit, Catalogue Number 23225) and 45 µl or 25 µl of eluate, depending on the used combs, were loaded.

6.10.1 Antibody Stripping

Removal of bound antibodies from nitrocellulose membranes, also called antibody 'stripping' was done with Pierce Restore Western Blot Stripping Buffer (Catalogue Number 21059). Nitrocellulose-membranes were kept in 1xPBS after chemiluminescence detection. Nitrocellulose-membranes were covered with Restore Western Blot Stripping Buffer and incubated at RT for 15 min under gentle agitation (laboratory 3D shaker). For washing, the Restore Western Blot Stripping Buffer was replaced by 1xPBS and kept for another 15 min on the 3D shaker. The stripped nitrocellulose-membrane was then re-incubated with primary and secondary antibodies as described in the standard western blot workflow (see above).

6.11 Recombinant ROPIP1 Expression

Recombinant His-tagged ROPIP1 protein was expressed in *E.coli* and purified as follows. Chemical competent Rosetta (DE3) (Catalogue Number 70954, Novagen, Darmstadt, Germany), alternatively BL21(DE3) (Catalogue Number 69450, Novagen, Darmstadt, Germany) were transformed with the pET28b(+) vector (Catalogue Number 69865, Novagen, Darmstadt, Germany) containing the ROPIP1 sequence as insert. ROPIP1 was first BamHI/SalI cloned into pET28b(+) resulting in ROPIP1-6His. Upstream ATG-start codons derived from the vector were removed by NdeI/BamHI restriction enzyme digestion and relegation of the vector. This achieved transcription start of 6His-ROPIP1-6His from one single ATG start codon located near the ribosome

binding site. The estimated size of 6His-ROPIP1-6His was about 12.5 kDa (ExPASy-Protparam tool; Gasteiger et al. 2003).

Recombinant 6His-ROPIP1-6His (recROPIP1) was expressed in small scale cultures. An overnight starter culture was prepared by inoculating 1 ml of LB Kan (Lysogeny Broth (Tryptone 10 g, Yeast Extract 5 g, NaCl 10 g) containing 50 µg/ml kanamycine) with several colonies of Rosetta-pET28b-6H-ROPIP1-6H, and heavy vortexing to get an even bacterial suspension. This suspension was used to inoculate 50 ml of LB Kan in a 250 ml Erlenmeyer flask. The starter culture was grown over-night at 37°C and 250 rpm. The next morning, the over-night culture was diluted 1:100 in LB Kan. Two cultures of 50-250 ml volume were grown at 37 °C and 250 rpm with hourly OD_{600} measurements until they reached an OD_{600} of 0.8 to 1.0, aliquots were taken, pelleted and stored at -20 °C. The expression of recROPIP1 was induced by adding a final concentration of 1 mM IPTG (Isopropyl β-D-1-thiogalactopyranoside) to induce the T7 *lac* promoter of one culture. Hourly OD_{600} measurements and taking of culture samples aliquots continued. The cultures were grown for an additional 1-3 h at 37 °C and 250 rpm until harvest in 50 ml falcons by centrifugation. Bacterial pellets were, when necessary, stored at -20 °C. Crude protein extracts were prepared by resuspending bacterial pellets in 100 µl Lysis Buffer (50 mM NaH_2PO_4-H_2O, 300 mM NaCl, 10% glycerol, 1% Triton X-100, 1mg/ml Lysozyme, pH 8.0) per 1 ml of culture volume and incubation on ice for 30 min. The lysate was then placed 3-times in an ultrasonic bath for 10 sec with incubation on ice in-between. Viscosity of the samples was reduced by addition of 50 u Benzonase (Catalogue Number 70746, Merck Millipore, Darmstadt, Germany) per 1 ml culture volume and a further incubation on ice for 15 min. Samples were denatured at 95°C for 5 min in 1x SDS loading buffer (see Standard Western Blot Workflow). 10 µl of crude lysate were loaded onto a SDS-PAGE gel. If necessary, the loading volumes of samples were normalized according to the OD_{600} of their respective cultures. Un-induced control samples and IPTG-induced samples were run as duplicates on the same gel. The Standard Western Blot Workflow, as described above, followed. The nitrocellulose membrane was cut into two halves. One was incubated with 1:10.000 diluted α-ROPIP1 as primary antibody and 1:80.000 diluted Anti-rabbit-Hrp (Catalogue Number A0545-1ML, Sigma-Aldrich, St. Louis, USA) as secondary antibody. The duplicate was

incubated with 1:10.000 diluted Anti-His-Hrp (Catalogue Number 3894.1, Carl Roth, Karlsruhe, Germany).

RecROPIP1 was purified by Immobilized Metal Affinity Chromatography (IMAC) using the Protino Ni-TED 2000 packed columns kit (Catalogue Number 745120.25, Macherey Nagel, Düren, Germany) and following the batch gravity-flow purification protocol under native conditions (User Manual, version Rev.04, protocol 5.5). A cleared lysate was prepared from 250 µl of IPTG-induced culture by 5 cycles of freezing in liquid N2 and thawing in an ultrasonic bath in Lysis-Equilibration-Wash (LEW) Buffer provided with the kit and taking the supernatant after collection of cell debris by centrifugation. 1 g of Ni-TED resin was removed from the column and added to the cleared lysate which was then rotated over-night at 4°C. Washing and elution steps followed as recommended. All flow-throughs were collected and aliquots thereof were analyzed by western blotting. The Ni-TED resin was additionally cooked in 3 ml of 1x SDS sample buffer centrifuged and the supernatant also kept.

6.12 Immunogoldlabeling and TEM

The adaxial side of 7 d old barley primary leaves was densely (~300 conidia/mm²) inoculated with *Bgh*. Samples for immunogoldlabeling were prepared 3 dai at University of Graz (Austria) in a cooperation with the lab of Bernd Zechmann (current address: Baylor University, Waco, USA), similar to [Heyneke et al. 2013]. 1.5 mm² pieces were cut out close to the middle vein of primary leaves of different inoculated plants in a drop of fixation buffer (2.5 % paraformaldehyde, 0.5 % glutaraldehyde in 0.06 M Sorensen's phosphate buffer, pH 7.2) on a modeling wax plate and then placed in a 4 ml glass vial containing fixation solution. The glass vials were evacuated with a vacuum pump and the samples were left for 90 min in the fixation buffer at RT. 4 wash steps with 0.06 M Sorensen's phosphate buffer, pH 7.2 followed with a 15 min wait between the buffer exchanges. Samples were dehydrated in a concentration series of 50 %, 70 % and 90 % acetone with an incubation time of 2-times 10 min of each step at RT. The acetone was then gradually replaced by Epon epoxy resin (Agar 100 Harz, Dodecenylsuccinic anhydride, Methylnadicanhydride, Benzyldimethylamine) with Epon : acetone ratios of 1:2 for 2 h, 1:1 for 3 h, 2:1 for 4 h and 100% Epon epoxy resin for 4 h. Fresh 100% Epon epoxy resin was then polymerized at 60°C for 48 h in cup. A Reichert Ultracut S

ultramicrotome (Leica Microsystems, Wetzlar, Germany) was used for preparation of 80 nm thick ultrathin cuts. The automated Leica EM IGL system (Leica Microsystems, Wetzlar, Germany) was used for immunogold labeling. The ultrathin cuts were first blocked with 2% BSA in PBS, pH 7.2 for 20 min before incubation with α-ROPIP1 antibody, respectively the control antibody, in PBS, pH 7.2 containing 1 % BSA for 2 h at RT. Samples were then washed 3-times with PBS, pH 7.2 for 5 min each before addition of the secondary antibody. The samples were incubates with anti-rabbit (goat IgG) antibodies coupled to 10 nm gold particles (BBI Solutions, Cardiff, UK) in PBS, pH 7,2 for 90 min at RT. Samples were again washed 3-times for 5 min in PBS, pH 7.2 and additionally 2-times for 5 min in H_2O_{dest}. The gold particles were then detected with a Philips CM10 transmission electron microscope. The obtained micrographs were digitized. I assisted in the sample embedding, Bernd Zechmann's lab prepared ultrathin cuts and did the immunogold-labeling, Bernd Zechmann shot the micrographs and digitized them.

6.13 MAGAP1-dependent ROPIP1 Recruitment to MTs

Barley epidermal cells of 7 d old primary leaves got transiently transformed by particle bombardment. The plasmid amounts per shot were 0.5 µg pGY1-GFP, respectively 0.75 µg pGY1-ROPIP1, 1.0 µg pGY1-RFP-MAGAP1, respectively 1.0 µg pGY1-RFP-MAGAP1-Cter. Transformed cells were imaged with confocal laser scanning microscopy using standard settings (see above) at 12-24 hat. Pictures were merged into maximum projection using Leica LAS AF software (version 2.5.1.6757) and exported. Pictures were visually categorized into (I) GFP-signal present at MTs or (II) absent from MTs. The distribution of the total numbers of cells assessed to category (I) and (II) were compared between cells co-expressing RFP-MAGAP1 or RFP-MAGAP1-Cter together with GFP-ROPIP1 in a X^2 test with df = 1.

6.14 ROPIP1 Promoted MT Network Destabilization

The experimental set up was identical to the GFP-ROPIP1 – RFP-MAGAP1/RFP-MAGAP1-Cter co-expression experiment (previous paragraph), except that 1.0 µg pGY1-RFP-MAGAP1-R185G were used instead of pGY1-RFP-MAGAP1-Cter.

Exported pictures were categorized based on the appearance of their MT-network into (I) intact, (II) disordered, or (III) fragmented MT network. The distribution of the total amount of cells of the categories was compared between cells co-expressing GFP or GFP-ROPIP1 along with RFP-MAGAP1 by a X^2 test with df = 2. The same was done for cells co-expressing RFP-MAGAP1-R185G instead of RFP-MAGAP1.

6.15 BiFC Experiment

The pUC-SPYNE and pUC-SPYCE plant-compatible BiFC plasmid pair [Walter et al. 2004] drive the expression of their inserts as fusion to YFP^N, respectively YFP^C from the constitutive CaMV35S promoter. To minimize the possibility of YFP self-assembly over time [Horstman et al. 2014], the transfected plasmid amount of pUC-SPYNE-ROPIP1 and pUC-SPYCE-CA RACB, respectively pUC-SPYCE-DN RACB was reduced to a necessary minimum and the time point for confocal laser scanning microscopy was chosen to be as early as possible. Additionally the experiment was analyzed in a quantitative instead of a qualitative manner by measurement of fluorescence intensities.

Barley epidermal cells of 7 d old primary leaves got transiently transformed by microparticle bombardment. 0.75 µg of pUC-SPYNE-ROPIP1 got co-transfected with 0.75 µg pUC-SPYCE-CA RACB, respectively pUC-SPYCE-DN RACB, 0.5 µg pGY1-CFP as transformation marker and 1.0 µg pGY1-RFP-MAGAP1-R185G. Transformed cells were identified by their CFP-fluorescence and documented by confocal laser scanning microscopy at 36 hat. The pinhole was set to 60.06 µm, the scan speed was 400 Hz. Whole cells were scanned as z-stacks in 2 µm increments in a sequential scan between frames with a frame average of 2. In the first scan, YFP was excited by the 514 nm laser line at 10 % power and detected using the HyD2 detector set to 524-549 nm detection range with smart gain set to 500 %. In the second scan, RFP was excited with the 561 nm laser line and detected using one Pmt detector set to 571-621 nm detection range and using 25 % laser power. Smart gain was set to 1250 V with -10 % smart offset. In the third scan, CFP was excited with the 458 nm laser line at 15 % power and detected by another Pmt detector in the detection range from 468 to 493 nm with smart gain set to 1150 V and smart offset set to -10 %. All settings were kept identical for all cells and repetitions. Lamda-scans of the signal in the YFP channel were performed at the upper cell cortex in xyλ scanning mode, the λ range was set to 400-650 nm and

travelled in 10 nm steps. The fluorescence intensities of the intervals were read out from the Leica LAS AF software (version 2.5.1.6757).

For quantitative analysis of the BiFC signal, the quantification tool of the Leica LAS AF software (version 2.5.1.6757) was used to obtain individual Mean Fluorescence Intensities (MFIs) of cells. The single layers of the z-stacks got first merged into a maximum projection. One region of interest (ROI) was drawn as longitudinal line from cell to cell border. The nucleus was excluded. A second, copy-pasted, ROI was placed close to the cell in the surrounding background. The MFIs of the ROIs, which are an arithmetic mean of the fluorescence intensity/pixel density within the ROI, of the YFP and of the CFP detector channel were read out. The MFI of the background was subtracted from the MFI of the cell-spanning ROI for each cell. The resulting cell-specific MFI of the YFP channel was divided by the analogously obtained cell-specific MFI of the CFP channel, which resulted in an YFP to CFP MFI ratio for each cell. This YFP/CFP ratios of CA RACB-YFP^C and DN RACB-YFP^C co-expressing cells were compared in a two-sided Student's t-test. The cell-specific MFIs of the CFP-channel of CA RACB-YFP^C and DN RACB-YFP^C co-expressing cells were additionally pairwise compared in a separate two-sided Student's t-test.

6.16 5'-RACE-PCR

Poly(A) mRNA was isolated from *Bgh*-infected (10 dai) barley primary leaves using the Dynabeads mRNA Direct Kit (Catalogue Number 61011, Thermo Scientific, Waltham, USA). The sample was prepared by grinding 2 *Bgh*-infected barley primary leaves in liquid N_2. The powder was transferred to a precooled 2 ml cryotube to a filling height of 0.25 ml which corresponds to ~100-125 mg of ground plant material. 1.25 ml of Lysis/Binding Buffer (provided with the kit) were added, followed by vortexing for 2 min. Genomic DNA was sheared by pressing the lysate 5-times through a 23G needle. The lysate was then kept on ice. Isolation of mRNA from the crude cell lysate was done by directly following the Direct mRNA Isolation Protocol in standard scale (user manual year 2012). Due to experienced gDNA contamination, a DNAse digestion step was included. 2 u DNAseI (Catalogue Number AM2222, Thermo Scientific, Waltham, USA) were added to the beads in a 50 µl reaction volume containing 1x DNAse I Reaction Buffer and 1 u/µl RiboLock RNAse Inhibitor (Catalogue Number EO0381, Thermo

Scientific, Waltham, USA) and incubation at 37°C for 0.5-1 h. The reaction was stopped by adding 5 µl of 50 mM EDTA and incubation at 65°C for 10 min. Then a second round of of mRNA isolation from the DNAse digested cell lysate followed by directly following the Direct mRNA Isolation Protocol in standard scale (user manual year 2012). Poly(A) mRNA was eluted from the magnetic Oligo (dT) beads in 20 µl Elution Buffer (10 mM Tris-HCl, pH 7.5). Tubes were placed in an 80°C hot heating block for 2min and then rapidly transferred into the magnetic rack. The supernatants were transferred into a pre-cooled test-tube, 1 u/µl RNAse Inhibitor (RiboLock RNase Inhibitor, Catalogue Number EO0381, Thermo Scientific, Waltham, USA) was added and the samples kept on ice.

0.5-1.0 µg of purified mRNA were used for first-strand cDNA synthesis by directly following protocol 3.1 Experimental Protocol for 5'-RACE of the Roche 5'/3' RACE Kit, 2nd Generation, version 12 (Catalogue Number 03353621001, Roche Diagnostics, Mannheim, Germany) and using 1 µl of 12.5 µM TW42A_R primer as cDNA synthesis primer. 5 µl of the obtained dA-tailed cDNA were used as template for PCR-amplification using Phusion High-Fidelity DNA Polymerase (Catalogue Number: #F-530L, Thermo Scientific, Waltham, USA). A 50 µl reaction was prepared using Phusion GC Buffer, 1 µl of dNTPs (Vial3 of RACE Kit), 1 µl Oligo dT-Anchor Primer (Vial8 of RACE Kit), 1 µl of 12.5 µM V42A-SP2 as gene-specific primer, 1.5 µl DMSO and 0.02 u/µl Phusion DNA Polymerase. The PCR run was: 1. 98°C-30 sec, 35 cycles of 2.-4.: 2. 98°C-10 sec, 3. 65°C-20 sec, 4. 72°C-15 sec, 5. final elongation at 72°C-10 min, 6. storage at 4°C. A second, nested PCR run followed. The reaction mixture was the same, except 1 µl of PCR Anchor Primer (Vial 9 of RACE Kit) replaced the Oligo dT-Anchor Primer, 1 µl of 12.5 µM V42A-SP3 nested gene specific primer replaced V42A-SP2 and 1 µl of PCR product was used as template instead of dA-tailed cDNA. The PCR run was also the same, except that 69°C where used for annealing. PCR products were separated by Agarose gel electrophoresis, cut out from the gel, purified, A-tailed, cloned into pGEM-T vector (Promega, Fitchburg, USA) and sent for sequencing (Eurofins Genomics, Ebersberg, Germany).

6.17 Semi-Quantitative Reverse Transcription PCR

Primary leaves of 7 d old barley plants were inoculated with ~150 conidia/mm² on their adaxial side or mock treated and harvested by cutting and immediate placement in liquid

N_2 in 50 ml falcons at 0, 4, 8, 12, 24 and 48 hai. Total RNA was prepared by Chomczynski and Sacchi's [1987] single-step method of RNA isolation with the following RNA extraction buffer: 38% (v/v) saturated phenol, 0.8 M guanidinium thiocyanate, 0.4 M ammonium thiocyanate, 0.1 M sodium acetate (pH 5), 5% glycerol. Total RNA was additionally NaAc/ethanol precipitated to achieve greater purity and adjusted to 500 ng/µl per sample. DNAseI digestion (Thermo Scientific, Waltham, USA) preceded first strand cDNA synthesis using Oligo$(dT)_{15}$ Primer (Promega, Fitchburg, USA) and RevertAid Reverse Transcriptase (Catalogue Number EP0441, Thermo Scientific, Waltham, USA) Equal cDNA quantity and purity was checked with a NanoDrop ND-1000 spectrophotometer (Wilmington, USA).

Barley *Ubiquitin Conjugating Enzyme 2* (*HvUBC2,* AY220735.1) gene was amplified using the oligo pair HvUBC2_fwd and HvUBC2_rev (see Appendix). Barley *Basic PR-1-Type Pathogenesis Related Protein* (*HvPR1b,* X74940.1) gene was amplified using the oligo pair T-PR1b/3´-2 and T-PR1b/5´-2. *Bgh Tub2 Gene For Beta Tubulin* (*Bgh tub2*, AJ313149) gene was amplified using the oligo pair *Bgh*_beta-tub_F and *Bgh*_beta-tub_R. *Bgh ROPIP1* transcript was amplified using the oligo pair V42fwd and V42rev.

6.18 Bioinformatics Web Servers

Submitted Sequences and server settings are described in the respective text passages of the Results or the Discussion section. See also the following table for an overview.

Table 4: Bioinformatics Web Servers Used in this Study

Name	URL	Purpose	Reference
Alternative Splice Site Predictor	http://wangcomputing.com/assp/	Alternative splice site prediction	Wang and Marín (2006)
BDGP	http://www.fruitfly.org/seq_tools/promoter.html	Neural network promoter prediction	Reese (2001)
BluGen BLAST	http://www.blugen.org/WebSearch-bin/search	BLAST against *Bgh* genome	Spanu (2010)
ClustalW2	http://www.ebi.ac.uk/Tools/msa/clustalw2/	Multiple sequence alignment	Larkin (2007), Goujon (2010)
DisEMBL	http://dis.embl.de/	Secondary structure disorder prediction	Linding (2003)
Hcpolya	http://bioinfo4.itb.cnr.it/~webgene/wwwHC_polya.html	Polyadenylation signal prediction	Milanesi (1996)
HHpred	http://toolkit.tuebingen.mpg.de/hhpred	Protein structure and homology prediction	Söding (2005)
NCBI BLAST	http://blast.ncbi.nlm.nih.gov/Blast.cgi	BLAST searches	Altschul (1997)
NCBI SRA BLAST	http://www.ncbi.nlm.nih.gov/sra/	Raw sequence read archive	Leinonen (2010)
NCBI Trace BLAST	http://www.ncbi.nlm.nih.gov/Traces/home/	Sequencing data storage	Leinonen (2010)
Pfam	http://pfam.xfam.org/	Protein domain prediction	Finn (2014)
PROSITE	http://prosite.expasy.org/	Protein domain prediction	Sigrist (2012)
ProtParam	http://web.expasy.org/protparam/	MW prediction	Gasteiger (2005)
QUARK	http://zhanglab.ccmb.med.umich.edu/QUARK/	Ab initio tertiary structure modelling	Xu, Zhang (2012)
Quick2D	http://toolkit.tuebingen.mpg.de/quick2_d	Secondary structure prediction	Biegert (2006)
Repbase	http://www.girinst.org/repbase/	Repetive elements database	Jurka (2005)
SecretomeP 2.0	http://www.cbs.dtu.dk/services/SecretomeP/	Non-classical protein secretion prediction	Bendtsen (2004b)
si-Fi v3.1.0-0001	http://labtools.ipk-gatersleben.de	RNAi off-target prediction	Douchkov (2014)
SignalP 4.1/3.0	http://www.cbs.dtu.dk/services/SignalP/	Signal peptide prediction	Peterson (2011), Bendtsen (2004)
SINEBase	http://sines.eimb.ru/	SINE database and analysis	Vassetzky (2013)
SMART	http://smart.embl-heidelberg.de/	Protein domain prediction	Letunic (2014)
TargetP 1.1	http://www.cbs.dtu.dk/services/TargetP/	Subcellular protein localization prediction	Emanuelsson (2000)
Translate	http://web.expasy.org/tools/translate/	Nucleotide to amino acid sequence	Gasteiger (2005)
WebLogo 3.4	http://weblogo.threeplusone.com/create.cgi	WebLogo	Crooks (2004)
WoLF PSORT	http://www.genscript.com/psort/wolf_psort.html	Subcellular protein localization prediction	Horton (2007)

7 References

Acevedo-Garcia J., Kusch S., Panstruga R. (2014): Magical mystery tour: MLO proteins in plant immunity and beyond. ***New Phytologist* 204: 273–281**.

Agrios G. N. (2005): Plant pathology. 5th ed. Amsterdam, Boston: Elsevier Acadaemic Press.

Ahmed A. A., Pedersen C., Schultz-Larsen T., et al. (2015): Barley powdery mildew effector candidate CSEP0105 inhibits chaperone activity of a small heat shock protein. ***Plant Physiology* 168: 321–333**.

Akamatsu A., Wong H. L., Fujiwara M., et al. (2013): An OsCEBiP/OsCERK1-OsRacGEF1-OsRac1 module is an essential early component of chitin-induced rice immunity. ***Cell Host & Microbe* 13: 465–476**.

Aktories K. (2011): Bacterial protein toxins that modify host regulatory GTPases. ***Nature Reviews Microbiology* 9: 487–498**.

Altschul S. F., Madden T. L., Schäffer A. A., et al. (1997): Gapped BLAST and PSI-BLAST: a new generation of protein database search programs. ***Nucleic Acids Research* 25: 3389–3402**.

Ambrose C. and Wasteneys G. O. (2014): Microtubule initiation from the nuclear surface controls cortical microtubule growth polarity and orientation in *Arabidopsis* thaliana. ***Plant and Cell Physiology* 55: 1636–1645**.

An Q., Ehlers K., Kogel K.-H., et al. (2006a): Multivesicular compartments proliferate in susceptible and resistant MLA12-barley leaves in response to infection by the biotrophic powdery mildew fungus. ***New Phytologist* 172: 563–576**.

An Q., Huckelhoven R., Kogel K.-H., et al. (2006b): Multivesicular bodies participate in a cell wall-associated defence response in barley leaves attacked by the pathogenic powdery mildew fungus. ***Cellular Microbiology* 8: 1009–1019**.

Anderson C. M., Wagner T. A., Perret M., et al. (2001): WAKs: Cell wall-associated kinases linking the cytoplasm to the extracellular matrix. ***Plant Molecular Biology* 47: 197–206**.

Anderson R., Deb D., Fedkenheuer K., et al. (2015): Recent Progress in RXLR Effector Research. ***Molecular Plant-Microbe Interactions* [Jahrgang fehlt!]: 150630065947006**.

Apel K. and Hirt H. (2004): Reactive Oxygen Secies: Metabolism, oxidative stress, and signal transduction. ***Annual Review of Plant Biology* 55: 373–399**.

Archuleta T. L., Du Y., English C. A., et al. (2011): The *Chlamydia* effector Chlamydial outer protein N (CopN) sequesters tubulin and prevents microtubule assembly. ***Journal of Biological Chemistry* 286: 33992–33998**.

Banfai B., Jia H., Khatun J., et al. (2012): Long noncoding RNAs are rarely translated in two human cell lines. ***Genome Research* 22: 1646–1657**.

Barlan K., Rossow M. J., Gelfand V. I. (2013): The journey of the organelle: Teamwork and regulation in intracellular transport. ***Current Opinion in Cell Biology* 25: 483–488**.

Bélanger R. R. (2002): The Powdery Mildews. St. Paul, Minn.: APS Press.

Bellincampi D., Cervone F., Lionetti V. (2014): Plant cell wall dynamics and wall-related susceptibility in plant-pathogen interactions. ***Frontiers in Plant Science* 5: 228**.

Bendtsen J. D., Jensen L. J., Blom N., et al. (2004a): Feature-based prediction of non-classical and leaderless protein secretion. ***Protein Engineering Design and Selection*** **17: 349–356**.

Bendtsen J. D., Nielsen H., Heijne G. VON, et al. (2004b): Improved prediction of signal peptides: SignalP 3.0. ***Journal of Molecular Biology*** **340: 783–795**.

Bergounioux J., Elisee R., Prunier A.-L., et al. (2012): Calpain activation by the *Shigella flexneri* effector VirA regulates key steps in the formation and life of the bacterium's epithelial niche. ***Cell Host & Microbe*** **11: 240–252**.

Berken A. (2006): ROPs in the spotlight of plant signal transduction. ***Cellular and Molecular Life Sciences*** **63: 2446–2459**.

Berken A., Thomas C., Wittinghofer A. (2005): A new family of RhoGEFs activates the Rop molecular switch in plants. ***Nature*** **436: 1176–1180**.

Berken A. and Wittinghofer A. (2008): Structure and function of Rho-type molecular switches in plants. ***Plant Physiology and Biochemistry*** **46: 380–393**.

Berti C., Fontanella B., Ferrentino R., et al. (2004): Mig12, a novel Opitz syndrome gene product partner, is expressed in the embryonic ventral midline and co-operates with Mid1 to bundle and stabilize microtubules. ***BMC Cell Biology*** **5: 9**.

Bhat R. A., Miklis M., Schmelzer E., et al. (2005): Recruitment and interaction dynamics of plant penetration resistance components in a plasma membrane microdomain. ***Proceedings of the National Academy of Sciences of the United States of America*** **102: 3135–3140**.

Bhuiyan N. H., Selvaraj G., Wei Y., et al. (2009): Gene expression profiling and silencing reveal that monolignol biosynthesis plays a critical role in penetration defence in wheat against powdery mildew invasion. ***Journal of Experimental Botany*** **60: 509–521**.

Biegert A., Mayer C., Remmert M., et al. (2006): The MPI Bioinformatics Toolkit for protein sequence analysis. ***Nucleic Acids Research*** **34: W335–W339**.

Bindschedler L. V., Burgis T. A., Mills D. J. S., et al. (2009): *In planta* proteomics and proteogenomics of the biotrophic barley fungal pathogen *Blumeria graminis* f. sp. *hordei*. ***Molecular & Cellular Proteomics*** **8: 2368–2381**.

Bindschedler L. V., McGuffin L. J., Burgis T. A., et al. (2011): Proteogenomics and *in silico* structural and functional annotation of the barley powdery mildew *Blumeria graminis* f. sp. *hordei*. ***Methods*** **54: 432–441**.

Black D. S. and Bliska J. B. (2000): The RhoGAP activity of the *Yersinia pseudotuberculosis* cytotoxin YopE is required for antiphagocytic function and virulence. ***Molecular Microbiology*** **37: 515–527**.

Bloch D. and Yalovsky S. (2013): Cell polarity signaling. ***Current Opinion in Plant Biology*** **16: 734–742**.

Block A., Toruño T. Y., Elowsky C. G., et al. (2014): The *Pseudomonas syringae* type III effector HopD1 suppresses effector-triggered immunity, localizes to the endoplasmic reticulum, and targets the *Arabidopsis* transcription factor NTL9. ***New Phytologist*** **201: 1358–1370**.

Bonifacino J. S., Dell'Angelica E. C., Springer T. A. (2001): Immunoprecipitation. ***Current Protocols in Molecular Biology.*** **48: VI: 10.16:10.: 16.1–10.16.29**.

Bos J. L., Rehmann H., Wittinghofer A. (2007): GEFs and GAPs: Critical elements in the control of small G proteins. ***Cell* 129: 865–877**.

Boutte Y., Vernhettes S., Satiat-Jeunemaitre B. (2007): Involvement of the cytoskeleton in the secretory pathway and plasma membrane organisation of higher plant cells. ***Cell Biology International* 31: 649–654**.

Bozkurt T. O., Schornack S., Banfield M. J., et al. (2012): Oomycetes, effectors, and all that jazz. ***Current Opinion in Plant Biology* 15: 483–492**.

Bozkurt T. O., Schornack S., Win J., et al. (2011): *Phytophthora infestans* effector AVRblb2 prevents secretion of a plant immune protease at the haustorial interface. ***Proceedings of the National Academy of Sciences of the United States of America* 108: 20832–20837**.

Brandizzi F. and Wasteneys G. O. (2013): Cytoskeleton-dependent endomembrane organization in plant cells: An emerging role for microtubules. ***The Plant Journal* 75: 339–349**.

Brownhill K., Wood L., Allan V. (2009): Molecular motors and the Golgi complex: Staying put and moving through. ***Seminars in cell & developmental biology* 20: 784–792**.

Brumell J. H., Goosney D. L., Finlay B. B. (2002): SifA, a type III secreted effector of *Salmonella typhimurium*, directs *Salmonella*-induced filament (Sif) formation along microtubules. ***Traffic* 3: 407–415**.

Brutus A., Sicilia F., Macone A., et al. (2010): A domain swap approach reveals a role of the plant wall-associated kinase 1 (WAK1) as a receptor of oligogalacturonides. ***Proceedings of the National Academy of Sciences of the United States of America* 107: 9452–9457**.

Caarls L., Pieterse C. M. J., Van Wees S. C. M. (2015): How salicylic acid takes transcriptional control over jasmonic acid signaling. ***Frontiers in Plant Science* 6: 170**.

Cai G., Faleri C., Del Casino C., et al. (2011): Distribution of callose synthase, cellulose synthase, and sucrose synthase in tobacco pollen tube is controlled in dissimilar ways by actin filaments and microtubules. ***Plant Physiology* 155: 1169–1190**.

Carayol N. and Tran Van Nhieu G. (2013): Tips and tricks about *Shigella* invasion of epithelial cells. ***Current Opinion in Microbiology* 16: 32–37**.

Carol R. J., Takeda S., Linstead P., et al. (2005): A RhoGDP dissociation inhibitor spatially regulates growth in root hair cells. ***Nature* 438: 1013–1016**.

Caron E., Crepin V. F., Simpson N., et al. (2006): Subversion of actin dynamics by *EPEC* and *EHEC*. ***Current Opinion in Microbiology* 9: 40–45**.

Causier B. and Davies B. (2002): Analysing protein-protein interactions with the yeast two-hybrid system. ***Plant Molecular Biology* 50: 855–870**.

Cesari S., Bernoux M., Moncuquet P., et al. (2014): A novel conserved mechanism for plant NLR protein pairs: The "integrated decoy" hypothesis. ***Frontiers in Plant Science* 5: 606**.

Cesari S., Thilliez G., Ribot C., et al. (2013): The rice resistance protein pair RGA4/RGA5 recognizes the *Magnaporthe oryzae* effectors AVR-Pia and AVR1-CO39 by direct binding. ***The Plant Cell* 25: 1463–1481**.

Cevallos R. C. and Sarnow P. (2004): Factor-independent assembly of elongation-competent ribosomes by an internal ribosome entry site located in an RNA virus that infects *Penaeid* shrimp. ***Journal of Virology* 79: 677–683**.

Chadha S., Sharma M., Han K.-H. (2014): Transposable elements as stress adaptive capacitors induce genomic instability in fungal pathogen *Magnaporthe oryzae*. ***PLoS ONE* 9: e94415**.

Chen X., Grandont L., Li H., et al. (2014): Inhibition of cell expansion by rapid ABP1-mediated auxin effect on microtubules. ***Nature* 516: 90–93**.

Cheong M. S., Kirik A., Kim J.-G., et al. (2014): AvrBsT acetylates *Arabidopsis* ACIP1, a protein that associates with microtubules and is required for immunity. ***PLoS Pathogens* 10: e1003952**.

Chomczynski P. and Sacchi N. (1987): Single-step method of RNA isolation by acid guanidinium thiocyanate-phenol-chloroform extraction. ***Analytical Biochemistry* 162: 156–159**.

Chowdhury J., Henderson M., Schweizer P., et al. (2014): Differential accumulation of callose, arabinoxylan and cellulose in nonpenetrated versus penetrated papillae on leaves of barley infected with *Blumeria graminis* f. sp. *hordei*. ***New Phytologist* 204: 650–660**.

Collins N. C., Thordal-Christensen H., Lipka V., et al. (2003): SNARE-protein-mediated disease resistance at the plant cell wall. ***Nature* 425: 973–977**.

Cornelis G. R. (2002): *Yersinia* type III secretion: Send in the effectors. ***The Journal of Cell Biology* 158: 401–408**.

Craddock C., Lavagi I., Yang Z. (2012): New insights into Rho signaling from plant ROP/Rac GTPases. ***Trends in Cell Biology* 22: 492–501**.

Crooks G. E., Hon G., Chandonia J.-M., et al. (2004): WebLogo: A sequence logo generator. ***Genome Research* 14: 1188–1190**.

Cui H., Tsuda K., Parker J. E. (2014): Effector-triggered immunity: From pathogen perception to robust defense. ***Annual Review of Plant Biology* 66: 6.1-6.25**.

Cvrčková F., Oulehlová D., Žárský V. (2015): Formins: Linking cytoskeleton and endomembranes in plant cells. ***International Journal of Molecular Sciences* 16: 1–18**.

Damasceno C. M. B., Bishop J. G., Ripoll D. R., et al. (2008): Structure of the glucanase inhibitor protein (GIP) family from *Phytophthora* species suggests coevolution with plant endo-beta-1,3-glucanases. ***Molecular Plant-Microbe Interactions* 21: 820–830**.

Dangl J. L. and Jones J. D. G. (2001): Plant pathogens and integrated defence responses to infection. ***Nature* 411: 826–833**.

Davis J., Wang J., Tropea J. E., et al. (2008): Novel fold of VirA, a type III secretion system effector protein from *Shigella flexneri*. ***Protein Science* 17: 2167–2173**.

Day B., Henty J. L., Porter K. J., et al. (2011): The pathogen-actin connection: A platform for defense signaling in plants. ***Annual Review of Phytopathology* 49: 483–506**.

Devoto A., Piffanelli P., Nilsson I., et al. (1999): Topology, subcellular localization, and sequence diversity of the Mlo family in plants. ***Journal of Biological Chemistry* 274: 34993–35004**.

Djamei A., Schipper K., Rabe F., et al. (2011): Metabolic priming by a secreted fungal effector. ***Nature* 478: 395–398**.

Dodds P. N. and Rathjen J. P. (2010): Plant immunity: Towards an integrated view of plant–pathogen interactions. ***Nature Reviews Genetics* 11: 539–548**.

Doehlemann G. and Hemetsberger C. (2013): Apoplastic immunity and its suppression by filamentous plant pathogens. ***New Phytologist*** **198: 1001–1016**.

Dong N., Zhu Y., Lu Q., et al. (2012): Structurally distinct bacterial TBC-like GAPs link Arf GTPase to Rab1 inactivation to counteract host defenses. ***Cell*** **150: 1029–1041**.

Dou D. and Zhou J.-M. (2012): Phytopathogen effectors subverting host immunity: Different foes, similar battleground. ***Cell Host & Microbe*** **12: 484–495**.

Douchkov D., Nowara D., Zierold U., et al. (2005): A high-throughput gene-silencing system for the functional assessment of defense-related genes in barley epidermal cells. ***Molecular Plant-Microbe Interactions*** **18: 755–761**.

Dovas A. and Couchman J. R. (2005): RhoGDI: multiple functions in the regulation of Rho family GTPase activities. ***Biochemical Journal*** **390: 1**.

Duan Q., Kita D., Li C., et al. (2010): Feronia receptor-like kinase regulates RHO GTPase signaling of root hair development. ***Proceedings of the National Academy of Sciences of the United States of America*** **107: 17821–17826**.

Eichmann R., Bischof M., Weis C., et al. (2010): Bax Inhibitor-1 is required for full susceptibility of barley to powdery mildew. ***Molecular Plant-Microbe Interactions*** **23: 1217–1227**.

Emanuelsson O., Nielsen H., Brunak S., et al. (2000): Predicting subcellular localization of proteins based on their N-terminal amino acid sequence. ***Journal of Molecular Biology*** **300: 1005–1016**.

Escobar-Restrepo J.-M., Huck N., Kessler S., et al. (2007): The Feronia receptor-like kinase mediates male-female interactions during pollen tube reception. ***Science*** **317: 656–660**.

Fàbrega A. and Vila J. (2013): *Salmonella enterica* serovar *Typhimurium* skills to succeed in the host: Virulence and regulation. ***Clinical Microbiology Reviews*** **26: 308–341**.

Faulkner C. (2015): A cellular backline: Specialization of host membranes for defence. ***Journal of Experimental Botany*** **66: 1565–1571**.

Flor H. H. (1971): Current status of the gene-for-gene concept. ***Annual Review of Phytopathology*** **9: 275–296**.

Foreman J., Demidchik V., Bothwell J.H.F., et al. (2003): Reactive Oxygen Species produced by NADPH oxidase regulate plant cell growth. ***Nature 422*****: 442-446**.

Forges H., Bouissou A., Perez F. (2012): Interplay between microtubule dynamics and intracellular organization. ***The International Journal of Biochemistry & Cell Biology*** **44: 266–274**.

Freialdenhoven A., Peterhansel C., Kurth J., et al. (1996): Identification of genes required for the function of non-race-specific mlo resistance to powdery mildew in barley. ***The Plant Cell*** **8: 5–14**.

Fu Y., Gu Y., Zheng Z., et al. (2005): *Arabidopsis* interdigitating cell growth requires two antagonistic pathways with opposing action on cell morphogenesis. ***Cell*** **120: 687–700**.

Fu Z. Q., Guo M., Jeong B.-R., et al. (2007): A type III effector ADP-ribosylates RNA-binding proteins and quells plant immunity. ***Nature*** **447: 284–288**.

Galagan J. E. and Selker E. U. (2004): RIP: The evolutionary cost of genome defense. ***Trends in Genetics*** **20: 417–423**.

Galindo M. I., Pueyo J. I., Fouix S., et al. (2007): Peptides encoded by short ORFs control development and define a new eukaryotic gene family. ***PLoS Biology* 5: e106**.

Gasteiger E., Gattiker A., Hoogland C., et al. (2003): ExPASy: The proteomics server for in-depth protein knowledge and analysis. ***Nucleic Acids Research* 31: 3784–3788**.

Geisler S. and Coller J. (2013): RNA in unexpected places: Long non-coding RNA functions in diverse cellular contexts. ***Nature Reviews Molecular Cell Biology* 14: 699–712**.

Genre A., Chabaud M., Timmers T., et al. (2005): Arbuscular mycorrhizal fungi elicit a novel intracellular apparatus in *Medicago truncatula* root epidermal cells before infection. ***The Plant Cell* 17: 3489–3499**.

Germane K. L., Ohi R., Goldberg M. B., et al. (2008): Structural and functional studies indicate that *Shigell*a VirA is not a protease and does not directly destabilize microtubules. ***Biochemistry* 47: 10241–10243**.

Gimenez-Ibanez S., Ntoukakis V., Rathjen J. P. (2009): The LysM receptor kinase CERK1 mediates bacterial perception in *Arabidopsis*. ***Plant Signaling & Behavior* 4: 539–541**.

Giraldo M. C. and Valent B. (2013): Filamentous plant pathogen effectors in action. ***Nature Reviews Microbiology* 11: 800–814**.

Glazebrook J. (2005): Contrasting mechanisms of defense against biotrophic and necrotrophic pathogens. ***Annual Review of Phytopathology* 43: 205–227**.

Godfrey D., Böhlenius H., Pedersen C., et al. (2010): Powdery mildew fungal effector candidates share N-terminal Y/F/WxC-motif. ***BMC Genomics* 11: 317**.

Göhre V., Spallek T., Häweker H., et al. (2008): Plant pattern-recognition receptor FLS2 is directed for degradation by the bacterial ubiquitin ligase AvrPtoB. ***Current Biology* 18: 1824–1832**.

Gotea V. and Makalowski W. (2006): Do transposable elements really contribute to proteomes? ***Trends in Genetics* 22: 260–267**.

Goujon M., McWilliam H., Li W., et al. (2010): A new bioinformatics analysis tools framework at EMBL-EBI. ***Nucleic Acids Research* 38: W695–W699**.

Grandaubert J., Lowe R. G. T., Soyer J. L., et al. (2014): Transposable element-assisted evolution and adaptation to host plant within the *Leptosphaeria maculans-Leptosphaeria biglobosa* species complex of fungal pathogens. ***BMC Genomics* 15: 891**.

Green M. R. and Sambrook J. (2012): Molecular cloning. 4th ed. Cold Spring Harbor, N.Y.: Cold Spring Harbor Laboratory Press.

Gu Y., Dowd P., Vernoud V., et al. (2005): A Rho family GTPase controls actin dynamics and tip growth via two counteracting downstream pathways in pollen tubes. ***The Journal of Cell Biology* 169: 127–138**.

Guan X., Buchholz G., Nick P. (2013): The cytoskeleton is disrupted by the bacterial effector HrpZ, but not by the bacterial PAMP flg22, in tobacco BY-2 cells. ***Journal of Experimental Botany* 64: 1805–1816**.

Guex, N. and Peitsch, M. C. (1997): SWISS-MODEL and the Swiss-PdbViewer: An environment for comparative protein modeling. ***Electrophoresis* 18: 2714-2723**.

Gurel P. S., Hatch A. L., Higgs H. N. (2014): Connecting the cytoskeleton to the endoplasmic reticulum and Golgi. ***Current Biology* 24: R660-72**.

Gutierrez R., Lindeboom J. J., Paredez A. R., et al. (2009): *Arabidopsis* cortical microtubules position cellulose synthase delivery to the plasma membrane and interact with cellulose synthase trafficking compartments. ***Nature Cell Biology* 11: 797–806**.

Guttman M., Russell P., Ingolia N. T., et al. (2013): Ribosome profiling provides evidence that large noncoding RNAs do not encode proteins. ***Cell* 154: 240–251**.

Haas B. J., Kamoun S., Zody M. C., et al. (2009): Genome sequence and analysis of the Irish potato famine pathogen *Phytophthora infestans*. ***Nature* 461: 393–398**.

Hacquard S., Kracher B., Maekawa T., et al. (2013): Mosaic genome structure of the barley powdery mildew pathogen and conservation of transcriptional programs in divergent hosts. ***Proceedings of the National Academy of Sciences of the United States of America* 110: E2219–E2228**.

Hall A. (2012): Rho family GTPases. ***Biochemical Society Transactions* 40: 1378–1382**.

Ham H., Sreelatha A., Orth K. (2011): Manipulation of host membranes by bacterial effectors. ***Nature Reviews Microbiology* 9: 635–646**.

Han J. S. (2010): Non-long terminal repeat (non-LTR) retrotransposons: Mechanisms, recent developments, and unanswered questions. ***Mobile DNA* 1: 15**.

Hansjakob A., Riederer M., Hildebrandt U. (2012): Appressorium morphogenesis and cell cycle progression are linked in the grass powdery mildew fungus *Blumeria graminis*. ***Fungal Biology* 116: 890–901**.

Hardham A. R. (2013): Microtubules and biotic interactions. ***The Plant Journal* 75: 278–289**.

Hardham A. R., Takemoto D., White R. G. (2008): Rapid and dynamic subcellular reorganization following mechanical stimulation of *Arabidopsis* epidermal cells mimics responses to fungal and oomycete attack. ***BMC Plant Biology* 8: 63**.

Hazak O., Bloch D., Poraty L., et al. (2010): A Rho scaffold integrates the secretory system with feedback mechanisms in regulation of auxin distribution. ***PLoS Biology* 8: e1000282**.

Hazak O., Obolski U., Prat T., et al. (2014): Bimodal regulation of ICR1 levels generates self-organizing auxin distribution. ***Proceedings of the National Academy of Sciences of the United States of America* 111: E5471–E5479**.

Heil M. and Land W. G. (2014): Danger signals-damaged-self recognition across the tree of life. ***Frontiers in Plant Science* 5: 578**.

Hemetsberger C., Herrberger C., Zechmann B., et al. (2012): The *Ustilago maydis* effector Pep1 suppresses plant immunity by inhibition of host peroxidase activity. ***PLoS Pathogens* 8: e1002684**.

Heyneke E., Luschin-Ebengreuth N., Krajcer I., et al. (2013): Dynamic compartment specific changes in glutathione and ascorbate levels in *Arabidopsis* plants exposed to different light intensities. ***BMC Plant Biology* 13: 104**.

Hoefle C. and Hückelhoven R. (2014): A barley Engulfment and Motility domain containing protein modulates Rho GTPase activating protein HvMAGAP1 function in the barley powdery mildew interaction. ***Plant Molecular Biology* 84: 469–478**.

Hoefle C., Huesmann C., Schultheiss H., et al. (2011): A barley ROP GTPase Activating Protein associates with microtubules and regulates entry of the barley powdery mildew fungus into leaf epidermal cells. ***The Plant Cell* 23: 2422–2439**.

Horio T. and Murata T. (2014): The role of dynamic instability in microtubule organization. ***Frontiers in Plant Science* 5: 511**.

Horstman A., Tonaco I., Boutilier K., et al. (2014): A cautionary note on the use of split-YFP/BiFC in plant protein-protein interaction studies. ***International Journal of Molecular Sciences* 15: 9628–9643**.

Horton P., Park K.-J., Obayashi T., et al. (2007): WoLF PSORT: Protein localization predictor. ***Nucleic Acids Research* 35: W585–W587**.

Hückelhoven R. (2007): Cell wall–associated mechanisms of disease resistance and susceptibility. ***Annual Review of Phytopathology* 45: 101–127**.

Hückelhoven R. (2014): The effective papilla hypothesis. ***New Phytologist* 204: 438–440**.

Hückelhoven R. and Panstruga R. (2011): Cell biology of the plant-powdery mildew interaction. ***Current Opinion in Plant Biology* 14: 738-746**.

Hückelhoven R., Dechert C., Kogel K.-H. (2003): Overexpression of barley BAX inhibitor 1 induces breakdown of mlo-mediated penetration resistance to *Blumeria graminis*. ***Proceedings of the National Academy of Sciences of the United States of America* 100: 5555–5560**.

Hückelhoven R., Eichmann R., Weis C., et al. (2013): Genetic loss of susceptibility: A costly route to disease resistance? ***Plant Pathology* 62: 56–62**.

Huesmann C., Reiner T., Hoefle C., et al. (2012): Barley ROP binding kinase1 is involved in microtubule organization and in basal penetration resistance to the barley powdery mildew fungus. ***Plant Physiology* 159: 311–320**.

Ichiyanagi K., Nishihara H., Duvernell D. D., et al. (2007): Acquisition of endonuclease specificity during evolution of L1 retrotransposon. ***Molecular Biology and Evolution* 24: 2009–2015**.

Ingolia N. T. (2014): Ribosome profiling: New views of translation, from single codons to genome scale. ***Nature Reviews Genetics* 15: 205–213**.

Inuma T., Khodaparast S. A., Takamatsu S. (2007): Multilocus phylogenetic analyses within *Blumeria graminis*, a powdery mildew fungus of cereals. ***Molecular Phylogenetics and Evolution* 44: 741–751**.

Jacob F., Vernaldi S., Maekawa T. (2013): Evolution and conservation of plant NLR functions. ***Frontiers in Immunology* 4: 297**.

Jankovics T., Komáromi J., Fábián A., et al. (2015): New insights into the life cycle of the wheat powdery mildew: Direct observation of ascosporic Infection in *Blumeria graminis* f. sp. *tritici*. ***Phytopathology* 105: 797–804**.

Jarosch B., Kogel K.-H., Schaffrath U. (1999): The ambivalence of the barley Mlo locus: Mutations conferring resistance against powdery mildew (*Blumeria graminis* f. sp. *hordei*) enhance susceptibility to the rice blast fungus *Magnaporthe grisea*. ***Molecular Plant-Microbe Interactions* 12: 508–514**.

Jones J. D. G. and Dangl J. L. (2006): The plant immune system. ***Nature* 444: 323–329**.

Jones M. A., Raymond M. J., Yang Z., et al. (2007): NADPH oxidase-dependent reactive oxygen species formation required for root hair growth depends on ROP GTPase. ***Journal of Experimental Botany* 58: 1261–1270**.

Jones M. A., Shen J.-J., Fu Y., et al. (2002): The *Arabidopsis* Rop2 GTPase is a positive regulator of both rRoot hair initiation and tip growth. ***The Plant Cell Online* 14: 763–776**.

De Jonge R. van Esse, H., Kombrink A., et al. (2010): Conserved fungal LysM effector Ecp6 prevents chitin-triggered immunity in plants. ***Science* 329: 953–955**.

Jørgensen I. H. (1992): Discovery, characterization and exploitation of Mlo powdery mildew resistance in barley. ***Euphytica* 63: 141-152**.

Jørgensen J. H. and Wolfe M. (1994): Genetics of powdery mildew resistance in barley. ***Critical Reviews in Plant Sciences* 13: 97–119**.

Jurka J., Kapitonov V. V., Pavlicek A., et al. (2005): Repbase Update, a database of eukaryotic repetitive elements. ***Cytogenetic and Genome Research* 110: 462–467**.

Käll L., Krogh A., Sonnhammer E. L. (2004): A combined transmembrane topology and signal peptide prediction method. ***Journal of Molecular Biology* 338: 1027–1036**.

Kamoun S. (2006): A catalogue of the effector secretome of plant pathogenic oomycetes. ***Annual Review of Phytopathology* 44: 41–60**.

Kämper J., Kahmann R., Bölker M., et al. (2006): Insights from the genome of the biotrophic fungal plant pathogen *Ustilago maydis*. ***Nature* 444: 97–101**.

Kankanala P., Czymmek K., Valent B. (2007): Roles for rice membrane dynamics and plasmodesmata during biotrophic invasion by the blast fungus. ***The Plant Cell Online* 19: 706–724**.

Kaschani F., Shabab M., Bozkurt T., et al. (2010): An effector-targeted protease contributes to defense against *Phytophthora infestans* and is under diversifying selection in natural hosts. ***Plant Physiology* 154: 1794–1804**.

Kawano Y., Kaneko-Kawano T., Shimamoto K. (2014): Rho family GTPase-dependent immunity in plants and animals. ***Frontiers in Plant Science* 5: 522**.

Kawasaki T., Koita H., Nakatsubo T., et al. (2006): Cinnamoyl-CoA reductase, a key enzyme in lignin biosynthesis, is an effector of small GTPase Rac in defense signaling in rice. ***Proceedings of the National Academy of Sciences of the United States of America* 103: 230–235**.

Kazan K. and Lyons R. (2014): Intervention of phytohormone pathways by pathogen effectors. ***The Plant Cell* 26: 2285–2309**.

Kazazian H. H. (2014): Processed pseudogene insertions in somatic cells. ***Mobile DNA* 5: 20**.

Keijzer J., Mulder B., Janson M. (2014): Microtubule networks for plant cell division. ***Systems and Synthetic Biology* 8: 187-194**.

Kemen A. C., Agler M. T., Kemen E. (2015): Host-microbe and microbe-microbe interactions in the evolution of obligate plant parasitism. ***New Phytologist* 206: 1207–1228**.

Kessler S. A., Shimosato-Asano H., Keinath N. F., et al. (2010): Conserved molecular components for pollen tube reception and fungal invasion. ***Science* 330: 968–971**.

Ketelaar T. (2013): The actin cytoskeleton in root hairs: All is fine at the tip. ***Current Opinion in Plant Biology* 16: 749–756**.

Kim M. G., da Cunha L., McFall A. J., et al. (2005): Two *Pseudomonas syringae* type III effectors Inhibit RIN4-regulated basal defense in *Arabidopsis*. ***Cell* 121: 749–759**.

Klahre U. and Kost B. (2006): Tobacco RhoGTPase Activating Protein1 spatially restricts signaling of RAC/Rop to the apex of pollen tubes. ***The Plant Cell Online* 18: 3033–3046**.

Kobayashi Y., Kobayashi I., Funaki Y., et al. (1997): Dynamic reorganization of microfilaments and microtubules is necessary for the expression of non-host resistance in barley coleoptile cells. ***The Plant Journal* 11: 525–537**.

Koch A. and Kogel K.-H. (2014): New wind in the sails: Improving the agronomic value of crop plants through RNAi-mediated gene silencing. ***Plant Biotechnology Journal* 12: 821–831**.

Koh S., André A., Edwards H., et al. (2005): *Arabidopsis thaliana* subcellular responses to compatible *Erysiphe cichoracearum* infections. ***The Plant Journal* 44: 516–529**.

Koolhaas J. M., Bartolomucci A., Buwalda B., et al. (2011): Stress revisited: A critical evaluation of the stress concept. ***Neuroscience & Biobehavioral Reviews* 35: 1291–1301**.

Kost B. (2008): Spatial control of Rho (Rac-Rop) signaling in tip-growing plant cells. ***Trends in Cell Biology* 18: 119–127**.

Kramerov D. A. and Vassetzky N. S. (2011): SINEs. ***Wiley Interdisciplinary Reviews: RNA* 2: 772–786**.

Krishnamoorthy P., Sanchez-Rodriguez C., Heilmann I., et al. (2014): Regulatory roles of phosphoinositides in membrane trafficking and their potential impact on cell-wall synthesis and re-modelling. ***Annals of Botany* 114: 1049–1057**.

Krull M., Petrusma M., Makalowski W., et al. (2007): Functional persistence of exonized mammalian-wide interspersed repeat elements (MIRs). ***Genome Research* 17: 1139–1145**.

Kuhle V., Jäckel D., Hensel M. (2004): Effector proteins encoded by *Salmonella* pathogenicity Island 2 interfere with the microtubule cytoskeleton after translocation into host cells. ***Traffic* 5: 356–370**.

Kumar J., Hückelhoven R., Beckhove U., et al. (2001): A compromised Mlo pathway affects the response of barley to the necrotrophic fungus *Bipolaris sorokiniana* (Teleomorph: *Cochliobolus sativus*) and its toxins. ***Phytopathology* 91: 127–133**.

Kunoh H., Aist J. R., Hayashimoto A. (1985): The occurrence of cytoplasmic aggregates induced by *Erysiphe pisi* in barley coleoptile cells before the host cell walls are penetrated. ***Physiological Plant Pathology* 26: 199–207**.

Kwaaitaal M., Keinath N. F., Pajonk S., et al. (2010): Combined bimolecular fluorescence complementation and Forster resonance energy transfer reveals ternary SNARE complex formation in living plant cells. ***Plant Physiology* 152: 1135–1147**.

Kwon C., Neu C., Pajonk S., et al. (2008): Co-option of a default secretory pathway for plant immune responses. ***Nature* 451: 835–840**.

Laemmli U. K. (1970): Cleavage of Structural Proteins during the Assembly of the Head of Bacteriophage T4. ***Nature* 227: 680–685**.

Landrein B. and Hamant O. (2013): How mechanical stress controls microtubule behavior and morphogenesis in plants: History, experiments and revisited theories. ***The Plant Journal* 75: 324–338**.

Larkin M. A., Blackshields G., Brown N. P., et al. (2007): Clustal W and Clustal X version 2.0. ***Bioinformatics* 23: 2947–2948**.

Lavy M., Bloch D., Hazak O., et al. (2007): A novel ROP/RAC effector links cell polarity, root-Meristem maintenance, and vesicle trafficking. ***Current Biology* 17: 947–952**.

Lee A. H.-Y., Hurley B., Felsensteiner C., et al. (2012): A bacterial acetyltransferase destroys plant microtubule networks and blocks Secretion. ***PLoS Pathogens* 8: e1002523**.

Lee W. L., Grimes J. M., Robinson R. C. (2015): *Yersinia* effector YopO uses actin as bait to phosphorylate proteins that regulate actin polymerization. ***Nature Structural & Molecular Biology* 22: 248–255**.

Lee Y. J., Szumlanski A., Nielsen E., et al. (2008): Rho-GTPase-dependent filamentous actin dynamics coordinate vesicle targeting and exocytosis during tip growth. ***The Journal of Cell Biology* 181: 1155–1168**.

Lehmann S., Serrano M., L'Haridon F., et al. (2014): Reactive oxygen species and plant resistance to fungal pathogens. ***Phytochemistry* 112: 54–65**.

Lei L., Li S., Bashline L., et al. (2014): Dissecting the molecular mechanism underlying the intimate relationship between cellulose microfibrils and cortical microtubules. ***Frontiers in Plant Science* 5: 90**.

Lemichez E., Wu Y., Sanchez J.-P., et al. (2001): Inactivation of AtRac1 by abscisic acid is essential for stomatal closure. ***Genes & Development* 15: 1808–1816**.

Levin H. L. and Moran J. V. (2011): Dynamic interactions between transposable elements and their hosts. ***Nature Reviews Genetics* 12: 615–627**.

Lev-Maor G., Sorek R., Shomron N., et al. (2003): The birth of an alternatively spliced exon: 3' splice-site selection in Alu exons. ***Science* 300: 1288–1291**.

Lewis J. D., Lee A. H.-Y., Hassan J. A., et al. (2013): The *Arabidopsis* ZED1 pseudokinase is required for ZAR1-mediated immunity induced by the *Pseudomonas syringae* type III effector HopZ1a. ***Proceedings of the National Academy of Sciences of the United States of America* 110: 18722–18727**.

Lewis J. D., Wan J., Ford R., et al. (2012): Quantitative Interactor Screening with next-generation Sequencing (QIS-Seq) identifies *Arabidopsis* thaliana MLO2 as a target of the *Pseudomonas syringae* type III effector HopZ2. ***BMC Genomics* 13: 8**.

Li S., Chen M., Yu D., et al. (2013): Exo70A1-mediated vesicle trafficking Is critical for tracheary element development in *Arabidopsis*. ***The Plant Cell* 25: 1774–1786**.

Li S., Lei L., Somerville C. R., et al. (2012): Cellulose Synthase Interactive protein 1 (CSI1) links microtubules and cellulose synthase complexes. ***Proceedings of the National Academy of Sciences of the United States of America* 109: 185–190**.

Li S., van Os G. M. A., Ren S., et al. (2010): Expression and functional analyses of EXO70 Genes in *Arabidopsis* implicate their roles in regulating cell type-specific exocytosis. ***Plant Physiology* 154: 1819–1830**.

Lin L., Shen S., Tye A., et al. (2008): Diverse splicing patterns of exonized Alu elements in human tissues. ***PLoS Genetics* 4: e1000225**.

Linding R., Jensen L. J., Diella F., et al. (2003): Protein disorder prediction. ***Structure* 11: 1453–1459**.

Lipka V., Dittgen J., Bednarek P., et al. (2005): Pre- and postinvasion defenses both contribute to nonhost resistance in *Arabidopsis*. ***Science* 310: 1180–1183**.

Liu T., Song T., Zhang X., et al. (2014): Unconventionally secreted effectors of two filamentous pathogens target plant salicylate biosynthesis. ***Nature Communications* 5: 4686**.

Lo Presti L., Lanver D., Schweizer G., et al. (2015): Fungal effectors and plant susceptibility. ***Annual Review of Plant Biology* 66: 513–545**.

López-Solanilla E., Bronstein P. A., Schneider A. R., et al. (2004): HopPtoN is a *Pseudomonas syringae* Hrp (type III secretion system) cysteine protease effector that

suppresses pathogen-induced necrosis associated with both compatible and incompatible plant interactions. ***Molecular Microbiology* 54: 353–365**.

Macho A. P. and Zipfel C. (2014): Plant PRRs and the activation of innate immune signaling. ***Molecular Cell* 54: 263–272**.

Maekawa T., Kracher B., Vernaldi S., et al. (2012): Conservation of NLR-triggered immunity across plant lineages. ***Proceedings of the National Academy of Sciences of the United States of America* 109: 20119–20123**.

Magny E. G., Pueyo J. I., Pearl F. M. G., et al. (2013): Conserved regulation of cardiac calcium uptake by peptides encoded in small open reading frames. ***Science* 341: 1116–1120**.

Makalowski W. (2003): Genomics: Not junk after all. ***Science* 300: 1246–1247**.

Manning V. A., Pandelova I., Dhillon B., et al. (2013): Comparative genomics of a plant-pathogenic fungus, *Pyrenophora tritici-repentis*, reveals transduplication and the impact of repeat elements on pathogenicity and population divergence. ***G3 Genes|Genomes|Genetics* 3: 41–63**.

Marck C., Kachouri-Lafond R., Lafontaine I., et al. (2006): The RNA polymerase III-dependent family of genes in hemiascomycetes: Comparative RNomics, decoding strategies, transcription and evolutionary implications. ***Nucleic Acids Research* 34: 1816–1835**.

Marshall, O. J. (2004): PerlPrimer: cross-platform, graphical primer design for standard, bisulphite and real-time PCR. ***Bioinformatics* 20: 2471-2472**.

Matsuzawa T., Kuwae A., Yoshida S., et al. (2004): Enteropathogenic *Escherichia coli* activates the RhoA signaling pathway via the stimulation of GEF-H1. ***The EMBO Journal* 23: 3570–3582**.

McLellan H., Boevink P. C., Armstrong M. R., et al. (2013): An RxLR effector from *Phytophthora infestans* prevents re-localisation of two plant NAC transcription factors from the endoplasmic reticulum to the nucleus. ***PLoS Pathogens* 9: e1003670**.

Melotto M., Underwood W., Koczan J., et al. (2006): Plant stomata function in innate immunity against bacterial invasion. ***Cell* 126: 969–980**.

Meyer D., Pajonk S., Micali C., et al. (2009): Extracellular transport and integration of plant secretory proteins into pathogen-induced cell wall compartments. ***The Plant Journal* 57: 986–999**.

Micali C. O., Neumann U., Grunewald D., et al. (2011): Biogenesis of a specialized plant-fungal interface during host cell internalization of *Golovinomyces orontii* haustoria. ***Cellular Microbiology* 13: 210–226**.

Miklis M., Consonni C., Bhat R. A., et al. (2007): Barley Mlo modulates actin-dependent and actin-independent antifungal defense pathways at the cell periphery. ***Plant Physiology* 144: 1132–1143**.

Milanesi L., Muselli M., Arrigo P. (1996): Hamming-Clustering method for signals prediction in 5′ and 3′ regions of eukaryotic genes. ***Bioinformatics* 12: 399–404**.

Miyawaki K. N. and Yang Z. (2014): Extracellular signals and receptor-like kinases regulating ROP GTPases in plants. ***Frontiers in Plant Science* 5: 449**.

Monshausen G. B., Bibikova T. N., Messerli M. A., et al. (2007): Oscillations in extracellular pH and reactive oxygen species modulate tip growth of *Arabidopsis* root hairs.

***Proceedings of the National Academy of Sciences of the United States of America* 104: 20996–21001**.

Moores C. A. and Milligan R. A. (2006): Lucky 13 - microtubule depolymerisation by kinesin-13 motors. ***Journal of Cell Science* 119: 3905–3913**.

Moriura N., Matsuda Y., Oichi W., et al. (2006): Consecutive monitoring of lifelong production of conidia by individual conidiophores of *Blumeria graminis* f. sp. *hordei* on barley leaves by digital microscopic techniques with electrostatic micromanipulation. ***Mycological Research* 110: 18–27**.

Mucha E., Fricke I., Schaefer A., et al. (2011): Rho proteins of plants – Functional cycle and regulation of cytoskeletal dynamics. ***European Journal of Cell Biology* 90: 394–943**.

Mucha E., Hoefle C., Hückelhoven R., et al. (2010): RIP3 and AtKinesin-13A - a novel interaction linking Rho proteins of plants to microtubules. ***European Journal of Cell Biology* 89: 906–916**.

Nekrutenko A. and Li W.-H. (2001): Transposable elements are found in a large number of human protein-coding genes. ***Trends in Genetics* 17: 619–621**.

Nibau C., Wu H.-M., Cheung A. Y. (2006): RAC/ROP GTPases: 'Hubs' for signal integration and diversification in plants. ***Trends in Plant Science* 11: 309–315**.

Nicaise V., Joe A., Jeong B.-R., et al. (2013): *Pseudomonas* HopU1 modulates plant immune receptor levels by blocking the interaction of their mRNAs with GRP7. ***The EMBO Journal* 32: 701–712**.

Nicholas K. B., Nicholas H. B. J., Deerfield D. W. I. (1997): GeneDoc: Analysis and visualization of genetic variation. ***EMBNEW.NEWS* 4**.

Nickel W. (2003): The mystery of nonclassical protein secretion. ***European Journal of Biochemistry* 270: 2109–2119**.

Nie L., Wu H.-J., Hsu J.-M., et al. (2012): Long non-coding RNAs: Versatile master regulators of gene expression and crucial players in cancer. ***American Journal of Translational Research* 4: 127–150**.

Nomura K., DebRoy S., Lee Y. H., et al. (2006): A bacterial virulence protein suppresses host innate immunity to cause plant disease. ***Science* 313: 220–223**.

Nowara D., Gay A., Lacomme C., et al. (2010): HIGS: Host-Induced Gene Silencing in the obligate biotrophic fungal pathogen *Blumeria graminis*. ***The Plant Cell* 22: 3130–3141**.

Oda Y. (2015): Cortical microtubule rearrangements and cell wall patterning. ***Frontiers in Plant Science* 6: 236**.

Oda Y. and Fukuda H. (2012): Initiation of cell wall pattern by a Rho- and microtubule-driven symmetry breaking. ***Science* 337: 1333–1336**.

Oda Y. and Fukuda H. (2013a): Rho of plant GTPase signaling regulates the behavior of *Arabidopsis* Kinesin-13A to establish secondary cell wall patterns. ***The Plant Cell* 25: 4439–4450**.

Oda Y. and Fukuda H. (2013b): Spatial organization of xylem cell walls by ROP GTPases and microtubule-associated proteins. ***Current Opinion in Plant Biology* 16: 743–748**.

Oda Y. and Fukuda H. (2014): Emerging roles of small GTPases in secondary cell wall development. ***Frontiers in Plant Science* 5: 428**.

Oda Y., Iida Y., Nagashima Y., et al. (2015): Novel coiled-coil proteins regulate exocyst association with cortical microtubules in xylem cells via the conserved oligomeric Golgi-Complex 2 protein. ***Plant and Cell Physiology* 56: 277–286**.

Oerke E.-C. (2006): Crop losses to pests. ***The Journal of Agricultural Science* 144: 31-43**.

Ogiwara I., Miya M., Ohshima K., et al. (2002): V-SINEs: A new superfamily of vertebrate SINEs that are widespread in vertebrate genomes and retain a strongly conserved segment within each repetitive unit. ***Genome Research* 12: 316–324**.

Ohshima K. (2012): Parallel relaxation of stringent RNA recognition in plant and mammalian L1 retrotransposons. ***Molecular Biology and Evolution* 29: 3255–3259**.

Ohshima K. (2013): RNA-mediated gene duplication and retroposons: retrogenes, LINEs, SINEs, and sequence specificity. ***International Journal of Evolutionary Biology* 2013: 1–16**.

Ohshima K. and Okada N. (2005): SINEs and LINEs: Symbionts of eukaryotic genomes with a common tail. ***Cytogenetic and Genome Research* 110: 475–490**.

Ökmen B. and Doehlemann G. (2014): Inside plant: Biotrophic strategies to modulate host immunity and metabolism. ***Current Opinion in Plant Biology* 20: 19–25**.

Opalski K. S., Schultheiss H., Kogel K.-H., et al. (2005): The receptor-like MLO protein and the RAC/ROP family G-protein RACB modulate actin reorganization in barley attacked by the biotrophic powdery mildew fungus Blumeria graminis f.sp. hordei. ***The Plant Journal* 41: 291–303**.

Ostertag E. M. and Kazazian Jr H. H. (2001): Biology of mammalian L1 retrotransposons. ***Annual Review of Genetics* 35: 501–538**.

Ostertag M., Stammler J., Douchkov D., et al. (2013): The conserved oligomeric Golgi complex is involved in penetration resistance of barley to the barley powdery mildew fungus. ***Molecular Plant Pathology* 14: 230–240**.

Paredez A. R., Persson S., Ehrhardt D. W., et al. (2008): Genetic evidence that cellulose synthase activity influences microtubule cortical array organization. ***Plant Physiology* 147: 1723–1734**.

Paredez A. R., Sommerville C. R., Ehrhardt D. W. (2006): Visualization of cellulose synthase demonstrates functional association with microtubules. ***Science* 312: 1491–1495**.

Parker J. M. R., Guo D., Hodges R. S. (1986): New hydrophilicity scale derived from high-performance liquid chromatography peptide retention data: Correlation of predicted surface residues with antigenicity and x-ray-derived accessible sites. ***Biochemistry* 25: 5425–5432**.

Parlange F., Oberhaensli S., Breen J., et al. (2011): A major invasion of transposable elements accounts for the large size of the *Blumeria graminis* f.sp. *tritici* genome. ***Functional & Integrative Genomics* 11: 671–677**.

Pathuri I. P., Eichmann R., Hückelhoven R. (2009a): Plant small monomeric G-proteins (RAC/ROPs) of barley are common elements of susceptibility to fungal leaf pathogens, cell expansion and stomata development. ***Plant Signaling & Behavior* 4: 109–110**.

Pathuri I. P., Imani J., Babaeizad V., et al. (2009b): Ectopic expression of barley constitutively activated ROPs supports susceptibility to powdery mildew and bacterial wildfire in tobacco. ***European Journal of Plant Pathology* 125: 317–327**.

Pathuri I. P., Reitberger I. E., Huckelhoven R., et al. (2011): Alcohol dehydrogenase 1 of barley modulates susceptibility to the parasitic fungus *Blumeria graminis* f.sp. *hordei*. ***Journal of Experimental Botany* 62: 3449–3457**.

Pathuri I. P., Zellerhoff N., Schaffrath U., et al. (2008): Constitutively activated barley ROPs modulate epidermal cell size, defense reactions and interactions with fungal leaf pathogens. ***Plant Cell Reports* 27: 1877–1887**.

Pauli A., Norris M. L., Valen E., et al. (2014): Toddler: An embryonic signal that promotes cell Movement via Apelin receptors. ***Science* 343: 1248636**.

Pavan S., Jacobsen E., Visser R. G. F., et al. (2010): Loss of susceptibility as a novel breeding strategy for durable and broad-spectrum resistance. ***Molecular Breeding* 25: 1–12**.

Pavlíček A., Pačes J., Zíka R., et al. (2002): Length distribution of long interspersed nucleotide elements (LINEs) and processed pseudogenes of human endogenous retroviruses: Implications for retrotransposition and pseudogene detection. ***Gene* 300: 189–194**.

Pedersen C., van Themaat E. V. L., McGuffin L., et al. (2012): Structure and evolution of barley powdery mildew effector candidates. ***BMC Genomics* 13: 694**.

Pel M. J. C., van Dijken A. J. H., Bardoel B. W., et al. (2014): *Pseudomonas syringae* evades host immunity by degrading flagellin monomers with alkaline protease AprA. ***Molecular Plant-Microbe Interactions* 27: 603–610**.

Petersen T. N., Brunak S., Heijne G. VON, et al. (2011): SignalP 4.0: Discriminating signal peptides from transmembrane regions. ***Nature Methods* 8: 785–786**.

Petrásek J. and Schwarzerová K. (2009): Actin and microtubule cytoskeleton interactions. ***Current Opinion in Plant Biology* 12: 728–734**.

Petre B., Kamoun S., McDowell J. M. (2014): How Do Filamentous Pathogens Deliver Effector Proteins into Plant Cells? ***PLoS Biology* 12: e1001801**.

Piffanelli P., Zhou F., Casais C., et al. (2002): The barley Mlo modulator of defense and cell Death is responsive to biotic and abiotic stress stimuli. ***Plant Physiology* 129: 1076–1085**.

Pliego C., Nowara D., Bonciani G., et al. (2013): Host-induced gene silencing in barley powdery mildew reveals a class of ribonuclease-like effectors. ***Molecular Plant-Microbe Interactions* 26: 633–642**.

Poraty-Gavra L., Zimmermann P., Haigis S., et al. (2013): The *Arabidopsis* Rho of plants GTPase AtROP6 functions in developmental and pathogen response pathways. ***Plant Physiology* 161: 1172–1188**.

Prehna G., Ivanov M. I., Bliska J. B., et al. (2006): *Yersinia* virulence depends on mimicry of host Rho-family nucleotide dissociation inhibitors. ***Cell* 126: 869–880**.

Radhakrishnan G. K. and Splitter G. A. (2012): Modulation of host microtubule dynamics by pathogenic bacteria. ***BioMolecular Concepts* 3: 571–580**.

Rae A. L., Bonfante-Fasolo P., Brewin N. J. (1992): Structure and growth of infection threads in the legume symbiosis with Rhizobium leguminosarum. ***The Plant Journal* 2: 385–395**.

Raffaele S. and Kamoun S. (2012): Genome evolution in filamentous plant pathogens: Why bigger can be better. ***Nature Reviews Microbiology* 10: 417–430**.

Raffaele S., Win J., Cano L. M., et al. (2010): Analyses of genome architecture and gene expression reveal novel candidate virulence factors in the secretome of *Phytophthora infestans*. ***BMC Genomics* 11: 637**.

Rafiqi M., Ellis J. G., Ludowici V. A., et al. (2012): Challenges and progress towards understanding the role of effectors in plant–fungal interactions. ***Current Opinion in Plant Biology* 15: 477–482**.

Rasmussen C. G., Wright A. J., Müller S. (2013): The role of the cytoskeleton and associated proteins in determination of the plant cell division plane. ***The Plant Journal* 75: 258–269**.

Rasmussen M., Rossen L., Giese H. (1993): SINE-like properties of a highly repetitive element in the genome of the obligate parasitic fungus *Erysiphe graminis* f.sp. *hordei*. ***Molecular Genetics & Genomics* 239: 298–303**.

Rath A., Glibowicka M., Nadeau V. G., et al. (2009): Detergent binding explains anomalous SDS-PAGE migration of membrane proteins. ***Proceedings of the National Academy of Sciences of the United States of America* 106: 1760–1765**.

Reese M. G. (2001): Application of a time-delay neural network to promoter annotation in the Drosophila melanogaster genome. ***Computers & Chemistry* 26: 51–56**.

Reiner T., Hoefle C., Hückelhoven R. (2015): A barley SKP1-like protein controls abundance of the susceptibility factor RACB and influences the interaction of barley with the barley powdery mildew fungus. ***Molecular Plant Pathology*: Article first published online: 7 Jun 2015**.

Reinstadler A., Muller J., Czembor J. H., et al. (2010): Novel induced mlo mutant alleles in combination with site-directed mutagenesis reveal functionally important domains in the heptahelical barley Mlo protein. ***BMC Plant Biology* 10: 31**.

Ridout C. J., Skamnioti P., Porritt O., et al. (2006): Multiple avirulence paralogues in cereal powdery mildew fungi may contribute to parasite fitness and defeat of plant resistance. ***The Plant Cell* 18: 2402–2414**.

Rooney H. C., van't Klooster J. W., van der Hoorn R. A., et al. (2005): *Cladosporium* Avr2 inhibits tomato Rcr3 protease required for Cf-2-dependent disease resistance. ***Science* 308: 1783–1786**.

Rose J. K., Ham K.-S., Darvill A. G., et al. (2002): Molecular cloning and characterization of glucanase inhibitor proteins: Coevolution of a counterdefense mechanism by plant pathogens. ***The Plant Cell Online* 14: 1329–1345**.

Ross J. L., Ali M. Y., Warshaw D. M. (2008): Cargo transport: Molecular motors navigate a complex cytoskeleton. ***Current Opinion in Cell Biology* 20: 41–47**.

Rounds C. M. and Bezanilla M. (2013): Growth mechanisms in tip-growing plant cells. ***Annual Review of Plant Biology* 64: 243–265**.

Rouxel T., Grandaubert J., Hane J. K., et al. (2011): Effector diversification within compartments of the *Leptosphaeria maculans* genome affected by repeat-induced point mutations. ***Nature Communications* 2: 202**.

Sacristán S., Vigouroux M., Pedersen C., et al. (2009): Coevolution between a family of parasite virulence effectors and a class of LINE-1 retrotransposons. ***PLoS ONE* 4: e7463**.

Sandberg A., Luheshi L. M., Sollvander S., et al. (2010): Stabilization of neurotoxic Alzheimer amyloid- oligomers by protein engineering. ***Proceedings of the National Academy of Sciences of the United States of America* 107: 15595–15600**.

Schaefer A., Höhner K., Berken A., et al. (2011a): The unique plant RhoGAPs are dimeric and contain a CRIB motif required for affinity and specificity towards cognate small G proteins. ***Biopolymers* 95: 420–433**.

Schaefer A., Miertzschke M., Berken A., et al. (2011b): Dimeric plant RhoGAPs are regulated by its CRIB effector motif to stimulate a sequential GTP hydrolysis. ***Journal of Molecular Biology* 411: 808–822**.

Scheffzek K. and Ahmadian M. R. (2005): GTPase activating proteins: Structural and functional insights 18 years after discovery. ***Cellular and Molecular Life Sciences* 62: 3014–3038**.

Schmidt S. M., Kuhn H., Micali C., et al. (2014): Interaction of a *Blumeria graminis* f. sp. *hordei* effector candidate with a barley ARF-GAP suggests that host vesicle trafficking is a fungal pathogenicity target. ***Molecular Plant Pathology* 15: 535–549**.

Schmitz J. and Brosius J. (2011): Exonization of transposed elements: A challenge and opportunity for evolution. ***Biochimie* 93: 1928–1934**.

Schornack S., Huitema E., Cano L. M., et al. (2009): Ten things to know about oomycete effectors. ***Molecular Plant Pathology* 10: 795–803**.

Schroeder N., Mota L. J., Méresse S. (2011): *Salmonella*-induced tubular networks. ***Trends in Microbiology* 19: 268–277**.

Schultheiss H., Dechert C., Kogel K.-H., et al. (2002): A small GTP-binding host protein Is required for entry of powdery mildew fungus into epidermal cells of barley. ***Plant Physiology* 128: 1447–1454**.

Schultheiss H., Dechert C., Kogel K.-H., et al. (2003): Functional analysis of barley RAC/ROP G-protein family members in susceptibility to the powdery mildew fungus. ***The Plant Journal* 35: 589–601**.

Schultheiss H., Hensel G., Imani J., et al. (2005): Ectopic expression of constitutively activated RACB in barley enhances susceptibility to powdery mildew and abiotic stress. ***Plant Physiology* 139: 353–362**.

Schultheiss H., Preuss J., Pircher T., et al. (2008): Barley RIC171 interacts with RACB in planta and supports entry of the powdery mildew fungus. ***Cellular Microbiology* 10: 1815–1826**.

Schweizer P., Pokorny J., Abderhalden O., et al. (1999): A transient assay system for the functional assessment of defense-related genes in wheat. ***Molecular Plant-Microbe Interactions* 12: 647–654**.

Seeholzer S., Tsuchimatsu T., Jordan T., et al. (2010): Diversity at the Mla powdery mildew resistance locus from cultivated barley reveals sites of positive selection. ***Molecular Plant-Microbe Interactions* 23: 497–509**.

Seifert G. J. and Blaukopf C. (2010): Irritable walls: The plant extracellular matrix and signaling. ***Plant Physiology* 153: 467–478**.

Sela N., Mersch B., Hotz-Wagenblatt A., et al. (2010): Characteristics of transposable element exonization within human and mouse. ***PLoS ONE* 5: e10907**.

Shao F., Merritt P. M., Bao Z., et al. (2002): A *Yersinia* effector and a *Pseudomonas* avirulence protein define a family of cysteine proteases functioning in bacterial pathogenesis. ***Cell* 109: 575–588**.

Shao F., Vacratsis P. O., Bao Z., et al. (2003): Biochemical characterization of the *Yersinia* YopT protease: Cleavage site and recognition elements in Rho GTPases. ***Proceedings of the National Academy of Sciences of the United States of America* 100: 904–909**.

Shaw R. K., Smollett K., Cleary J., et al. (2005): Enteropathogenic *Escherichia coli* type III effectors EspG and EspG2 disrupt the microtubule network of intestinal epithelial cells. ***Infection and Immunity* 73: 4385–4390**.

Shen Q.-H., Saijo Y., Mauch S., et al. (2007): Nuclear activity of MLA immune receptors links isolate-specific and basal disease-desistance responses. ***Science* 315: 1098–1103**.

Sieberer B. J., Timmers A. C. J., Emons A. M. C. (2005): Nod factors alter the microtubule cytoskeleton in *Medicago truncatula* root hairs to allow root hair reorientation. ***Molecular Plant-Microbe Interactions* 18: 1195–1204**.

Skamnioti P., Pedersen C., Al-Chaarani G. R., et al. (2008): Genetics of avirulence genes in *Blumeria graminis* f.sp. *hordei* and physical mapping of AVRa22 and AVRa12. ***Fungal Genetics and Biology* 45: 243–252**.

Slavoff S. A., Mitchell A. J., Schwaid A. G., et al. (2012): Peptidomic discovery of short open reading frame–encoded peptides in human cells. ***Nature Chemical Biology* 9: 59–64**.

Smertenko A. and Franklin-Tong V. E. (2011): Organisation and regulation of the cytoskeleton in plant programmed cell death. ***Cell Death and Differentiation* 18: 1263–1270**.

Smith J. E., Alvarez-Dominguez J. R., Kline N., et al. (2014): Translation of small open reading frames within unannotated RNA transcripts in *Saccharomyces cerevisiae*. ***Cell Reports* 7: 1858–1866**.

Söding J., Biegert A., Lupas A. N. (2005): The HHpred interactive server for protein homology detection and structure prediction. ***Nucleic Acids Research* 33: W244–W248**.

Song J., Win J., Tian M., et al. (2009): Apoplastic effectors secreted by two unrelated eukaryotic plant pathogens target the tomato defense protease Rcr3. ***Proceedings of the National Academy of Sciences of the United States of America* 106: 1654–1659**.

Sorek R., Lev-Maor G., Reznik M., et al. (2004): Minimal conditions for exonization of intronic sequences: 5′ splice site formation in Alu exons. ***Molecular Cell* 14: 221–231**.

Spanu P. D., Abbott J. C., Amselem J., et al. (2010): Genome expansion and gene loss in powdery mildew fungi reveal tradeoffs in extreme parasitism. ***Science* 330: 1543–1546**.

Sperschneider J., Gardiner D. M., Taylor J. M., et al. (2013): A comparative hidden Markov model analysis pipeline identifies proteins characteristic of cereal-infecting fungi. ***BMC Genomics* 14: 807**.

Spoel S. H. and Dong X. (2012): How do plants achieve immunity? Defence without specialized immune cells. ***Nature Reviews Immunology* 12: 89–100**.

Stam R., Jupe J., Howden, A. J. M., et al. (2013): Identification and characterisation CRN effectors in *Phytophthora capsici* shows modularity and functional diversity. ***PLoS ONE* 8: e59517**.

Stergiopoulos I. and Wit P. J. DE (2009): Fungal effector proteins. ***Annual Review of Phytopathology* 47: 233–263**.

Synek L., Sekereš J., Žárský V. (2014): The exocyst at the interface between cytoskeleton and membranes in eukaryotic cells. ***Frontiers in Plant Science* 4: 543**.

Tamura K, Stecher G., Peterson D., et al. (2012): MEGA6: Molecular evolutionary genetics analysis version 6.0. ***Molecular Biology and Evolution* 30: 2725-2729**.

Tanaka K., Choi J., Cao Y., et al. (2014): Extracellular ATP acts as a damage-associated molecular pattern (DAMP) signal in plants. ***Frontiers in Plant Science* 5**.

Timmers A. C. J. (2008): The role of the plant cytoskeleton in the interaction between legumes and rhizobia. ***Journal of Microscopy* 231: 247–256**.

Trdá L., Boutrot F., Claverie J., et al. (2015): Perception of pathogenic or beneficial bacteria and their evasion of host immunity: pattern recognition receptors in the frontline. ***Frontiers in Plant Science* 6: 219**.

Troch V., Audenaert K., Wyand R. A., et al. (2014): *Formae speciales* of cereal powdery mildew: Close or distant relatives? ***Molecular Plant Pathology* 15: 304–314**.

Tulin A., McClerklin S., Huang Y., et al. (2012): Single-molecule analysis of the microtubule cross-linking protein MAP65-1 reveals a molecular mechanism for contact-angle-dependent microtubule bundling. ***Biophysical Journal* 102: 802–809**.

Tusnády G. E. and Simon I. (1998): Principles governing amino acid composition of integral membrane proteins: Application to topology prediction. ***Journal of Molecular Biology* 283: 489–506**.

Underwood W. (2012): The plant cell wall: A dynamic barrier against pathogen invasion. ***Frontiers in Plant Science* 3: 85**.

Üstün S., Bartetzko V., Börnke F., et al. (2013): The *Xanthomonas campestris* type III effector XopJ targets the host cell proteasome to suppress salicylic-acid mediated plant defence. ***PLoS Pathogens* 9: e1003427**.

Üstün S. and Börnke F. (2015): The *Xanthomonas campestris* type III effector XopJ proteolytically degrades proteasome subunit RPT6. ***Plant Physiology* 168: 107–119**.

Vallenius T. (2013): Actin stress fibre subtypes in mesenchymal-migrating cells. ***Open Biology* 3: 130001**.

Van de Wouw A. P., Cozijnsen A. J., Hane J. K., et al. (2010): Evolution of linked avirulence effectors in *Leptosphaeria maculans* is affected by genomic environment and exposure to resistance genes in host plants. ***PLoS Pathogens* 6: e1001180**.

van den Burg H. A., Harrison S. J., Joosten M. H. A. J., et al. (2006): *Cladosporium fulvum* Avr4 protects fungal cell walls against hydrolysis by plant chitinases accumulating during infection. ***Molecular Plant-Microbe Interactions* 19: 1420–1430**.

van Esse H. P., van't Klooster J. W., Bolton M. D., et al. (2008): The *Cladosporium fulvum* virulence protein Avr2 inhibits host proteases required for basal defense. ***The Plant Cell Online* 20: 1948–1963**.

van Schie C. C. and Takken F. L. (2014): Susceptibility genes 101: How to be a good host. ***Annual Review of Phytopathology* 52: 551–581**.

Vassetzky N. S. and Kramerov D. A. (2012): SINEBase: A database and tool for SINE analysis. ***Nucleic Acids Research* 41: D83–D89**.

Vetter I. R. and Wittinghofer A. (2001): The guanine nucleotide-binding switch in three dimensions. ***Science* 294: 1299–1304**.

Vetukuri R. R., Åsman, A. K. M., Tellgren-Roth C., et al. (2012): Evidence for small RNAs homologous to effector-encoding genes and transposable elements in the oomycete *Phytophthora infestans*. ***PLoS ONE* 7: e51399**.

Vetukuri R. R., Tian Z., Avrova A. O., et al. (2011): Silencing of the PiAvr3a effector-encoding gene from *Phytophthora infestans* by transcriptional fusion to a short interspersed element. ***Fungal Biology* 115: 1225–1233**.

Viboud G. I. and Bliska J. B. (2005): *Yersinia* Outer Proteins: Role in modulation of host cell signaling responses and pathogenesis. ***Annual Review of Microbiology* 59: 69–89**.

Vlot A. C., Dempsey D. A., Klessig D. F. (2009): Salicylic acid, a multifaceted hormone to combat disease. ***Annual Review of Phytopathology* 47: 177–206**.

Voegele R. T., Struck C., Hahn M., et al. (2001): The role of haustoria in sugar supply during infection of broad bean by the rust fungus *Uromyces fabae*. ***Proceedings of the National Academy of Sciences of the United States of America* 98: 8133–8138**.

Voigt C. A. (2014): Callose-mediated resistance to pathogenic intruders in plant defense-related papillae. ***Frontiers in Plant Science* 5: 168**.

Vorechovsky I. (2010): Transposable elements in disease-associated cryptic exons. ***Human Genetics* 127: 135–154**.

Walter M., Chaban C., Schütze K., et al. (2004): Visualization of protein interactions in living plant cells using bimolecular fluorescence complementation. ***The Plant Journal* 40: 428–438**.

Walters D. R. and McRoberts N. (2006): Plants and biotrophs: A pivotal role for cytokinins? ***Trends in Plant Science* 11: 581-586.**

Wang M. and Marín A. (2006): Characterization and prediction of alternative splice sites. ***Gene* 366: 219–227**.

Wang X., Parashar K., Sitaram A., et al. (2014): The GAP Activity of type III effector YopE triggers killing of *Yersinia* in macrophages. ***PLoS Pathogens* 10: e1004346**.

Wang Y., Chantreau M., Sibout R., et al. (2013): Plant cell wall lignification and monolignol metabolism. ***Frontiers in Plant Science* 4: 220**.

Wang Y., Li J., Hou S., et al. (2010): A *Pseudomonas syringae* ADP-ribosyltransferase inhibits *Arabidopsis* Mitogen-Activated Protein Kinase kinases. ***The Plant Cell* 22: 2033–2044**.

Wasteneys G. O. (2002): Microtubule organization in the green kingdom: Chaos or self-order? ***Journal of Cell Science* 115: 1345–1354**.

Wei Y. D., Collinge D. B., Smedegaard-Petersen V., et al. (1996): Characterization of the transcript of a new class of retroposon-type repetitive element cloned from the powdery mildew fungus, *Erysiphe graminis* repetitive element *Erysiphe graminis*. ***Molecular and General Genetics* 250: 477–482**.

Weiberg A., Wang M., Bellinger M., et al. (2014): Small RNAs: A new paradigm in plant-microbe interactions. ***Annual Review of Phytopathology* 52: 495–516**.

Weiberg A., Wang M., Lin F.-M., et al. (2013): Fungal small RNAs suppress plant immunity by hijacking host RNA interference pathways. ***Science* 342: 118–123**.

Weis C., Hückelhoven R., Eichmann R. (2013): Lifeguard proteins support plant colonization by biotrophic powdery mildew fungi. ***Journal of Experimental Botany* 64: 3855–3867**.

West N. C., Roy-Engel A. M., Imataka H., et al. (2002): Shared protein components of SINE RNPs. ***Journal of Molecular Biology* 321: 423–432**.

Whigham E., Qi S., Mistry D., et al. (2015): Broadly conserved fungal effector BEC1019 suppresses host cell death and enhances pathogen virulence in powdery mildew of barley (*Hordeum vulgare* L.). ***Molecular Plant-Microbe Interactions*: Accepted for Publication**.

Whisson S. C., Vetukuri R. R., Avrova A. O., et al. (2014): Can silencing of transposons contribute to variation in effector gene expression in *Phytophthora infestans* ? ***Mobile Genetic Elements* 2: 110–114**.

Wiberg A. (1974): Genetical studies of spontaneous sources of resistance to powdery mildew in barley. ***Hereditas* 77: 89–148**.

Wicker T., Sabot F., Hua-Van A., et al. (2007): A unified classification system for eukaryotic transposable elements. ***Nature Reviews Genetics* 8: 973–982**.

Wilhelm M., Schlegl J., Hahne H., et al. (2014): Mass-spectrometry-based draft of the human proteome. ***Nature* 509: 582–587**.

Wolter M., Hollricher K., Salamini F., et al. (1993): The mlo resistance alleles to powdery mildew infection in barley trigger a developmentally controlled defence mimic phenotype. ***Molecular and General Genetics MGG* 239: 122-128**.

Wright M. W. and Bruford E. A. (2011): Naming 'junk': Human non-protein coding RNA (ncRNA) gene nomenclature. ***Human Genomics* 5: 90**.

Wu G., Li H., Yang Z. (2000): *Arabidopsis* RopGAPs are a novel family of Rho GTPase-activating proteins that require the Cdc42/Rac-Interactive Binding motif for Rop-specific GTPase stimulation. ***Plant Physiology* 124: 1625–1636**.

Wu M., Li L., Sun Z. (2007): Transposable element fragments in protein-coding regions and their contributions to human functional proteins. ***Gene* 401: 165–171**.

Wu S., Lu D., Kabbage M., et al. (2011): Bacterial effector HopF2 suppresses *Arabidopsis* innate immunity at the plasma membrane. ***Molecular Plant-Microbe Interactions* 24: 585–593**.

Xiang T., Zong N., Zhang J., et al. (2011): BAK1 is not a target of the *Pseudomonas syringae* effector AvrPto. ***Molecular Plant-Microbe Interactions* 24: 100–107**.

Xu D. and Zhang Y. (2012): *Ab initio* protein structure assembly using continuous structure fragments and optimized knowledge-based force field. ***Proteins: Structure, Function, and Bioinformatics* 80: 1715–1735**.

Xu J. and Zhang Y. (2010): How significant is a protein structure similarity with TM-score = 0.5? ***Bioinformatics* 26: 889–895**.

Yan A., Xu G., Yang Z.-B. (2009): Calcium participates in feedback regulation of the oscillating ROP1 Rho GTPase in pollen tubes. ***Proceedings of the National Academy of Sciences of the United States of America* 106: 22002–22007**.

Yang G., Gao P., Zhang H., et al. (2007): A mutation in MRH2 kinesin enhances the root hair tip growth defect caused by constitutively activated ROP2 small GTPase in *Arabidopsis*. ***PLoS ONE* 2: e1074**.

Yorimitsu T., Sato K., Takeuchi M. (2014): Molecular mechanisms of Sar/Arf GTPases in vesicular trafficking in yeast and plants. ***Frontiers in Plant Science* 5: 411**.

Yoshida S., Handa Y., Suzuki T., et al. (2006): Microtubule-severing activity of *Shigella* is pivotal for intercellular spreading. ***Science* 314: 985–989**.

Yoshida S., Katayama E., Kuwae A., et al. (2002): *Shigella* deliver an effector protein to trigger host microtubule destabilization, which promotes Rac1 activity and efficient bacterial internalization. ***The EMBO Journal* 21: 2923–2935**.

Yoshida S. and Sasakawa C. (2003): Exploiting host microtubule dynamics: A new aspect of bacterial invasion. ***Trends in Microbiology* 11: 139–143**.

Zarnack K., König J., Tajnik M., et al. (2013): Direct competition between hnRNP C and U2AF65 protects the transcriptome from the exonization of Alu elements. ***Cell*** **152: 453–466**.

Zárský V., Cvrcková F., Potocký M., et al. (2009): Exocytosis and cell polarity in plants - exocyst and recycling domains. ***The New Phytologist*** **183: 255–272**.

Zárský V., Kulich I., Fendrych M., et al. (2013): Exocyst complexes multiple functions in plant cells secretory pathways. ***Current Opinion in Plant Biology*** **16: 726–733**.

Zhang J., Shao F., Li Y., et al. (2007): A *Pseudomonas syringae* effector inactivates MAPKs to suppress PAMP-induced immunity in plants. ***Cell Host & Microbe*** **1: 175–185**.

Zhang W.-J., Pedersen C., Kwaaitaal M., et al. (2012a): Interaction of barley powdery mildew effector candidate CSEP0055 with the defence protein PR17c. ***Molecular Plant Pathology*** **13: 1110–1119**.

Zhang Y. and McCormick S. (2007): A distinct mechanism regulating a pollen-specific guanine nucleotide exchange factor for the small GTPase Rop in *Arabidopsis thaliana*. ***Proceedings of the National Academy of Sciences of the United States of America*** **104: 18830–18835**.

Zhang Z., Wu Y., Gao M., et al. (2012b): Disruption of PAMP-induced MAP kinase cascade by a *Pseudomonas syringae* effector activates plant immunity mediated by the NB-LRR Protein SUMM2. ***Cell Host & Microbe*** **11: 253–263**.

Zhou J., Wu S., Chen X., et al. (2014): The *Pseudomonas syringae* effector HopF2 suppresses *Arabidopsis* immunity by targeting BAK1. ***The Plant Journal*** **77: 235–245**.

Zhu C., Ganguly A., Baskin T. I., et al. (2015): The fragile Fiber1 kinesin contributes to cortical microtubule-mediated trafficking of cell wall components. ***Plant Physiology*** **167: 780–792**.

Zipfel C. (2014): Plant pattern-recognition receptors. ***Trends in Immunology*** **35: 345–351**.

8 Appenidx

Table A 1: Nucleotide and Amino Acid Sequences

>ROPIP1 ATGTCAACACCTGTCAGTGGTGTCCCCTACGAACCTCCAGCTCTCACTGTAGAGTCTGCAGAGCC AAGATTGAGTAACAACCTCCTCACTTCGATGAGGATTCCCAGTCGCCTTCGCGATCTGTATCGTC TTCATTTCTCATCACATCCCCCTATCACCATTATCATGAAGCTAACCACGATCAGATCAGACGTT AGGGTCGAAGCCCTTCTCGTCACCAACCCTTGA
Nucleotide Sequence of ROPIP1. Please note, the underlined ATG is artificial.
>ROPIP1-translated MSTPVSGVPYEPPALTVESAEPRLSNNLLTSMRIPSRLRDLYRLHFSSHPPITIIMKLTTIRSDV RVEALLVTNP-
Amino Acid Sequence of ROPIP1. Please note, the underlined M is artificial.
>ROPIP1-Cter ATGAGGATTCCCAGTCGCCTTCGCGATCTGTATCGTCTTCATTTCTCATCACATCCCCCTATCAC CATTATCATGAAGCTAACCACGATCAGATCAGACGTTAGGGTCGAAGCCCTTCTCGTCACCAACC CTTGA
Nucleotide Sequence of ROPIP1-Cter.
>ROPIP1-Cter-translated MRIPSRLRDLYRLHFSSHPPITIIMKLTTIRSDVRVEALLVTNP-
Amino Acid Sequence of ROPIP1-Cter.
>gi|763091|emb|X86077.1| E.graminis mRNA for a retroposon-type repetitive element CTCAACACCTGTCAGTGGTGTCCCCTACGAACCTCCAGCTCTCACTGTAGAGTCTGCAGAGCCAA GATTGAGTAACAACCTCCTCACTTCGATGAGGATTCCCAGTCGCCTTCGCGATCTGTATCGTCTT CATTTCTCATCACATCCCCCTATCACCATTATCATGAAGCTAACCACGATCAGATCAGACGTTAG GGTCGAAGCCCTTCTCGTCACCAACCCTTGATCATGGAGGAAAAGCCATCCGATGAGTTTCCGGA GCGAACCCAGCACCCGATACAGAGATGGTGGATTGGATCAAGATGGCCTCGAATGCTACAAAGAA GGGAGATATAGATGAATATGCGCACCTCATGTGGTCCCGGTGTCTAGGCCTCGCCTGGCTGGGGC TGCAGGTTTTTTGAGACTTTTTCCCGCGCACGCAGTTTCCATTGCTACCATTTTTATTTTTTTTT GGGTAGAAGGTTCCGTGGAAAAGGTGGCTGAATTCCACGGGTAAATACTGAGCTGAATGGCTATT CATCATGGGCAATATATCAATGATCTTACAAGTAACAAGAGAGGACAGGAGCACTGTACAAGGTG TGGCCTGGGCCAGAGAGGAGCCCAATGTGCTAGATAGTCGAAGACTCAAGTAGTACAATAAAAAC CCACCCACTCATTACTCCAAAAAAAAAAAAAAAAAA
Annotated Nucleotide Sequence of Eg-R1. GenBank: X86077.1.

Table A 1 continued

>Eg-R1_CONSENUS
-----gGGGGACTATTCTCAACACCTGTCAGTGGTGTCCCCTACGAACCTCCAGCtCTCa
CTgtAgAGTCTGCAGAGCCaAGATTGAGTaACAAccTCCTCACTtCGATGAGGaTTCCCA
gTCGCcTTCGCgaTCTGTATCgTCTTCATttcTcAtCACATCcCCcTATCACCATTATCA
TGAAGCTAACCACgATCAGATCAGAcGtTAgggTCgaAGCCCTtCTcgTCACCAACCCTT
GATCATGGAgGAAAAGCCATCCgATGAGTTTCCGGAGcGaACCCAGCACCCGATACggAG
ATGGTGGATTGGATCAAGatGGCcTCGAaTgcTAcAAAGAAGGGAGATATAGATGAATAT
GCGCACCTCaTGTGGTCCCGGTGTCTAGGCCTCGCCTGGCTGGGGCTGCAGGTTTTTTGA
GACTTTTtCCCgCGCACgcAGTTTCCATTGCTACCatttttatttttTTT-GGGTAGAAG
GTTCCgTGGAaAAGGTGgCTGAATTCcA-GGGTAAATACTGAGCTGAATgGCTAtTCATC
A-gGGCAAtaTAtCAATGATCTTaCAAGtAACAagAGAGGacAgGAGCACTGTACAAGgT
GtGGccTGGGCCAGAGAGGAgCCCAATGTGCTAgATAGTCgaaGACTCAAgTAGTACAAT
AAA--AaCcCACtcactcac--------------

Consensus Sequence of 23 'Full-Length' Genomic Insertions of the Eg-R1 Element Bordered by Target Site Duplications (TSDs) and Being Longer than 670 bp Identified in the Genome v3b (contigs) Database of BluGen. The underlined nucleotides were newly identified as part of Eg-R1.

>5-RACE_cand_2-1
~~TTTTTTTTTTTTTTT~~GGGGGACTATTCTCAACACCTGTCAGTGGTGTCCCCTACGAACCTCCAG
CTCTCACTGTAGAGTCTGCAGAGCCAAGATTGAGTAACAACCTCCTCACTTCGATGAGGATTCCC
AGTCGCCTTCGCGGTCTGTATCGTCTTCATTTCTCATCACATCCCCCTATCACCATTATCATGAA
GCTAACCACGATCAGATCAGAC

One Exemplary Sequence Derived from 5'-RACE PCR Using ROPIP1-specific Oligos. The striked-through Oligo(dT) stretch derived from process-dependent A-tailing. The underlined nucleotides are identical to the newly identified nucleotides of the Eg-R1 element.

>ROPIP1-translated
->ROPIP1-Cter
MSTPVSGVPYEPPALTVESAEPRLSNNLLTSMRIPSRLRDLYRLHFSSHPPITIIMKLTTIRSDV
RVEALL
SCOP domain: YigF-like superfamily
[55298]
VTNP-

Localization of the putative YigF-like homo-trimerization domain (SCOP 55298) in the translated ROPIP1 sequence, predicted with HHpred. A motif reminiscent of the *P. infestans* RXLR host translocation motif is highlighted in red.

Table A 2: Sequence Alignments.

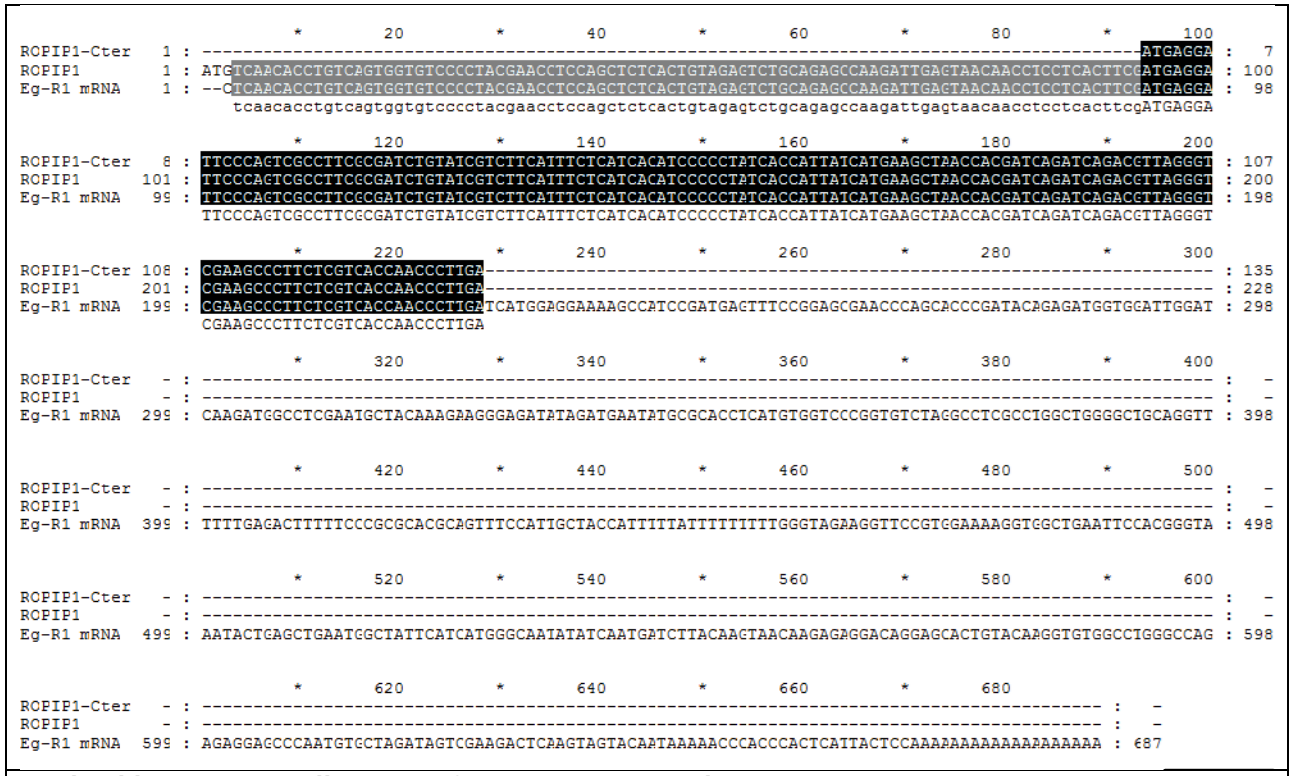

Nucleotide Sequence Alignment of Eg-R1, ROPIP1 and ROPIP1-Cter.

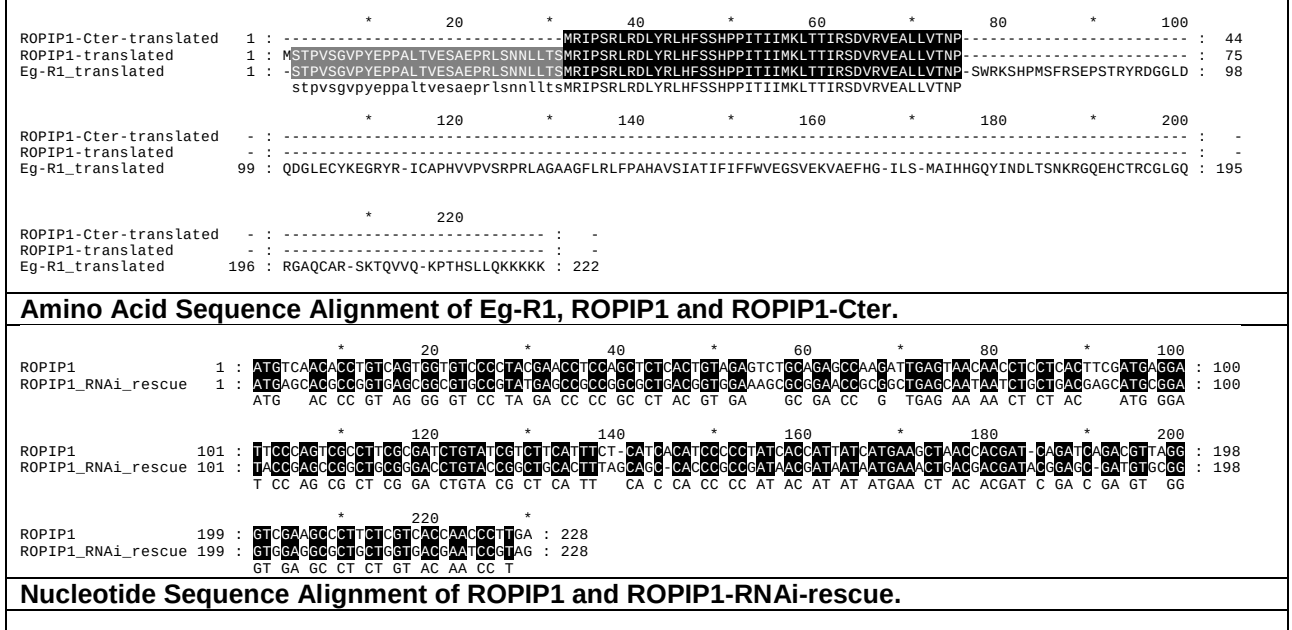

Amino Acid Sequence Alignment of Eg-R1, ROPIP1 and ROPIP1-Cter.

Nucleotide Sequence Alignment of ROPIP1 and ROPIP1-RNAi-rescue.

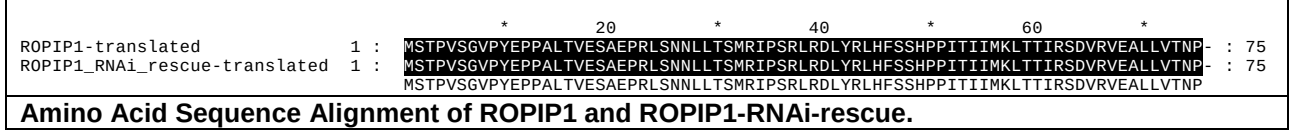

Amino Acid Sequence Alignment of ROPIP1 and ROPIP1-RNAi-rescue.

Table A 2 continued

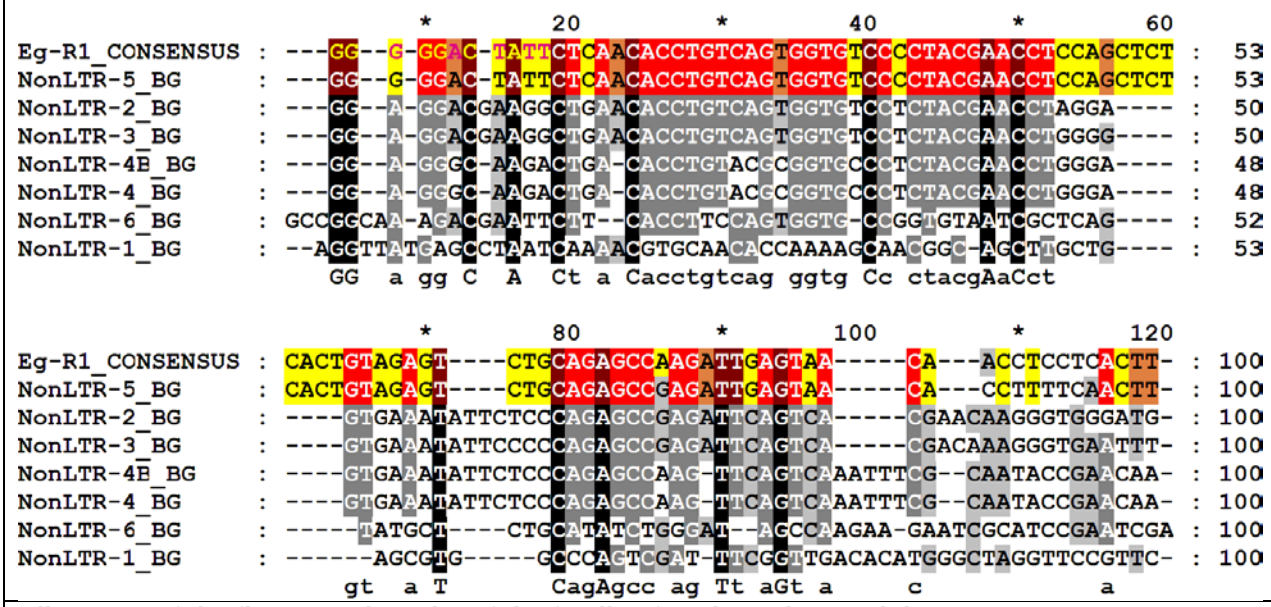

Alignment of the first 5'-end 100 bp of the family of 8 *Blumeria graminins* Non-LTR retrotransposons. EGRT1 Non-LTR Retrotransposon, which is identical to Eg-R1 was replaced with Eg-R1_CONSENSUS, containing the newly identified 5'-extension of Eg-R1. The image is given in 4-colour code. The at their 5'-end nearly identical Eg-R1_CONSENSUS and NonLTR-5_BG are highlighted in colour.

Table A 3: 8 ROPIP1 Sequence Variants with Positive Signal Peptide Prediction.

#	Source	Identifier	Length	SignalP	Name
1	BluGen	contig_000529:1..1000 = CAUH01000529:1..1000	106	v3.0	sp42-1
2	BluGen	contig_001259:1..1000 = CAUH01001259:1..1000	91	v3.0	sp42-2
3	BluGen	contig_002559:9000..11000 = CAUH01002559:9000..11000	88	v3.0	sp42-3
4	BluGen	contig_002841:27000..29500 = CAUH01002841:27000..29500	105	v3.0 & v4.1	sp42-4
5	BluGen	contig_010510:1..1419 = CAUH01010509:1..1419	108	v3.0	sp42-5
6	NCBI Trace Archive	ti|2268612253	118	v3.0	104770672
7	NCBI Nucleotide Collection	GenBank: EU098096.1	74	v3.0 & v4.1	EKA42A
8	Thomas Wicker/BluGen	CAUH01002575:2300..3800	133	v3.0	TW42A

Name	Sequence
sp42-1	MNPPLILPGFSPFLVCGDFYCLSLPSFGGLFSTPVSGVPYEPPALTVESAEPRLSNNLLTSMRIPSRLRDLYRLHFSSHPPITIIMKLTTIRSDVRVEALLVTNP*
sp42-2	MDCRLEGVVLGILGGLFSTPVSGVPYEPPALTVESAEPRLSNNLLTSMRIPSRLRDLYRLHFSSHPPITIIMKLTTIRSDVRVEALLVTNP
sp42-3	MWWNFAPVAGGLFSTPVSGVPYEPPALTVESAEPRLSNNLLTSMSIPSRLRDLYRLHFSSHPPITIIMKLTTIRSDVRVEALLVTNP*
sp42-4	MAGDQWGKLLFAIGVTSLLVAEARWSGGLFSTPVSGVPYEPPALTVESAEPRLSNNLLTSMRIPSRLRDLYRLHFSSHPPITIIMKLTTIRSDVRVEALLVTNP*
sp42-5	MTGTLFTYKMTLLTLETLLLWISIANTTMGGGLFSTPVSGVPYEPPALTVESAEPRLSNNLLTSMRIPSRLRDLYRLHFSSHPPITIIMKLTTIRSDVRVEALLVTNP
104770672	MFFSSLAPQAHYSWLAPLAPKLWQTWSGKRPFHTLHPPLGGGLFSTPVSGVPYEPPALTVESAEPRLSNNLLTSMRIPSRLRDLYRLHFSSHPPITIIMKLTTIRSDVRVEALLVTNP
EKA42A	MGRSSGGHPALVAACSCDFLLGAAGGLFSTPVSGVPYEPPALTVESAEPRLNDKVLTSMRIPKRFRGLYRLHP*
TW42A	MNHLHGLQSQSKIWIISWMDPFFLVRGKPVLSVDLSTQHTMVLGSNEFQMKQVTSGLFSTPVSGVPYEPPALTVESAEPRLSNNLLTSMRIPSRLRDLYRLHFSSHPPITIIMKLTTIRSDVRVEALLVTNP*

Sequence extensions of ROPIP1 generating a positive signal peptide prediction score using SIgnalP server in the indicated versions are underlined.

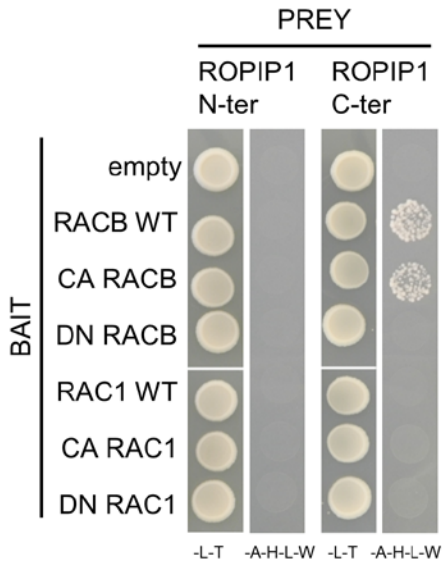

Figure A 1: Targeted Y2H with ROPIP1-Nter and ROPIP1-Cter as preys and bait vectors as indicated. The ROPIP1 sequence was split into an N-terminal (ROPIP1-Nter) and a C-terminal (ROPIP1-Cter) fragment. ROPIP1-Cter interacted with RACB (WT/CA) but not with RAC1. Left stripes: Transformation control medium (SD –L/-W); Right stripes: selection medium (SD –A/-H/-L/-W). Drops of 10^6 cells per combination are shown.

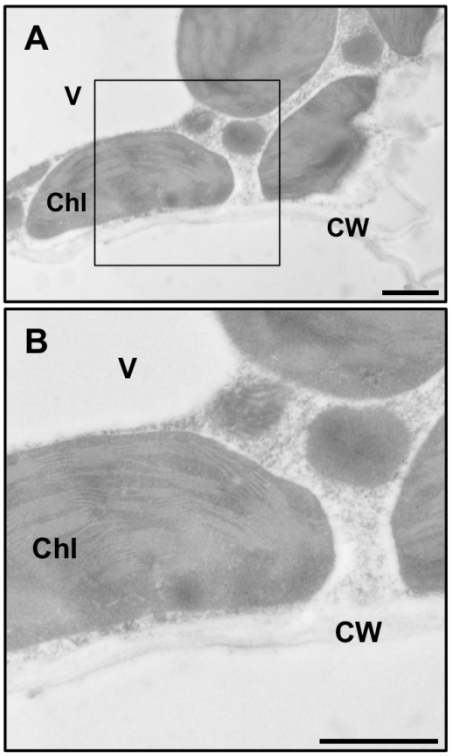

Figure A 2: Immunogold labeling mesophyll control. (A) Transmission electron microscopy (TEM) micrograph of an immunogold-stained mesophyll cell of a *Bgh*-infected barley primary leaf chemically fixed at 3 dai. α-ROPIP1 was used as primary antibody and detected with anti-rabbit secondary antibodies conjugated to 10 nm gold particels. Gold-particles were only occasionally observed. (B) Detail picture of A. Chl: chloroplast, CW: cell wall, V: vacuole. Scale bars are 1 µm.

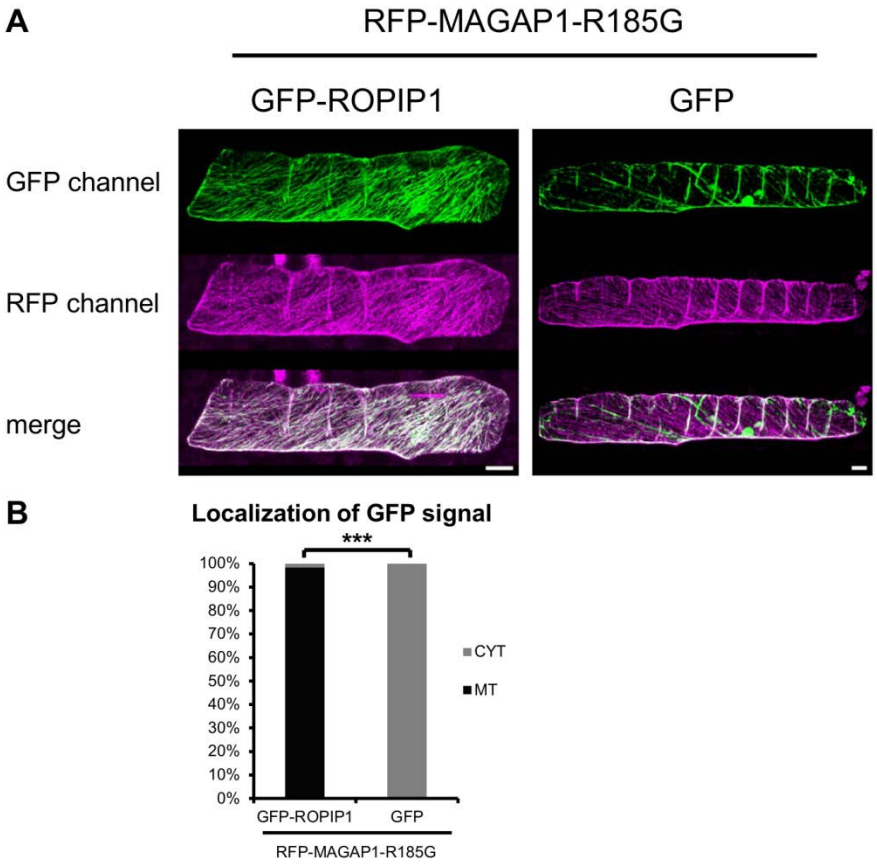

Figure A 3: GFP-ROPIP1 and RFP-MAGAP1-R185G co-localize at microtubules. The R185G mutation of MAGAP1 did not abolish recruitment of GFP-ROPIP1 to microtubules. Whole cell projections of barley epidermal cells co-expressing (A) GFP-ROPIP1 or (B) GFP together with catalytic inactive RFP-MAGAP1-R185G are shown. Barley epidermal cells were transiently co-transformed with 1.0 µg/shot pGY1-RFP-MAGAP1-R185G plus 0.75 µg/shot GFP-ROPIP1, respectively 0.5 µg/shot GFP. Transformed cells were sequentially scanned as z-stacks in 2 µm increments by confocal laser scanning microscopy at 12-24 hat and merged into maximum projection. White colour in the merge picture indicates co-localization. (B) 59 GFP-ROPIP1 and 53 GFP co-expressing cells derived from 3 independent repetitions were categorized by the GFP signal being located at microtubules (MT) or in the cytoplasm (CYT). The relative frequencies of the categories are depicted. The distribution of the absolute values of the categories were compared between GFP-ROPIP1 and GFP co-expressing cells in a X^2-test and found to be highly significant different ($X^2 = 108.06$; $\alpha = 0.001$; $df = 1$; $n = 59, 53$). *** $p \leq 0.001$ (X^2). Scale bars are 20 µm.

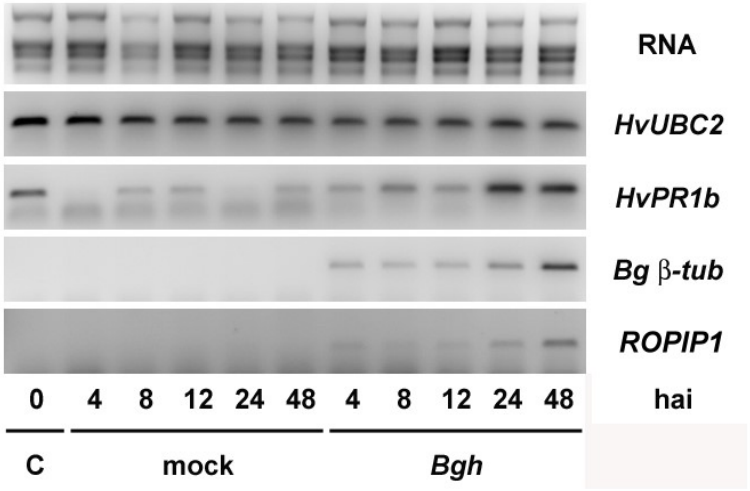

Figure A 4: Semi-quantitative Reverse Transcription PCR.
7d old barley primary leaves were inoculated with *Bgh* or mock treated and harvested at the indicated time points. Total RNA was extracted, digested with DNAse I and reverse transcribed into cDNA. Barley *Ubiquitin Conjugating Enzyme 2* (*HvUBC2*, AY220735.1) was amplified as control for cDNA quantity. Successful inoculation was checked by the induction of the barley *Basic PR-1-Type Pathogenesis Related Protein* (*HvPR1b*, X74940.1) gene. The amount of Blumeria graminis f.sp. hordei *Tub2 Gene For Beta Tubulin* (*Bgh tub2*, AJ313149) transcript monitored the development of fungal biomass. The *ROPIP1* transcript appeared not to be induced after pathogen challenge. Being part of the SINE-like Eg-R1 retrotransposon the amplified ROPIP1 sequence is indistinguishable from Eg-R1. The experiment was repeated with similar results.

Table A 4: Plasmids Used in this Study

Plasmid	Purpose	Source
pGEM-T	A/T-Cloning	Promega
pGEM-T putX80677 K15	Cloning of Eg-R1	This study
pGEM-T sp42-2 K1	Cloning of sp42-2	This study
pGEM-T sp42-3 K2	Cloning of sp42-5	This study
pGEM-T sp42-5 K4	Cloning of sp42-4	This study
pGY1-empty	Control OE ROPIP1	Patrick Schweizer Lab
pGY1-ROPIP1	Transient OE	Hückelhoven Lab
pGY1-ROPIP1-Cter	Transient OE	Hückelhoven Lab
pGY1-GFP	Life Cell Imaging	Hückelhoven Lab
pGY1-GFP+2	Cloning of GFP-ROPIP1-RNAi rescue	Hückelhoven Lab
pGY1-mCherry	Life Cell Imaging	Hückelhoven Lab
pGY1-CFP	Life Cell Imaging	Hückelhoven Lab
pGY1-GFP-ROPIP1	Life Cell Imaging	Hückelhoven Lab
pGY1-GFP-ROPIP1-Cter	Life Cell Imaging	Hückelhoven Lab
pEXA2-ROPIP1-RNAi rescue	Synthetic ROPIP1-RNAi rescue	Eurofins MWG Operon
pGY1-ROPIP1-RNAi-rescue	RNAi rescue ROPIP1	This study
pGY1-GFP-ROPIP1-RNAi-rescue	Test pIPKTA30N-ROPIP1	This study
pGY1-RFP-MAGAP1	Life Cell Imaging	Hückelhoven Lab
pGY1-RFP-MAGAP1-R185G	Life Cell Imaging	Hückelhoven Lab
pGY1-RFP-MAGAP1-Cter	Life Cell Imaging	Hückelhoven Lab
pGY1-RACB WT	Cloning of pGY1-mCherry-RACB WT	Hückelhoven Lab
pGY1-CA RACB	Cloning of pGY1-mCherry-CA RACB	Hückelhoven Lab
pGY1-DN RACB	Cloning of pGY1-mCherry-DN RACB	Hückelhoven Lab
pGY1-mCherry-RACB WT	Life Cell Imaging	This study
pGY1-mCherry- CA RACB	Life Cell Imaging	This study
pGY1-mCherry-DN RACB	Life Cell Imaging	This study
pIPKTA30N-empty	Control HIGS ROPIP1	Patrick Schweizer Lab
pIPKTA38N-ROPIP1	Gateway Entry Vector	Hückelhoven Lab
pIPKTA30N-ROPIP1	HIGS ROPIP1	This study
pUC-SPYNE-ROPIP1	BiFC	Hückelhoven Lab
pUC-SPYCE-CA RACB	BiFC	Hückelhoven Lab
pUC-SPYCE-DN RACB	BiFC	Hückelhoven Lab
pGADT7-empty	Targeted Y2H	Clonetech
pGADT7-ROPIP1	Targeted Y2H	Hückelhoven Lab
pGADT7-ROPIP1-Nter	Targeted Y2H	This study
pGADT7-ROPIP1-Cter	Targeted Y2H	This study
pGBKT7-empty	Targeted Y2H	Clonetech
pGBKT7-RACB WT	Targeted Y2H	Hückelhoven Lab
pGBKT7-CA RACB	Targeted Y2H	Hückelhoven Lab
pGBKT7-DN RACB	Targeted Y2H	Hückelhoven Lab

Table A 4 continued		
pGBKT7-RAC1 WT	Targeted Y2H	Hückelhoven Lab
pGBKT7-CA RAC1	Targeted Y2H	Hückelhoven Lab
pGBKT7-DN RAC1	Targeted Y2H	Hückelhoven Lab
pGBKT7-RAC3 WT	Targeted Y2H	Hückelhoven Lab
pGBKT7-CA RAC3	Targeted Y2H	Hückelhoven Lab
pGBKT7-CA RACD	Targeted Y2H	Hückelhoven Lab
pGBKT7-CA ROP6	Targeted Y2H	Hückelhoven Lab
pGBKT7-MAGAP1	Targeted Y2H	Hückelhoven Lab
pET28b 6H-V42A-6H	Recombinant Expression 6H-ROPIP1-6H	This study

Table A 5: Oligos Used in this Study

Name	Sequence 5'→3'	Gene	Purpose
V42fwd	ACCTGTCAGTGGTGTCCC	ROPIP1	Amplification ROPIP1
V42rev	CAAGGGTTGGTGACGAGAAGG	ROPIP1	Amplification ROPIP1
B8B,V21B_BamH1fwd	GGGGATCCATGTCAACACCTGTTAGTGGT	ROPIP1	Equipment BamHI 5' ROPIP1
V20A,V42ABamH1fwd	GGGGATCCATGTCAACACCTG	ROPIP1	Equipment BamHI 5' ROPIP1
V42A_SmaI_F	CCCGGGATGTCAACACCTGTCAGTGGTG	ROPIP1	Equipment SmaI 5' ROPIP1
V42A,V20Bsalrev	TCAGTCGACCGGGTTGGTGACGAG	ROPIP1	Equipment SalI 3' ROPIP1 w/o stop
V42A,V20Brev	CATGATCACGGGTTGGTGAC	ROPIP1	ROPIP1 with stop codon
42A,42k-NotI-rev	GCGGCCGCACGGGTTGGTGACGAG	ROPIP1	Equipment NotI 3' ROPIP1
F-V42ACter_Sma	CCCGGGATGAGGATTCCCAGTC	ROPIP1-Cter	Equipment SmaI 5' ROPIP1-Cter
R_V42ACter_Bam	GGATCCTCAAGGGTTGGTGACGAG	ROPIP1-Cter	Equipment BamHI 3' ROPIP1-Cter
V42A,V20B-BamH1kurz	AACCTCCTCGGATCCATGAGGATTCC	ROPIP1-Cter	Equipment BamHI 5' ROPIP1-Cter
V42A_Nter_XbaI_R	TCTAGATCACGAAGTGAGGAGGTTGTTAC	ROPIP1-Nter	Equipment XbaI 3' ROPIP1-Nter
R_V42A_Nter_BamHI	GGATCCTCACGAAGTGAGGAGGTTGTTAC	ROPIP1-Nter	Equipment BamHI 3' ROPIP1-Nter
V42A-SP2	GTCTGATCTGATCGTGGTTAGC	ROPIP1	5'-RACE PCR ROPIP1
V42A-SP3	AGACGATACAGATCGCGAAGGC	ROPIP1	5'-RACE PCR ROPIP1
S42A_EcoRI-fwd-1	GAATTCGGGCTAATGAATCCGCCT	sp42-1	Amplification sp42-1
S42A_EcoRI-fwd-2	GAATTCGTGGATGGATTGTCGGCT	sp42-2	Amplification sp42-2
S42A_EcoRI-fwd-3	GAATTCTATGTGGTGGAATTTCGC	sp42-3	Amplification sp42-3
S42A_EcoRI-fwd-4	GAATTCATGGCCGGTGATCAATGG	sp42-4	Amplification sp42-4
S42A_EcoRI-fwd-5	GAATTCGCTATGACACATGACCGG	sp42-5	Amplification sp42-5
Sp42_2_BamHI_F	GGATCCGTGGATGGATTGTCGGCT	sp42-2	Equipment BamHI 5' sp42-2
Sp42_3 BamHI_F	GGATCCTATGTGGTGGAATTTCGC	sp42-3	Equipment BamHI 5' sp42-3
TW42A_F	ATGAATCATCTTCATGGGTTGC	TW42A	Amplification TW42A
TW42A_R	TCAAGGGTTGGTGACGAG	TW42A	Amplification TW42A
TW42A_Intron_F	ACAAGTAACTAGGGGACTATTC	TW42A	Amplification TW42A
TW42A_Intron_F2	CAGATGAAACAAGTAACTAGGG	TW42A	Amplification TW42A
X80677_anchored_dT	TTTTTTTTTTTTTTTTTTGGAG	Eg-R1	Amplification Eg-R1 RNA
HvUBC2_fwd	TCTCGTCCCTGAGATTGCCCACAT	HvUBC2	Amplification HvUBC2 sqRT-PCR

Table A 5 continued			
HvUBC2_rev	TTTCTCGGGACAGCAACACAATCTTCT	HvUBC2	Amplification HvUBC2 sqRT-PCR
T-PR1b/3´-2	AGGTGTTGGAGCCGTAGTC	HvPR1b	Amplification HvPR1b sqRT-PCR
T-PR1b/5´-2	AAGCTGCAAGCGTTCGCC	HvPR1b	Amplification HvPR1b sqRT-PCR
*Bgh*_beta-tub_F	TCTGCCATTTTCCGCGGTAA	*Bgh*β-tub	Amplification *Bgh*β-tub sqRT-PCR
*Bgh*_beta-tub_R	CGTTGCTTACTTCCTCTGGA	*Bgh*β-tub	Amplification *Bgh*β-tub sqRT-PCR
GFP+0fwd	ATGGTGAGCAAGGGCGAG	GFP	Amplification GFP
GFP3'Stop	TCATTTGTACAGCTCGTCCAT	GFP	GFP with 3' stop codon
GFP5'BamHI	GGATCCATGGTGAGCAAGGGCGAG	GFP, mCherry	Equipment BamHI 5' GFP, mCherry
GFP3'BamHI	GGATCCTTGTACAGCTCGTCCAT	GFP, mCherry	Equipment BamHI 3' GFP, mCherry
NdeI_GFP_F	CATATGGTGAGCAAGGGCGAG	GFP	Equipment NdeI 3' GFP
SalI_Thrombin_F	GTCGACAGCAGCGGCCTGGTG	Thrombin cleavage site (TCS) pET28b	Cloning of 6H-ROPIP1-TCS-GFP
M13fwd(-40)	GTTTTCCCAGTCACGAC	MCS pGEM-T	Colony check PCR, sequencing
M13rev	AACAGCTATGACCATGA	MCS pGEM-T	Colony check PCR, sequencing
pGY1-fwd	TGACGCACAATCCCACTAT	MCS pGY1	Colony check PCR, sequencing
pGY1-rev	AGAGAGACTGGTGATTTCAGC	MCS pGY1	Colony check PCR, sequencing
pGADT7_seq_rev	TGGCGAAGAAGTCCAAA	MCS pGADT7	Colony check PCR, sequencing
pGADT7_seq_rev	TGGCGAAGAAGTCCAAA	MCS pGADT7	Colony check PCR, sequencing
T7	TAATACGACTCACTATAGGG	MCS pET28b	Colony check PCR, sequencing
T7_Terminator_rev	TATGCTAGTTATTGCTCAG	MCS pET28b	Colony check PCR, sequencing
RGA2intronBie371	GAAGGGATAGCCCTCATAGATAG	Recombination Site pIPKTA30N	Colony check PCR, sequencing
RGA2intronBie372	AAACAAATGCAGTATGAAGATACAC	Recombination Site pIPKTA30N	Colony check PCR, sequencing

Table A 6: Software Used in this Study

Name	Version	Purpose	Reference
BioEdit	39454	Local BLAST searches	Hall (1999)
GeneDoc	2.7.000	Processing sequence alignment files	Nicholas et al. (1997)
Mega6	6140226	Computating phylogenetic trees	Tamura et al. (2013)
DeepView	v4.1.0	3D-rendering tertiary protein structures	Guex and Peitsch (1997)
PyMOL	v1.3r1-edu	3D-rendering tertiary protein structures	DeLano Scientific LLC
PerlPrimer	v1.1.21	Designing oligos	Marshall (2004)
pDRAW	1.0	Virtual cloning	Acaclone Software
SPSS	21.0.0.0	Statistical analysis	IBM Corp. 2012

Danksagung

Ich bedanke mich bei Prof. Hückelhoven für das in mich gesetzte Vertrauen, für die Förderung und auch für die Forderung, sowie Diskussionen. Danke, Ralph.

Ich bedanke mich bei meiner Prüfungskommisson, dem Zweitprüfer Prof. Aurélien Tellier, dem Drittprüfer Prof. Erich Glawischnig und dem Vorsitzenden Prof. Alfons Gierl für die Übernahme der Aufgaben.

Ich bedanke mich bei Prof. Hans Thordal-Christensen für die Rolle des Mentors (Graduate School).

Ich möchte mich weiter bei Dr. Ruth Eichmann für meine Rekrutierung an den Lehrstuhl für Phytopathologie und für die Förderung während meiner Studentenzeit bedanken. Danke, Ruth.

Bei Dr. Bernd Zechmann bedanke ich mich für die Kooperation und die freundliche Aufnahme in Graz.

Der Deutschen Forschungsgemeinschaft (DFG) danke ich für die finanzielle Unterstützung dieser Arbeit (Sachbeihilfe Projekt ’Characterization of *Blumeria graminis* peptides as potential effectors targeting barley RAC/ROP proteins‘).

… und natürlich bei allen, die zum Gelingen dieser Arbeit beigetragen haben!